UNIVERSITY OF SOUTHAMPTON
FACULTY OF ENGINEERING AND PHYSICAL SCIENCES
SCHOOL OF ENGINEERING, DEPARTMENT OF BIOMEDICAL ENGINEERING

ULTRASOUND-MEDIATED THERAPIES FOR THE TREATMENT OF BIOFILMS IN CHRONIC WOUND INFECTIONS

Gareth William Edward LuTheryn BSc (Hons), MSc, MRSB

THESIS FOR THE DEGREE OF DOCTOR OF PHILOSOPHY
DECEMBER 2020

- SUPERVISORY TEAM -
Dr Dario Carugo[1,2,3,5], Dr Peter Glynne-Jones[2], Professor Jeremy S Webb[3, 4, 5]

[1] Department of Pharmaceutics, School of Pharmacy, University College London, London, UK.
[2] Faculty of Engineering and Physical Science, University of Southampton, Southampton, UK.
[3] Centre for Biological Sciences, University of Southampton, Southampton, UK.
[4] Institute for Life Sciences, University of Southampton, Southampton, UK.
[4] National Biofilms Innovation Centre (NBIC), Southampton, UK

ABSTRACT

Bacterial biofilms are an ever growing concern for public health; featuring both inherited genetic resistance and a conferred innate tolerance to traditional antibiotic therapies. Consequently, there is a growing interest in novel methods of drug delivery, in order to increase the efficacy of antimicrobial agents. One such method is the use of acoustically activated microbubbles, which undergo volumetric oscillations and collapse upon exposure to an ultrasound field. This facilitates physical perturbation of the biofilm, and provides the means to control drug delivery both temporally and spatially. In line with current literature in this area, this report offers a rounded argument and research evidence to outline why ultrasound-responsive agents could be an integral part of advancing wound care. The fabrication of a stable ultrasound-responsive carrier of nitric oxide was an important first step in this research, this was achieved by exploring two primary lipid microbubble shell constituents: 1,2-distearoylphosphatidylcholine (DSPC) and 1,2-dibehenoyl-sn-glycero-3-phosphocholine (DBPC). It was successfully demonstrated that DBPC shelled microbubbles exhibited the greatest stability in ambient temperature over 60 minutes. Targeting biofilms to increase the efficacy of antimicrobial delivery and optimised local concentrations has proved challenging, due to the complex and heterogeneous nature of the biofilm extracellular matrix. This research assessed the utility of cationic microbubbles, as a means of non-selective electrostatic targeting of the anionic biofilm structure. Cationic microbubbles demonstrated the ability enhance microbubble-biofilm contact by up to 37%, with a binding strength comparable to that seen in specific ligand-receptor targeting of biofilm extracellular matrix constituents. The anti-biofilm and bactericidal efficacy of neutral and cationic air- and nitric oxide-loaded microbubbles, were assessed both in terms of their passive nitric oxide-mediated action and active response to ultrasound stimulation. To facilitate growth of biofilms with morphological and phenotypic characteristics of biofilms found in chronic wounds, a wound constituent media that featured key pathophysiological components of the *in vivo* wound environment was developed. It was successfully demonstrated that insonified DBPC nitric oxide microbubbles could elicit a clinically significant 99.9% (3-log reduction) in viable cells recovered from treated biofilms, by enhancing the efficacy of sub-inhibitory (4 µg/mL) concentrations of the antibiotic gentamicin. Moreover, the combination of the nitric oxide and the ultrasound mediated physical perturbation of biofilms by microbubbles, was also shown to elicit a significant 99.9% reduction in surface area covered by *P. aeruginosa* biofilms.

TABLE OF CONTENTS

LIST OF FIGURES

LIST OF TABLES

RESEARCH THESIS: DECLARATION OF AUTHORSHIP

Print name: Gareth William Edward LuTheryn

Title of thesis: Ultrasound-mediated therapies for the treatment of biofilms in chronic wound infections

I declare that this thesis and the work presented in it are my own and has been generated by me as the result of my own original research.

I confirm that:

1. This work was done wholly or mainly while in candidature for a research degree at this University;
2. Where any part of this thesis has previously been submitted for a degree or any other qualification at this University or any other institution, this has been clearly stated;
3. Where I have consulted the published work of others, this is always clearly attributed;
4. Where I have quoted from the work of others, the source is always given. With the exception of such quotations, this thesis is entirely my own work;
5. I have acknowledged all main sources of help;
6. Where the thesis is based on work done by myself jointly with others, I have made clear exactly what was done by others and what I have contributed myself;
7. Parts of this work have been published as:-

LuTheryn, G., Glynne-Jones, P., Webb, J. S. and Carugo, D. (2019) 'Ultrasound-mediated therapies for the treatment of biofilms in chronic wounds: a review of present knowledge', *Microbial Biotechnology*. Wiley Online Library. doi: 10.1111/1751-7915.13471.

LuTheryn, G., Hind, C., Glynne-Jones, P., Webb, J. S., Sutton, J. M., and Carugo, D. (2019). Ultrasound-responsive bioactive-microbubbles for the eradication of biofilms. 24th Eur. Symp. Ultrasound Contrast Imaging. DOI: 10.13140/RG.2.2.29250.84169

De Grazia, A.; LuTheryn, G.; Meghdadi, A.; Mosayyebi, A.; Espinosa-Ortiz, E.J.; Gerlach, R.; Carugo, D. A Microfluidic-Based Investigation of Bacterial Attachment in Ureteral Stents. Micromachines 2020, 11, 408.

Signature: .... Date:..........................

ACKNOWLEDGEMENTS

I began this PhD journey with an email to Dr Dario Carugo, explaining that I was very interested in the research topic, but as a medical microbiologist who lacked any skills in acoustics or bioengineering was not sure if I was a suitable candidate. It is only fitting therefore that my first thank you is to Dario, for seeing potential in me and providing me with the opportunity to grow as a researcher with his phenomenal support and friendship for the last three years. I would also like to thank my wider supervisory team at the University of Southampton:- Dr Peter Glynne-Jones and Professor Jeremy S Webb, and Public Health England:- Dr Mark J Sutton and Dr Charlotte Hind, for their guidance and respective expertise that facilitates the success of this interdisciplinary research. Making progress at times would not have been possible without my colleagues in the Bioengineering office, who have become wonderful friends and provided an essential support group through this period of my life. Erik and Sara, I think of as a mischievous brother and sister and can't thank you enough for all the times you've made me laugh and been there to talk to, Alisha you're the most motivational fitness guru I have ever met and I would have finished my PhD with several more kilograms without you. A special thank you must also be made to Fiona Haigh, who has been a much needed source of counselling, laughter and escapism since the very beginning. Additionally, to Gwyneth Skiller for making my first months at the University of Southampton feel like home.

To my family who have supported my ambition since I was a child; despite not having a clue what I am doing most of the time, I owe you more than I could ever repay. Nin, your pride in me and support has encouraged me to keep going no matter what, I could never fully articulate how much that has meant. For being a constant support during the best and hardest of times in this journey, I owe a huge debt of gratitude to Kian Clark and Deborah Jones for always being there to make me feel loved and supported. To Mamma Den, who has been there for me since undergraduate, your kindness, affection and encouragement has always been unconditional and meant immeasurably more than you could imagine. Nonna Emilietta, Elena e tutta la famiglia Sartori mi hai insegnato che il duro lavoro, la passione e la determinazione per avere successo ti porteranno molto lontano nella vita. Nonno Anthony 'Father' mi ha insegnato ad essere sempre gentile e di dare il massimo, non importa quanto piccolo sia il compito, è per questo motivo che dedico questa tesi alla sua memoria.

ABBREVIATIONS

BB	Bolton Broth
BOCS	Biofilm on coupon sonicator
c-di-GMP	Cyclic-di-guanosine monophosphate
CFU	Colony forming units
DBPC	1,2-dibehenoyl-sn-glycero-3-phosphocholine
DFU	Diabetic foot ulcers
DHR	Dihydrorhodamine 123
DPPC	Dipalmitoyl phosphatidylcholine
DPPE	1,2-Bis(diphenylphosphino)ethane
DSEPC	1,2-Distearoyl-sn-Glycero-3-ethylphosphocholine
DSPC	1,2-distearoylphosphatidylcholine
EPS	Extracellular polymeric substances
FI	Fluorescent intensity
FFT	Fast fourier transform
GFP	Green fluorescent protein
HPLC	High-performance liquid chromatography
LB	Lysogeny broth
LHB	Laked horse blood
MBs	Microbubbles
MDR	Multi-drug resistant
MIC	Minimum inhibitory concentration
NO	Nitric oxide
NOMB	Nitric oxide microbubble
PBS	Phosphate-buffered saline
PEG40s	Polyoxyethylene (40) stearate
PEG	Polyethylene glycol
PCD	Passive cavitation detection
PHE	Public Health England
PRF	Pulse repetition frequency
PVA	Polyvinyl alcohol
RAMB	Room air microbubble
RFP	Red fluorescent protein
SAT	System for acoustic transfection
SNP	Sodium nitroprusside
SUMIT	System for ultrasound mediated interventional therapy
TSB	Tryptone soy broth
WCM	Wound constituent media
VBNC	Viable but non-culturable

CHAPTER I

1 ULTRASOUND MEDIATED THERAPIES FOR THE TREATMENT OF BIOFILMS IN CHRONIC WOUNDS: A REVIEW OF PRESENT KNOWLEDGE

1.1 Introduction

1.1.1 *The bacterial biofilm: Development and aetiology*

Though the microbial world is vastly diverse, the development of a biofilm remains perhaps the most ubiquitous means by which microbial cells can thrive within their given environment (H. Wu *et al.*, 2015; Flemming *et al.*, 2016). A biofilm can be described as a localised aggregation of microorganisms in a heterogeneous, sessile community, embedded in a dynamic matrix of extracellular polymeric substances (EPS) (Singh *et al.*, 2017b). From biogeochemical cycling in the ecosystem and the human microbiome, to biofouling and disease; biofilms are simultaneously an essential part of life and a prominent concern for industry and public health (Donlan, 2002; Flemming *et al.*, 2016; Kuliasha *et al.*, 2017). The gross architecture of the biofilm is complex; proteomic investigation has shown that at least in *Pseudomonas aeruginosa* biofilm development is regimented and sequential (**Figure 1**) (Hall-Stoodley *et al.*, 2004). Though the specific stages of biofilm development have not been characterised for each prokaryotic organism individually, it should be noted that the development archetype is markedly conserved *in vitro* (Figueiredo *et al.*, 2017; Lohse *et al.*, 2017; Bartell *et al.*, 2018).

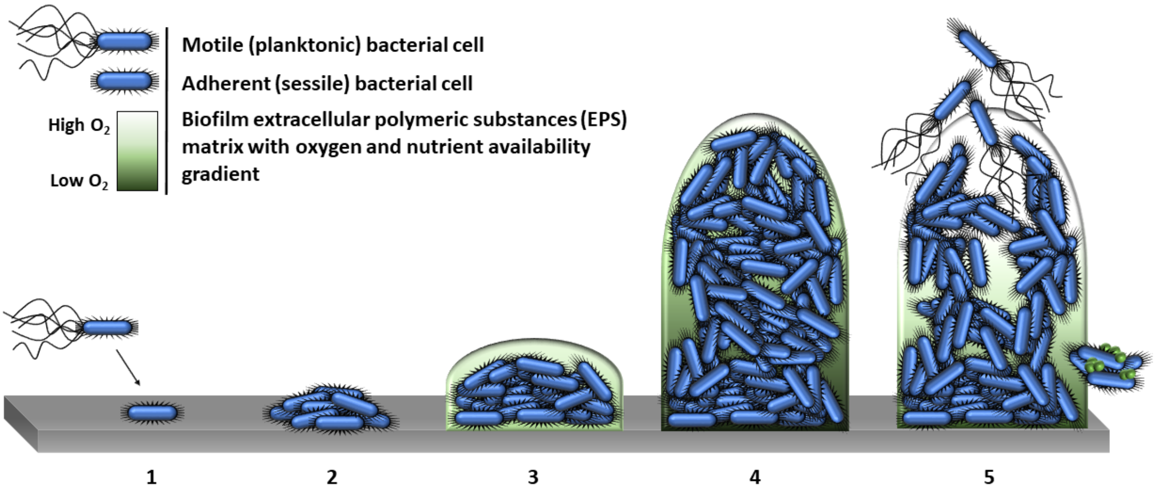

Figure 1 A simplified schematic representation of the sequential biofilm formation described by (Hall-Stoodley *et al.*, 2004) (1) Initial attachment can be transient, but this association can become robust and lead to the aggregation of cells (2). This stabilised attachment leads to the production of extracellular polymeric substances (EPS), which encapsulate aggregated cells forming micro-colonies (3). The maturation of the biofilm structure is achieved through inter-cellular signalling (4), a mature biofilm commonly features a concentration gradient of oxygen and nutrient availability. At superficial layers of the biofilm oxygen is consumed at a faster rate than it can diffuse in, which coincides with the gradient of nutrient availability. Consequently, the majority of metabolically active cells are located at the periphery of the biofilm, whilst persister, dormant or dead cells are found at the biofilm-substratum interface. In its final stages the biofilm undergoes programmed dispersal of cells, which includes cellular mass and EPS sloughing off (5).

The initial stages of biofilm formation are characterised by an impermanent association of planktonic cells with a surface, which is superseded by a robust adhesion and the production of EPS (Hall-Stoodley *et al.*, 2004; Holt *et al.*, 2017). Although proteins, carbohydrates, lipids, DNA, RNA and water are staple constituents of the EPS (Taglialegna *et al.*, 2016), there is a notable variability in the quantity of each macromolecule present between biofilms (Flemming *et al.*, 2007). The mucoid phenotype of *P. aeruginosa* is found extensively in the cystic fibrosis lung, and usually arises from the overproduction of the exopolysaccharide alginate (Schurr, 2013). This serves as a good example of the individual differences seen in the EPS of biofilms, exemplifying that variation can be both species specific and influenced by the immediate environment (Maleki *et al.*, 2016). Adherent cells will then begin to propagate and assemble into micro-colonies; the initiation of this process is attributed to monomeric adhesins (Jamal *et al.*, 2015). Aggregation and micro-colony formation in *P. aeruginosa* is attributed to the Type IV pili surface adhesin, whereas in *Staphylococcus aureus* it is thought to be induced by polysaccharide intercellular adhesin (Persat *et al.*, 2015; Maleki *et al.*, 2016). Maturation of a biofilm into its distinctive three dimensional structure, is achieved through sophisticated cell-cell communication termed quorum sensing (Laganenka and Sourjik, 2017). Quorum sensing is facilitated by the production of auto-inducer signalling molecules, which allow microbial cells to determine cell density and collectively adjust gene expression in response (Rutherford and Bassler, 2012). This ensures the formation of an encapsulating extracellular matrix, with water-filled channels for the transport and exchange of nutrients and waste products within the biofilm (Parsek and Singh, 2003). Programmed dispersal of microbial cells is the final stage of biofilm development, which is achieved by either the release of newly formed cells from biofilm aggregates, or detachment of constituent peripheral cells by species specific saccharolytic enzymes (Marsh and Zaura, 2017). Erosion and sloughing may also occur due to mechanical (i.e. shear) stress upon the biofilm (**Figure 1 - 5**), which causes peripheral cells to disengage indiscriminately from the biofilm and enter the local environment (Rmaile *et al.*, 2014; Jamal *et al.*, 2018). Though dispersed cells regain motility, they remain physiologically unique from cells in the planktonic and biofilm phase; these dispersed cells are highly virulent in nature towards macrophages, which is a useful attribute given their main purpose is the colonisation of new sites (Chua *et al.*, 2014). Dispersion represents one of the most virulent stages in the biofilm lifecycle, but perhaps also one of the easiest to target and in turn potentiate killing of microbial cells (Hall and Mah, 2017).

1.1.2 *The physiological mechanism of acute wound healing*

In response to a wound derived from acute trauma, tissue will undergo a sequential process of reparation that results in the reinstitution of anatomical integrity (Clark, 1993). Under normal physiological conditions, the progression of wound healing can be broadly categorised into four phases: haemostasis, inflammation, proliferation and remodelling (Guo and DiPietro, 2010). The phases within the process of wound repair are not mutually exclusive, but involve dynamic integration of cellular processes that overlap temporally (Robson, 2004). The haemostatic phase of wound repair occurs immediately upon damage to the epidermis; platelets rapidly bind to damaged blood vessels initiating coagulation and local aggregation of growth factors and inflammatory cytokines (Smith *et al.*, 2015). An important distinction between cytokines is that pro-inflammatory cytokines such as tumour necrosis factor (TNF- α) promote inflammation, whilst anti-inflammatory cytokines such as transforming growth factor (TGF-β) promote healing and cell proliferation (Dinarello, 2000). Coagulation ends at the formation of a platelet plug with a fibrin extracellular matrix, which provides the primary substratum that recruited cells interact with (Laurens *et al.*, 2006). As inflammatory cells such as leukocytes and macrophages are recruited to the wound site by platelet derived and transforming growth factors, there is a significant overlap between the coagulation and inflammatory phases of repair.

The general environment of a wound provides a warm, moist, nutrition rich niche for microbial colonisation; however, in an immunocompetent patient antimicrobial proteases released by recruited phagocytic cells clear the wound of bacteria quickly (Bowler *et al.*, 2001). In order for tissue formation to progress successfully, there is a requirement for adequate blood supply that ensures gas and metabolite exchange; the process of forming new blood vessels (termed angiogenesis) is an integral part of preventing the wound from maintaining an ischaemic state (Tonnesen *et al.*, 2000). Macrophages in particular serve an important role in stimulating both angiogenesis and cellular proliferation, which are critical in the resolution of a wound (Koh and DiPietro, 2011). The inflammatory phase usually subsides within 5 days of initial trauma; this is superseded by the proliferative phase in which re-epithelisation begins by sustained migration and controlled proliferation of keratinocytes (Demidova-Rice *et al.*, 2012). Keratinocytes form 90% of the population of epidermal skin cells and are essential to wound healing, particularly in the production of cytokines and growth factors that exhibit autocrine activity during skin remodelling (Findlay and Gurtner, 2017; Kwan *et al.*, 2018). The transition into the remodelling phase of wound repair is principally due to the neo-vascularisation of the area, which restores physiological function to the tissue. The increased blood supply creates an optimal microenvironment for epidermal cell and fibroblast proliferation, which mediate the synthesis of a collagen based matrix that restores the integrity of the epidermis to complete the healing process (Gurtner *et al.*, 2008).

1.1.2.1 **The pathophysiology of chronic wounds**

A chronic wound can be broadly classified as any wound that is subject to poor wound healing; this is typically associated with recalcitrant infection, ischaemia of the tissue and a prolonged or arrested inflammatory phase (Wolcott *et al.*, 2008). Diabetic foot ulcers (DFU) are a severe complication observed in 15% of neuropathic diabetic patients, making DFUs one of the most prevalent examples of a chronic wound worldwide (Alexiadou and Doupis, 2012). One of the hallmarks of a chronic wound is high microbial burden and diversity, which is typically attributed to the formation of poly-microbial drug-resistant biofilms in the wound bed (Banu *et al.*, 2015). In response to infection there is increased recruitment of pro-inflammatory cytokines and production of proteolytic enzymes, which causes the degradation of growth factors and early extracellular matrix in the wound (McCarty and Percival, 2013). Without the specific growth factors and matrices produced across the haemostatic and inflammatory phases of wound repair, the migration and proliferation of keratinocytes is impaired (Martinasso *et al.*, 2010). These factors are exacerbated by impaired angiogenesis and subsequent neo-vascularisation of the wound tissue, maintaining a hypoxic environment in the wound preventing metabolic exchange and potentiating necrosis of the tissue (Demidova-Rice *et al.*, 2012; Yazdanpanah *et al.*, 2015)

1.1.3 *The significance of biofilms in chronic wounds*

The causality between pathogenic microorganisms and infection has been understood for over a century; yet most research into the pathogenesis of microorganisms has focused solely on acute infection by planktonic cells. Over the last decade this focus has shifted; greater emphasis is now placed on the role of multi-drug resistant (MDR) organisms and biofilms, which mediate over 90% of chronic wound infections (Attinger and Wolcott, 2012; Bjarnsholt, 2013). The augmented persistence of biofilms can be attributed in part to inherited genetic antibiotic resistance traits, which actively reduce the efficacy of an administered antimicrobial agent. This commonly includes the use of membrane localised efflux pumps, which prevent antimicrobial agents reaching lethal intracellular concentrations; and antibiotic degradation enzymes such as beta-lactamase, which alter the pharmacokinetic properties of beta-lactam antibiotics (Høiby *et al.*, 2011; Geisinger and Isberg, 2017). However, of particular concern is that when compared to their planktonic counterparts, it has been conclusively shown that the biofilm phenotype confers an innate physical tolerance to antimicrobial agents (Hengzhuang *et al.*, 2012; Algburi *et al.*, 2017). It is also noted that the extracellular polysaccharides within the dynamic EPS matrix potentiate this effect by acting as a shield, compromising the ability of the host immune system to detect the biofilm infection (Limoli *et al.*, 2015; Kumar *et al.*, 2017). Moreover, the production of extracellular toxins and lytic enzymes facilitates destruction of local immune cells, which provides a source of cellular components that can be utilised by microbial cells (Cooper *et al.*, 2014).

There is a pronounced heterogeneity associated with bacterial colonisation of wounds, which has an intrinsic effect on morphology, mechanical properties and development of biofilms in chronic wounds (Thomson, 2011). It has been demonstrated that a typical wound can consist of approximately 17 different bacterial genera, with 12-20 different aerobic and anaerobic species of pathogenic bacteria dominating the commensal microflora (Omar *et al.*, 2017). There are a number of important attributes that contribute to the success of biofilms in chronic wounds, which include microenvironments with oxygen and nutrient gradients throughout the biofilm structure (**Figure 1**).

Hypoxic regions within the biofilm are integral to the proliferation of pathogenic anaerobes such as *Clostridium* and *Bacteroides* species (Bowler *et al.*, 2001), which under normal culture conditions would fail to grow. It is therefore possible that whilst endogenously derived anaerobic bacteria contribute to the pathophysiology of a chronic wound, their significance in terms of treating polymicrobial infections is overlooked in favour of perceived causative agents such as *P. aeruginosa* and *S. aureus* (Cowan, 2011). In addition to being polymicrobial, constituent cells of the biofilm will be undergoing each respective stage of the bacterial growth cycle simultaneously: lag phase, log phase, stationary phase and death (**Figure 2**)(Percival *et al.*, 2011). Whilst cells at the peripheral interface are metabolically active, deep layers of the biofilm can accumulate dead cells in addition to exhibiting reduced rates of growth; this can contribute to biofilm persistence by rendering antimicrobial agents that target growing cells ineffective (Hall and Mah, 2017).

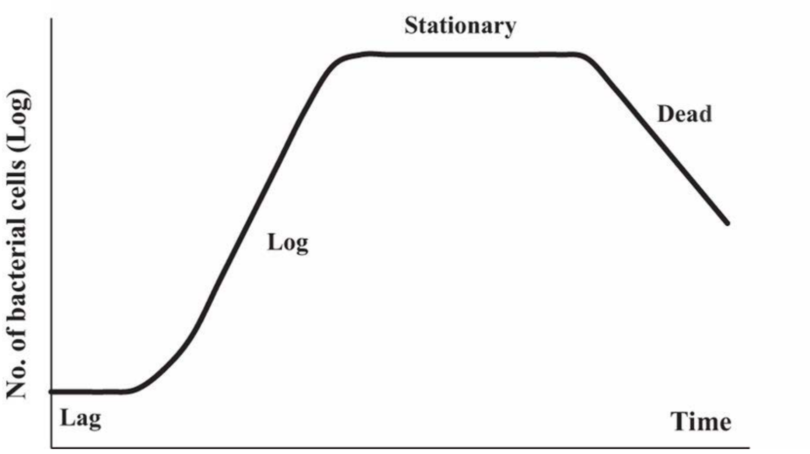

Figure 2 In a typical population of bacteria with access to appropriate nutrients, the growth dynamics exhibits the general trend depicted. During the lag phase, the bacteria will take some time to adjust to the immediate environment. This is followed by the log phase of exponential growth, in which bacteria divide in the process of asexual reproduction termed binary fission. The population of bacteria will reach their maximum growth rate, at which point growth will plateau due to depletion of nutrients and enter the stationary phase. In the stationary phase, the number of actively dividing cells is equalled by the number of dead cells. At the point of total nutrient exhaustion bacteria will enter

the death phase, whereby the number of dead cells outnumbers those that are alive (Wang *et al.*, 2015).

Due to poor absorption in the digestive tract, gentamicin is one of the most common topical broad-spectrum aminoglycoside antibiotics used in the treatment of wounds (Price *et al.*, 2016). A common feature of aminoglycosides such as gentamicin is that they bind the 30s ribosomal subunit of bacteria, which is critical to the translation of mRNA and subsequent production of functional bacterial proteins (Mehta and Champney, 2002). Gentamicin is particularly effective against gram negative organisms such as *P. aeruginosa;* the antibiotic interaction results in the restructuring of the outer membrane, and the subsequent formation of transient pores alters the permeability of bacterial cells to antibiotics (Leggett, 2017). The minimum inhibitory concentration (MIC) of an antibiotic, can be defined as the lowest concentration required to inhibit visible growth of an organism (Andrews, 2001). A problem with this method is that MIC is typically measured using planktonic bacterial cultures, whereas the concentration required to eliminate a competent biofilm can be up to 10 fold higher (Tassew *et al.*, 2017). As a typical example of a chronic wound, DFUs commonly arise from comparatively minor trauma to the foot and have been strongly associated with substantial morbidity and mortality (Walsh *et al.*, 2016). The key pathophysiological difference between a typical acute wound and a chronic wound, is that the latter fails to progress past the inflammatory phase of repair (Attinger and Wolcott, 2012). Given the pathogenicity and associated virulence factors of biofilms, there is credible evidence that they are implicit in preventing normal mechanisms of wound healing (Malone *et al.*, 2017). A comparative study of the foot microbiome demonstrated that when compared to a non-diabetic, the diabetic foot was host to substantially more opportunistically pathogenic species of bacteria such as *S. aureus* (Jneid *et al.*, 2017). Though studies have specifically implicated the microbial burden of DFUs in delayed healing, there must also be consideration of the species present and their importance in the pathophysiology of chronic wounds (Gardner *et al.*, 2013). It is reported that every 30 seconds worldwide, there is a lower-limb amputation as a direct result of DFU

(Yazdanpanah *et al.*, 2015). This is undoubtedly accompanied by significant physical and emotional stress, as well as an increase in mortality rate (Costa *et al.*, 2017). In addition, there is an undeniable economic burden associated with the cost of health care, from disease management to major intervention (Walsh *et al.*, 2016). It is evident that current treatment options available for biofilms are both limited in availability and effectiveness; thus, seeking to resolve a chronic infection by eradicating a competent biofilm formed in a wound bed, is a multifactorial challenge.

1.1.4 ***Composition of gas-filled microbubbles***

The architecture of gas-filled microbubbles (MBs) is variable according to their intended application, though they commonly consist of a surfactant, polymer, protein or phospholipid shell, which encapsulates a gaseous-core (**Figure 3**) (Sirsi and Borden, 2009; Owen *et al.*, 2018a). The composition of the MB shell is integral to conferring mechanical stability, preventing coalescence, and determining its acoustic response to stimulation by ultrasound (Borden *et al.*, 2005; Stride, 2008; Carugo *et al.*, 2017). The range in MB size is typically 1 – 10 µm, but this is heavily influenced by the shell composition and fabrication method used (Lee *et al.*, 2015a). Characterising MB size is an important step not only for determining its acoustic response and drug-loading capacity, but also its longevity in circulation and thereby its safety for *in vivo* applications (Lee *et al.*, 2015a). Phospholipids are perhaps the most common excipients of the MB shell; key examples include distearoyl phosphatidylcholine (DSPC) and dipalmitoyl phosphatidylcholine (DPPC) (Swanson *et al.*, 2010). The lipid molecules assemble in a monolayer at the hydrophilic-hydrophobic interface to stabilise the gas core, exposing their hydrophilic polar head to the aqueous environment and their hydrophobic tails towards the gaseous core (**Figure 3**).

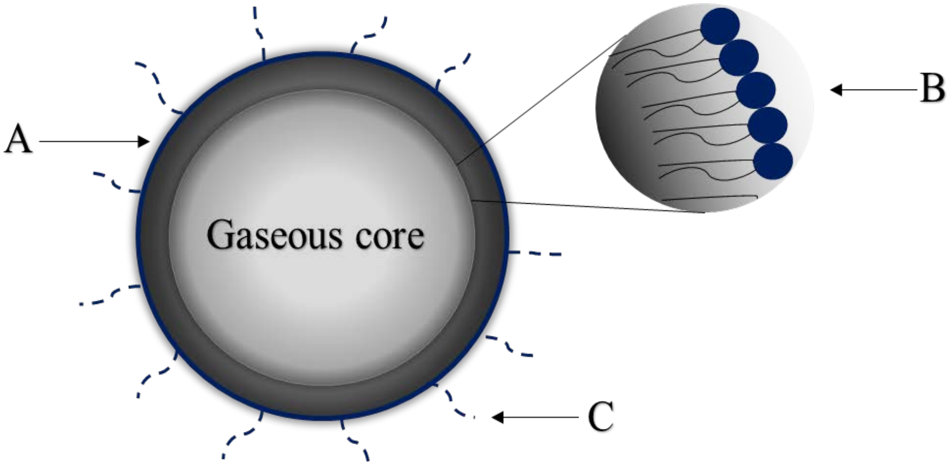

Figure 3 A schematic representation of a microbubble depicting a gaseous core encapsulated by (A) a stabilising lipid-shell. An expanded view (B) shows the orientation of the phospholipid monolayer at the gas-liquid interface, with polar heads in contact with the aqueous phase and polar tails internalised towards the gaseous core. The addition of polyethylene glycol surfactant chains is represented by (C).

The acyl chain length of a lipid dictates the permeability of the MB shell to gases (Borden, 2016); longer hydrophobic acyl chains provide greater cohesion (or packing density) between adjacent lipid molecules (Hosny *et al.*, 2013). Moreover, they increase the distance of diffusion compared to shorter chain lengths, these factors consequently reduce the MB shell permeability to gases and increase its stability both during storage and upon administration (Zhuang *et al.*, 2016). Additional surfactants can be integrated into the MB shell, which can be particularly important for biomedical applications of MBs such as drug delivery (Abou-Saleh *et al.*, 2014). The addition of the polyethylene glycol (PEG) derivatives such as PEG40s that possess surfactant-like properties to stabilise a MB shell, simultaneously provide a means to functionalise the MB shell with biological components or assemblies such as targeting ligands, antibodies and liposomes (Abou-Saleh *et al.*, 2014), whilst mitigating immunogenicity to lipid antigens and preventing phagocytosis of the MB by macrophages (Paolino *et al.*, 2017). The content of the MBs gaseous core, is arguably just as important as the composition of the encapsulating shell, as it dictates some of the MB properties (Vohra and Jasuja, 2016). High molecular weight perfluorocarbon compounds and sulphur hexafluoride are commonly used as the gaseous core for MBs *in vivo*; the poor water solubility and low diffusion rate of fluorinated gases prolongs MB longevity by enhancing stability (Casini *et al.*, 2016; Carugo *et al.*, 2017).

The drug loading capacity of a MB is strongly linked to the efficacy of the treatment, as it directly impacts the amount of a given therapeutic agent that can be delivered to a target site (Tzu-Yin *et al.*, 2013). The use of electrostatic force to bond drugs to the MB surface (Rychak and Klibanov, 2014), insertion into the MB shell (Lentacker *et al.*, 2009), loading the drug into the gaseous void (Fix *et al.*, 2015), and placing a layer of oil at the interface between the gaseous core and MB shell (Tinkov *et al.*, 2009), are all considered relatively low-capacity methods of drug loading (**Figure 4**) (Sirsi and Borden, 2009). A limiting factor of these methods is that the MB formulation is governed by the physicochemical properties of the drug intended for use; to allow incorporation or association of a drug, the MB formulation must have a complementary charge, hydrophobicity or hydrophilicity. To yield a greater MB drug loading capacity, it is common for nanoparticles or liposomes to be conjugated to MBs covalently or with the use of biotin-avidin bridges (Lentacker *et al.*, 2010; Liang *et al.*, 2018). However, methods of achieving a greater drug loading capacity also directly impact upon the stability and acoustic properties of the MB, due to changes in the shell thickness and composition (Tzu-Yin *et al.*, 2013; Kooiman *et al.*, 2014). Methods of microbubble fabrication and their biophysical effects, have been extensively reviewed elsewhere (Stride and Edirisinghe, 2008; Fix *et al.*, 2015; Lee *et al.*, 2015a).

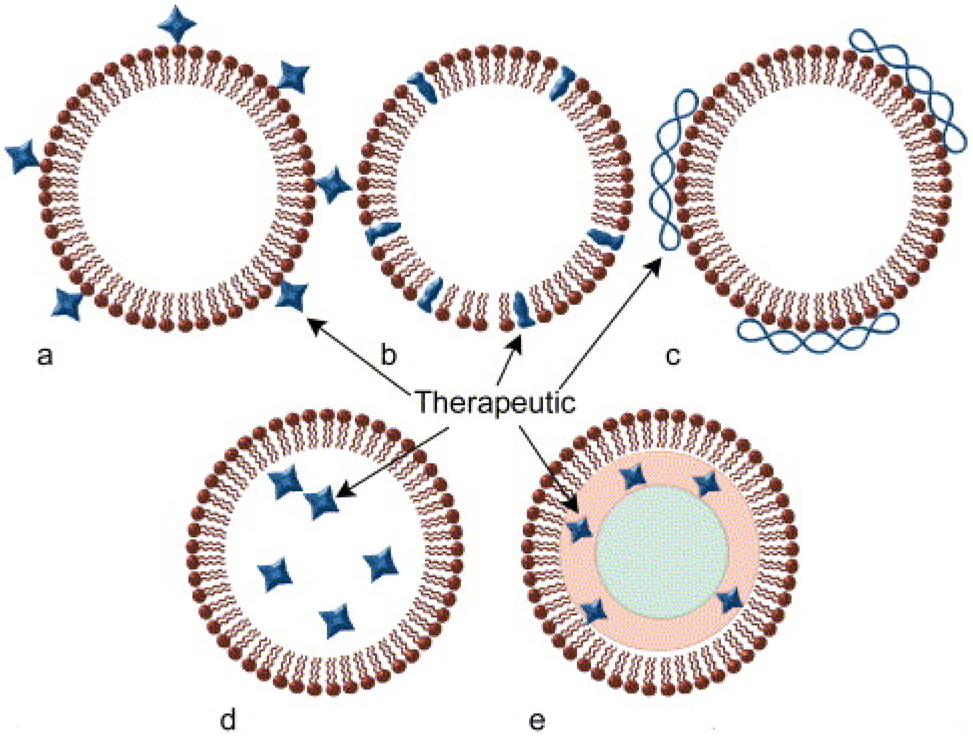

Figure 4 Drug loading modalities associated with MBs adapted from (Unger *et al.*, 2002): (a) the loading of therapeutic agents onto the shell, or embedding them directly into the shell of the MBs (b). Charged molecules such as DNA, can be associated with the MB shell by electrostatic forces (c). A target drug or gas can be encapsulated in the internal void of the MB (d), or solubilised in an oil layer under the MB shell (e). For the purpose of visualisation the MB shells used here are constructed from lipids, but the shell could equally be composed of other stabilising polymeric materials.

1.1.4.1 **Commercially available preparations of MBs**

As shown in **Table 1**, a number of MB formulations are commercially available for clinical use, with Albunex® being one of the first approved in the early 1990s (Appis *et al.*, 2015). Though commercially available, not all formulations have continued to meet increasingly strict regulatory standards imposed by government bodies such as the FDA. As two examples SonoVue® and Optison™ have a demonstrably excellent record for safety, in that they are non-immunogenic, non-thrombotic and are fabricated from biocompatible materials that can be neutralised and excreted from the body (Paefgen *et al.*, 2015). SonoVue® MBs are comprised of DSPC, DPPG and palmitic acid; 99% of the MBs in a

1 – 5 x 10^8 MB/mL suspension are found to be smaller than 10 µm, with a typical size of 1.5 - 2.5 µm though a small proportion can be as large as 20 µm (Borden and Song, 2018). Optison™ MBs are stabilised by human serum albumin and are typically larger than the lipid shelled SonoVue® MBs at 3 – 4.5 µm, however they are more concentrated too at 5 – 8 x 10^8 MB/mL with 95% of the MBs less than 10 µm and a maximum size of 32 µm (Borden and Song, 2018).

Table 1 Examples of microbubble formulations currently available commercially; formulations that also have FDA approval have been indicated (*). (Wong *et al.*, 2004; Stride and Edirisinghe, 2009; Sun *et al.*, 2014; McDannold *et al.*, 2017; Borden and Song, 2018).

Formulation	Manufacturer	Shell composition	Gas core
SonoVue®*	Bracco diagnostics, Inc.	Phospholipid	Sulphur hexafluoride
Optison™*	Amersham Health plc.	Human serum albumin *(Cross-linked)*	Octafluoropropane
Albunex®	Molecular Biosystems	Human serum albumin *(Sonicated)*	Air
Sonazoid™	Amersham Health plc.	Phospholipid	Perfluorocarbon
Bisphere™	Point Biomedical Corp.	Polymer-protein bilayer	Air

1.1.4.2 Ultrasound-mediated physical effects of MBs

Ultrasound is perhaps most widely known for its use as a rapid, cost effective and safe method of medical diagnostic scanning (Stride and Saffari, 2003), however an ever increasing body of research is seeking to further develop its original intended use as a therapeutic agent (ter Haar, 2007). Ultrasound can be defined as mechanical pressure waves resulting from vibrations, which are transmissible through materials such as fluids, soft tissue and solids. Transmission of ultrasound through a medium is governed by acoustic impedance, which is derived from $Z = \rho v$, where ρ is the density of the medium (in kg/m^3) and v is the speed of sound through the medium (in m/s). The units for Z are therefore $kg/(m^2 \cdot s)$. At the boundary between media of different acoustic impedance we see reflection and transmission of the ultrasound energy; when the difference in acoustic impedance between two media is high, there is greater reflection and reduced transmission (O'Brien, 2007). The acoustic impedances between soft tissues such as the epidermis, fat, muscle and blood varies by less than 1%, which results in more transmission than reflection of the ultrasound (Alkins and Hynynen, 2014). However, it is important to note that the propagation of ultrasound in soft tissue is limited by attenuation of the signal, this corresponds to the loss of signal amplitude as distance from the transmission source increases (Suzuki *et al.*, 2018). Attenuation in tissue is largely due to absorption or scattering; where absorption occurs due to a proportion of the ultrasound being converted into heat, and scattering is a result of the transmitted ultrasound changing direction (radiating) (Aubry and Derode, 2011; T. Chen *et al.*, 2016). Ultrasound is generated by applying voltage to transducers that most commonly use piezoelectric materials, which have the ability to convert electrical energy to mechanical energy or vice versa (van der Zwaag *et al.*, 2013). The frequency of ultrasound is determined by the number of waves per second, this is often reported in MHz (where 1 MHz corresponds to 1,000,000 Hz and 1 Hz = 1 cycle per second) and for medical ultrasound devices this is typically in the range of 1 – 15 MHz (Abu-Zidan *et al.*, 2011; Rutkowska *et al.*, 2017). The intensity of an ultrasound wave is determined by the flow of energy per second through a cross-sectional area (W/cm^{-2}); the greater the intensity of the ultrasound, the more energy is transmitted (Neppiras, 1980). Biophysical effects such as acoustic cavitation, acoustic radiation forces and heat generation, are achieved at a range of ultrasound intensities (0.1–10,000 W/cm^{-2}) (Rediske *et al.*, 1999; Dong *et al.*, 2013). For diagnostic ultrasound imaging intensities of 0.05–0.50 W/cm^{-2} are common, with most clinical devices having a peak output of 0.70 W/cm^{-2} (ter Haar, 2007; Xin *et al.*, 2016). The ultrasound intensities seen in surgical and therapeutic applications such as bone fracture repair and high intensity focused ultrasound for selective tissue heating, range respectively from 0.03–1,000 W/cm^{-2} (Ng and Liu, 2002).

Manipulation of the MB fabrication method and shell composition dictates their physicochemical properties and size, allowing them to elicit different modes of action in response to acoustic stimulation. These ultrasound-mediated behaviours of the MBs can be further regulated by adjusting the parameters of the ultrasound delivered (e.g. frequency, acoustic pressure, duration); this makes MBs perhaps one of the most versatile tools available in biomedicine. In biomedical applications of MBs their efficacy for a given task is correlated to their acoustic response (Datta *et al.*, 2006; Choi *et al.*, 2014), which is typically categorised into either stable or inertial cavitation (**Figure 5**) (Lentacker *et al.*, 2014). In response to the pressure changes of ultrasound waves, MBs experience alternating volumetric compression and expansion (or rarefaction) (De Jong *et al.*, 2002). Upon exposure to low-intensity US, the nature of these oscillations is typically repetitive over several US cycles; this behaviour is referred to as stable cavitation (Stride and Coussios, 2009). Above a critical US intensity, the periodicity of this oscillation is lost; MBs expand rapidly, and the inertia of the surrounding fluid during contraction causes them to collapse violently (Wu and Nyborg, 2008; Stride and Coussios, 2009). This process is known as inertial or transient cavitation and often leads to MB fragmentation into smaller bubbles. It should be noted that whilst there is a simple relationship between US intensity and pressure for a plane travelling wave, it is more complex in 2D fields and standing wave fields. The propensity for fragmentation of lipid-shelled MBs is inversely correlated to the phospholipid alkyl chain length and also depends upon the type of emulsifier used (Borden *et al.*, 2005). Notably, the MB resonant frequency and amplitude of oscillation, the transition pressure from stable to inertial cavitation, and MB fragmentation diameter all strongly depend upon the initial MB size (for a given shell formulation and suspension medium) (Povey and Mason, 1998; Borden *et al.*, 2005). Therefore, the selection of a specific US frequency to elicit a desired acoustic response should take into account the typically broad size distribution of a MB suspension and variations in MB size during sample storage and/or handling.

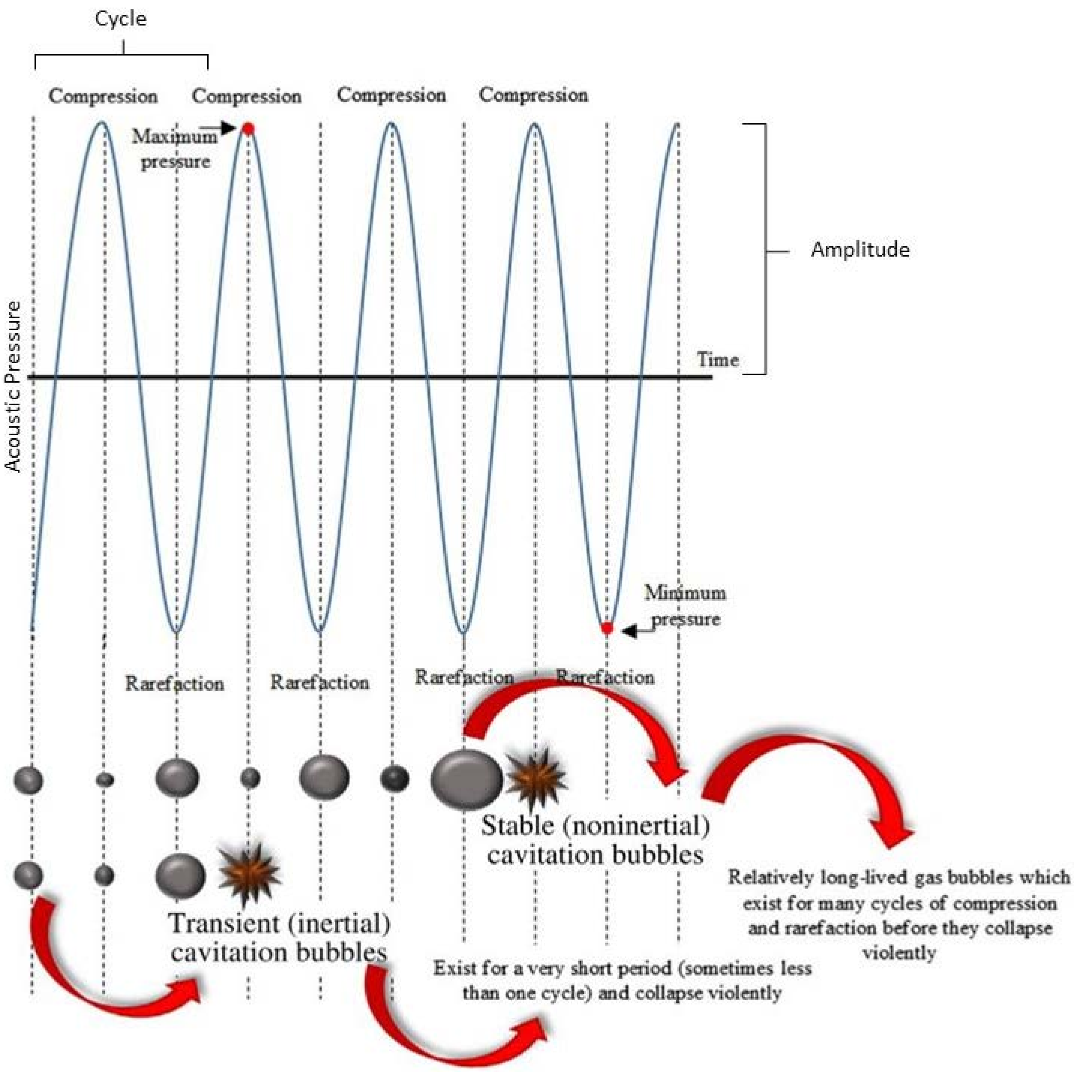

Figure 5 (Adapted from Rutkowska *et al.*, 2017) In response to the pressure changes induced by an ultrasound wave, MBs will resonate at specific frequencies according to factors such as size and composition. Stable cavitation results in in the linear or non-linear oscillation (sustained compression and expansion (rarefaction) over time), where a bubble of resonant size equilibrates to its initial diameter over many cycles (Lentacker *et al.*, 2014). Inertial cavitation is more likely to occur when during rarefaction the bubble diameter grows to at least twice its original diameter, this will occur generally during a single or small number of cycles (Fabiilli *et al.*, 2009). Inertial cavitation causes the bubble to collapse violently, driven by the inertia of the fluid, and can cause fragmentation into multiple smaller bubbles. Although inertial cavitation can release energy in the form of heat, this is rapidly dissipated in the surrounding fluid which has a greater total volume than the volume occupied by MBs (Ye *et al.*, 2013).

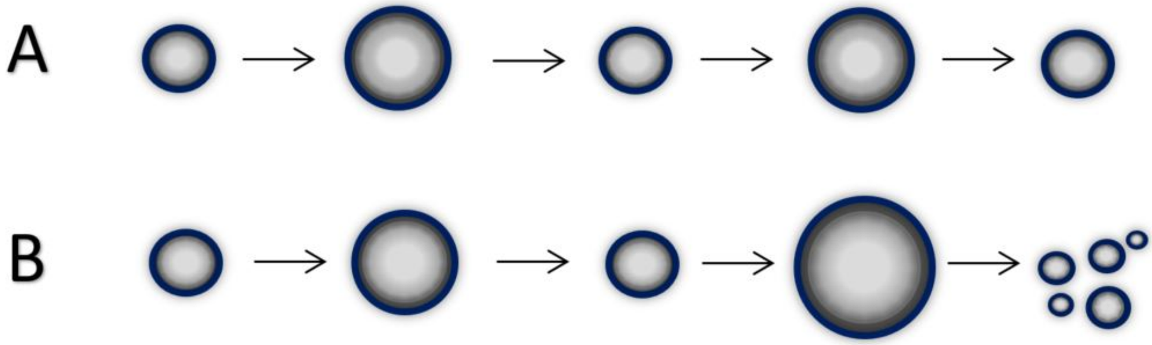

Figure 6 A schematic representation of (A) stable cavitation and (B) inertial cavitation in MBs of resonant size, in response to acoustic stimulation by ultrasound. Cavitation is the sequential expansion and contraction of the microbubble, which is induced by the low and high deviations in the pressure of the ultrasound wave. Stable cavitation (A) is characterised by low amplitude microbubble oscillation, which generates localised microstreaming of the fluid and shear stress on cell membranes. When ultrasound intensity is increased, MBs expand and compress at a faster rate. The inertia of the surrounding fluid upon compression causes the microbubble to collapse or fragment into a number of smaller MBs; this is termed inertial cavitation (B).

It is possible for MB oscillation to induce micro-streaming in the surrounding fluid, which exerts shear stress over a cell membrane causing transmembrane pores to form (**Figure 7**A) (Ferrara *et al.*, 2007). The systematic expansion and compression of MBs in stable cavitation creates localised pushing and pulling forces, which in turn cause disruption to the integrity of cell membranes located in their vicinity (**Figure 7**B) (Lee *et al.*, 2015b). Micro-jet formation and shockwaves are more transient biophysical effects attributed to the collapse of MBs in inertial cavitation, which respectively puncture proximal membranes and increase membrane permeability through mechanical stress (**Figure 7**C and **Figure 7**D) (H Yu *et al.*, 2014; Leow *et al.*, 2015). In comparison to the mechanical and thermal stresses imparted by inertial cavitation, it could be inferred that stable cavitation is a comparatively gentle means of facilitating drug uptake.

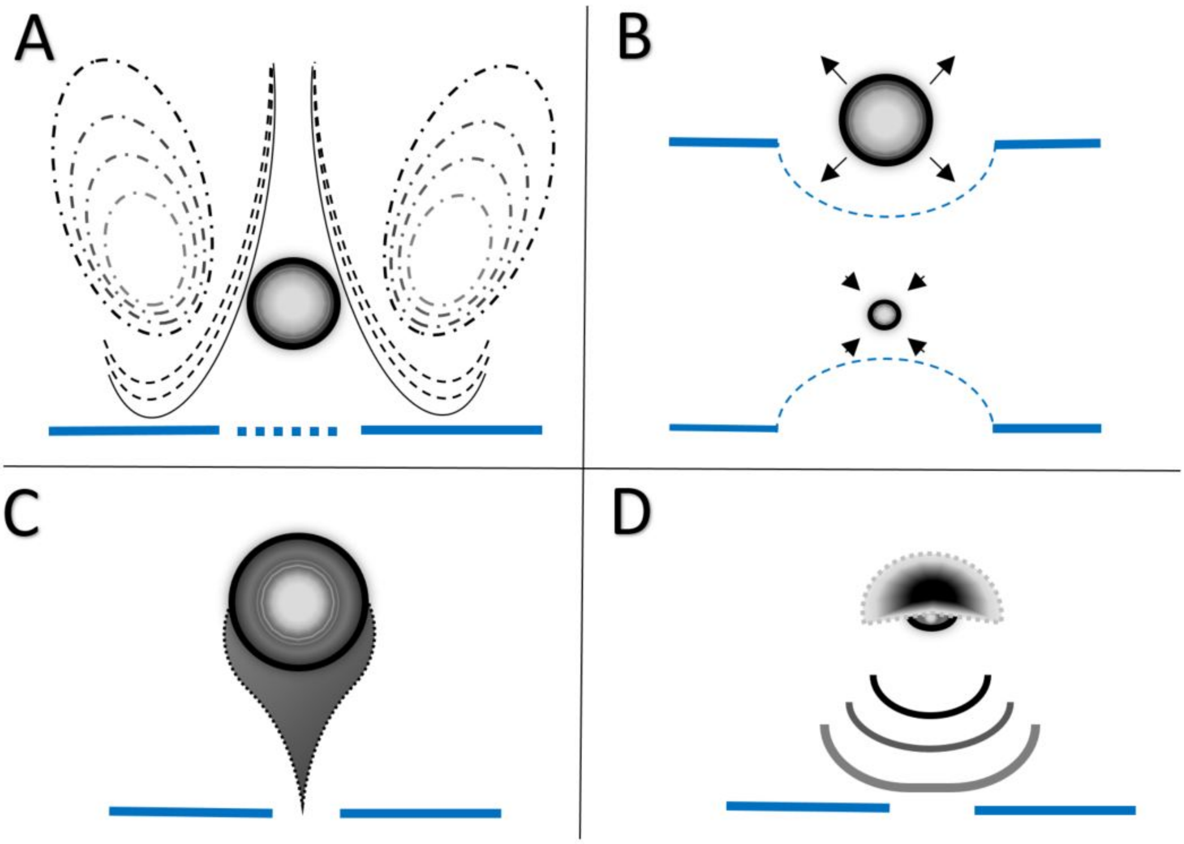

Figure 7 Examples of the biophysical effects of MBs on cell membranes (▬), when exposed to varied ultrasound parameters: (A) Micro-streaming of fluid and (B) microbubble pushing upon expansion and pulling upon compression are characteristic effects of stable cavitation induced by low intensity ultrasound. However, asymmetrical collapse causing liquid jetting (C) and shock waves induced by forceful microbubble collapse (D), are hallmarks of inertial cavitation induced by ultrasound of a higher intensity. This work will investigate the efficacy of MBs cavitation regimes, as a treatment modality for biofilms.

1.1.4.3 **Assessing microbubble activity by passive cavitation detection**

The acoustic behaviour of MBs can be characterised by passive cavitation detection (PCD); this is often carried out by stimulating a suspension of MBs with ultrasound from a transducer, whilst using a second transducer to detect the acoustic emissions from the cavitating MBs. The detector specifically is used to record the pressure waves that are emitted as a result of volume changes in oscillating MBs generating acoustic waves (Leighton, 1997). The pressure of the wave received and recorded by the PCD, depends upon the temporal variations of the MB volume. Therefore the spectral peaks in volumetric oscillations are output as spectral peaks in pressure emissions, which provides information about the periodicity and stability of the oscillating MB (Gyöngy and Coussios, 2010). When MBs oscillate in response to their resonance frequency the temporal response can be separated into two phases; the first is their harmonic response during ultrasound stimulation, in which the MB will undergo periodic volumetric compression and rarefaction with a fixed frequency (Doinikov *et al.*, 2009; Efthymiou *et al.*, 2018). The second broadband response is termed post excitation signal (PES) and can occur 1 – 5 µs subsequent to the end of stimulation (Santin *et al.*, 2010). Carrying out PCD testing provides information about the cavitation regime of a MB suspension upon exposure to US; specifically, the appearance of harmonics, subharmonics and ultra-harmonics provides some evidence of stable cavitation of MBs, whilst broadband noise emissions are linked to inertial cavitation. The ability to broadly distinguish between cavitation regimes is valuable, as it is well documented that MB behaviour is closely linked to their cavitation activity (O'Brien, 2007; Collis *et al.*, 2010; de Saint Victor *et al.*, 2019). The pressure emissions recorded by PCD can be processed in three ways: frequency-domain, time-domain, or time-frequency. The frequency-domain method is perhaps the most commonly used, in which a Fast Fourier Transform (FFT) of the spectrum is performed to visualise the frequency content of the signal (**Figure 8**).

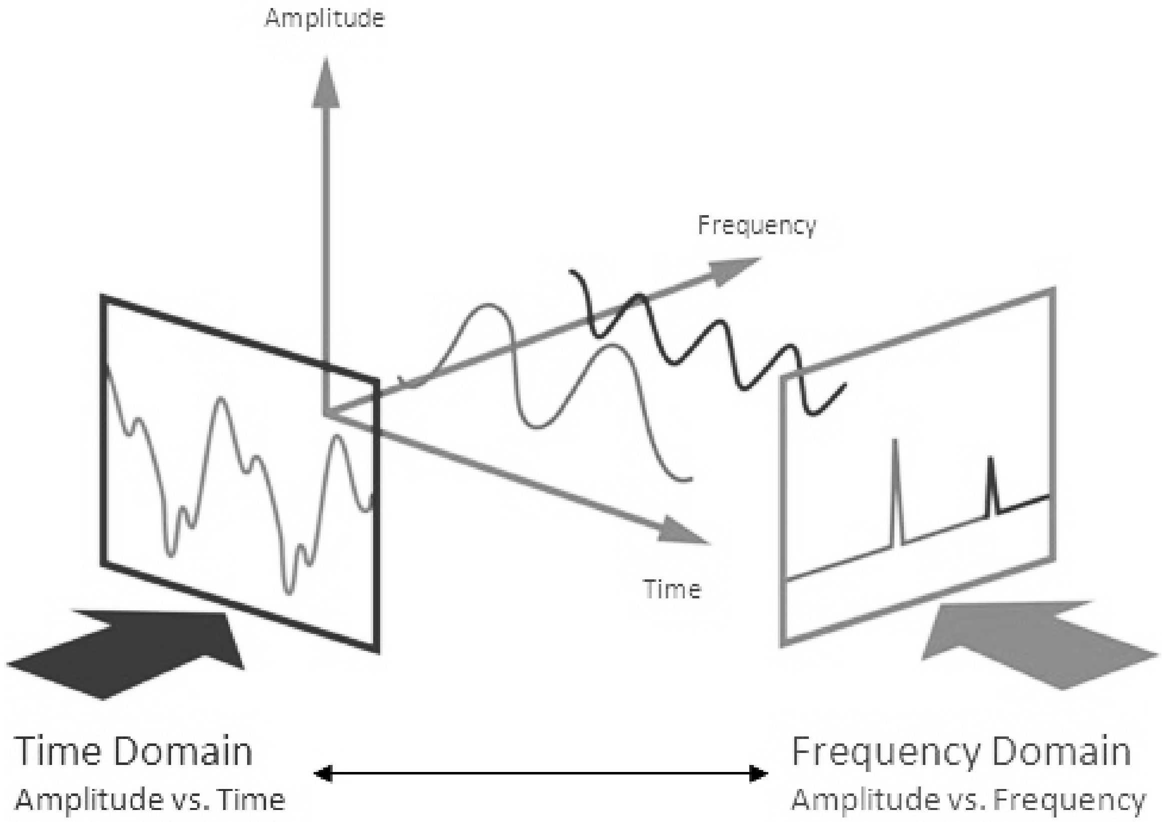

Figure 8 A FFT provides a quantification of the frequency content of a time-dependent signal, which allows the visualisation of the frequency content of a signal obtained by PCD. Image adapted with permission from Mastriani, (2018).

An example of FFT spectra showing different MB acoustic behaviours can be found in **Figure 9**: (a) demonstrates the effect of a low acoustic pressure applied where only the driving frequency is present; (b) shows the appearance of harmonic components indicating the stable cavitation of MBs due to an increase in the acoustic pressure; (c) sub- and ultra- harmonics become apparent upon further increase in the acoustic pressure; finally, in (d), the broadband noise level increases and the sub- and ultra- harmonic components are suppressed which is indicative of inertial cavitation of MBs (Mastriani, 2018).

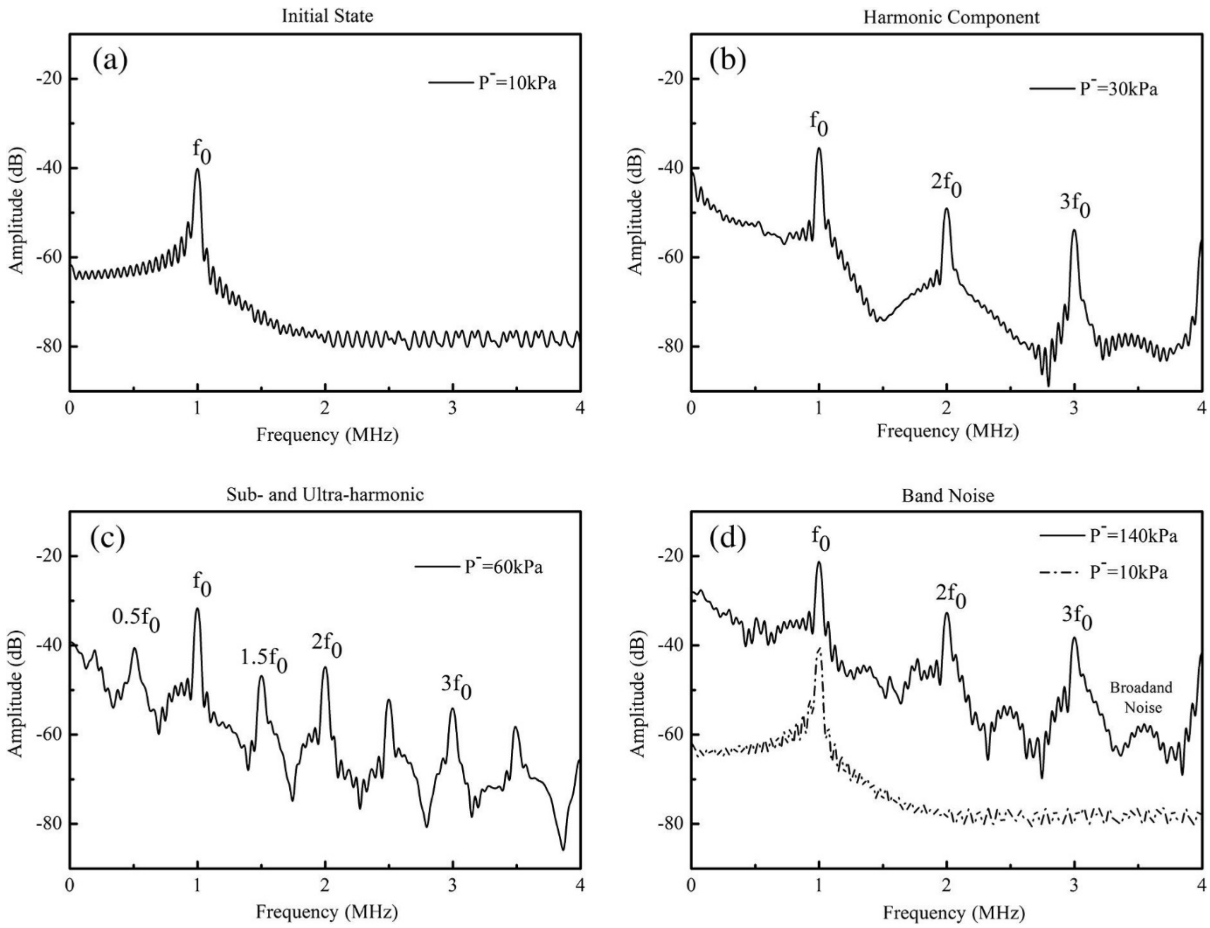

Figure 9 Example FFT spectra obtained at different acoustic driving pressures, which corresponds to different cavitation regimes and thus MB behaviours. These tests were carried out with superparamagnetic iron oxide nanoparticles, the frequency, pulse repetition rate and pulse length of the driving signals are 1 MHz, 100 Hz, and 20 cycles, respectively. (a) 10 kPa driving frequency only, no harmonic features are evident. (b) 30 kPa harmonic components appear which is indicative of stable cavitation of MBs. (c) 60 kPa sub- and ultra- harmonic components appear. (d) 140 kPa sub- and ultra-harmonics are suppressed and the broadband noise level increases, which is usually indicative of inertial cavitation and collapse of MBs. Figure adapted with permission from (Gu *et al.*, 2016).

1.2 Literature review

1.2.1 *Current treatment strategies for biofilms in chronic wounds*

The longest established method of removing necrotic tissue and biofilms from chronic wounds is sharp debridement, but this mechanical method of biofilm disruption lacks both efficiency and effectiveness (Cooper *et al.*, 2014). A prospective study by Williams *et al.* (2005) assessed the effect of debridement of chronic wounds in 53 patients over a period of 12 months; debridement was shown to significantly reduce the mean surface area of the chronic wound by 7.4 cm^2, but only achieved complete healing in 16% of patients. The mean surface area of chronic wounds that did not receive debridement was shown to increase by 1.3 cm^2 but, complete healing was still achieved in 4.3% of patients. Though studies have shown that debridement alone expedites wound healing, reduction in wound size and complete healing only occur over weeks of treatment (Cardinal *et al.*, 2009; Kim *et al.*, 2018). The presence of persister cells allows the regeneration of the biofilm within the wound bed, which means that debridement is by no means a complete or permanent solution (Lebeaux *et al.*, 2014). Persister cells are typically a sub-population of dormant cells present close to the initial site of biofilm attachment, they typically constitute 1% or less of the total biomass and occur at these lower levels of the biofilm due to the depletion of oxygen and nutrients over time (Miyaue *et al.*, 2018). The efficacy of debridement can be improved by chemical and biological adjuvants, such as hydrogen peroxide and enzymes respectively (Watters *et al.*, 2016). By causing the EPS matrix of the biofilm to degrade, and thus removing its principal means of protection and nutrition, the rate of wound healing is significantly increased (Kim *et al.*, 2018). The physical perturbation of the biofilm caused by debriding has also been shown to temporarily restore antibiotic sensitivity; as the biofilm begins to regenerate, key antibiotic targets such as cell-wall synthesis (glycopeptides) and protein synthesis (aminoglycosides) become viable (Wolcott *et al.*, 2009; Hall and Mah, 2017).

Quorum sensing is an important regulator of biofilm development; it is the principal means by which microbial cells communicate within a given environment (Miller and Bassler, 2001; Rutherford and Bassler, 2012). The ability of microbial cells to carry out such sophisticated communication is a potent advantage, therefore quorum sensing can also be considered as a valuable therapeutic target (Singh *et al.*, 2017b). By incapacitating this signalling mechanism, the regulation of gene expression, essential metabolic processes and virulence can be irreparably altered (Khmel, 2006). Natural and synthetic inhibitors of quorum sensing such as furanones and Manuka honey, work by downregulating four major quorum sensing genes, which in turn has downstream consequences for genes associated with the biofilm phenotype (Wang *et al.*, 2012; Jakobsen *et al.*, 2018). However, it is important to note that this is principally a method to render a biofilm more inert; it does not offer an immediate solution to detachment or physical eradication (LaSarre and Federle, 2013).

An additional means of controlling biofilms in chronic wounds is impeding their attachment to surfaces; one way in which this has been achieved is with the iron chelating glycoprotein, lactoferrin (García-Montoya *et al.*, 2012). Lactoferrin is an important endogenous antimicrobial component of the innate immune system; it is principally found in tears, saliva, mucous secretions, and breast milk of mammals (Cooper *et al.*, 2014). Its most potent properties include sequestering iron essential for bacterial motility, and direct interaction with Gram-negative bacterial cell walls to induce lysis at the site of infection (Valenti *et al.*, 2015). This consequently means that its bacteriostatic effect can prevent biofilm development, but also disrupt cells which have already become adherent. Lactoferrin has the additional benefit of exhibiting anti-inflammatory properties, which may play an important role in mitigating chronic inflammation associated with delayed wound healing (Valenti *et al.*, 2017). Allison *et al.,* (2015) showed that as a component of breast milk, lactoferrin at a concentration of 3 mg/mL significantly decreased S*treptococcus mutans* biofilm formation *in vitro.* The artificial sweetener xylitol has been shown to bind to Gram-positive organisms, preventing them from adhering to other cells or surfaces (Ferreira *et al.*, 2015). The co-administration of lactoferrin and xylitol has shown great efficacy in eliminating *Pseudomonas aeruginosa* biofilms *in vitro* (Ammons *et al.*, 2011). The acquisition of iron by lactoferrin causes membrane disruption, while xylitol prevents *P. aeruginosa* biofilms successfully repairing the damage caused to the membrane (Rhoads *et al.*, 2008). This treatment modality has been successfully implemented for the treatment of chronic wounds; a lactoferrin and xylitol hydrogel, in conjunction with a silver wound dressing, were shown to achieve a significant log reduction in *Staphylococcus aureus and P. aeruginosa* biofilm viability of 6.5 ± 2.4 and 4.9 ± 0.9, respectively (Ammons *et al.*, 2011). However, this method is comparably only as efficacious as sharp debridement and still requires treatment over a number of weeks to months, but may provide a means to prevent recalcitrant and exacerbated infection (Kim *et al.*, 2018). By avoiding mechanisms of microbial resistance, quorum sensing inhibition, bacteriostasis and adhesion prevention, are pertinent alternatives to traditional antimicrobial therapies. To meet the multi-factorial challenge presented by biofilms in chronic wounds, it is herein proposed that gas-filled MBs can be the versatile biomedical-tool required.

1.2.2 ***Therapeutic applications of gas-filled MBs***

Naturally occurring pockets of echogenic gas were seen to enhance contrast in ultrasound imaging; over the course of 40 years, this discovery has evolved into the use of ultrasound responsive agents for targeted therapy (Kooiman *et al.*, 2014). The term *'theranostic'* agent has been applied to MBs, since they have therapeutic drug transport and delivery potential, while maintaining their echogenic characteristics and diagnostic potential (Sirsi and Borden, 2009). As described earlier (1.1.4), therapeutic agents can be co-administered intravenously with MBs or incorporated into the MB itself in a number of ways, which includes being attached to or embedded in the MB shell (Unger *et al.*, 2004). The incorporation of targeting ligands into the MB shell or conjugation with PEG moieties means that MBs can be functionalised for precision delivery to a specific cell type or location, and they can then be acoustically stimulated to administer the drug they are transporting (Fan *et al.*, 2014). Though a potential limitation of this application is that MBs have a relatively low drug loading capacity, as such the typical anti-cancer agents, peptides and biomolecules they carry must be sufficiently potent in small doses *(Unger et al*>, 2004; Mahringer and Gert, 2017).

One of the first theranostic applications of MBs was in the cardiovascular system; for instance, MBs have been employed in sonothrombolysis to both detect and treat thrombi (Unger *et al.*, 1998), as exemplified by *in vitro* animal models and clinical trials (Unger *et al.*, 2002; Ricci *et al.*, 2012). Without rapid intervention the occlusion of blood vessels leads to ischemic stroke and myocardial infarction, which are associated with significant rates of morbidity and mortality (Dronkers *et al.*, 2017). By using targeting ligands to specifically bind MBs to activated platelets and ultrasound to induce localised MB cavitation, it is possible to deliver thrombolytic drugs and restore normal blood flow (Wang *et al.*, 2016; de Saint Victor *et al.*, 2019). The majority of MBs presently used for this application contain a fluorinated gas core, which increases the lifetime of the MB in circulation (Unger *et al.*, 2014). This is principally because fluorinated gases diffuse poorly into fluids, which consequently means the MB diameter remains relatively stable over time preventing MB induced gas embolism. This treatment modality is not limited to acute thrombosis, but may offer some resolution of the underlying atherosclerotic plaque (Damianou *et al.*, 2015).

Perhaps the most significant advantage of using MBs for drug delivery *in vivo*, is that the material encapsulated in a MB is prevented from interacting directly with the external environment until activated by acoustic stimulation (Sirsi and Borden, 2014). This makes MBs a particularly effective theranostic agent for the delivery of cytotoxic chemotherapeutic drugs; for instance, it could be employed for contrast imaging of a tumour environment, followed by rapid and concentrated drug release at the target site (Emerich *et al.*, 2002). Systemically administered chemotherapeutic drugs are quite limited, with only a small fraction of the therapeutic dose able to reach the tumour and a side effect of damaging healthy tissues (Ibsen *et al.*, 2013). In addition to delivery of chemotherapy agents, MBs have been utilised for gene delivery for the treatment of cancer. The targeted transfection of tissues with acoustically activated MBs has demonstrated the ability to both induce apoptosis and prevent angiogenesis in tumours, which has the significant advantage of being an entirely non-invasive and non-cytotoxic treatment modality (Fujii *et al.*, 2013).

The unique vasculature that controls the movement of substances from the blood to the brain, is termed the blood brain barrier. Its dense network of capillaries with a specialised endothelium supported by neurovascular cells, maintains normal neural physiology by highly selective transport of materials to prevent toxins and pathogens reaching the central nervous system (Daneman and Prat, 2015). Therefore, the blood brain barrier also presents a significant challenge in the administration of therapeutic agents, for the treatment of disease or dysfunction in the central nervous system. However, the use of MBs in combination with focused ultrasound, generating *in situ* peak rarefactional acoustic pressures between 0.3 and 0.6 MPa has been shown to disrupt the blood brain barrier (Wang *et al.*, 2014). The peak acoustic pressure used within studies remains quite consistent, however MB size and the specific ultrasound frequency and intensity used lack congruency and rigorous safety assessment (Meairs and Alonso, 2007; McDannold *et al.*, 2017). Despite these challenges, early data has shown that phospholipid shelled MBs (SonoVue, SF_6), stimulated by focused ultrasound (400 kHz), can increase the penetration of chemotherapeutic drugs across the blood brain barrier by 202% in rodents with implanted brain tumours (Liu *et al.*, 2010). Research interest in this area is high, and studies are beginning to address the issues of ultrasound-responsive agent toxicity, translation to clinical application, and potential negative health implications (Lin *et al.*, 2016; Wu *et al.*, 2018).

1.2.3 ***The use of ultrasound alone as an anti-biofilm treatment***

The ability of low frequency ultrasound to improve the efficacy of antibiotics was shown as early as 1994 (Pitt *et al.*, 1994); the minimum inhibitory concentration (MIC) of aminoglycoside and macrolide antibiotics was consistently reduced by up to 50%, in planktonic cultures of *P. aeruginosa* and *S. aureus* exposed to continuous ultrasound at 67 kHz and 0.3 W/cm^{-2} intensity (Runyan *et al.*, 2006). In contrast a study conducted by Pitt and Ross (2003), showed that low frequency ultrasound (70 kHz) of low acoustic intensity (< 2 W/cm^{-2}) increased the growth rate of planktonic *Escherichia coli* and *P. aeruginosa* compared to cultures grown in the absence of ultrasound. This has since been applied to biofilms and the prevailing theory is that ultrasound alters the permeability of cell membranes to systemically available antibiotics, without physically disrupting or dispersing the biofilm (Mohammad *et al.*, 2015). Investigations conducted *in vivo* on the effect of adjuvant ultrasound on biofilms implanted subcutaneously in rabbits, showed that after 24 hours of continuous ultrasound exposure

(28.48 kHz, 100 and 300 mW/cm^{-2}) recovered *E. coli* colony forming units (CFU) were significantly reduced, whereas there was no observable effect on *P. aeruginosa* (Rediske *et al.*, 1999). The literature in this area is clear that ultrasound alone has no effect on cell viability, though they do lack congruency in the ultrasound frequency, intensity, and pulse length or repetition frequency used (Jiang *et al.*, 2016; Cai *et al.*, 2017). The principal limitation of this approach is that it currently lacks translation to a viable clinical application; the most efficacious low-frequency ultrasound (28.48 kHz) and low-power-density (100 and 300 mW/cm^{-2}) used *in vitro,* was shown to induce tissue damage when applied *in vivo* (Rediske *et al.*, 1999; Jiang *et al.*, 2016). It should also be noted that the majority of studies have continuous treatment times of 24-48 hours, which is unlikely to be considered economically or socially practical. Moreover, this method of utilising the synergistic relationship between ultrasound and antibiotic efficacy is not the most effective means of achieving targeted drug delivery, as even though ultrasound can be directed to specific regions it does not allow for targeted or controlled delivery of the antibiotic to a localised region. The limitation of this is that the antibiotic would still have an impact on unintended systemic targets, which would include dysbiosis of the host commensal microbiota (Carding *et al.*, 2015).

1.2.4 ***Acoustically-stimulated gas MBs for the treatment of bacterial biofilms***

The success of low frequency ultrasound (20–100 kHz) in facilitating the uptake of systemic antibiotics by biofilms has been variable, therefore the use of ultrasound responsive MBs in light of their controllable physical response may be viewed as an evolution in antimicrobial drug delivery (Kooiman *et al.*, 2020). Alteration in the permeability of biofilms to macromolecules such as antimicrobial compounds, has been routinely demonstrated with the use of the red-fluorescent nucleic acid stain, propidium iodide (PI). Dong *et al.* (2017) demonstrated that acoustically activated MBs were capable of enhancing the permeability of *Staphylococcus epidermidis* biofilms grown in OptiCell™ chambers (Thermo Fisher Scientific, Waltham, MA, USA) *in vitro,* to propidium iodide. The fluorescent signal emitted increases proportionally with the quantity of PI that has intercalated with DNA, therefore it can be utilised as a direct means of assessing how MBs facilitate uptake of macromolecules (Stiefel *et al.*, 2015). These effects have been further characterised in more physiologically relevant *in vitro* biofilm models of *S. aureus* infective endocarditis; Lattwein *et al.* (2018) demonstrated that infected thrombi treated with combinations of MBs, plasma, thrombolytic, antibiotic and low frequency ultrasound (120-kHz, 0.44 MPa peak-to-peak pressure) could reduce infected clot mass by 99.3% (± 1.7%), this was determined by the authors a 'sonobactericidal' effect as the treatment was signifcantly better than any other combination of the treatment agents. However, it is important to note that this study measured treatment efficacy by reduction in thrombi size and did not conduct a direct assessment of bactericidal or bacterostatic activity of the treatment, therefore there is no conclusive evidence from this study that cell death of bacteria within biofilm was achieved (Lattwein *et al.*, 2018). Consequently, viable biofilm-residing bacteria may become disseminated upon destruction of the thrombi, which would facilitate redevelopment of biofilms elsewhere (Müsken *et al.*, 2018). It can be hypothesised from the current literature that ultrasound activated MBs facilitate the uptake of antibiotics by biofilms (**Figure 10**); principally through increasing membrane permeability of bacterial cells and *via* heterogeneous alterations to the biofilm architecture, which can include the development of pores in the EPS matrix as well as dispersal and sloughing (Dong *et al.*, 2013; Jang *et al.*, 2017; Hu *et al.*, 2018; Lattwein *et al.*, 2018).

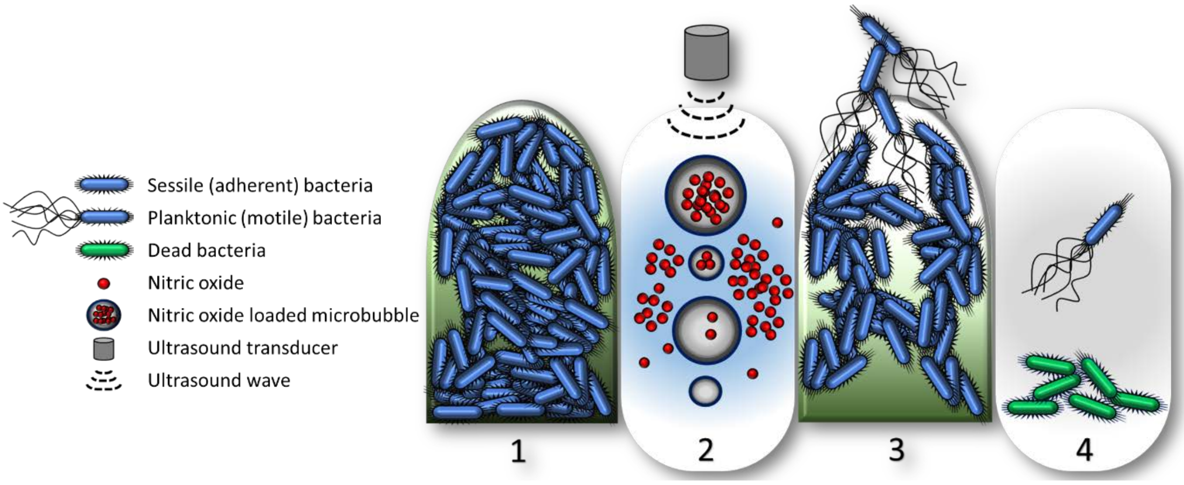

Figure 10 Upon exposure to ultrasound, gas MBs undergoing stable cavitation have been shown to enhance membrane permeability; this enhances the local intracellular concentration of a target drug. By encapsulating biologically active nitric oxide within the lipid shell of the microbubble, the mechanical action of the oscillating microbubble and the biological effect of nitric oxide may induce targeted dispersal and elimination of biofilms from a surface. The co-administration of antibiotic and MBs, may provide means to overcome biofilm associated antibiotic tolerance.

Fluid shear stress has also been shown to significantly affect biofilm morphology; at shear stresses under 1 Pa biofilms are shown to grow in a lab-typical mushroom-like shape with interstitial channels and voids (Salta *et al.*, 2013). However, is some species when the shear stress overcomes the biofilm adhesion strength (> 2 Pa) erosion and sloughing of the biofilm is more pronounced, which leads to low density, biofilm aggregates with large interspaces (Rmaile *et al.*, 2014). The effect of fluid shear stress on the detachment of biofilms has shown to be compounded in the presence of MBs, clearing up to 70% of biofilm in a species dependent manner *in vitro* (Sharma *et al.*, 2005). It has been shown that the *in vitro* application of 0.08 MHz, 1.0 W/cm^{-2}, 50% duty cycle, and 10-min duration ultrasound, MBs and vancomycin can significantly decrease the number of viable cells (7.17 $\log_{10}$ CFU/mL) from *S. epidermidis* biofilms compared to an untreated control (10.51 $\log_{10}$ CFU/mL) (He *et al.*, 2011). It is important to note however, that this study could not demonstrate a significant difference between these groups using an *in vivo* rabbit model, in which *S. epidermidis* biofilms grown on polyethylene disks were subcutaneously implanted bilateral to the vertebral column. The work carried out by He *et al.* (2011), demonstrated that ultrasound activated sulphur hexafluoride MBs with a mean diameter of 2.5 µm and vancomycin create micro-pores within the biofilm architecture (0.08 MHz, 1.0 W/cm^{-2}, 50% duty cycle, and 10-min duration), which does support the hypothesis of facilitated uptake mediated by membrane/EPS disruption. An interesting point is that not only does the membrane disruption facilitates antibiotic uptake, but the influx of nutrients may induce a phase of active growing in deeper layers of the biofilm, potentiating the efficacy of the antibiotic (Dong *et al.*, 2013). In addition, studies have consistently shown that the combination of low frequency ultrasound (40 – 80 KHz) and MBs can halve the MIC of the administered antibiotic (Kasimanickam *et al.*, 2013). It should not be overlooked that to date, research on enhancing efficacy of ultrasound activated MBs has only been performed on naive single-species biofilm models. As discussed in section 1.1.4.2, the ultrasound-dependant response of a MB is strongly influenced by their size; a number of the studies considered here do not assess the impact of alteration to MB size under treatment conditions or carry out cavitation detection, consequently there is no quantitative evidence of a sustained response of MBs to ultrasound over the treatment period or link to which (stable or inertial) cavitation regime may be responsible for the effect seen (He *et al.*, 2011). Furthermore, although the biophysical effect of acoustically activated MBs is evident, the underlying mechanisms of interaction between the bubbles and the biofilm have not been elucidated yet.

1.2.5 ***The applications of nitric oxide for the treatment of bacterial biofilms***

Nitric oxide (NO) has been utilised to facilitate healing of chronic wounds such as DFU for a number of years, this is motivated by the role of NO as an important biological signalling molecule (Witte and Barbul, 2002). Cellular proliferation, angiogenesis and remodelling are key biological and physiological processes mediated by NO, which have been principally applied to wounds in the form of inducible NO synthase (Dhall *et al.*, 2014). It is important to note that traditionally NO has only been applied to chronic wounds in the context of tissue repair, and not with the specific intention to treat the underlying biofilm (Saidkhani *et al.*, 2016; Han and Ceilley, 2017). The administration of NO in a therapeutic capacity has historically been difficult; at high concentrations NO is bactericidal and cytotoxic, which significantly impairs the progression of the normal healing process (Schulz and Stechmiller, 2006). Studies of the biofilm life cycle have elucidated endogenous mechanisms which can be exploited as therapeutic targets, these principally involve the use of NO in the sub-micromolar range to induce the biofilms dispersal phase (Barraud *et al.*, 2015). By inducing dispersal of the biofilm with NO, the physical barrier imposed by the EPS matrix can be negated entirely. Research has shown that the dispersed cells are considerably more susceptible to antimicrobial treatments; it can therefore be inferred that adjuvant NO potentiates antibiotics against biofilms (Howlin *et al.*, 2017). Utilising the spontaneous NO donor sodium nitroprusside (SNP), Howlin *et al.* (2017) successfully showed that NO disrupted *P. aeruginosa* biofilms from cystic fibrosis sputum samples *in vitro*. The same study also highlighted the importance of dispersal as a means of therapy, since the administration of the antibiotic tobramycin alone caused a significant increase in biomass and biofilm thickness compared to untreated controls. Xu *et al.* (2017) have proposed and tested the implementation of NO releasing agents for indwelling medical device surfaces, and they were able to successfully prevent biofilm formation on a functionalised polyurethane surface. Utilising NO to prevent bacterial growth and adhesion on implanted surfaces in conjunction with antimicrobial therapy, may result in better clinical outcomes for patients and significant cost savings for health service providers. There is relatively little published data either *in vivo* or *in vitro,* on the successful implementation of exogenous NO in a gaseous form for biofilm dispersal. The inhalation of NO has been an FDA approved therapeutic agent for nearly two decades, and clinical trials have shown that NO gas at 5-10 ppm can achieve a 3.5 log reduction in respiratory *P. aeruginosa* biofilm aggregates (Howlin *et al.*, 2017). The major problem with the delivery of NO in a gaseous form is that it is highly reactive, which translates to a half-life of only seconds (Thomas *et al.*, 2001). A solution to this challenge is to utilise an ultrasound responsive agent such as the MB, which could provide the means to successfully control the delivery and release of NO.

1.2.5.1 The mechanism of action for nitric oxide induced dispersal of biofilms

The transition between motile and sessile states in the bacterial life cycle are linked to the intracellular second messenger molecule cyclic-di-guanosine monophosphate (c-di-GMP), which is regulated by cellular phosphodiesterase (Reinders *et al.*, 2016). Recent studies have shown that the activity of cellular phosphodiesterase is increased in the presence of NO at concentrations in the pico- and nano-molar range, which results in the degradation of c-di-GMP and subsequent dispersal of sessile cells (Algburi *et al.*, 2017; Howlin *et al.*, 2017). The dispersed cells return to a motile planktonic state and become susceptible to antimicrobial treatment, this effect is shown to be conserved across species such as *P. aeruginosa* and *Staphylococcus aureus* and in both single and complex multispecies biofilms (Barraud *et al.*, 2009). Dispersal has been achieved with NO concentrations as low as 450 pM, reaching peak efficacy at 450 nM (Howlin *et al.*, 2017).

1.2.6 *Biologically active nitric oxide gas MBs and their applications*

Though high molecular weight gases are most commonly used as the MB core constituent, it is also possible to generate MBs that possess a biologically active gaseous core. Recent research has already highlighted the advantages of using MBs with an oxygen core, to increase the therapeutic efficacy of chemo-sonodynamic therapy (SDT) in the targeted treatment of solid malignant tumours (McEwan *et al.*, 2015; Nesbitt *et al.*, 2018). Bioactive gases such as NO have significant therapeutic potential, as they mediate a number of important biological signal pathways (Basudhar *et al.*, 2016). However, the molecule is highly reactive with both exogenous molecules such as oxygen, as well as endogenous scavengers like haemoglobin (Azarov *et al.*, 2005). NO is only moderately soluble in aqueous solutions (< 2 mMol) under standard room temperature and pressure conditions, its concentration is specifically limited by its rate of oxidation (Kelm, 1999). This can be mitigated by utilising the gas as the core of acoustically active MBs; protected by the MB shell, the release of NO can then be both spatially and temporally controlled by ultrasound (Fix *et al.*, 2015). Exposure to ultrasound at frequencies of approximately 1 MHz and relatively low acoustic pressures (< 1 MPa), induces stable volumetric oscillation of MBs. This expansion and contraction of the MB is an important part of its associated biophysical effects, but the effects of cavitation-enhanced gas exchange have been less investigated. During MB compression there is an efflux of core-gas into the local environment, followed by a net influx of gas upon expansion (Crum, 1984; Lentacker *et al.*, 2014; Yusof *et al.*, 2016). This is particularly important in regard to the use of nitric oxide microbubbles (NOMBs), since it shows that the MB has the capacity to deliver a locally concentrated therapeutic NO payload.

There have been few studies to date, which investigated the use of MBs for the delivery of NO. Tong *et al.* (2013) and Wang *et al.* (2013), generated NOMBs with a mean diameter of 3.85 µm by continuous sonication of a lipid suspension at 100 W. 1,2-Bis(diphenylphosphino)ethane (DPPE-PEG_{2000}) and phosphatidylcholine were used to encapsulate NO, which was administered at a constant stream of 4 mL/min for five minutes under anoxic conditions. In contrast, Grishenkov *et al.* (2015) and Cavalieri *et al.* (2008), used biocompatible polyvinyl alcohol (PVA) and high shear stirring to fabricate air-filled MBs, which were then freeze-dried with liquid nitrogen. The subsequent 4 µm diameter PVA capsules were enclosed in a pressure chamber purged with nitrogen, before loading with NO and re-suspend in water. All four studies focused on the intravascular application of NOMBs, thus their research is linked by some common themes.

The work by Cavalieri *et al.* (2008) was the first *in vitro* study of its kind, utilising NOMBs for localised delivery of NO for the prevention of clot formation. Similarly, the NOMBs developed by Grishenkov *et al.* were implemented in a theranostic capacity for myocardial ischemia, showing that they are a highly effective tool for the localised and targeted delivery of NO. Unlike the work by Tong *et al.* (2013), this study sought to use NOMBs as a prophylaxis for patients at risk of thromboembolism. In a rodent model of myocardial infarction, 60 seconds of continuous ultrasound (1 MHz, 1 W/cm^{-2}) applied to NOMBs in conjunction with mesenchymal stem cells, was successfully used to promote angiogenesis (Tong *et al.*, 2013). The applications of this as a successful therapy are promising, with the scope to prevent heart failure by restoring adequate blood flow to damaged cardiac tissue (Cochain *et al.*, 2013). The use of NOMBs without ultrasound for the resolution of deep vein thrombosis was investigated by Wang *et al.* (2013), which successfully showed a reduction in thrombus size by 40% and mitigated development of chronic inflammation. More recently the innate bactericidal activity of NOMBs has been demonstrated; using planktonic *S. aureus* suspensions NOMBs showed a statistically significant decrease in CFU compared to MBs containing air, however the observed reduction in CFU was < 1 Log (Lafond *et al.*, 2020). Further research would be needed to better understand the applicability of NOMBs as a novel bactericidal or bacteriostatic agent, in addition to characterising its ability to potentiate antibiotic therapy.

Grishenkov *et al.* (2015) and Lafond *et al.* (2020), are to date the only studies to assess the final NOMB gas content and dissolution rate in solution, with and without the application of ultrasound (1 - 15 MHz, < 100 kPa). Grishenkov *et al.* utilised high-performance liquid chromatography (HPLC) to measure nitrite and nitrate in both aerated and degassed saline, which are oxidised products of NO. Passive release of NO from degassed saline occurred in 17 minutes and this is increased to 55 minutes in aerated saline; the application of ultrasound reduced the exponential time constant to 10 minutes and 4 minutes respectively (Grishenkov *et al.*, 2015). The assessment of nitrate and nitrite in solution is concordant with expected parameters of diffusion; NO enters the degassed solution at a faster rate than an aerated solution. This was confirmed by Lafond *et al.* (2020) who successfully demonstrated the inclusion and temporal resolution of NO in MBs with an Apollo 4000 with ISO-NOP electrode (World Precision Instruments, Sarasota, FL, USA), in their NOMBs co-loaded with octafluoropropane the concentration of NO ranged from 2-5 mM with rapid release over 340 seconds in an NO saturated solution.

1.2.7 ***Multifunctional agents for the delivery of nitric oxide to biofilms: Present and future perspectives***

To the best of the authors' knowledge, very few previous studies have investigated the use of a NO releasing particle for the treatment of biofilms. The research carried out by Hetrick *et al.* (2009) investigated the use of NO-releasing silica nanoparticles, however it focused only on the bactericidal efficacy of the NO and not on biofilm dispersal. Similarly, in recent work carried out by Choi *et al.* (2019) on NO delivery by perfluorocarbon micro-emulsion, only its antibacterial efficacy was assessed. This work importantly showed the effect that different NO concentrations can have on bacterial activity; using NO concentrations of 0.175 – 2.622 µM a 50% decrease in bacterial viability was observed in planktonic suspensions of *S. aureus*, however no discernible bactericidal activity was seen in planktonic suspensions of *P. aeruginosa* (Choi *et al.*, 2019).

There are a number of unexplored and novel aspects in this area, pertaining specifically to the application of NOMBs for the treatment of bacterial biofilms. There are currently no acoustically stimulated NOMBs used for the treatment of biofilms *in vitro* or *in vivo*, consequently there is currently no evidence on the efficacy of NOMBs or NO loaded nanoparticle induced dispersal of biofilms. Furthermore, though its effects have been observed, the specific interaction between MBs and the biofilm has not been fully elucidated. Previous research has shown that lipid transfer occurs between MBs and biological membranes, which undoubtedly impacts upon cellular integrity, permeability and signalling (Carugo *et al.*, 2017). This effect could be successfully employed to exert a priming effect upon biofilms, to stimulate disruption of the biofilm prior to the administration of ultrasound. One of the greatest challenges faced in the administration of MBs for biofilm treatment, is in achieving a viable clinical translation. It is essential that any proposed treatment is not only efficacious *in vivo*, but can be implemented with minimal training or expertise. The transmission of ultrasound *via* a fluid stream to biotic and abiotc surfaces for the purpose of biological decontamination, has recently demonstrated that clinical translation and utility is achievable (Birkin *et al.*, 2015, 2016).

1.3 Research Aim and Objectives

The principal aim of this research is to develop an effective treatment for biofilms in chronic wounds. The objectives of this project were to (i) characterise an ultrasound-responsive agent capable of delivering nitric oxide contained in MBs, which can be administered with free antimicrobial compounds for dispersal and elimination of biofilms respectively; (ii) validate the use of electrostatic interaction as a means of inducing non-selective binding of the engineered ultrasound responsive NO carrier to a bacterial biofilm; (iii) evaluate the therapeutic efficacy of the developed ultrasound responsive agents in terms of their anti-biofilm and bactericidal effects, using relevant pathophysiological models of biofilm infection, cell viability assessments and fluorescence imaging techniques; and (iv) evaluate the potential for a clinically viable translation of this research subject to its findings.

CHAPTER II

2 FABRICATION AND CHARACTERISATION OF ULTRASOUND-RESPONSIVE MICROBUBBLES

2.1 Introduction

As discussed in Chapter I, the composition of the MB shell is important for determining MB size, stability, response to ultrasound, and subsequent biophysical effects (O'Brien, 2007; ter Haar, 2007; Lentacker *et al.*, 2014). An important first step undertaken in this research was to fabricate a MB stable enough to retain NO, without compromising the mechanical action of the MB. The compositions used in this research are lipid based, using 1,2-distearoyl-sn-glycero-3-phosphocholine (DSPC), 1,2-dibehenoyl-sn-glycero-3-phosphocholine (DBPC) or 1,2-Distearoyl-sn-Glycero-3-EthylPhosphocholine (DSEPC), and polyoxyethylene (40) stearate (PEG40s) as an emulsifier. Lipid coated MBs are widely used in biomedical applications, due to their versatility as biocompatible diagnostic and therapeutic agents (Talu *et al.*, 2006). These particular formulations have been shown by numerous studies to produce stable MBs, which can be successfully used for ultrasound-mediated drug delivery (Helfield *et al.*, 2012; Gong *et al.*, 2014). The incorporation of PEG40s into the MB shell allows the conjugation of bioactive components and targeting agents whilst reducing immunogenicity, without negatively impacting MB stability or responsiveness to ultrasound (Carugo *et al.*, 2017; Owen *et al.*, 2018b). It has also been demonstrated that constituent lipids of the MB shell can incorporate into cell membranes; this alters mechanical properties and permeability even in the absence of ultrasound stimulation, which could contribute to the successful application of MBs in drug delivery (Carugo *et al.*, 2017). A secondary factor, which is important to consider, is the method used to produce MBs, for the most effective balance between cost, yield and MB stability.

2.1.1 *Common gas microbubble fabrication methods*

2.1.1.1 Sonication

The most common method by which micron sized gas MBs are produced is sonication. This is achieved by administering high intensity, low-frequency ultrasound to a suspension of MB shell constituents, particularly phospholipids (Xu *et al.*, 2008), within an environment of controlled gas composition. The principal advantage of this method is rapid production with high yield, however a limiting factor is the large range in the size distribution of the MBs produced (1 – 100 µm) (**Table 2**) (Stride and Edirisinghe, 2008). The size dispersity of MBs produced by sonication may be influenced by factors such as ultrasound frequency, pulse regime, and power, however differential centrifugation or filtration may be used to achieve a more uniform MB dispersity (Feshitan *et al.*, 2009). The MB suspension for all intravascular applications must have a clinically acceptable size dispersity; most importantly, centrifugation may successfully remove MBs with a diameter that exceeds 10 µm. Although it would not be necessary to strictly control MB size for extra-vascular applications, there must be a balance between attaining MBs large enough to have sufficient drug/gas loading capacity, whilst maintaining the ability of the MB to resonate at an ultrasound frequency of 1 MHz. It is possible to simulate larger MBs (> 10 µm) with lower ultrasound frequencies (20-200 kHz), however there are obstacles in its administration *in vivo* due to significant gaps in the knowledge of appropriate safety limits that have been extensively evaluated elsewhere (Ahmadi *et al.*, 2012). It has been shown that MBs with a lipid shell can maintain their stability after centrifugation; however, the fluorinated-gas core of the MBs tested are inherently less susceptible to diffusing out of the MB shell (Feshitan *et al.*, 2009; S.-Y. Wu *et al.*, 2015). To the best of the author's knowledge no research has explored the effect of centrifugation on the stability of NOMBs, consequently the impact that centrifugation would have on NOMB stability is unclear. It could be hypothesised that due to the diffusivity and highly reactive nature of NO, NOMBs would be susceptible to dissolution under centrifugal force.

2.1.1.2 High shear stirring

High shear stirring is used particularly for generating MBs with a polymer coating; the polymer is dissolved in a volatile solvent and emulsified in an aqueous suspension with an immiscible fluid (Jiang *et al.*, 2006). Evaporation of the solvent produces fluid-filled, polymer-coated microspheres at the fluid interface, while secondary processing by freeze drying produces the final gas-filled shells (Stride and Edirisinghe, 2008). The polymer used dictates the porosity of the MB shell assembled by this method. If the structure is too porous its stability would be compromised; if it is not sufficiently porous it will retain liquid and exhibit a poor response to acoustic stimulation (Elsayed *et al.*, 2016). This method has been used to produce polymer shelled NOMBs in studies by both Cavalieri *et al.* (2008) and Grishenkov *et al.* (2015).

2.1.1.3 Membrane emulsification

A less energy intensive alternative to both sonication and high shear stirring is membrane emulsification, which also produces MBs that are more reliably monodisperse (Vladisavljević, 2016). Using a gaseous dispersed phase, MBs are produced by forcing a liquid suspension of shell components through a porous membrane with emulsifiers to prevent coalescence (Lee *et al.*, 2015b). By varying the velocity of the flow, emulsifiers and membrane characteristics such as wettability and stiffness, it is possible to exert a high level of control over MB size and size distribution (Stride and Edirisinghe, 2008).

2.1.1.4 Microfluidic devices

The requisite feature of microfluidic flow focusing or T-junction devices to produce MBs, is an orifice that interfaces with a flow of liquid to perturb gas flow (**Figure 11**) (Dhanaliwala *et al.*, 2015). The instability created at the gas-liquid interface by flow of liquid, allows the MB to form by a process of ‘pinching off’ (Pulsipher *et al.*, 2018). Microfluidic devices have been utilised with great success to generate MBs with precise dimensions; dictated by liquid viscosity, flow rate, gas pressure and orifice diameter (Lee *et al.*, 2015a). Though microfluidic methods allow comprehensive control over MB size and dispersity, the principal limitations of this method are i) a comparatively low MB yield, ii) frequent blockage of micro-channels, and iii) relatively high manufacturing costs (Fiabane *et al.*, 2016). It is also worth noting that in a direct comparison of fabrication methods, microfluidic devices have been shown to produce less stable and lower concentrations of MBs compared to the sonication method (Hosny *et al.*, 2013). The work carried out by Hosny *et al.* (2013) showed that the viscosity of sonicated MB suspensions was significantly higher than those produced by 'T-junction devices, this would result in a lower diffusivity in the sonicated suspension and thus greater stability over time (**Table 2**). With the view of generating a viable clinical translation of this research, this method of MB production and its associated technology would likely be too complex and labour intensive for practical application.

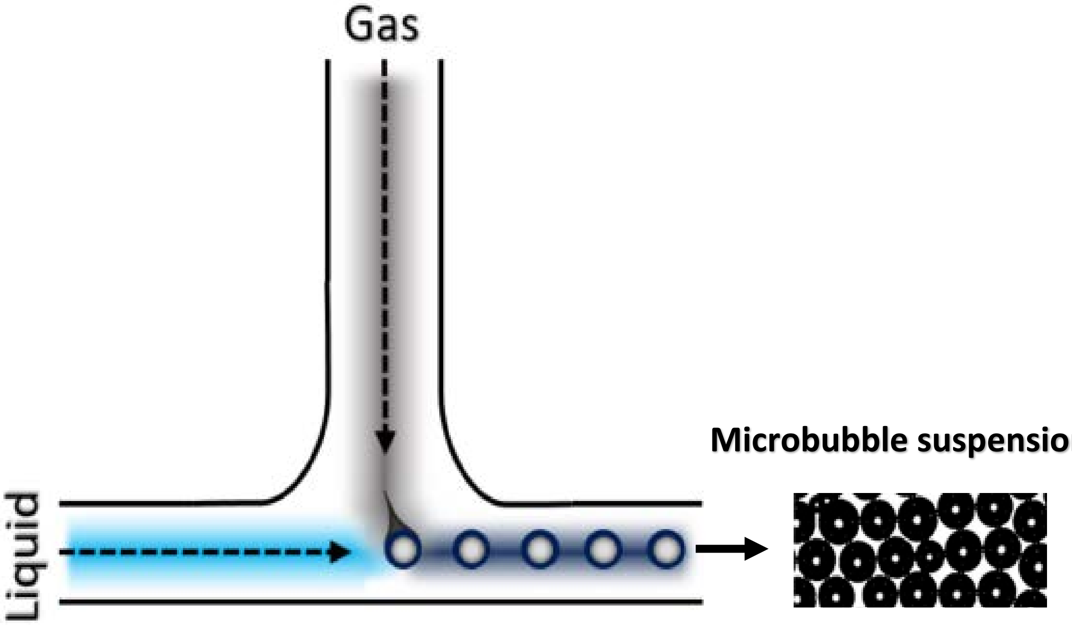

Figure 11 Schematic view of a standard T-junction microfluidic device used in MB fabrication. The flow of the dispersed phase (gas) is perturbed by the carrier phase (liquid). At the point where the liquid impinges on the flow of gas, the MB is formed by an emulsion being 'pinched off'.

Table 2 A summary of the respective advantages and limitations associated with the two prevailing methods of MB production, adapted from Stride and Edirisinghe, 2008.

	Sonication	Microfluidic 'T' junction
Mean microbubble diameter range (µm)	1 – 100	2 - 100
Control over MB diameter	Low	High
Acoustic response	Broadband	Narrow band
Stability	High	Low
Production rate (MB/min)	~ 1×10^{10}	~ 2×10^{7}
Production volume (mL/min)	~ 1×10^{10}	~ 2×10^{8}
Cost	Low	Moderate

2.1.2 *Factors affecting the stability of MBs in fluid suspension*

A MB can be defined as stable if it has a constant diameter and concentration over time. In general, the MB diameter (µm) increases while concentration decreases over time (MB/mL). MB stability is influenced by factors such as diameter, filling gas, shell composition and concentration. The dissolution, Ostwald ripening, coalescence and collapse of MBs are physical phenomenon, accountable for the increase in MB size and reduction in concentration over time (Talu *et al.*, 2006). The Laplace pressure is the pressure difference across a curved boundary, between two immiscible fluids (a gas and a liquid in this work), and this is the principal cause of Ostawald ripening. In a MB, the Laplace pressure is specifically the pressure difference at the boundary between the inside and outside of the MB, which is caused by the surface tension at the interface between the surrounding medium and the gas encapsulated by the MB. This pressure difference drives gas out of the MB core into the surrounding medium. The Laplace pressure can be determined by **Equation 1**, where ΔP = the difference in pressure inside (P_I) to outside (Po), γ = surface tension, r = MB radius (**Figure 12**).

Equation 1 Young-Laplace equation

$$\Delta P = \frac{2\gamma}{r}$$

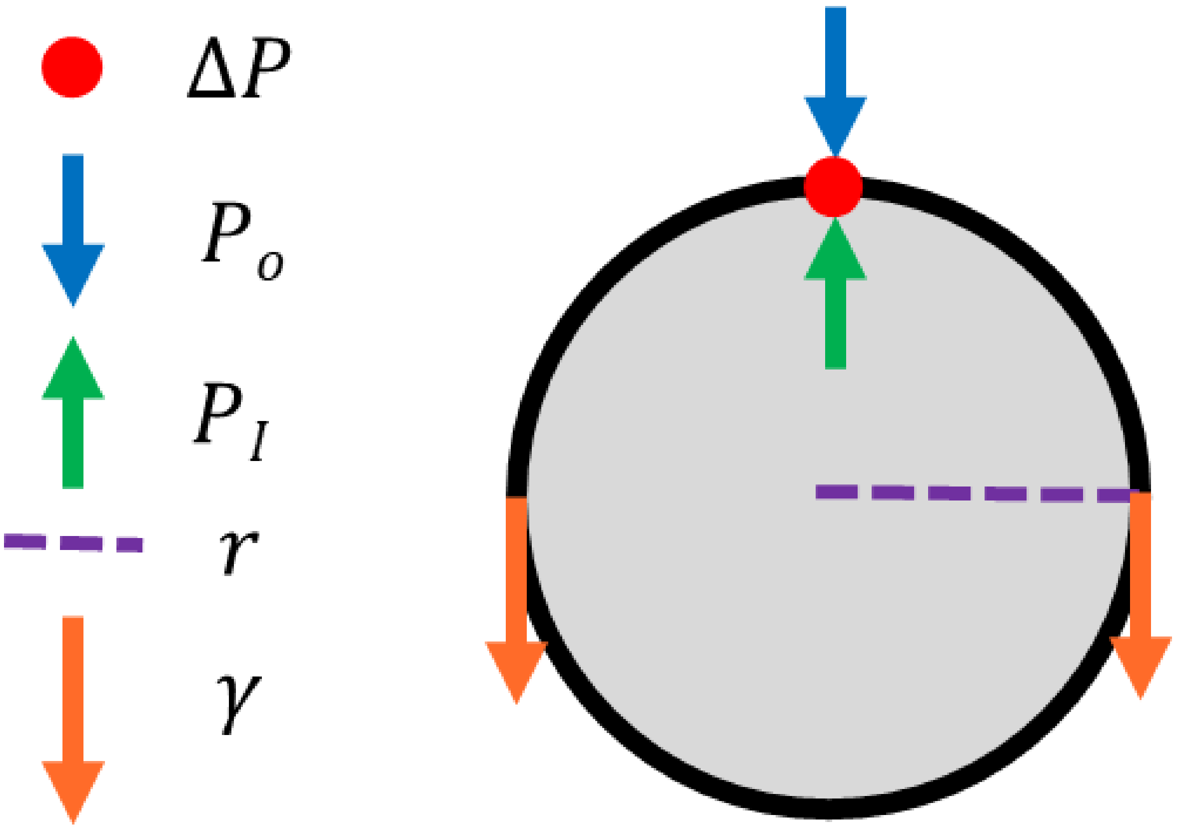

Figure 12 Schematic representation of the Young-Laplace pressure equation; where ΔP indicated by a red dot at the boundary between the inside and outside of the MB, is the difference in pressure inside (P_I) (green arrow) to outside (Po) (blue arrow), γ = surface tension (orange arrows), r = MB radius (purple dashed line).

It can be inferred that a smaller MB diameter results in larger Laplace pressure; thus small MBs dissolve in aqueous media more rapidly, which has been confirmed elsewhere (Shih and Lee, 2016). Larger bubbles form over time and lower the concentration of MBs as the gas diffuses from the smaller to the larger MBs by dissolution, coalescence occurs due to reduced surface tension of larger bubbles allowing them to fuse, and smaller bubbles overcome by the external pressure collapse (**Figure 13**). Some of these effects may be overcome by reducing the diffusion rate of the gas from the MB, by utilising a thicker MB shell or altering the properties of the suspension media (e.g. using a gas saturated solution).

The data collected on MB stability in this research, can attest to the impact of these effects in reducing MB concentration over time. Epstein and Plesset proposed a mathematical model of bubble dissolution shown in **Equation 2**, where *dR/dt* = change in MB radius over time, *D* = diffusivity of the gas, K_H = Henry's constant, *B* = ideal gas constant, *T* = temperature, *f* = gas saturation fraction of the surrounding medium, M_W = molecular weight of the gas species, ρ = density of the suspension medium and σ = surface tension (Epstein and Plesset, 1950).

Equation 2 Epstein-Plesset Equation

$$\frac{dR}{dt} = -DK_HBT\left(\frac{1-f+\frac{2M_W\sigma}{\rho BTR}}{1+\frac{4M_W\sigma}{3\rho BTR}}\right)\frac{1}{R}$$

The rate of bubble dissolution, or the change in MB radius over time, varies inversely with MB radius, so smaller MBs have a higher rate of dissolution. However, an important caveat is that the Epstein-Plesset model does not account for inter-MB interactions, i.e. it assumes that MB stability is independent of MB concentration. In reality, MB suspensions will produce larger MBs by Ostwald ripening over time (**Figure 13**).

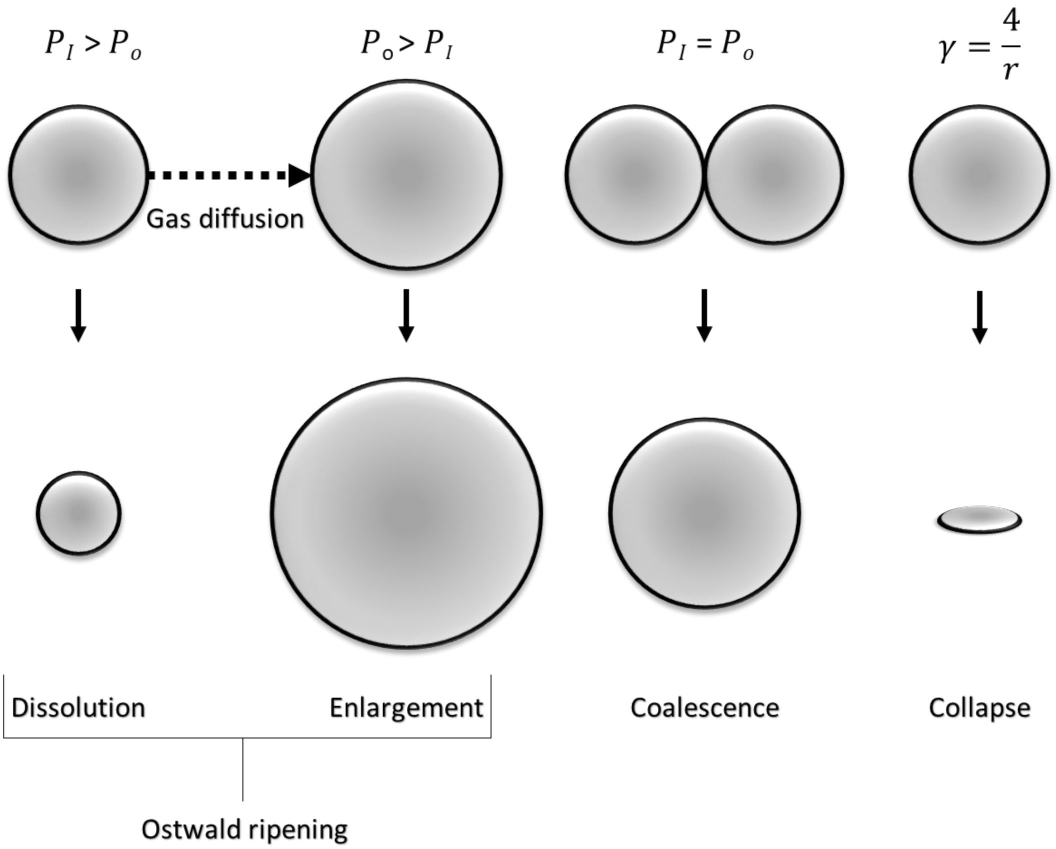

Figure 13 An illustration of the effect of Laplace pressure on MB stability; MBs with a smaller radius have a greater internal pressure, which drives the diffusion of gas from the bubble into the surrounding medium causing dissolution. Consequently, MBs with a larger radius that have a lower internal pressure will enlarge as gas diffuses into them from the medium; this is known as Ostwald ripening (Feshitan *et al.*, 2009). When the internal and external pressure of proximal bubbles are in equilibrium, coalescence of MBs occurs and MBs fuse together forming a single larger bubble (Talu *et al.*, 2006; Borden and Song, 2018). Collapse of MBs with a large radius is likely to occur when the external pressure on the shell exceeds the Laplace pressure, principally caused by a low surface tension forces (Sarkar *et al.*, 2009; Mulvana *et al.*, 2010).

2.2 Statement of objectives

This chapter will outline the development and stability testing of lipid-shelled ultrasound-responsive agents capable of delivering nitric oxide contained in MBs, which can be administered with free antimicrobial compounds for dispersal and elimination of biofilms respectively.

2.3 Materials and methods

2.3.1 *Method rationale*

A number of MB formulations were assessed in this research, including the use of long (22 carbon) chain DBPC lipids, shorter (18 carbon) chain of DSPC and positively charged DSEPC lipids. The use of lipids for the fabrication of MBs is well documented; comparable formulations in other research have informed and supported the methods used here, including specific molar ratios of lipids utilised (McEwan *et al.*, 2015; Carugo *et al.*, 2017; Paolino *et al.*, 2017; Owen *et al.*, 2018a; Owen *et al.*, 2018b; Horsley *et al.*, 2019; Browning *et al.*, 2020). This was an integral step in this research in order to determine the most efficacious MB formulation, which balances the loading capacity and resonant frequency of the MB with its stability over time. The fabrication and stability characterisation of MBs that incorporate DSEPC lipids to create cationic MBs are discussed here, however their utility and application is discussed specifically in Chapter 3. In line with the objective of achieving a viable clinical translation of this research, stability data was obtained at ambient temperature (~ 23 °C ± 2 °C) to replicate the conditions in which MBs are most likely to be handled clinically. The ambient temperature observed in the research, is a consequence of centrally controlled negative-pressure air-handling and heat supplied to the containment level two laboratory at different times of the year.

2.3.2 *Fabrication of MBs with an air or nitric oxide core*

The MB shell constituents DSPC (850365P, Avanti, Sigma-Aldrich) or DBPC (850371C, Avanti, Sigma-Aldrich) and PEG40s (P3440, Sigma-Aldrich) dissolved in chloroform, were combined in a 20 mL capacity 23 mm diameter glass vial (15394769, Fisherbrand™, Fisher Scientific) in a 9:1 molar ratio, using a 1 mL Luer lock glass syringe (1MR-GT, S.G.E Gas Tight Syringe, Supelco) to achieve a final lipid concentration of 4 mg/mL (**Table 3**). The suspension was covered with Parafilm® that was pierced a number of times with a needle, then placed in a fume hood to allow the solvent to evaporate overnight at ambient temperature ~ 23 °C ± 2 °C.

Table 3 Stock concentrations and relative quantities of MB constituents required to make a MB suspension with a final volume of 5 mL

MB constituent	**DSPC**	**OR**	**DBPC**	**AND**	**PEG40s**
Stock Concentrations (mg/mL)	25	/	10	+	10
Molar Ratio	9	/	9	+	1
Volume (μL) for 5 mL of MBs	~ 621	/	~ 639	+	~ 400-450

The dry lipid film obtained was rehydrated with 5 mL of degassed 0.01 M sterile phosphate-buffered saline (PBS) (P4417, Sigma-Aldrich), a magnetic stirrer was added to the vial before it was capped. For DSPC lipid suspensions the vial was placed on a stirring hotplate (Fisherbrand™, Isotemp™) for 30 minutes at a temperature of 90 °C and 700 rpm, whereas DBPC lipid suspensions remained on the hotplate for 60 minutes at 100°C and 700 rpm due to the greater energy required to melt the longer (22 carbon) chain of the lipid. Using a 120 W, 3.175 mm diameter tip sonicator (20 kHz, Fisher Scientific FB120, Pittsburgh, USA) the DSPC and DBPC suspensions at transition temperature (> 55 °C) were homogenously dispersed for 150 or 240 seconds respectively, at 40% power (48 W) with the sonicator tip fully immersed in the lipid suspension. As described by Carugo *et al.* (2017), after this first sonication step the homogenous DBPC suspension was returned to the hotplate for 5 minutes at 100 °C to ensure that the suspension was above its transition temperature of 75 °C for the second sonication step. This was not required for DSPC suspensions as the initial sonication time is shorter, this means the suspension does not drop below its transition temperature of 55°C. Microbubbles were formed in a second sonication step, by placing the tip sonicator at the fluid-air interface of the homogenised lipids suspension for 30 seconds at 70% power (84 W). Upon completion of the second sonication, the vial is place immediately into an ice bath to rapidly cool the MB suspension. For the generation of NOMBs the same sonication steps were performed; however, the dry lipid film was reconstituted with deoxygenated PBS, which was prepared by purging the solution with pure nitrogen for 20 minutes (Gu and Chen, 2008). A constant flow of nitrogen was used to purge air from the headspace of the vial. The eNO generator (NitricGen Inc., Madison, WC) was used to flush 40 ppm NO at 1.5 L/min through the degassed PBS during the first sonication steep, during the second sonication step the flow of NO was maintained with the needle placed at the interface between the fluid and the sonicator tip (**Figure 14**).

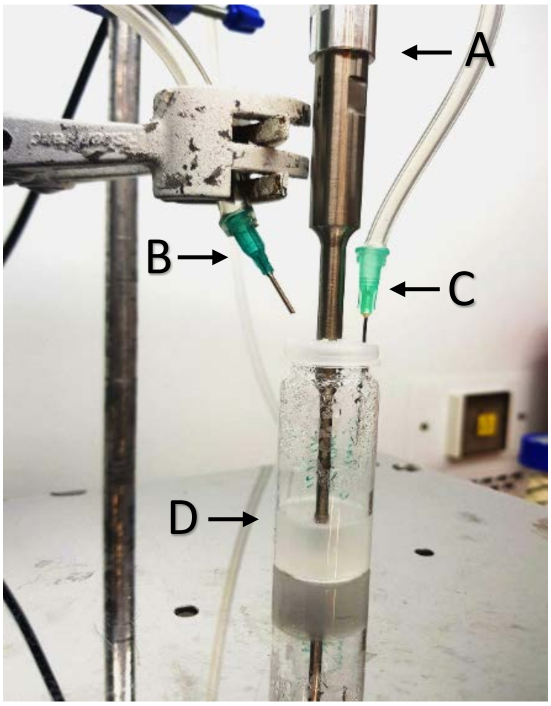

Figure 14 Photograph depicting the setup used for the generation of NOMBs: (A) tip sonicator fully immersed in the liquid (B) outlet for nitrogen gas to displace air around the vial; (C) outlet for NO gas with needle piecing the lid of the vial to deliver NO close to the fluid-air interface; and (D) the DSPC-PEG40s suspension, heated above the transition temperature of DBPC to 90 °C.

2.3.3 *Production of cationic MBs*

Cationic MBs were produced by adding a cationic phospholipid DSEPC (Avanti Polar Lipids, Alabama, USA) dissolved in chloroform to the DSPC and PEG40s mixture in quantities determined by the desired molar ratio, lipid concentration and sample volume as described in other research (Delalande *et al.*, 2017; Owen *et al.*, 2018b) (**Table 4**). The lipid suspension was sonicated in accordance with the procedure outlined in 2.2.2.

Table 4 Stock concentrations, molar ratio compositions and volumes used for neutral and cationic MBs.

MB constituent	DSPC	OR	DBPC	PEG40s	DSEPC
Stock Concentrations (mg/mL)	25	/	25	10	10
	Molar ratio				
Neutral (N)	9	/	9	0.5	0
Cationic (+)	9	/	9	0.5	1
	Preparation volumes (μL) to prepare 2 mL MB suspension with a final lipid concentration of 3 mg/mL				
Neutral (N)	210	/	213	75 / 67	0 / 0
Cationic Microbubbles (+)	190	/	195	68 / 61	57 / 51

2.3.4 *Characterisation of MBs stability*

To assess the stability of MBs at environmental temperature, three vials each of air MBs (control) and NOMBs were prepared as outlined in section 7.3.1. A 10 μL sample was pipetted onto a Neubauer haemocytometer with a 0.2 mm thick cover slip placed on top, samples were taken from each vial at intervals of 10, 20, 40 and 60 minutes after the initial reading. Between the readings at each time point, the vials remained sealed with a polyethylene cap on a bench at room temperature (23 °C ± 2 °C). The MBs were observed using bright field microscopy (Olympus, IX71) with a 50x (Olympus, LMPLFLN) objective lens, ten images were acquired at each time point for all vials using a CCD camera (Hamamatsu ORCA-ER, C4742-80). The images were processed using ImageJ (Fiji) to determine the MB diameter, size distribution and volume. The contrast of each image was normalised to differentiate between the white background and dark MB, before the threshold was automatically calculated by ImageJ to differentiate the MBs from the surrounding fluid and identify individual MBs. The images taken had a width of 1344 pixels and a height of 1024 pixels; in this experiment 700 pixels equated to 100 μm (**Figure 15**). The area in pixels of all particles was determined by using the set-scale function in ImageJ, using the dimensions of the picture with a known distance on each image. The circularity threshold was set between 0.7 and 1, this eliminated any debris from counting. MB concentration was determined using **Equation 3**; where the number of MBs was the total number of MBs in all the images (three vials, ten images per vial = 30 images per MB composition), *b* = length covered in field of view (µm) = 192 µm, *h* = height covered in field of view (µm) = 146 µm, *t* = thickness of MB suspension imaged on haemocytometer (µm) = 100 µm, number of images = ten images taken per vial, number of vials = three vials per composition. The post-production number of MBs per 5 mL vial was approximately 8.5 x10^{8}.

Equation 3 Calculation for determining concentration of MB/mL

$$[Mean\ MB] = \frac{No.of\ MBs}{b\ \times h \times t \times No.of\ images\ per\ vial\ \times No.of\ vials}$$

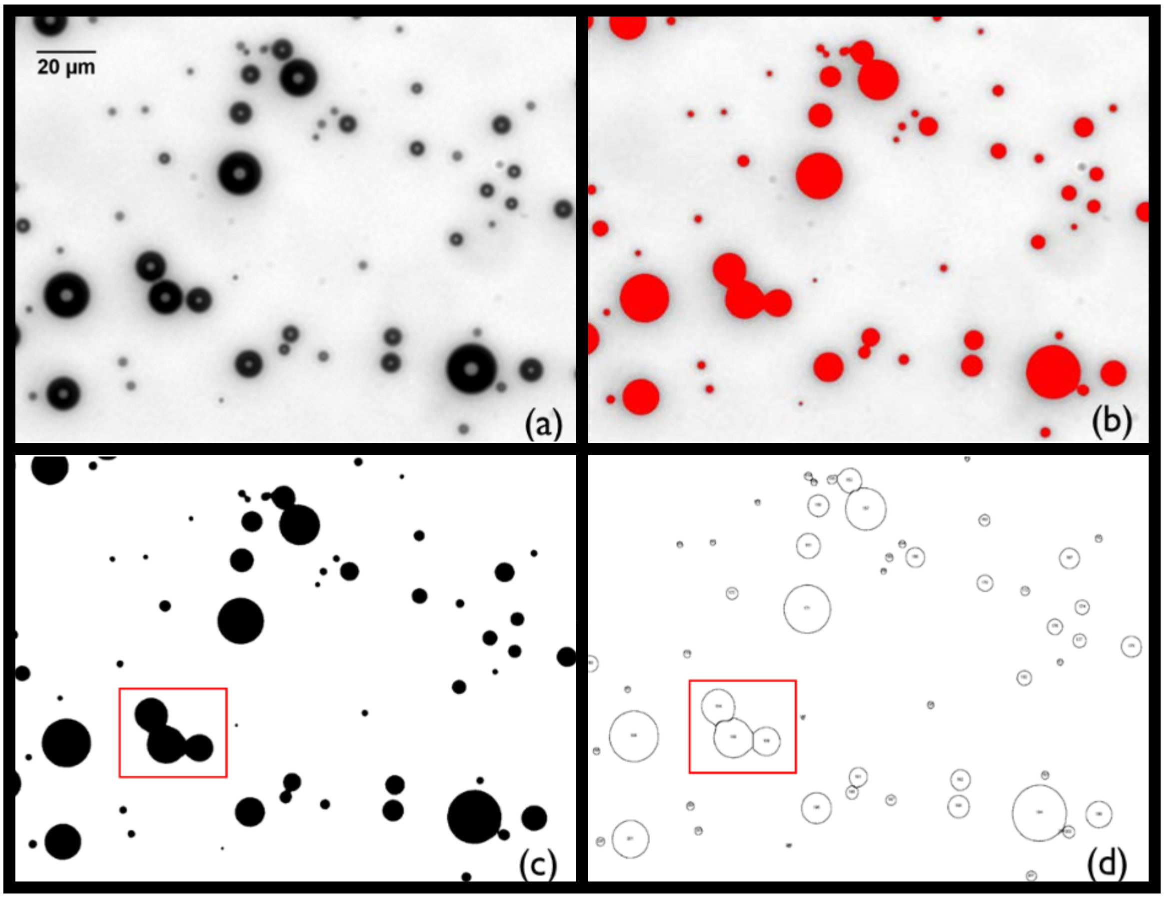

Figure 15 Image analysis protocol for determining size and concentration of MBs by microscopy. Images were taken with 50x objective; the scale bar represents a 20 µm distance in each image. (a) Bright field image of MBs suspended in PBS. (b) Automatic threshold was applied to the image. (c) A mask was created based on the thresholded image. (d) Watershed algorithm was applied to count MBs which appear to be touching as separate MBs (see red boxes in (c) and (d)). Only features with circularity > 0.7 were selected to remove any cropped MBs. The area and diameter of each MB was determined by calibrating a scale in which the number of pixels corresponds to a known distance in µm; specifically in these experiments 700 pixels corresponded to 100 µm, therefore the number of pixels per MB could be used to automatically calculate the dimensions of each MB in the image.

2.3.5 *Verification of nitric oxide inclusion in MBs by dihydrorhodamine 123*

The use dihydrorhodamine 123 (DHR) as a means of detecting NO has been fully defined elsewhere (Barraud *et al.,* 2006); briefly, DHR is a small lipophilic and cationic dye that is able to diffuse across membranes; it remains non-fluorescent until oxidised to rhodamine 123 ($^{\lambda}$excitation = 505 nm, $^{\lambda}$emission = 529 nm), by the interaction between O_2 and NO (Volk and Moreland, 2014) (**Figure 16**).

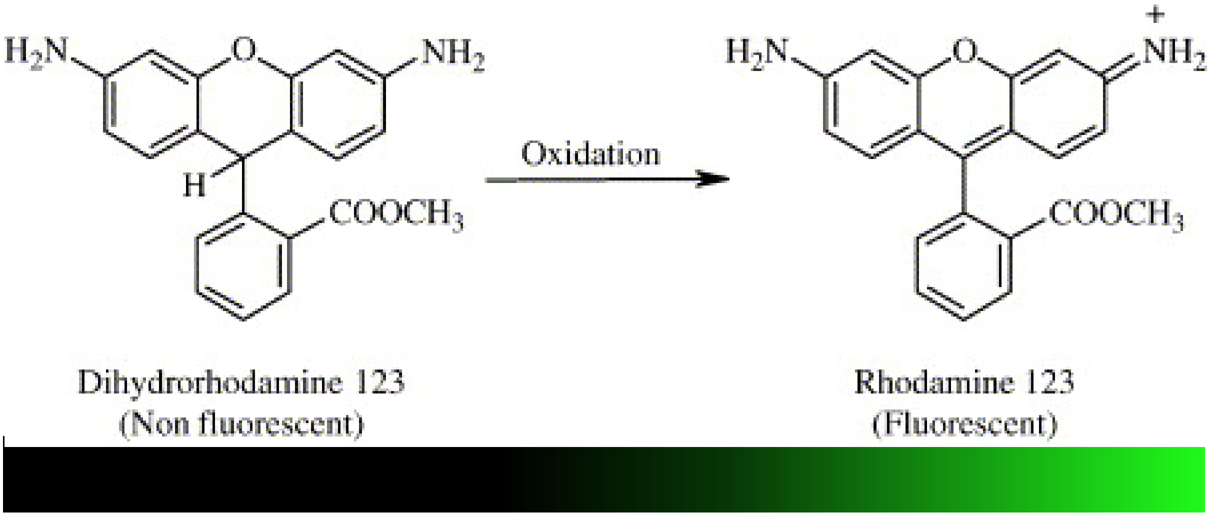

Figure 16 Dihydrorhodamine is non-fluorescent until it is oxidised to the fluorescent product rhodamine 123, which is induced by the reaction between O_2 and NO in solution. The relative FI of rhodamine 123 is proportional to the quantity of fully reacted peroxynitrite (Almeida *et al.*, 2019).

The relative fluorescence intensity (FI) observed in these experiments, is proportional to the quantity of reacted peroxynitrite (Almeida *et al.*, 2019). Consequently the higher the proportion of NO present in the original solution that has reacted with oxygen, the greater the FI of rhodamine 123 will be. In accordance with the method described by Barraud *et al.* (2006); DHR (D23806, Invitrogen™, ThermoFisher Scientific) was applied at a concentration of 15 µM to MB suspensions for 30 minutes in an ice bath, before images were captured with fluorescence microscopy: $^{\lambda}$emission 510 nm, gain 5.0, light source intensity 0.5, brightness 0.5, exposure time 20 ms (EVOS M5000, 20x Plan Fluor EVOS AMEP42924 objective, LED cube GFP AMEP4653, Invitrogen™, ThermoFisher Scientific). Images were analysed with ImageJ, to determine the relative FI of the fluorescent oxidised product rhodamine 123.

Images imported to ImageJ were converted to RGB and the RGB channels split to isolate the green channel. Each isolated image was converted to 8-bit greyscale and the multipoint tool was used to select 10 points within each image that did not contain MBs i.e. suspending fluid only. At each point the minimum, maximum and mean pixel intensity of the greyscale image was recorded. Each image analysed represented an independent suspension of NOMBs (n=5) or room air microbubbles (RAMB) (n=5).

2.3.6 *Statistical analysis*

A one-way ANOVA was used to identify any significant difference between diameter and concentration of MBs with different compositions over time, all data was analysed and plotted using Prism 7.04 (GraphPad) with a significance threshold of < 0.05. In DHR detection of NO experiments, an unpaired T-test of the data was used to determine if there was a significant difference between the relative fluorescence of the RAMB and NOMB suspensions.

2.4 Results

2.4.1 *Effect of gas composition and lipid shell constituents on MB size and stability*

2.4.1.1 Air filled MBs

The results showed that immediately after production DSPC RAMBs were > 70% less concentrated than both DSPC and DBPC NOMBs; equivalent to 5.63 x10^{7} MB/mL, 1.92 x10^{8} MB/mL and 1.71 x10^{8} MB/mL, respectively. Interestingly, the 2.85 µm mean diameter of DSPC NOMBs was 18.10% smaller than the 3.48 µm initial diameter of RAMBs (**Figure 17**). Though the DSPC RAMBs started with a higher initial diameter compared to DSPC NOMBs, their growth rate plateaued around 20 minutes (**Figure 17**).

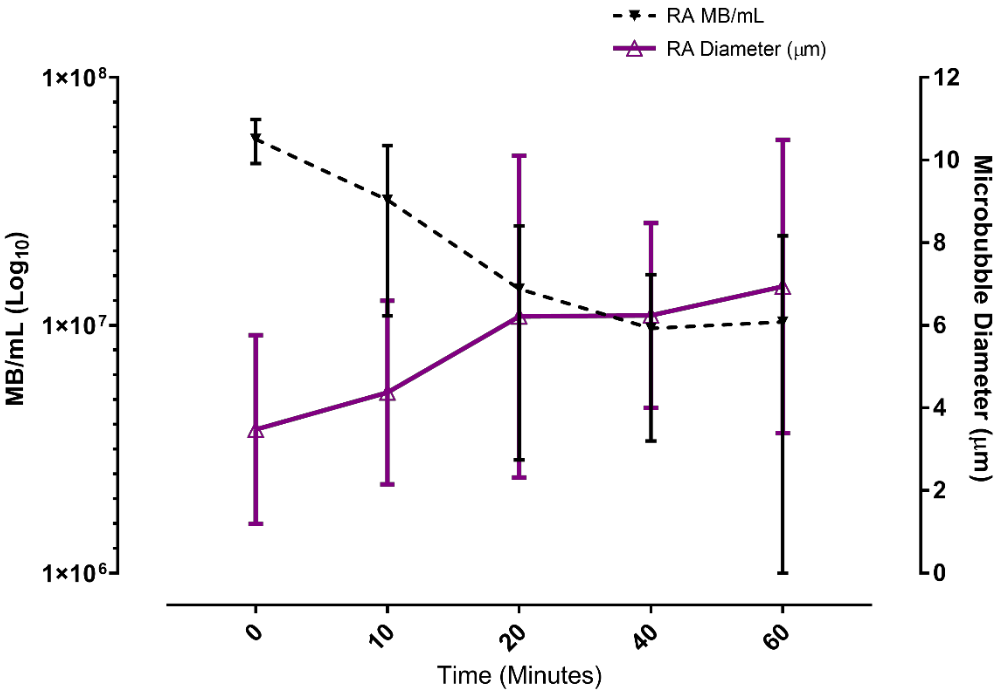

Figure 17 Characterisation of DSPC:PEG40s shelled RAMB stability at environmental temperature over 60 minutes, assessed by change in mean diameter (µm) and concentration of MBs (MBs/mL). Immediately after production, air MBs had an average diameter of 3.48 µm and a concentration of 5.63 x10^7 MB/mL. After 20 minutes at ambient temperature the mean diameter of the MB started to plateau, the concentration at 60 minutes was reduced by 81.69% compared to the original concentration. Error bars represent the standard deviation, assessed by comparing three independent MB suspensions. The standard deviation of the mean diameter seen at each time point, would indicate that the MBs were quite dispersed in size, which is not unusual for MBs produced by sonication.

To better demonstrate the size dispersity of the MB suspension, a box plot has been included showing the distribution of MB diameter (**Figure 18**). There is a clear positive skew in the data exemplifying that despite a small number of outliers that possess a very large diameter, there are considerably more MBs of a smaller diameter in the suspension. The mean diameter of the MBs in suspension is largely congruent with the median size of the MBs, therefore the mean and standard deviation values for MB diameter reported in **Figure 17** can be considered a valid representation of the overall size distribution of MBs in suspension.

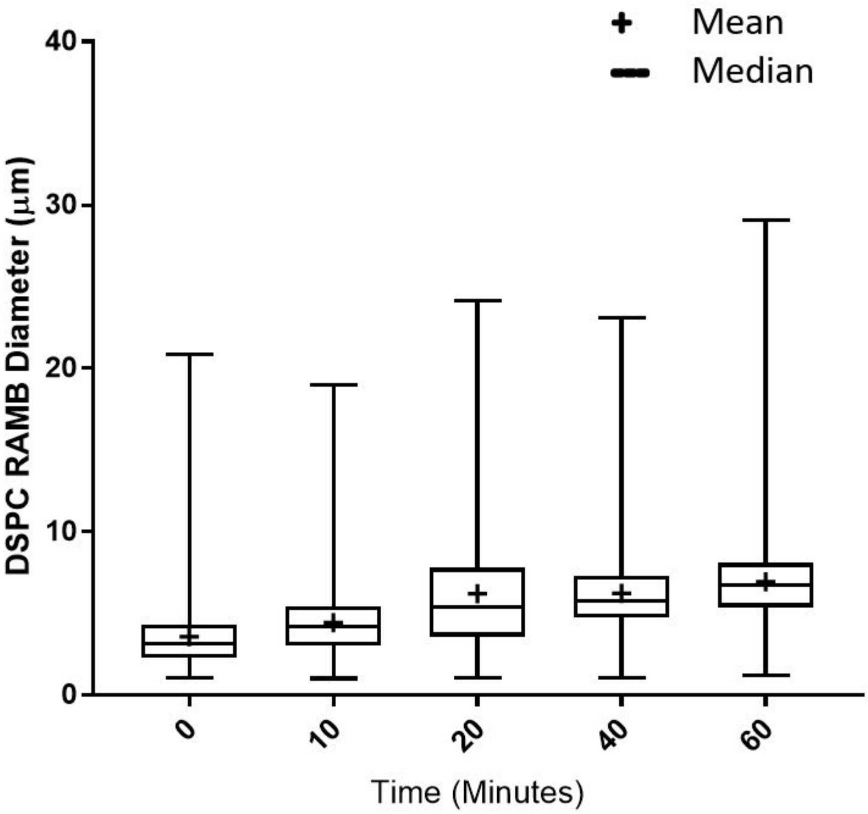

Figure 18 Box plot to comprehensively demonstrate the range in MB size distribution (μm), averaged across three vials of DSPC RAMBSs for each time point. The upper and lower whiskers of the box demonstrate the lowest and highest observed values respectively, while the lower and upper quartile of the data set is indicated by the lower and upper boundary of the box. The proximity of the box to the lower whisker indicates a positive skew in the data, this would mean that the majority of MBs in suspension are closer to the lowest diameter outliers than the largest. The minimum size observed across all time points was 1.02 μm, whilst the outliers at the maximum of the range varied from 18.98 μm and 29.06 μm. The majority of the MB population possess a diameter within ± 2 μm of the median diameter; there is very little disparity observed between the mean and median size of MBs over 60 minutes.

2.4.1.2 DSPC Nitric oxide MBs

DSPC NOMBs remained stable at environmental temperature for up to 10 minutes post-production, but their growth thereafter appeared exponential (**Figure 19**). DSPC NOMBs had a smaller post-production mean diameter (2.85 µm) and higher concentration (1.92 x10^8 MB/mL) than DSPC RAMBs (**Figure 17**). However, it is important to note that the dissolution rate of DSPC NOMBs was more than 10% higher than their RAMB analogues, with less than 8% of the MB population remaining after 60 minutes (**Figure 19**).

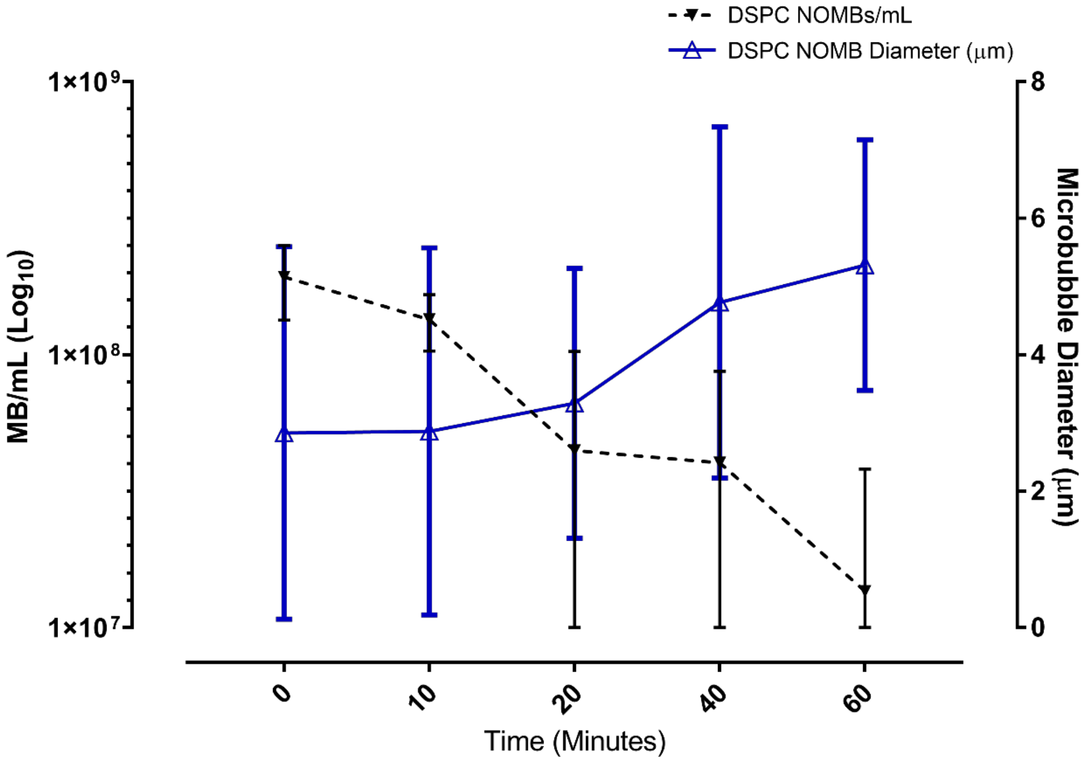

Figure 19 Characterisation of DSPC:PEG40s shelled NOMB stability at environmental temperature over 60 minutes, assessed by change in mean diameter (µm) and concentration of MBs (MB/mL). Immediately after production, NOMBs had an average diameter of 2.85 µm and a concentration of 1.92 x10^8 MB/mL. After 20 minutes at ambient temperature the mean diameter of the MB began to increase, and the final diameter at 60 minutes was 5.31 µm; the reduction in MB concentration after 60 minutes was 92.95%. Error bars represent the standard deviation, assessed by comparing three independent MB suspensions. The range in mean diameters would indicate that the MBs were quite dispersed in size, which is not unusual for MBs produced by sonication.

The dispersity in MB size has been demonstrated using a box plot (**Figure 20**), that exhibits a positive skew indicative of values in the inter-quartile range being closer to the lowest observed values. MBs produced by sonication are inherently subject to high dispersity in diameter, however the data suggests that the majority of MBs produced would be within the range of resonant size (1 – 10 µm) for a 1 MHz stimulus.

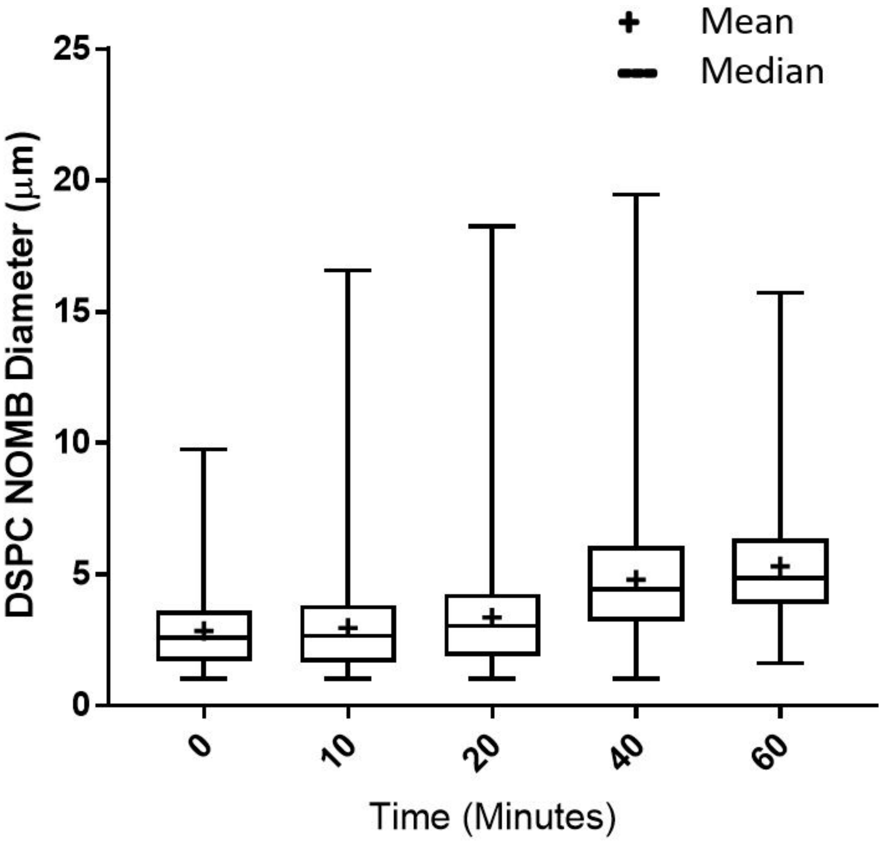

Figure 20 Box plot to comprehensively demonstrate the range in MB size distribution (µm), averaged across three vials of DSPC NOMBSs for each time point. The upper and lower whiskers of the box demonstrate the lowest and highest observed values respectively, while the lower and upper quartile of the data set is indicated by the lower and upper boundary of the box. The proximity of the box to the lower whisker indicates a positive skew in the data, this would mean that the majority of MBs in suspension are closer to the lowest diameter outliers than the largest. The minimum size observed across all time points was 1.02 µm, whilst outliers at the maximum of the range were between 9.75 µm and 19.44 µm. The majority of the MB population possess a diameter within ± 2 µm of the median diameter; there is little disparity observed between the mean and median size of MBs over 60 minutes.

2.4.1.3 DBPC Nitric oxide MBs

Although all MBs in this research had comparable size dispersity after production, DBPC shelled NOMBs exhibited the greatest stability over 60 minutes with a negligible incremental change in diameter of 0.02 µm/per minute and less than 40% reduction in concentration (**Figure 21**). There was no significant difference (p 0.0578) between mean diameter of RAMBs or NOMBs regardless of shell composition, however DBPC shelled MBs were significantly more concentrated over time compared to all other compositions ($p < 0.0001$).

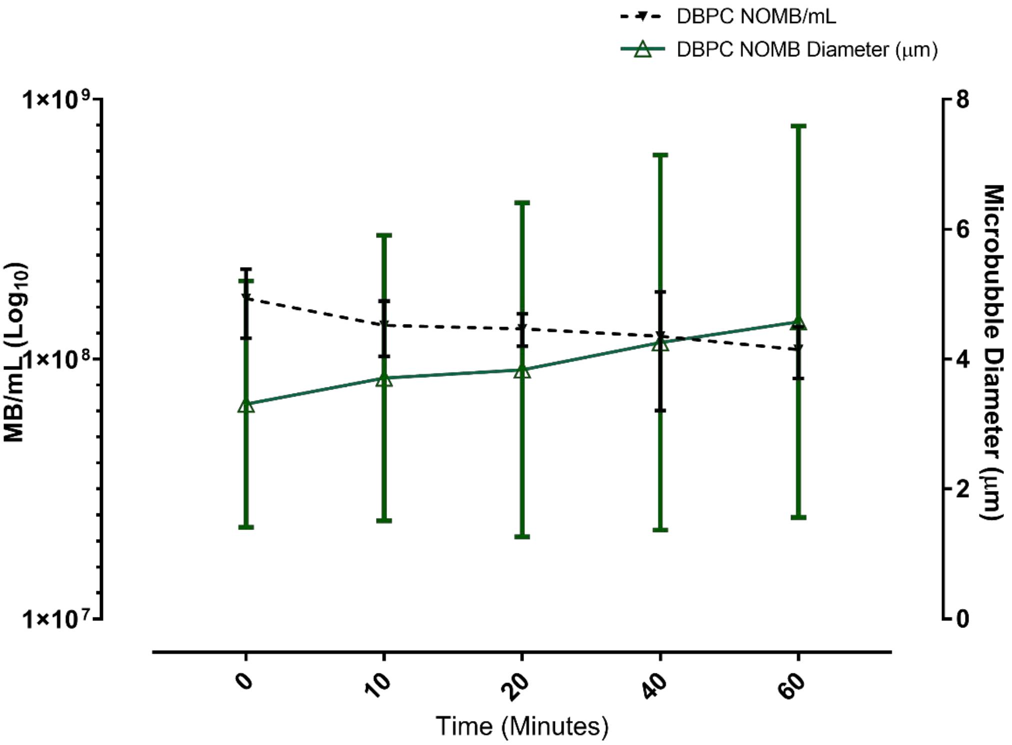

Figure 21 Characterisation of DBPC:PEG40s shell NOMBs stability at environmental temperature over 60 minutes, assessed by change in mean diameter (µm) and concentration of MBs (MB/mL). Immediately after production, NOMBs had an average diameter of 3.31 µm and a concentration of 1.71 x108 MB/mL. At each time point the diameter of the NOMBs only increased by a maximum of 0.4 µm, with a final diameter at 60 minutes of 4.57 µm; the reduction in MB concentration after 60 minutes was only 36.41%. Error bars represent the standard deviation, assessed by comparing three independent MB suspensions. The comparatively small decrease in MB concentration, and slow increase in diameter over 60 minutes with a low standard deviation would indicate that this formulation is more stable than DSPC shelled NOMBs.

The data still exhibit a strong positive skew, indicative of a population of MBs in which the majority are considerably smaller than outliers indicated by the upper whisker of the box plot (**Figure 22**). Moreover, DBPC NOMBs have the smallest inter-quartile range (1.87 µm) of any formulation, which would indicate a significant majority of MBs in suspension would respond to an US stimulation of therapeutically relevant frequency.

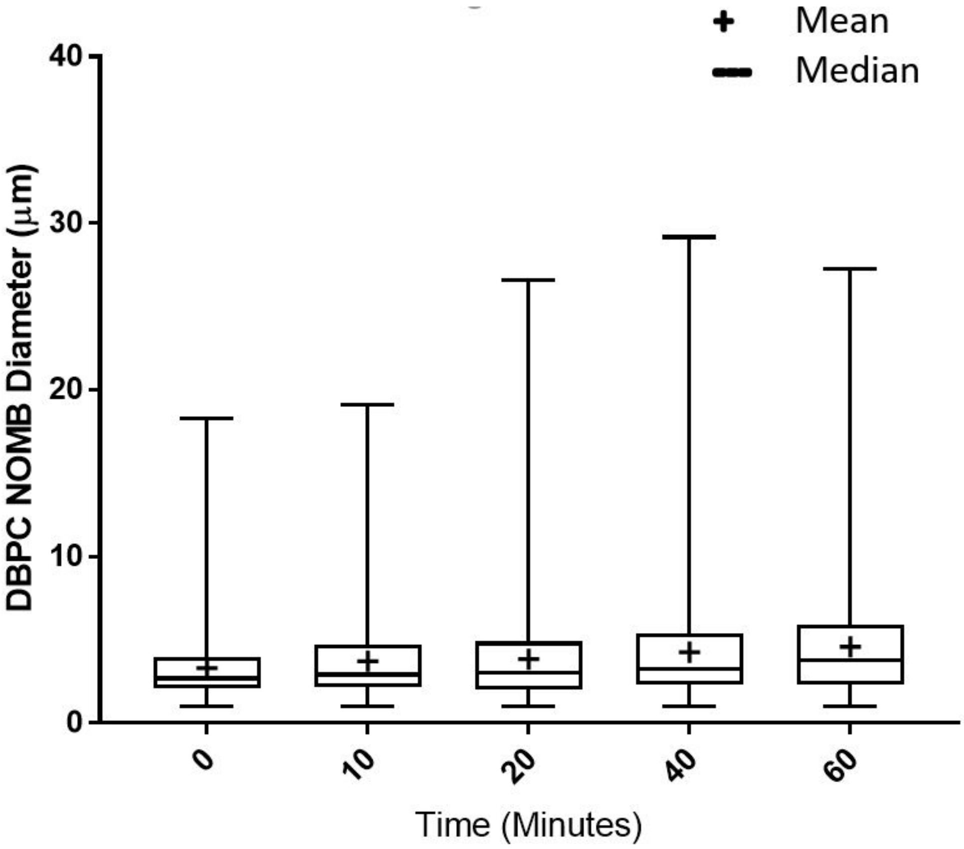

Figure 22 Box plot to comprehensively demonstrate the range in MB size distribution (µm), averaged across three vials of DBPC NOMBSs for each time point. The upper and lower whiskers of the box demonstrate the lowest and highest observed values respectively, while the lower and upper quartile of the data set is indicated by the lower and upper boundary of the box. The proximity of the box to the lower whisker indicates a positive skew in the data, this would mean that the majority of MBs in suspension are closer to the lowest diameter outliers than the largest. The minimum size observed across all time points was 1.02 µm, whilst the outliers at the maximum varied from 18.29 µm to 29.15 µm. The majority of the MB population possess a diameter consistently within ± 2 µm of the median diameter; there is little disparity observed between the mean and median size of MBs over 60 minutes.

2.4.2 *Effect of phospholipid charge on MB size and stability*

The stability of DSPC:PEG40s:DSEPC shelled cationic $RAMB^+$ and $NOMB^+$ suspensions in this experiment was assessed at room temperature (~ 23 °C ± 2 °C) over 60 minutes. The changes in $RAMB^+$ (**Figure 23**) and $NOMB^+$ (**Figure 24**) size and concentration over time exhibited a high level of congruity with the trends in the data of their non-charged RAMB (**Figure 17**) and NOMB (**Figure 19**) counterparts.

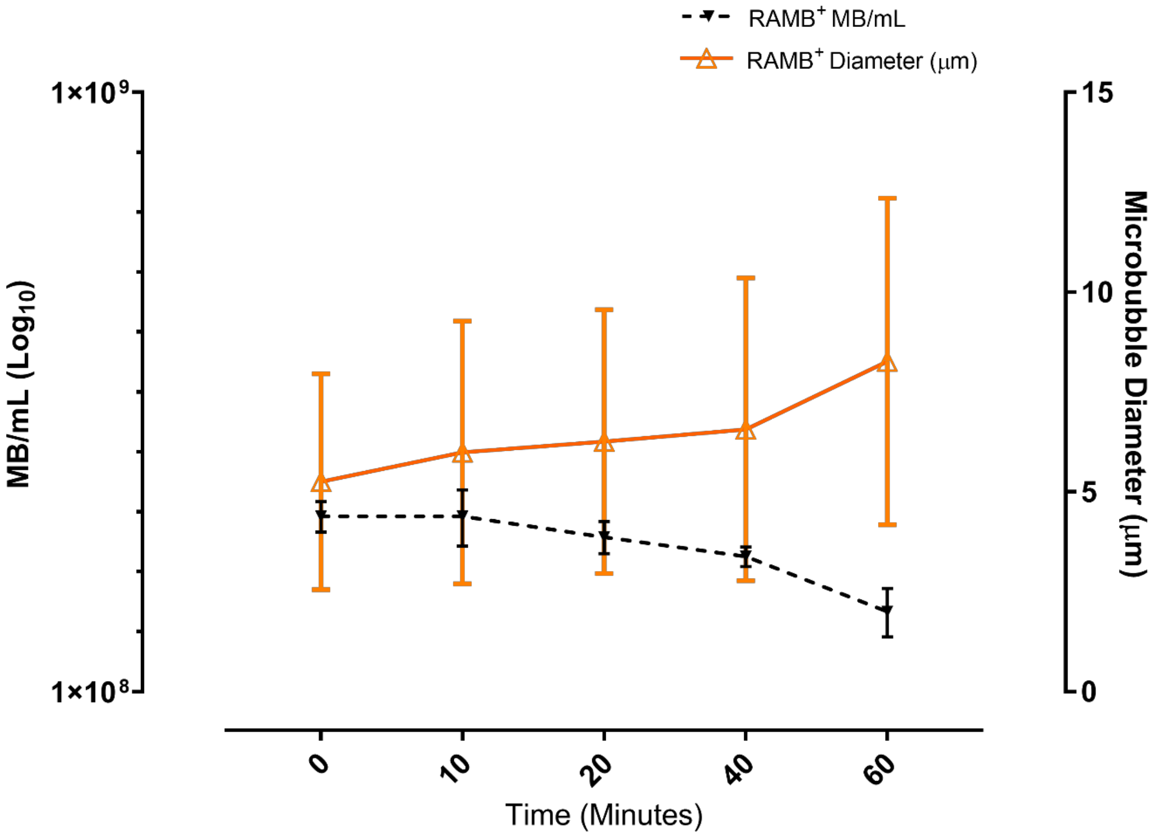

Figure 23 Characterisation of 9:0.5:1 molar ratio DSPC:PEG40s:DSEPC shelled cationic $RAMB^+$ suspensions stability at environmental temperature, assessed by change in mean diameter (µm) and concentration of MBs (MB/mL) over 60 minutes. Immediately after production, $RAMBs^+$ had an average diameter 5.25 µm and a concentration of 1.96 $x10^8$ MB/mL. Error bars represent the standard deviation, assessed by comparing three independent MB suspensions.

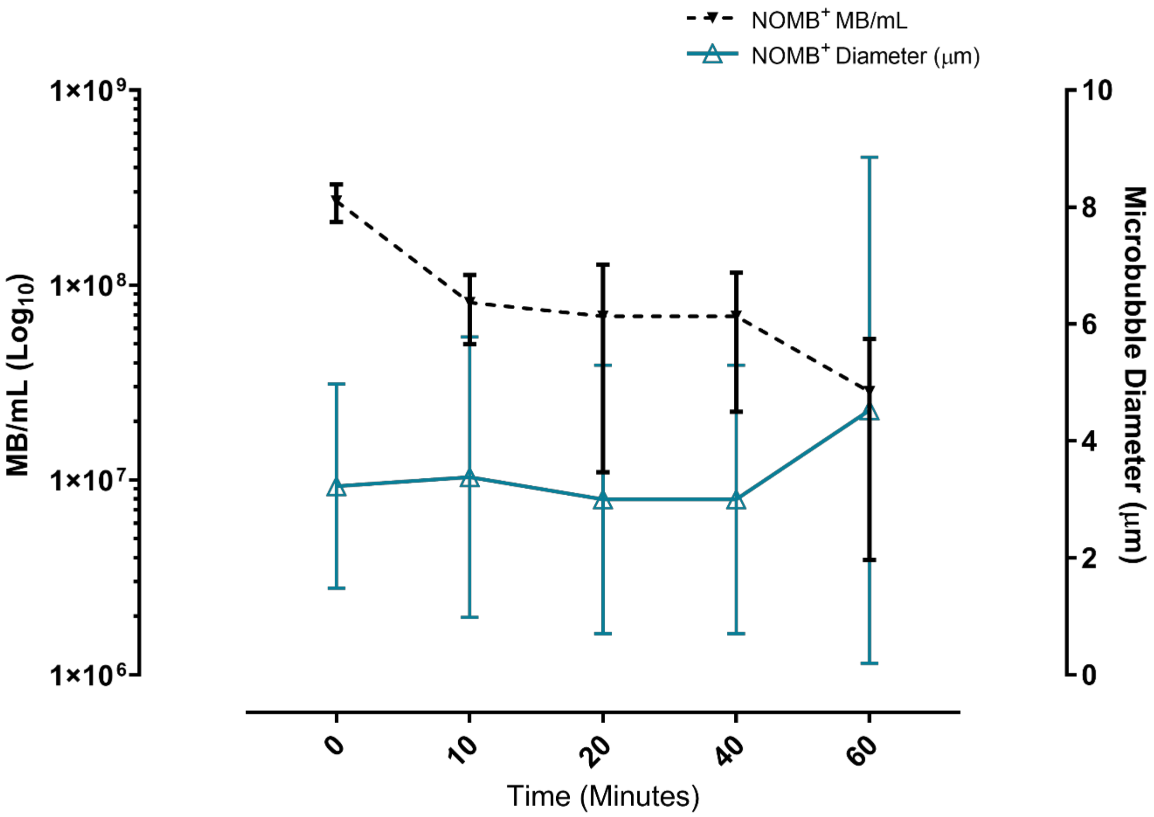

Figure 24 Characterisation of 9:0.5:1 molar ratio DSPC:PEG40s:DSEPC shelled cationic NOMB$^+$ suspensions stability at environmental temperature, assessed by change in mean diameter (µm) and concentration of MBs (MB/mL) over 60 minutes. Immediately after production, NOMBs$^+$ had an average diameter 3.22 µm and a concentration of 2.69 x10^8 MB/mL. Error bars represent the standard deviation, assessed by comparing three independent MB suspensions.

2.4.3 *Presence of nitric oxide in MBs assessed by dihydrorhodamine 123*

In order to determine the relative FI of rhodamine 123, the pixel intensity of the MB suspension fluid was assessed at 10 points in 5 independent RAMB or NOMB suspensions for a total of 50 data points per formulation (**Figure 25**). The relative FI of rhodamine 123 in RAMB and NOMB suspensions was determined by comparing pixel intensity values in suspensions containing DHR, to control RAMB and NOMB suspensions that did not contain DHR. The values for pixel intensity are integers that range from 0 (dark/black) to 255 (bright/white); the intensity value of a pixel is proportional to the concentration of fluorophores present in a selected area, therefore a higher value of pixel intensity is indicative of a greater concentration of rhodamine 123. There was a significant difference (P < 0.0001) between the mean intensity in the fluid of RAMB suspensions (9.02), compared to NOMB suspensions (60.46) (**Figure 26**).

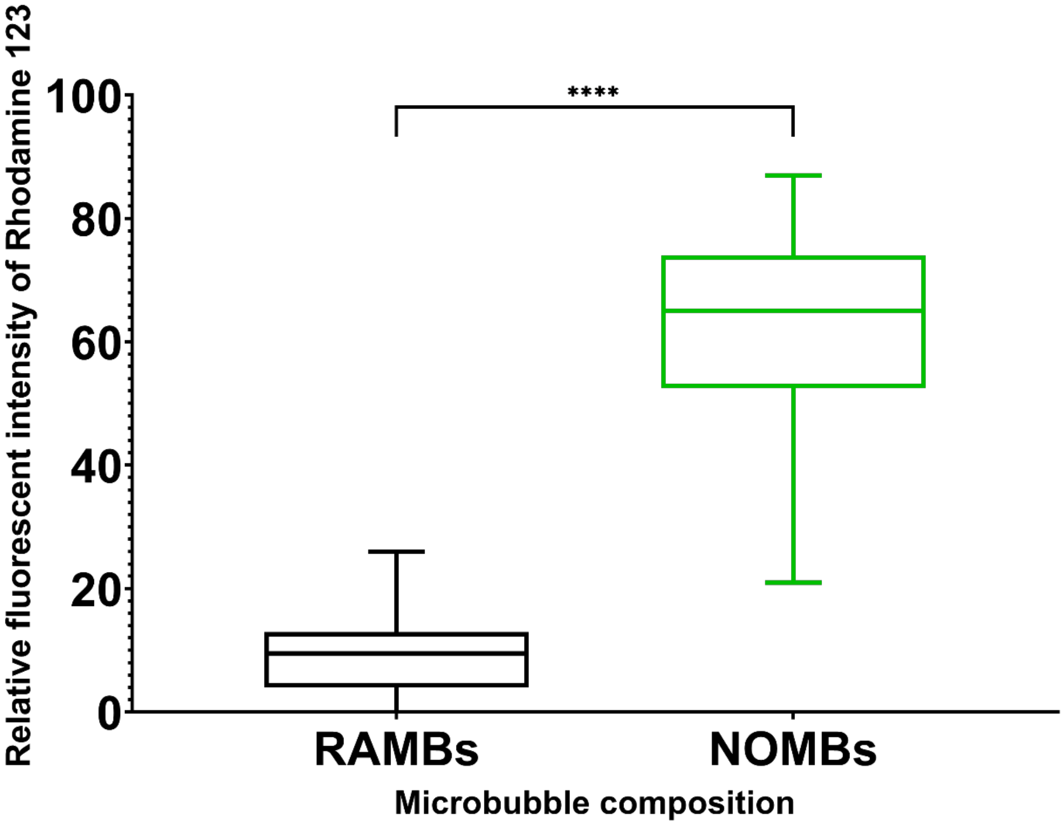

Figure 25 The relative FI of rhodamine 123 in the fluid surrounding MBs in RAMB and NOMB suspensions, was determined by assessing the change in pixel intensity over multiple (n = 10) points per image. The mean relative fluorescent intensity observed in the RAMB suspension was 9.02, compared to 60.46 in the NOMB suspension, the data can be used to confirm the presence of NO in MB suspension. An unpaired T-test of the data indicated that there was a significant difference between the relative fluorescence of the RAMB and NOMB suspension (**** P = <0.0001).

As DHR is only reduced to fluorescent rhodamine 123 in the presence of the oxygenated products of NO, the data can be used to confirm the presence of NO at significantly higher proportions in NOMB suspensions. The level of fluorescence in the MB shell seen in both RAMB and NOMB shells was unexpected; thus, further testing was carried out to investigate the cause of this. It was hypothesised that the process of obtaining a dry lipid film by evaporating chloroform overnight in air caused auto-oxidation of the lipids; in MB suspensions where the dry lipid film is obtained by blowing off the chloroform under a constant stream of nitrogen, the fluorescence in the MB shell is removed entirely (**Figure 27**). This method of chloroform evaporation is a direct recommendation by the lipid supplier; with a controlled stream of nitrogen to ensure no solvent splashed from the glass vial, this method of removing chloroform is both reliable and highly consistent.

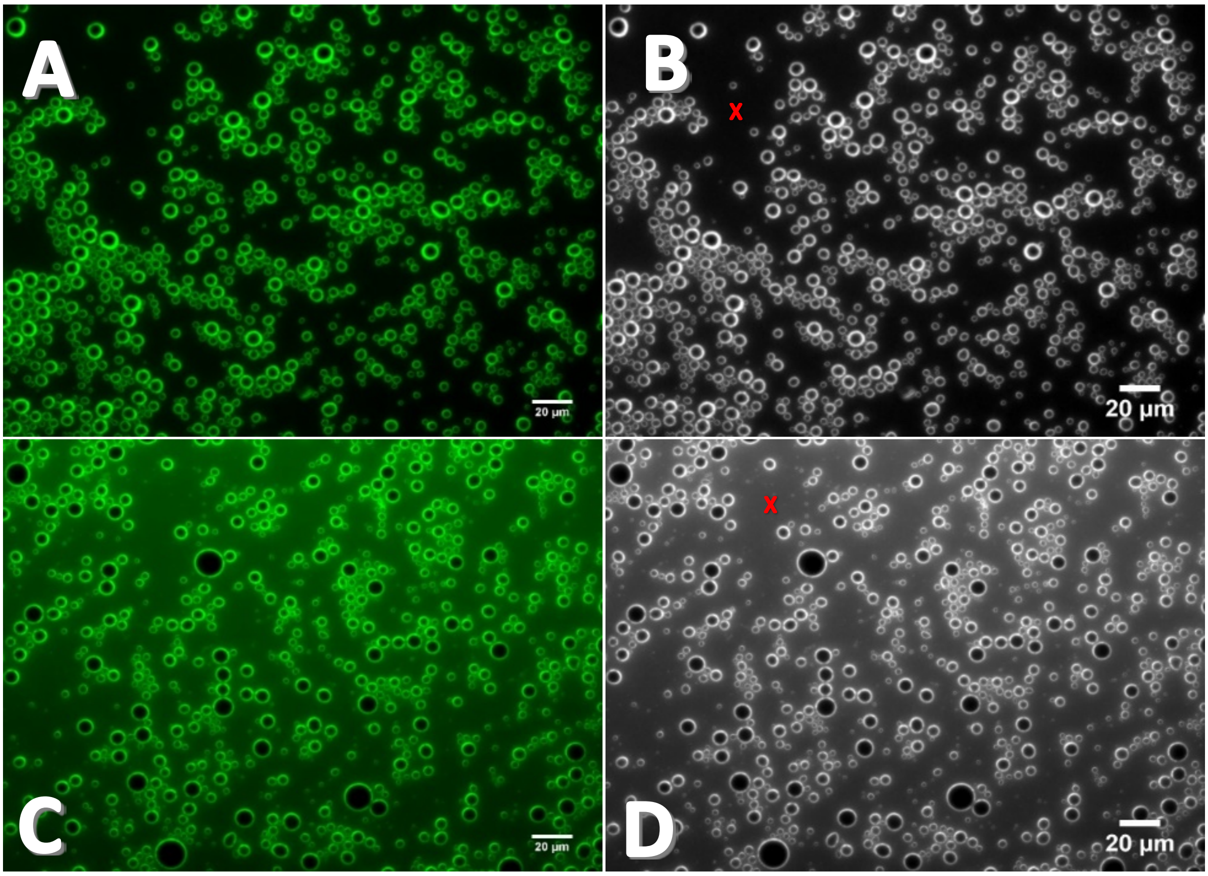

Figure 26 Example Image set of MB suspensions stained with dihydrorhodamine 123. A) RAMB suspension stained with DHR, (B) RAMB suspension isolated green channel only, 8-bit, greyscale image. (C) NOMB suspension stained with DHR, (D) NOMB suspension isolated green channel only, 8-bit, greyscale image. There is a clearly discernible visual difference in the quantity of fluorescent rhodamine 123 present in NOMB suspensions, which results in the fluid surrounding NOMBs appearing turbid due to background fluorescence. Points marked with (X) in images B and D, provide one representative example of the marker placement used in the assessment of pixel intensity.

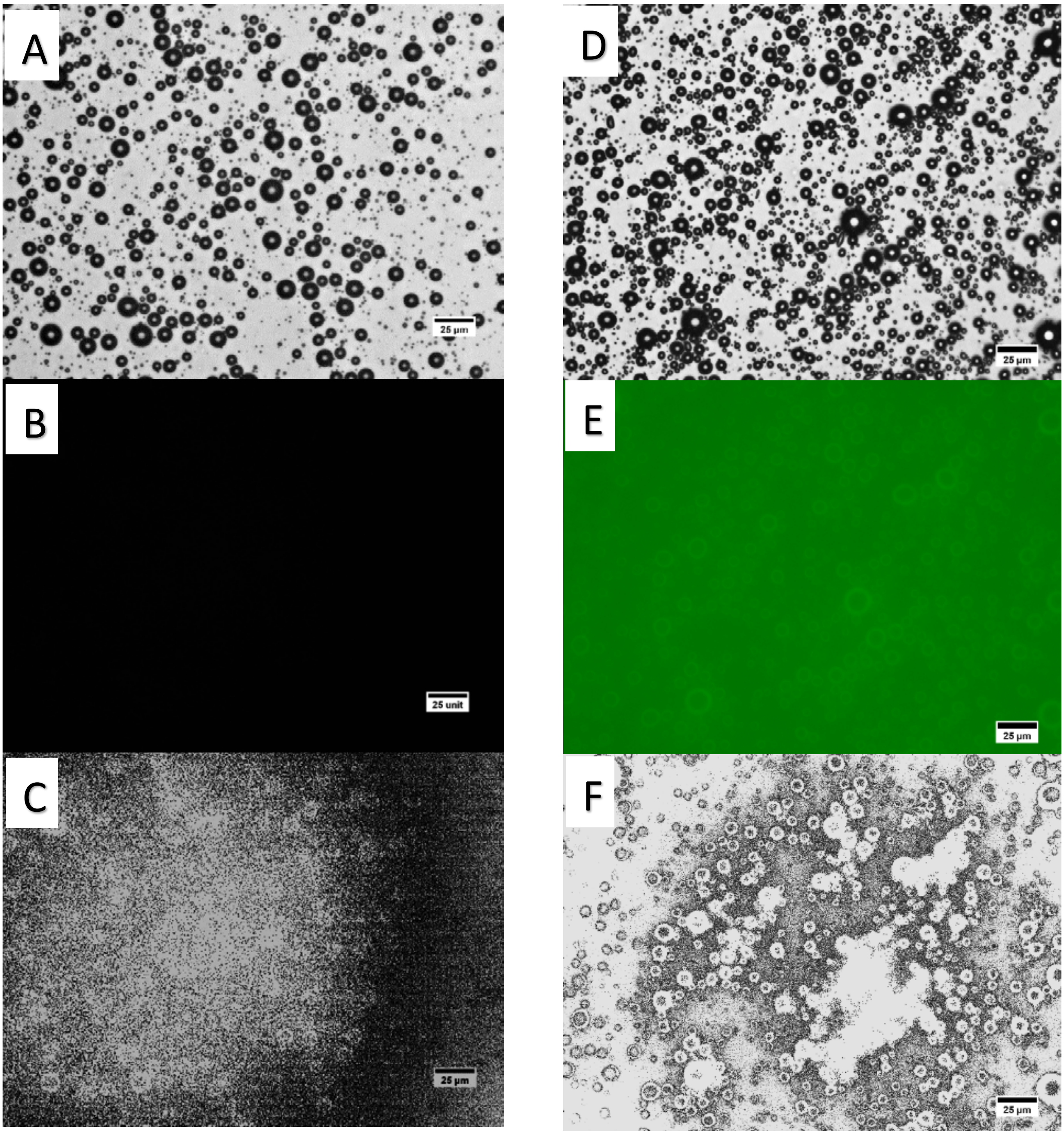

Figure 27 The images show (A) the bright field microscopy image of RAMBs where the lipid film was prepared under nitrogen, (B) the isolated green fluorescent channel of the image isolated to show there is no fluorescence in the presence of DHR. In (C) the green channel has been converted to a binary and any structural outlines enhanced. A suspension of NOMBs under bright field microscopy (D), with the isolated green fluorescent channel showing response of NOMBs to DHR and light scattering allowing depiction of MB shell outlines (E) and the binary converted image with structural outlines enhanced demonstrating high fluorescence in the fluid being diffracted by MBs (F).

2.5 Discussion

2.5.1 *Fabrication and stability characterisation of air and nitric oxide MBs*

The first step in this research was to fabricate ultrasound responsive MBs that maintain integrity to transport NO, but with enough elasticity to be responsive to ultrasound waves. Sonication was chosen as the most suitable method of MB production in this study, due to the ability to obtain a high yield of MBs within a short time frame at low cost. The stability of the MBs was only assessed at environmental temperature, as superficial wounds are the intended target for NOMBs and exhibit a temperature range of 31 °C to 34 °C (Dini *et al.*, 2015). Therefore the data is more applicable, since they would be required to function at approximately ambient temperature (~ 23 °C ± 2 °C) for the duration of treatment. The mean diameter of DSPC RAMBs increased from 3.48 µm to 6.94 µm over 60 minutes (**Figure 17**), whilst DSPC NOMBs ranged from 2.85 µm to 5.31 µm (**Figure 19**). After 60 minutes held at ambient temperature, the concentration of DSPC:PEG40s shelled MBs was reduced by 81.69% for RAMBs and further to 92.95% for NOMBs. When compared to DBPC:PEG40s shelled MBs there was no significant difference in the size distribution; DBPC NOMBs had an initial diameter of 3.31 µm which increased steadily over 60 minutes to 4.57 µm (**Figure 21**). However, there was a significant difference ($p < 0.0001$) between the concentration of NOMBs with a DBPC:PEG40s shell over time, compared to both RAMBs and NOMBs with a DSPC:PEG40s shell. The final concentration of DBPC:PEG40s NOMBs was 1.087 $\times 10^8$ MB/mL, which is only a 36.41% reduction compared to the initial concentration of the MB suspension of 1.710 $\times 10^8$ MB/mL. Within a suspension of MBs produced by sonication it is commonplace for the size distribution to be relatively broad (Stride and Edirisinghe, 2008; Feshitan *et al.*, 2009; Swanson *et al.*, 2010); although the majority of MBs in suspension (75%) are within ± 2 µm of the median value, there are inevitably some extreme outliers. It should be noted that this wide variation in MB size is also seen in clinically approved MB formulations (**Table 1**). This research demonstrated that in MB suspensions produced by sonication, dispersity in MB size was independent of shell composition; DBPC:PEG40s shelled NOMBs (**Figure 22**), DSPC:PEG40s shelled

RAMBs (**Figure 18**) and DSPC:PEG40s shelled NOMBs had an average standard deviation in mean MB diameter of approximately 2 µm (**Figure 20**).

Due to a longer carbon chain length associated with the DBPC phospholipid (22 carbon), the shell of DBPC MBs is comparatively thicker than those of DSPC MBs (18 carbon). Concurrent with theoretical dissolution rates determined by the Epstein and Plesset equation (**Equation 2**); the increased thickness of DBPC MB shells translates into greater MB stability over time, principally by reducing the diffusivity of the constituent gas core (Owen *et al.*, 2018b). The lower post-production concentration of DSPC RAMB (5.63 x10^7 MB/mL) observed compared to DSPC and DBPC NOMB concentration (1.92 x10^8 MB/mL and 1.71 x10^8), could be attributed to the difference in gas delivery during production; air is incorporated into RAMBs passively due to atmospheric air present in the headspace of the vial as MBs form at the fluid-air interface, whereas in the production of NOMBs the flow of NO is directed at a high flow rate (1.5 L/min). The directed flow of NO would result in a higher concentration of dissolved NO in the formerly degassed PBS, which would then become entrapped in the core of the MB. This would ultimately result in a decrease of the gas concentration gradient in a NOMB suspension compared to RAMBs in a degassed fluid, which would result RAMBs having a higher initial dissolution rate as described in the equation by Epstein and Plesset (Stride and Edirisinghe, 2009). However, due to the solubilisation of atmospheric gasses back into the NOMB solution this reduced diffusion coefficient will not be maintained, its impact is therefore likely to be limited to a short-term period post-production. An additional mechanism that is more likely to impact the long-term stability of MBs is the effect of temperature. As previously stated, during production of NOMBs a constant flow of nitrogen into the headspace of the vial and flow of NO at the interface between the sonicator tip and the fluid, this will invariably induce cooling of the fluid during sonication. Consequently, after the second 30 second sonication period when NOMB suspensions are placed in an ice bath, the fluid will already be closer to dropping below the lipid transition temperature (> 55 °C). We can hypothesise that the reduced period of time at which the temperature of the suspension is > 55 °C, will invariably limit the impact of Ostwald ripening in the fluid. This effect is clearly evident in this research, as NOMB suspensions consistently exhibit both a smaller diameter and greater concentration than RAMBs after production; as there is no cooling of RAMB suspensions during sonication by airflow, the cooling time post-production in the ice bath will be longer. In support of this hypothesis, other research has conclusively shown that the more rapidly a MB suspensions is cooled post-production, the greater the long-term stability of the MBs will be (Segers *et al.*, 2019).

In previous studies that also generated NOMBs by sonication, the flow rate of NO into the lipid suspension was 4 mL/min (Tong *et al.*, 2013; Wang *et al.*, 2013). This is 0.02% of the NO flow rate used in this experiment, however the studies did not quantify the final amount of NO encapsulated in the MB. The mean diameter of the NOMBs immediately post-production was 2.85 µm, this was over 19.54% smaller than both the 3.48 µm DSPC RAMBs in this study (**Figure 19**), and 3.85 µm NOMBs generated by other research (Tong *et al.*, 2013; Wang *et al.*, 2013). It is worth noting that the studies by both Tong *et al.* and Wang *et al.* used a lipid MB shell composed of DPPE and PEG_{2000}, the key difference between this formulation and the DBPC/DSPC and PEG40s shell used in this research is stability. Owen *et al.* (2018b) demonstrated that the inclusion of PEG_{2000} in the MB shell conferred greater stability at ambient temperature than MBs containing PEG40s. In this research this may be mitigated by the use of DBPC, as its longer carbon chain length has demonstrated the ability to significantly enhance MB stability at ambient temperatures (**Figure 21**) (Garg *et al.*, 2013). The key difference in shell composition is that DBPC and DPPE possesses longer hydrocarbon chains than DSPC; this results in stronger polar-head group interactions. Due to the greater cohesive forces between DPPE and DBPC phospholipids the MBs produced are more stable over time, but this is also means these MBs have lower elasticity than DSPC shelled MBs (Li *et al.*, 2015). This is exemplified well with the data in this research, which has shown that the diameter of DSPC shelled MBs increases gradually over time whilst MB concentration falls significantly (**Figure 18**, **Figure 20**). On the other hand, the stronger inter-molecular forces and thicker shell of DBPC MBs, allows them to maintain a more stable size and concentration over time (**Figure 21**). This would be an important consideration for the sustained release of NO, and mechanical stability of the MB to be maintained for the duration of any prospective treatment. The increase in diameter and decrease in MB concentration over time shown in **Figure 17**, **Figure 19** and **Figure 21**, is a commonly observed trend. This is perhaps best explained by spontaneous MB dissolution induced by Laplace pressure differences; the internal pressure of a MB is far greater than that of the surrounding medium which results in Ostwald ripening (Sarkar *et al.*, 2009). It is important to note that due to the solubilisation of atmospheric gasses into NOMB suspensions; the rate of NO diffusion down its concentration gradient out of the bubble and into solution will increase, this would certainly explain the decline in MB concentration over time. Though short term MB stability is commonly affected by coalescence, long-term stability on MBs is almost certainly predominantly influenced by Ostwald ripening (Talu *et al.*, 2006; Segers *et al.*, 2019). Despite this influence the mean diameters of DBPC and DSPC NOMBs was 4.57 and 5.31 µm ± 2 µm respectively after 60 minutes; therefore the bulk concentration of MBs in suspension would still be responsive to the 1 MHz ultrasound frequency that this research explores, for the stimulation of MBs for the treatment of biofilms. Consequently, there would be no need at present for differential centrifugation of MB suspensions to remove MBs that exceed 10 µm, or for safety reasons as the intended target of these MBs is topical application to extraneous wounds (Feshitan *et al.*, 2009). The stability data reported here provides confidence that NOMB suspensions would remain a viable size, for a potential treatment timescale of 60 minutes. However, though the NOMBs remain a suitable size over this period, they are unlikely to retain their bioactive effects over the same period due to the rapid diffusion of NO from the MB. The total proposed treatment time explored in Chapter 4, would take a clinician less than 10 minutes. This is in line with current research data, which suggests release of NO from lipid shelled MBs occurs over a period of 340 seconds (Lafond *et al.*, 2020). If the application of MBs for the delivery of NO is to be successful, there must be a good balance between elasticity and stability of the MB over time that correlates with successful encapsulation and controlled release of NO. Other research has demonstrated that NOMBs retain a therapeutic size distribution and concentration range, and remain biologically active for approximately one week if stored at 4 °C (Grishenkov *et al.*, 2015). However, the composition of NOMB shell in the cited study is polyvinyl alcohol based, whereas the present study uses a DSPC or DBPC lipid based shell with PEG40s as a surfactant. The comparatively rapid decline in concentration of MBs stored at room temperature seen in this research, is concurrent with literature that has directly compared the stability MBs stored at 4 °C and room temperature (Rovers *et al.*, 2016). At the time of writing, MBs with a DSPC or DBPC lipid shell have not been used for the delivery of nitric oxide exclusively to biofilms for dispersal. However, recent publications on the sonobactercidal effect NOMB in planktonic suspensions, have validated the use of MBs stabilised with a comparable DSPC:PEG$_{2000}$ shell comparable to the NOMB formulation explored here (Lafond *et al.*, 2020). Similar to this research, Lafond *et al.* postulated that DSPC with an 18-carbon chain would confer greater stability to the MB than the 16-carbon lipid DPPC. One of the significant advantages of this composition is that lipid shelled MBs are inherently biocompatible, their biophysical effects are well documented and approved for *in vivo* applications (Wu *et al.*, 2015a; Paolino *et al.*, 2017).

2.5.2 *Fabrication and characterisation of DSEPC cationic MBs stability*

It was hypothesised that the concentration of cationic MBs would be significantly lower than that of neutral MBs such as DSPC RAMBs, as charged lipids undergo electrostatic double layer repulsion that impairs MB formation (Kwan and Borden, 2012). The repulsion between similarly charged lipids can reduce cohesion between adjacent lipids in the MB shell, consequently this should lower the overall integrity of the shell and thus the stability of the MB more rapidly. This effect is not apparent in the suspensions tested here, as both cationic RAMBs$^+$ and NOMBs$^+$ were able to maintain their concentration in ambient conditions for the 60 minute period the test was run (**Figure 23**, **Figure 24**). As an equivalent maximum period of time that MBs would be utilised at ambient temperature after preparation in either an experimental or clinical setting, the 60 minute time frame assessed in this research was deemed substantial enough to validate the stability of MBs. Contrary to the findings in this research, Wang *et al*. found that neutral MBs were consistently more stable and had a longer half-life than cationic MBs (Wang *et al*., 2012). However, there were differences in MB shell constituents, MB production and initial MB concentrations compared to Wang *et al*. so an accurate comparison could not be made. It is important to note that the impact on cationic MB stability if assessed for a longer period of time may become more apparent; however, recent research by Browning *et al.*, who carried out stability testing of DSEPC shelled MBS over a 90 minute period, found no significant increase in MB diameter (< 5%) and only a 9% reduction in concentration over this period. The stability work by Browning *et al.* (2020) is directly comparable to this research, as the MB shell constituents and environmental conditions for stability testing were all consistent with this work; the findings therefore support and validate the stability data shown herein.

The Epstein-Plesset model of MB dissolution considers several MB characteristics such as MB radius, filling gas, shell surface tension and suspension medium. However, an important parameter is ignored in this model as the Epstein-Plesset equation only models the behaviour of a single bubble in a suspension medium, without considering the effect of inter-MB interactions such as Ostwald ripening. Over time Ostwald ripening causes smaller MBs shrink due to their high Laplace pressure; this induces growth of larger MBs and results in an increase in mean MB diameter in the suspension over time. Ostwald ripening is more pronounced when MBs are closer to each other, i.e. concentrated MB suspensions are more likely to undergo Ostwald ripening (Talu *et al*., 2008). Cationic MBs were more stable than neutral MBs despite there being no significant difference in initial MB diameter, which implies that they should have similar dissolution rates. However, cationic MBs did have moderately lower initial concentrations than neutral MBs, so they were potentially less affected by Ostwald ripening. The sustained concentration and diameter over the 60 minute period assessed here of the NO-filled cationic MBs compared to other MB formulations, demonstrated that although Ostwald ripening played a significant part in MB stability in this study the effects can be mitigated by altering the physical properties of the MB shell. Furthermore, repulsion between similarly charged cationic MBs is also likely to reduce the impact of Ostwald ripening, by increasing the physical distance and association between each MB; demonstrated in later experiments (Chapter 3, **Figure 38**).

2.5.3 *Fluorescent detection of nitric oxide products in MB suspensions*

DHR is a small lipophilic and cationic dye that is able to diffuse across membranes, it remains non-fluorescent until oxidised to rhodamine 123 by the interaction between O_2 and NO (Volk and Moreland, 2014). The relative FI observed in these experiments, is proportional to the quantity of reacted peroxynitrite (Almeida *et al.*, 2019). Consequently the higher the proportion of NO present in the original solution that has reacted with oxygen, the greater the FI of rhodamine 123 will be. The relative FI of rhodamine 123 was assessed across 5 independent MB suspensions for RAMBs and NOMBs, to demonstrate consistency in the preparation and values obtained. The mean FI observed in RAMB suspensions was 9.02, it could be assumed that this value should be zero as the suspension was not made with NO. However this residual low level of fluorescence is expected, due to the residual proportion of highly soluble nitrate and nitrite ions present in water used to constitute PBS in this experiment (Richard *et al.*, 2014; Karwowska and Kononiuk, 2020). As there is a substantial statistically significant difference between the mean FI of RAMB and NOMB suspensions (**Figure 26**), we can assert that the increase can only be the result of the addition of NO in NOMBs. It is worth noting that the lipid shell of MBs in both the RAMB and NOMB suspensions was highly fluorescent; due to the lipophilic and cationic nature of DHR the incorporation of the dye into the MB shell was not surprising, however the equal FI (mean pixel intensity = 215) of the shell in both RAMBs and NOMBs was unexpected (**Figure 27**). Further research lead to the development of the hypothesis that during evaporation of chloroform in air to obtain a dry lipid film (Fabrication and Characterisation of Ultrasound-Responsive Microbubbles: 2.2.2), the well documented phenomenon of lipid oxidation occurs and results in association of DHR to polar residues of oxidised lipids in the MB shell (Liljeblad *et al.*, 2010; Ayala *et al.*, 2014; Khanum and Thevanayagam, 2017). To verify that the fluorescence was indeed caused by lipid degradation by reactive species present in air, the solvent chloroform was evaporated under a constant stream of nitrogen to protect the lipid film. The results of this experiment validated the initial hypothesis, as no fluorescence was detected in fluid or shell of RAMB suspensions (**Figure 27**). Due to the ability of MBs scatter the green light being transmitted through the sample the outlines of the RAMBs were detectable in post processing (**Figure 27**C), the inclusion of this image is to verify the presence of RAMBs in the image in the absence of a fluorescent signal from rhodamine 123. Similarly in NOMB suspensions where chloroform was evaporated under nitrogen, there was no fluorescence in the shell. However due to the detection of significant levels of nitrate and nitrite in solution, the fluorescence of rhodamine 123 in the background of the fluid makes the outlines of MBs easily distinguishable in the green fluorescent channel image (**Figure 27**E). This is again caused by the diffraction of light due to the difference in refractive index of gas filled MBs compared to the surrounding fluid (Leung *et al.*, 2013), the strength of the fluorescent signal creating a 'backlit' effect is evident when the image is made binary and individual MB outlines enhanced (**Figure 27**F). This experiment confirmed fluorescence in the MB shell was not due to higher concentrations of NO at the diffusion boundary, but verified that upon release from the MB it quickly becomes homogenously distributed through the fluid. Though this method can be used to reliably infer the presence of NO, a major limitation of this method is that it does not directly assess the release kinetics or initial concentration of the NO in solution. These measurements have been attempted with various electrochemical (Unisense, Nitric Oxide Sensor) and chemical assays (Greiss) without success. A recent paper on the 'bactericidal activity of lipid-shelled nitric oxide loaded MBs' in planktonic suspensions, did successfully demonstrate the inclusion and temporal resolution of NO in MBs with an Apollo 4000 with ISO-NOP electrode (World Precision Instruments, Sarasota, FL, USA) (Lafond *et al.*, 2020). In MBs co-loaded with octafluoropropane and nitric oxide, the concentration of NO was noted to range from 2-5 mM with rapid release over 340 seconds. There are a number of parallels between the MB fabrication and NO loading method in this research and the Lanfond *et al.* paper, notably the same lipid molar ratios and method of voiding the headspace of the vial of air before the addition of NO under anoxic conditions were applied. This provides confidence in our method of fabrication and provides an approximation at least of the potential orders of magnitude for nitric oxide concentration and release, that we should expect from lipid shelled MBs.

2.6 Conclusion

The research conducted on the fabrication and characterisation of NOMB has fulfilled the first aim of this project, i.e. to engineer an ultrasound-responsive agent capable of transporting nitric oxide for the dispersal and elimination of biofilms. Through theoretical evaluation and robust practical assessment, we have successfully demonstrated the utility of sonication as a means of producing RAMB and NOMB suspensions. With supporting evidence from comparable MB formulations in the literature, we have verified that the MBs produced were sufficiently stable for current *in vitro* and prospective downstream *in vivo* applications. A significant challenge within this work has been the accurate assessment of nitric oxide incorporation, release and quantification from MBs. Using fluorescent detection methods we have demonstrated that NOMB suspensions contain a highly significant quantity of peroxynitrite, which can only occur as a direct result of oxidation of NO in solution over time. This essential investigative work on MB formulations and fabrication methodology has allowed the progression of the research into investigating the efficacy of RAMBs and NOMBs, for the dispersal and elimination of single species *P. aeruginosa* biofilm models.

CHAPTER III

3 THE USE OF CATIONIC ULTRASOUND-RESPONSIVE MICROBUBBLES FOR INDUCING AND SUSTAINING NON-SELECTIVE INTERACTION WITH BIOFILMS

3.1 Introduction

As previously discussed (Chapter 1, paragraph 1.1.4), the composition of the MB shell is a key determining factor of MB stability, biophysical effects, and therapeutic outcome. Enhancing the localisation of MBs to the target treatment site is acutely linked to their therapeutic efficacy; some strategies employed for targeted drug delivery and gene therapy with functionalised MBs include: biochemical ligand-receptor targeting, acoustic radiation force and magnetic manipulation (Weller *et al.*, 2002; Zhao *et al.*, 2004; Martin *et al.*, 2007; Owen *et al.*, 2015). The incorporation of charged lipids is one way in which the MB shell can be functionalised, principally for the purpose of non-selective targeting. The incorporation of cationic lipids allows MBs to electrostatically interact with negatively charged molecules; this method has already been used to bind nucleic acids to MBs for gene delivery (Carugo *et al.*, 2015; Huang *et al.*, 2017). The specific binding in this research between MB and biofilms occurs via electrostatic interaction, between the positively charged lipids associated with the MB shell and the net-negative charged molecules associated with the biofilm. An interesting point to note is that MBs augmented with a charge, have not been used as an explicit means to direct the MB to a specific site or feature based on the electrostatic interaction alone. As the non-selective nature of this targeting approach applied systemically to intravascular applications of MBs, could lead to MB interactions with endothelial cells or blood constituents before reaching their intended target site leading to occlusion or embolism in the circulatory system. For the treatment of superficial wound infections however, the presence of negatively charged teichoic acids of Gram-positive bacteria (Caveney *et al.*, 2018), and highly negative lipopolysaccharides on the surface of Gram-negative bacteria may provide a unique means of inducing non-selective contact between the MB and bacteria (Salazar *et al.*, 2017). Combining this information with what is known about the composition of the

EPS matrix of biofilms, it can be deduced that the biofilm should also exhibit a net negative charge (Jain *et al.*, 2015; Pen *et al.*, 2015). Utilising positively charged MBs could therefore provide the means to induce a prolonged MB-biofilm interaction, thereby aiding localised, precision release of NO from MBs to induce dispersal. Furthermore, an important consideration is that cationic DSEPC MBs may reduce the diffusion distance of NO from the MB to the biofilm, which may increase the efficacy of the treatment proposed.

3.2 Statement of objectives

This chapter will investigate the functionalisation of ultrasound-responsive agents developed in Chapter 2, utilising specific electrostatic interactions as a means of inducing non-selective binding of MBs applied topically to a bacterial biofilm.

3.3 Materials and methods

3.3.1 *Method rationale*

Biofilms exhibit a net negative surface charge, therefore it was hypothesised MBs modified to have cationic properties would be electrostatically attracted to biofilms (Khelissa *et al.*, 2019). Due to the heterogeneous nature of the biofilm and EPS of the matrix, specific targeting methods such as ligand-receptor interactions would be less reliably implemented. Electrostatic interactions offer a promising method of inducing non-selective interaction between MBs and biofilms, which has potential to increase the proximity of MBs to the treatment site. This not only reduces the diffusion distance of NO from the MB to the biofilm to potentiate dispersal, but also has the potential to increase the number of MBs in contact with or proximal to the biofilm; that may increase the efficacy of the biophysical effects imparted on the biofilm by a MB oscillating in response to US stimulation. To date, there have been very few quantitative studies on targeting efficacy of MBs to biofilms. Flow cells can be used to perform such studies as the shear stress exerted over a surface can be altered by changing the flow rate.

3.3.2 *Statistical analysis*

All data were assessed for normal distribution; for normally distributed data both paired and independent t-tests have been used to compare data depending on the relationship between the variables. For multiple treatment conditions, a one-way ANOVA was used to identify any significant difference between groups. All data was analysed and plotted using Prism 8.4.3 (GraphPad), with a threshold value for significance of < 0.05 where * = $P < 0.05$, ** = $P < 0.005$, *** = $P < 0.0005$, **** = $P < 0.0001$.

3.3.3 *Development of flow cells for creating surfaces with augmented electrostatic charge*

Flow cells were designed using Solidworks (Solidworks 2018, Dassault Systèmes, France) and converted to DXF files, which were compatible with the software of a laser cutting machine (Lasercut 5.3, HPC Laser Ltd., Yorkshire, UK). The flow cells were designed to fit a 75 mm x 25 mm glass slide. The inlet and outlet holes were laser cut (LS1690, HPC Laser Ltd., Yorkshire, UK) from a layer of 600 mm thick clear acrylic. Double sided tape 0.19 mm thick (3M™ Double Coated Polyester Tape 9731, Self-Adhesive Supplies, UK) was laid over the acrylic and the channels were laser cut from the tape. A glass substrate was then fixed over the double sided tape (**Figure 28**). Untreated borosilicate glass coverslips (0CON-161, 75 x 25 mm glass coverslips, Logitech, Glasgow, UK) were used for the uncharged flow cells. Quartz coverslips (Alfa Aesar™ Quartz Microscope Slides, Fisher Scientific UK Ltd.) were used for creating flow cells with an anionic electrostatic charge. The surface charge of flow cells can be altered as quartz slides become relatively anionic when in contact with a solution (e.g. PBS at pH 7.4) (Behrens and Grier, 2001). To ensure the flow cell was fluid-tight, water containing a red food dye was pumped through the flow cell at increasing flow rates until failure (i.e. visible leakage) occurred. The optimal inlet and outlet diameter was determined by laser cutting several holes of different diameters into the clear acrylic and testing the fit of the tubing in each orifice (Appendix A: 6.1.1). Two parallel channels were used to increase the throughput of the device and allow comparison studies to be performed with biofilms grown under the same conditions. A high aspect-ratio design was used for the channel cross-section to provide uniform shear-stress over the channel surface.

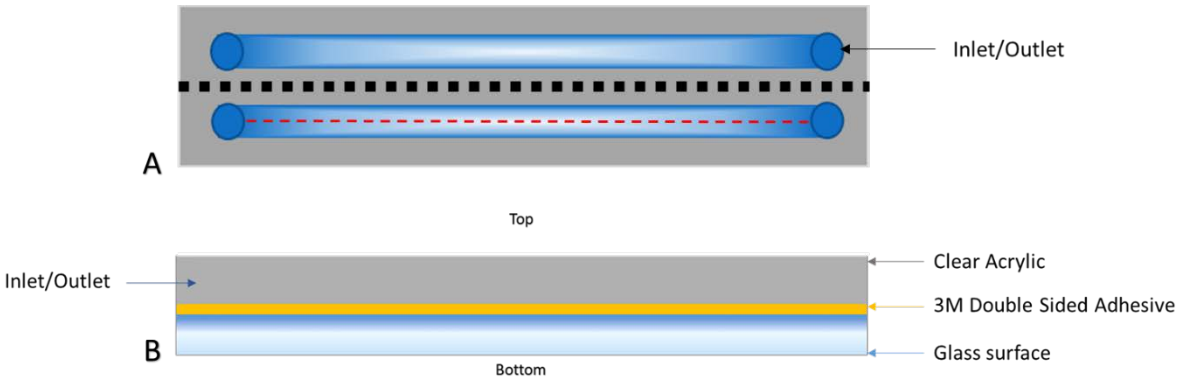

Figure 28 Schematic diagram of flow cell with main features highlighted. The flow cell measures 75 x 25 mm, and the fluid channel is 0.14 mm deep and 3.5mm wide. A) Top view of the flow cell with a dashed red line indicating the centreline of the channel, which is approximately 1.7 mm equidistant from the walls of the channel. B) Cross-sectional view of A taken at the dotted black line, with ‘top’ and ‘bottom’ orientation indications (Figure not to scale).

3.3.4 *Biofilm growth in neutral charge flow cells*

Firstly, the flow cell, required tubing and fittings were sterilised with 80 mL of 70% ethanol solution followed by 80 mL of deionised water in a laminar flow cabinet with syringes (BD Plastipak, 80 mL syringes, Becton-Dickinson UK Ltd., Berkshire, UK). The apparatus was then arranged as shown in **Figure 29**. An overnight culture of *P. aeruginosa* (PA01) was grown by selecting three identical colonies from an agar plate and inoculating 5 mL of TSB before incubating at 37 °C. The overnight culture was diluted 1/100 into sterile TSB before being inoculated into the flow cell and allowed to sit for 1 hour with the flow cell glass side down. This step ensures that the biofilm grows on the glass side of the flow cell. The entire apparatus was then placed in an incubator at 37 °C and sterile media was pumped through the flow cell at 0.01 mL/min over 24 hours. The waste outlet tubing was fed into 2% Virkon solution (Day Impex™ 330012, Fisher Scientific UK) and the tubing for the bacterial culture inlet was removed and sterilised. After 24 hours, the level of biofilm growth was assessed by microscopy (Appendix A - 6.1.2, **Figure 65**). Due to the small channel height of 140 µM, 24 hour growth was deemed to be the optimal time point to balance biofilm development with prevention of channel occlusion due to biofilm growth.

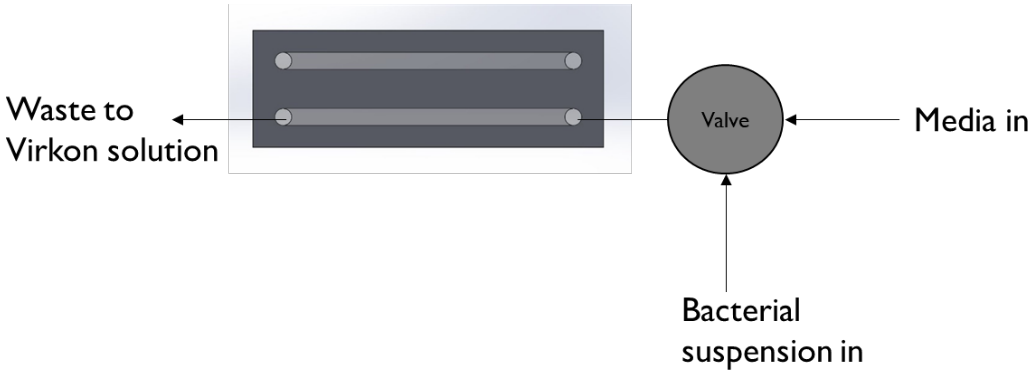

Figure 29 Apparatus set up for biofilm growth in flow cell. Both channels were set up in the same way, but only one channel is shown here for clarity. Media was pumped into the flow cell at a rate of 0.01 mL/min for 24 hours.

3.3.5 *Determination of MB binding characteristics under static conditions*

To determine if the incorporation of a positive charge into the MB shell can promote contact with negatively charged surfaces, an artificially charged environment was created for controlled preliminary testing; this method is summarised in **Figure 30**. Firstly, a flow cell with a neutral glass cover slip was primed with PBS. Short lengths (approximately 3 cm) of tubing (4 mm diameter, Masterflex Transfer Tubing, Platinum-Cured Silicone, WZ-95802-03, Cole Parmer, UK) were fitted to the inlet and outlet of the flow cell. Three vials each of RAMB, RAMB$^+$, NOMB and NOMBs$^+$ produced in accordance with the method outlined in 2.2.2 and 2.2.3, all MBs were initially produced with DSPC:PEG40s with cationic MBs also containing DSEPC, in later tests DSPC was substituted with DBPC.

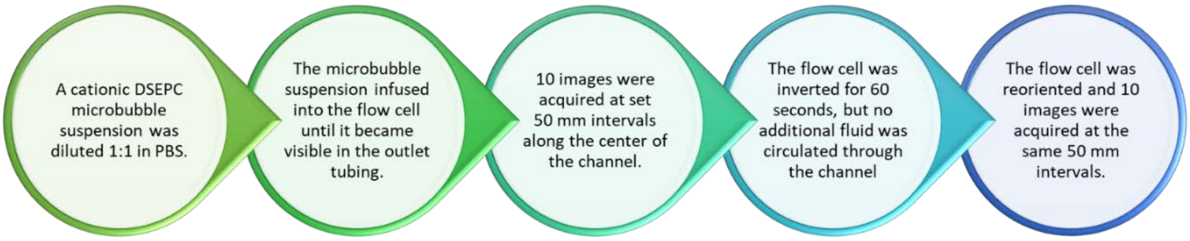

Figure 30 Summary flow chart of static flow cell experiment. The experiment was carried out in triplicate for each MB composition and both neutral and charged flow cells.

Approximately 1000 µL of an undiluted MB suspension was manually injected into the flow cell through tubing connected to the inlet hole, until the suspension was visible in the outlet tubing.

To prevent back flow of the MB suspension, the outlet tubing was then clamped to create a seal. Ten 'before interaction' images were acquired at 50 mm intervals from the inlet (left) to the outlet hole (right), along the centreline of the flow cell channel. Images were captured under bright field microscopy (Olympus, IX71), with a 50x (Olympus, LMPLFLN) objective lens using a CCD camera (Hamamatsu ORCA-ER, C4742-80) and analysed in accordance with Section 2.2.4. The centreline of the channel that was approximately 1.7 mm equidistant from the channel walls, as indicated in **Figure 28**, was selected as the wall shear stress acting on the glass surface here would exhibit greater uniformity. Each MB suspension was allowed to interact with the charged or uncharged surface for 60 seconds; a further 10 'post interaction' images were then captured and analysed in the same way. A 60 second interaction period was selected as a representative clinically viable treatment timescale, this also aligns with the time taken for the majority of the MBs in suspension to passively float towards the surface. This procedure was repeated for three vials of each MB composition with a neutral and charged surface. The percentage change in MB interaction with each surface was calculated with **Equation 4**; where V_1 corresponds to the number of MB/mL present before contact with the charged or neutral surface was induced (i.e. glass surface facing upwards), V_2 corresponds to the number of MBs that remain in contact with the charged or neutral surface after induced interaction is stopped (i.e. glass surface facing downwards).

Equation 4 Percentage change in MB concentration.

$$\begin{bmatrix} Change\ in \\ MB\ concentration\ (\%) \end{bmatrix} = \frac{V_2 - V_1}{|V_1|}\ x100$$

3.3.6 *Assessment of MB non-selective binding strength*

The mean wall shear stress exerted by the fluid flow over the channel substrate was altered by adjusting the flow rate of fluid through the channel. The volumetric flow rate required to generate a given mean wall shear stress was calculated by first determining the pressure drop along the channel length (for a given shear stress value). The pressure drop was calculated from **Equation 5** (Westerhof *et al.*, 2010), where ΔP = pressure drop (Pa), τ = mean wall shear stress (Pa), P_W = wetted channel perimeter (m) = 2 x channel width + 2 x channel depth (assuming channel was completely filled, P_W = 0.00728 m, L = channel length (m) = 0.0655 m, A = cross-sectional area of the channel (m^2) = $4.9 \text{x} 10^{-7}$ m^2.

Equation 5 Pressure drop within a channel.

$$\Delta P = \frac{\tau \times P_w \times L}{A}$$

The required volumetric flow rate was subsequently calculated from the pressure drop along the channel using Hagen-Poiseuille's law, corrected for calculating volumetric flow rate within a rectangular channel (**Equation 6**) (Lewis and Boose, 1995) where Q = volumetric flow rate (mL/min), ΔP = pressure drop along channel length (Pa), D_H = channel hydraulic diameter (m) = 4 x cross-sectional area / wetted perimeter = $2.7 \text{ x } 10^{-4}$ m, μ = dynamic viscosity of water = 0.00089 kg/ms, L = channel length (m) and 0.2 is the correction factor for a rectangular channel with a width of 3.5 mm, depth of 0.14 mm. The calculated volumetric flow rates required to achieve mean wall shear stress values of 0.1, 0.2, 0.5 and 1 Pa are shown in **Table 5**.

Equation 6 Hagen-Poiseuille's law corrected for estimating flow rate in a rectangular channel

$$Q = \frac{\Delta P \times \pi \times D_H^4}{128 \times \mu \times L \times 0.2} \times \frac{10^6}{60}$$

Table 5 Volumetric flow rates for PBS corresponding to mean wall shear stress to be exerted on MBs bound to the glass surface. The volumetric flow rates for each required mean wall shear stress were calculated from the pressure drop along the channel using **Equation 5** and **Equation 6**.

Mean wall shear stress (Pa)	**0.1**	**0.2**	**0.5**	**1**
Pressure drop along channel (Pa)	97.31	194.63	486.57	973.14
Volumetric flow rate (mL/min)	0.06	0.13	0.32	0.65

The MB concentration was assessed after increasing mean wall shear stress (acting on the glass slide) to determine the MB binding strength to neutral and anionic glass slides, a summary of the method is shown in **Figure 31**. Three vials containing 5 mL each of 9:0.5:0 (neutral) and 9:0.5:1 (cationic) molar ratio DSPC:PEG40s:DSEPC MBs were produced, according to the method outline in 2.2.2 and 2.2.3 respectively using the compositions shown in **Table 4**. After production, all MB suspensions were stored in an ice bath prior to use.

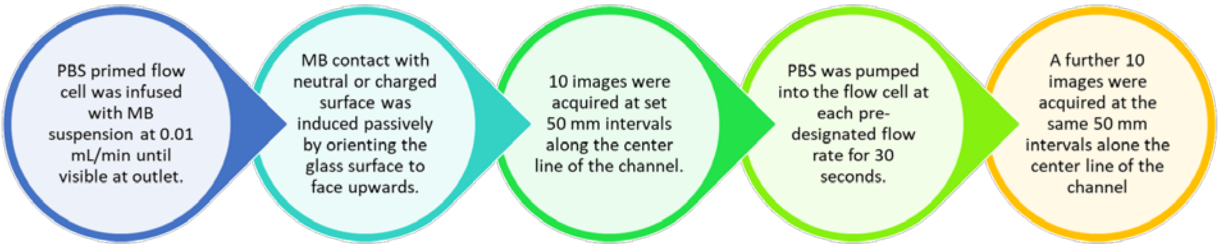

PBS primed flow cell was infused with MB suspension at 0.01 mL/min until visible at outlet.

MB contact with neutral or charged surface was induced passively by orienting the glass surface to face upwards.

10 images were acquired at set 50 mm intervals along the center line of the channel.

PBS was pumped into the flow cell at each pre-designated flow rate for 30 seconds.

A further 10 images were acquired at the same 50 mm intervals alone the center line of the channel

Figure 31 Summary flow chart of MB binding strength determination. The experiment was carried out in triplicate for each MB composition and both neutral and charged flow cells.

The flow cell and syringe system were assembled as shown in **Figure 32**. The MB suspension was drawn into 5 mL syringe (BD Luer Lock, 309649), and manipulated by inversion to ensure homogeneous distribution of MBs. A second 10 mL Luer Lock syringe (BD Luer Lock, SYR912) was filled with sterile 0.01 M PBS. Both syringes were connected to a three-way valve (Masterflex Fitting, Polycarbonate, Three-Way, Stopcock with Male Luer Lock, UY-30600-02, Cole Parmer, UK), with outlet tubing connected to the flow cell channel inlet. The tubing and channel was primed with PBS, before the MB suspension was pumped into the flow cell at a flow rate of 0.01 mL/min until the channel was filled. When the channel was full of MB suspension in a 1:1 volumetric ratio with PBS; the flow cell was placed with the glass surface facing up for 60 seconds, to allow interaction of the MBs with the neutral/charged surface. PBS was then pumped through the channel at 0.01 mL/min for 90 seconds, to remove any unbound or weakly associated MBs.

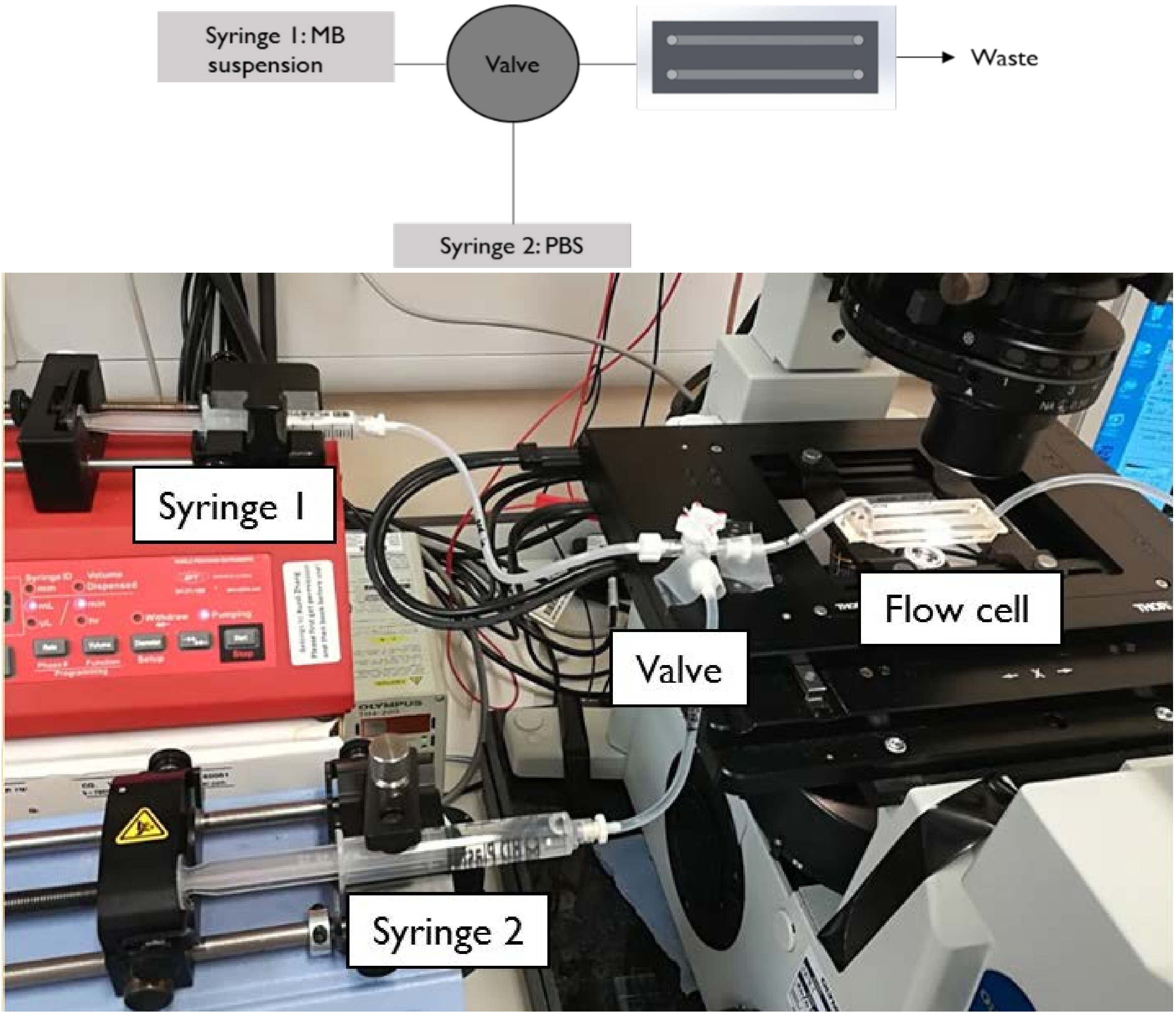

Figure 32 The experimental setup shown was used to assess the binding strength of cationic MBs, to a negatively charged surface. Syringe 1 was used to control the flow of MBs whilst syringe 2 contained PBS for flushing MBs out of the system; this could be alternated by controlling the position of the valve. The flow cell was placed on an inverted microscope, using a 50x objective to conduct bright field microscopy and acquire images to determine MB concentration as outline in section 2.2.4.

After visual inspection confirmed MBs were stationary within the channel, ten images were acquired at 50 mm intervals along the centreline of the flow channel. This ensured the full length of the channel occupied by MBs was analysed, with a direct comparison of the same areas of the channel before and after application of flow. PBS was pumped into the flow cell for 15 seconds at a time with flow rates of 0.06, 0.13, 0.32 and 0.65 mL/min respectively, to achieve wall shear stress values shown in **Table 5**. After the application of each flow rate, ten images at the same 50 mm positions along the centreline of the channel were acquired after visual confirmation that MBs had become stationary.

The procedure was repeated in triplicate with both MB compositions, in neutral and charged flow cells. Segmentation of individual MBs was not possible for this experiment as there was significant aggregation of the MBs. Therefore, in an adaptation of the method outlined in 2.2.4, the total percentage area covered by the MBs in each image was determined by image thresholding and binarisation in ImageJ. The total area covered by MBs obtained through thresholding was calculated for each set of 10 images, at each flow rate, for each MB composition. For each formulation the mean area covered by MBs derived from 10 images at each flow rate, was normalised dividing the mean by the initial area covered by MBs. This is represented by **Equation 7**; $\bar{x}$ corresponds to the mean percentage area of MB population present in the channel after flow rates of 0.06, 0.13, 0.32 or 0.65 mL/min respectively were applied, and the mean percentage area of MBs present in the channel prior to the application of flow is denoted as μ. The results of **Equation 7** equate the initial percentage coverage for each formulation to 100%, whilst preserving the proportional the change in MB population due to the application of various wall shear stress values.

Equation 7 Normalisation of percentage area covered by MBs.

$$\begin{bmatrix} Normalised \\ MB\ Area\ (\%) \end{bmatrix} = \frac{\bar{x}}{\mu}\, x100$$

3.3.7 *Assessment of non-selective interaction of MBs with P. aeruginosa biofilms*

P. aeruginosa biofilms were grown in Ibidi® dishes (µ-Dish 35 mm, Glass Bottom, Thistle Scientific) for 24 hours in wound constituent medium (WCM) at 37 °C as described in section 4.2.3. Biofilms were washed three times with sterile PBS, to remove any planktonic or weakly attached cells from the dish growth area. Biofilms were live/dead stained with 2.5 µM Syto9 (S34854, Invitrogen™, ThermoFisher Scientific) and 9 µM propidium iodide (P3566, Invitrogen™, ThermoFisher Scientific) for 5 minutes, and stored under foil to prevent exposure to light. Excess stain was removed by washing with sterile PBS and visual confirmation of biofilms presence was performed with fluorescence microscopy before the application of MBs (EVOS, M5000).

Cationic DBPC RAMB$^+$, NOMB$^+$ and uncharged DBPC RAMB and NOMB suspensions prepared in accordance with the methods outlined in 2.4.1 and 2.4.2, were diluted 1:5 in sterile PBS and 1000 µL was gently pipetted onto the previously live/dead stained biofilm. Each MB formulation was tested in triplicate using three independent biofilm samples (n=18); the total MB-biofilm interaction time was 60 seconds for each biofilm. After 60 seconds the Ibidi® dish was held at a 45° angle and washed gently from the top with 1000 µL of sterile PBS three times; this ensured removal of any transient MBs not interacting strongly with the biofilm. Each biofilm was imaged with the EVOSM5000, green fluorescent Syto9 was assessed under $^{\lambda}$emission 510 nm, gain 5.0, light source intensity 0.5, brightness 0.5, exposure time 20 ms (EVOS M5000, 20x Plan Fluor EVOS AMEP42924 objective, (Green fluorescent protein) GFP LED cube AMEP4653, Invitrogen™, ThermoFisher Scientific); red fluorescent propidium iodide was assessed under $^{\lambda}$emission 593 nm, gain 5.0, light source intensity 0.5, brightness 0.5, exposure time 20 ms (EVOS M5000, 20x Plan Fluor EVOS AMEP42924 objective, red fluorescent protein (RFP) LED cube AMEP4653, Invitrogen™, ThermoFisher Scientific); MBs were observed under in bright field to assess their localisation pattern and biofilm association as percentage area.

3.4 Results

3.4.1 *Assessing flow cells for leakage under increasing flow rates*

In leakage testing of the flow cell it proved able to withstand flow rates of up to 25 mL/min before failure, the use of red food dye ensured any leakages from tubing or bleeding of fluid into the tape would be clearly visible (**Figure 33**). All flow rates for experimentation were kept below 1 mL/min, significantly minimising any risk of leakage during experimentation.

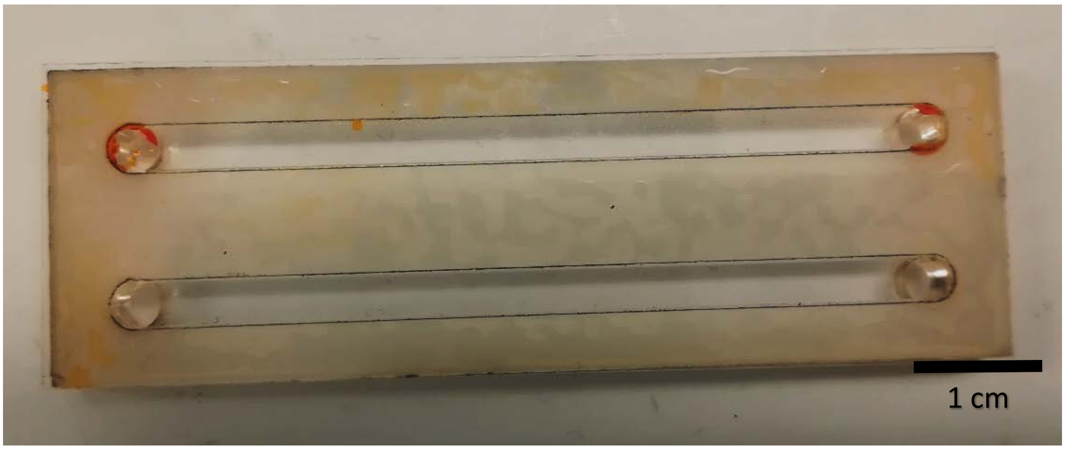

Figure 33 Example of a flow cell subjected to leakage testing, which failed upon exposure to a flow rate of 25 mL/min. There is indication of leakage of fluid and precipitation of the dye into the tape bonding the glass surface to the acrylic manifold.

3.4.2 *Biofilm growth in flow cell*

Bacterial biofilms were found to grow successfully within the flow cell, however MB experiments could not be performed when there was a biofilm in the flow cell. Both the biofilm and MBs need to be visible at high magnification for the experiment, but only the substance closest to or on the glass was visible under the microscope at any time. Biofilm growth was assessed on both the glass surface and acrylic manifold of the flow cell experiments. Biofilms grown on the flow cell manifold provided excellent visualisation of MB suspensions added to the channel (**Figure 34**), however, in bright field the microscope could not focus to a great enough depth beyond the MB suspension in the foreground, to simultaneously visualise the biofilm and MBs. Consequently, only the most superficial layer of the biofilm containing mostly planktonic cells could be observed, in subsequent testing where biofilms were grown on the glass surface of the flow cell the converse was true. The density of biofilm growth on the glass surface, did not permit simultaneously visualisation of both the biofilm and MBs within the channel. Research development aimed at overcoming the issues associated with visualisation of biofilms and MBs in this flow cell system were assessed further and reported in Appendix A – Supplementary experimental material, 6.1.4.

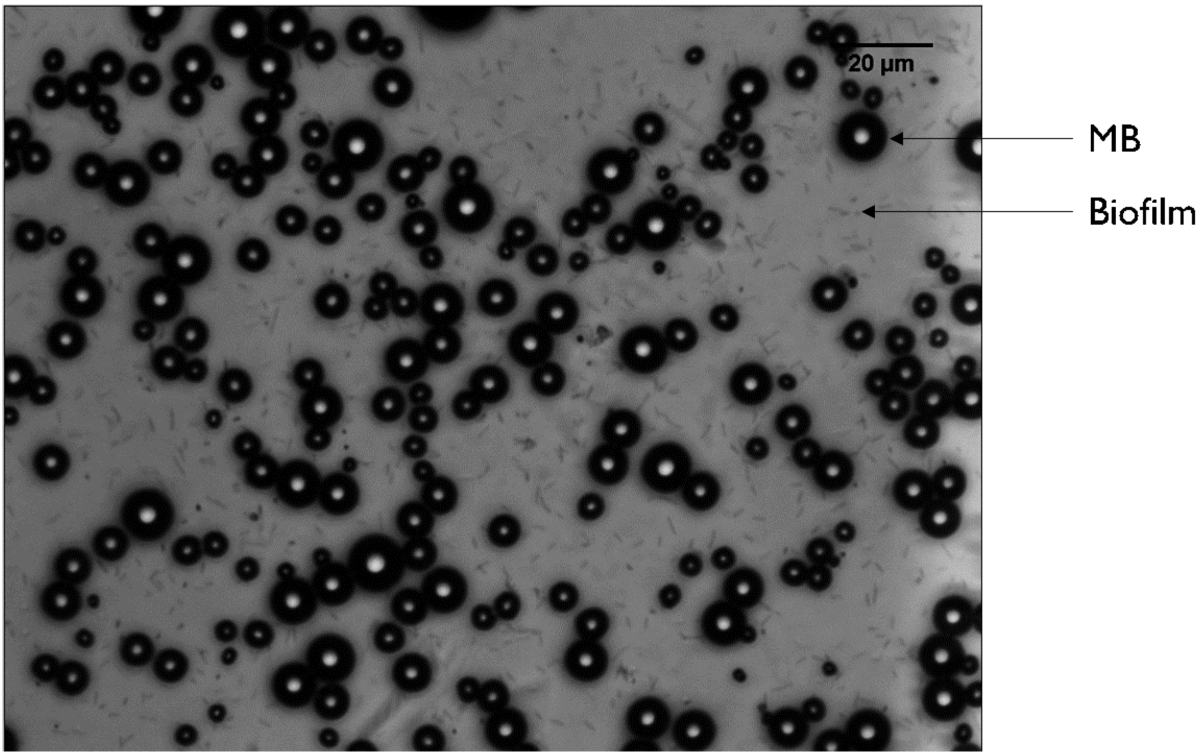

Figure 34 Image of MBs on the surface of the biofilm in the flow cell. The biofilm was grown over 24 hours in the incubator at 37 ˚C. In this case, the biofilm was grown on the acrylic manifold and MBs on the biofilm surface are closest to the glass surface. This provides defined view of the MBs, but provides weak visualisation of the biofilm and its features. In this image specifically, only the planktonic bacterial phase at the most superficial layer of the biofilm was simultaneously visible with MBs.

3.4.3 *Microbubble binding characteristics in static conditions*

In passive testing which involved no flow of fluid into the chamber after MB administration, cationic charged MBs with an air core (DSPC RAMBs$^+$) showed a significant ($P < 0.05$) increase in surface interaction compared to their uncharged counterparts (**Figure 35**). There was approximately a 40% increase in surface associated MBs; when the charged lipid is removed from the shell (DSPC RAMBs), the increase in surface interaction is lost. With NO as the gas core of the MB, any effect of the charged lipid in promoting interaction is removed. For both DSPC NOMBs$^+$ (-25%) and DSPC NOMBs (-65%) there is an apparent repulsion of the MB from a negatively charged surface.

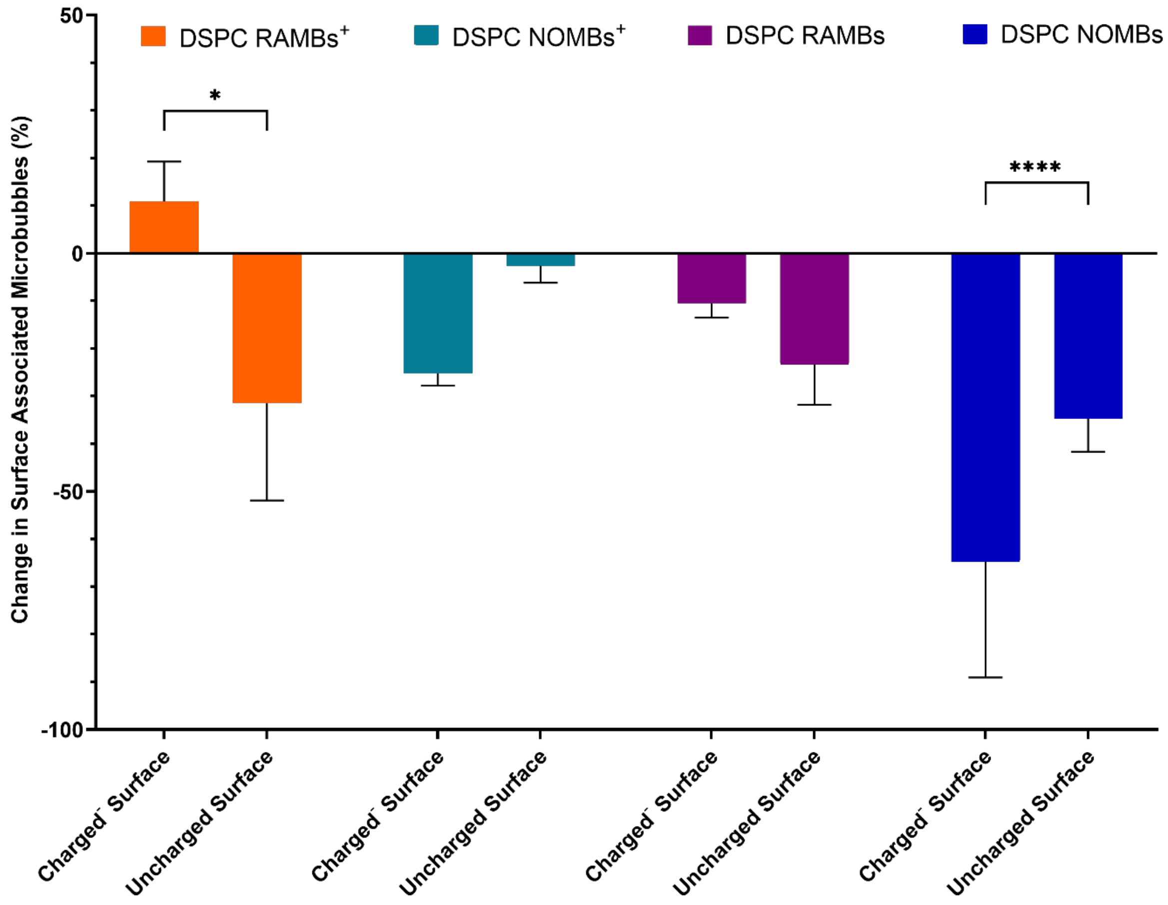

Figure 35 Assessment of the change in surface associated cationic DSPC RAMBs$^+$ and NOMBs$^+$ and their respective uncharged equivalents, after a 60 second interaction with either a negatively charged or uncharged surface. The data shows that the inclusion of the positively charged DSEPC lipid in the shell of DSPC RAMB$^+$, significantly increased the quantity of MBs that can maintain contact with a negatively charged surface by 40%. For both DSPC NOMB and NOMB$^+$ suspensions there was a consistent net-loss of MBs that interacted with either surface, but this loss was increased significantly in the presence of a negatively charged surface. Approximately 65% of NOMBs failed to remain in contact with the negatively charged surface, compared to a loss of 40% from the uncharged surface. This apparent repulsion of NOMBs from the negatively charged surface is mitigated somewhat by the presence of the cationic DSEPC lipid in NOMBs$^+$, of which only 25% were lost from the negatively charged surface and < 10% were lost from an uncharged surface.

3.4.4 *Assessment of MB non-selective binding strength*

A large proportion of RAMBs$^+$ (> 75%) were able to sustain an effective interaction with a negatively charged surface up to wall shear stress values of 0.5 Pa; in contrast when the charged surface is removed there is a substantial loss of RAMBs$^+$ (> 40%) exposed to the same wall shear stress (**Figure 36**). This attests to the relative strength of electrostatic interaction of RAMBs$^+$ with the negatively charged surface. In neutral RAMBs and RAMB$^+$ suspensions, there was no statistically significant difference in their ability to sustain an interaction with either a charged or uncharged surface. Contrary to the findings of static binding experiments NOMBs$^+$ appear better able to maintain an interaction with the artificially charged surface than RAMBs$^+$, however there was no significant difference in between the charged and neutral NOMBs or RAMBs ability to sustain an interaction with the negatively charged surface under increasing wall shear stress (**Figure 37**). At 1 Pa > 90% of RAMBs irrespective of formulation were flushed out of the system, indicative that the non-selective interaction of MBs with surfaces is non-permanent and easily reversible. It should be noted in contrast that at 1 Pa 72.9% of NOMBs$^+$ were still in contact with the negatively charged surface, compared to 41.4% with the uncharged surface. The 10 images used to assess the percentage change in MB surface area covered taken at 50 mm intervals, ensured the full length of the channel was observed in a reliable and repeatable manner between experiments.

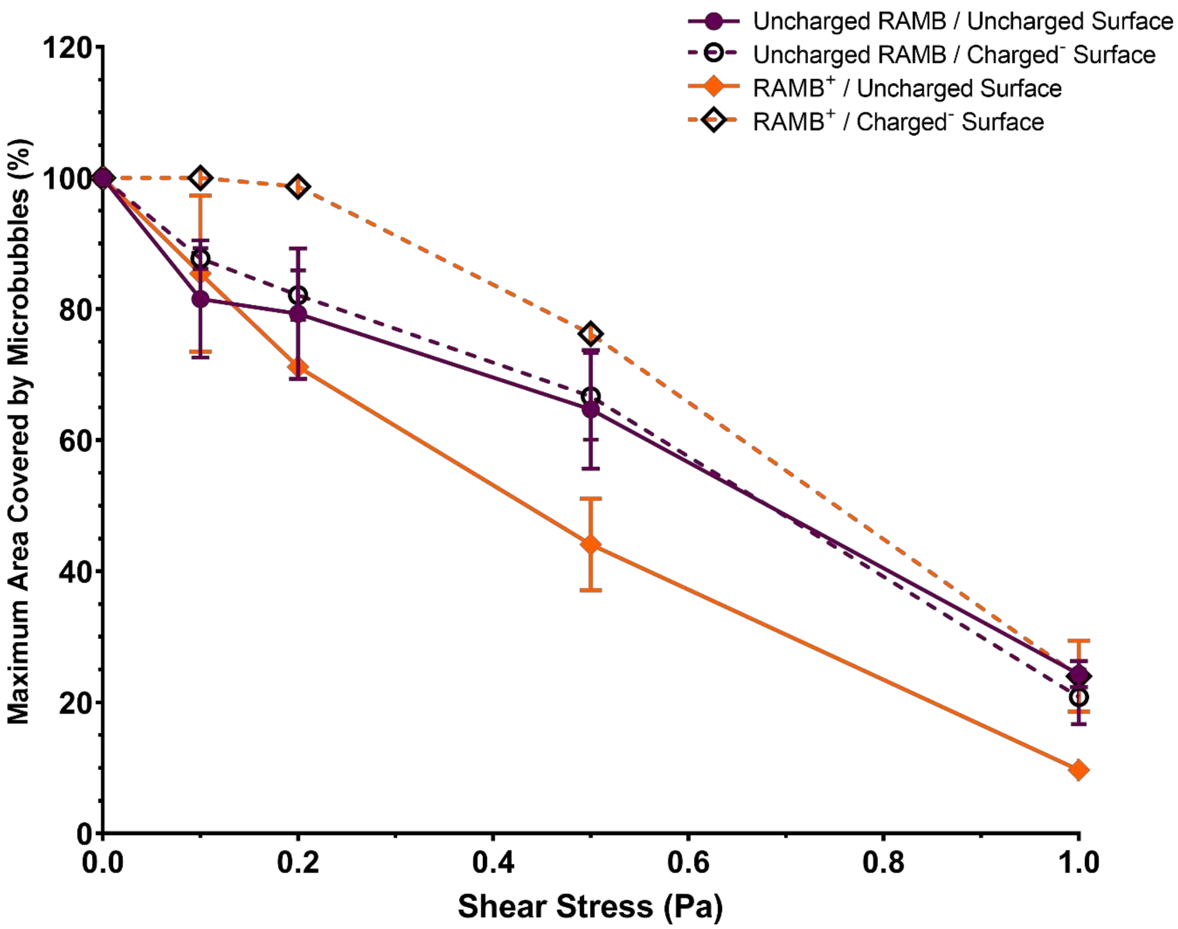

Figure 36 Percentage of maximum area covered by MBs for RAMBs of neutral (9:0.5 DSPC:PEG40s) and cationic RAMB$^+$ (9:0.5:1 DSPC:PEG40s:DSEPC) composition. The total area covered by each MB composition was assessed over 10 images, captured at after the application of incremental wall shear stress values from 0 to 1 Pa. Solid lines represent MB association with the uncharged surface, dashed lines represent MB association with the negatively charged surface. RAMBs$^+$ demonstrated the highest affinity for the negatively charged surface, with no substantial loss of MBs in contact with the surface until wall shear stress values < 0.2 Pa. All values were normalised by taking the percentage value of the area covered by MBs at 0 as the baseline maximum percentage area covered (100%). Error bars represent the standard deviation of the mean.

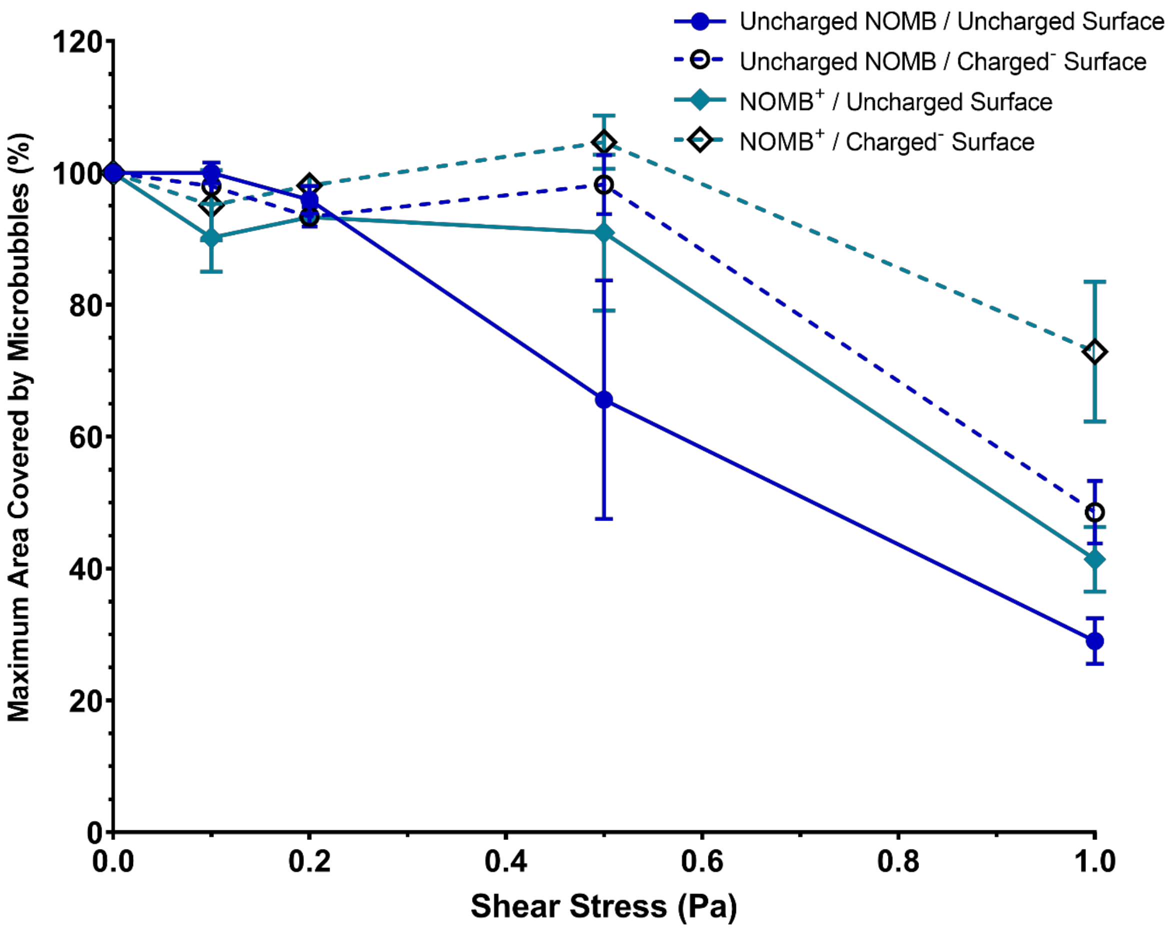

Figure 37 Percentage of maximum area covered by MBs for NOMBs of neutral (9:0.5 DSPC:PEG40s) and cationic NOMB$^+$ (9:0.5:1 DSPC:PEG40s:DSEPC) composition. The total area covered by each MB composition was assessed over 10 images, captured at after the application of incremental wall shear stress values from 0 to 1 Pa. Solid lines represent MB association with the uncharged surface, dashed lines represent MB association with the negatively charged surface. Uncharged NOMBs interacted with the uncharged surface as expected, where there is a rapid decline in MBs associated with the surface in response to wall shear stress < 0.2 Pa. For both NOMB and NOMB$^+$ suspensions there was an accumulation of MBs on the charged surface up to 0.5 Pa, with only 50% and 30% loss respectively in maximum coverage at 1 Pa. All values were normalised by taking the percentage value of the area covered by MBs at 0 as the baseline maximum percentage area covered (100%). Error bars represent the standard deviation of the mean.

3.4.5 *Characterisation of MB interaction with P. aeruginosa biofilms*

Images of biofilms captured with fluorescence microscopy and MBs captured with bright field and epifluorescence microscopy (EVOS, M5000), have been overlaid in ImageJ to provide a comprehensive visual representation of the interaction between MBs and the *P. aeruginosa* biofilm (**Figure 38**). Visual inspection of the interaction between both cationic MBs$^+$ and uncharged MB suspensions with *P. aeruginosa* biofilms and the glass growth substratum, indicated there was a low level of innate MB association to both strata irrespective of net charge. As observed in **Figure 38**A, clusters of MBs were clearly associated with the glass surface of the growth area, but there is no specific interaction with the distinct areas of biofilm growth. In contrast, DBPC$^+$ RAMBs exhibit a significantly ($P < 0.001$) increased quantity of MBs (38%) (**Figure 39**), which appear to be more highly localised and non-selectively bound to areas of biofilm (**Figure 38**B). From visual inspection there also appears to be a positive correlation between the quantity of bound MBs and depth of biofilm growth; specifically that in areas where the biofilm is thicker there is a visibly discernible increase in the aggregation of MBs (**Figure 38**B).

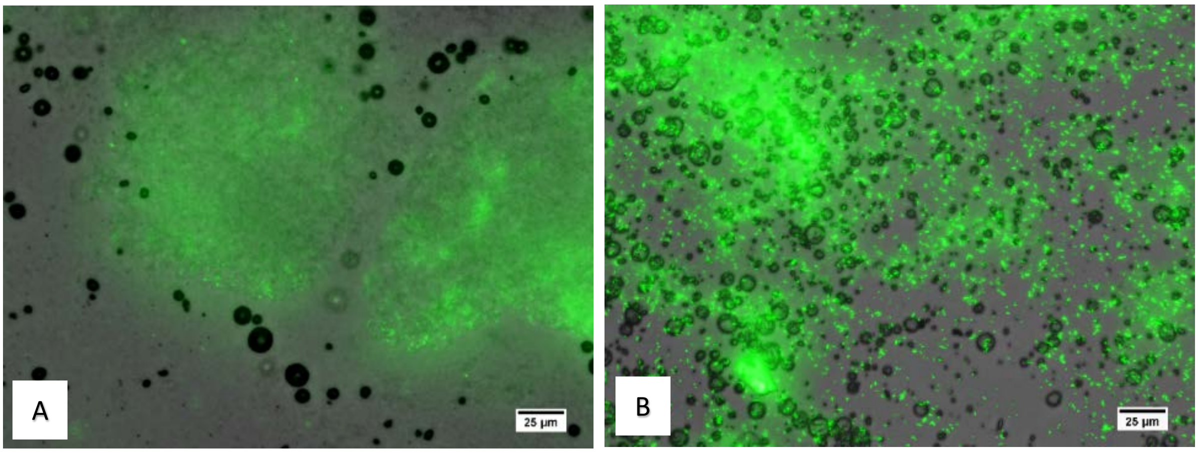

Figure 38 Visual assessment of the interaction between neutral DBPC RAMBs (A) and cationic DBPC RAMBs$^+$ (B) with a *P. aeruginosa* biofilm (stained with Syto9, green). Visual inspection confirms there is an increased level of non-selective binding of cationic DBPC RAMBs$^+$ to defined areas of biofilm growth, compared to a low level of residual uncharged MB interaction with the glass growth surface and little to no association of uncharged MBs to defined areas of biofilm growth.

In this experiment the innate level of uncharged MB interaction with biofilms and growth surface, was on average 10% for uncharged RAMBs and 2% for uncharged NOMBs (**Figure 39**). Sharing consistency with binding experiments conducted in flow cells with an artificially charged surface (**Figure 35**), RAMBs$^+$ exhibit a significantly ($P < 0.001$) increased level of association to the biofilm (38%) compared to all other formulations; with NOMBs$^+$ second most effective (28%). The incorporation of cationic charge into the NOMBs$^+$ shell was shown to significantly increase ($P < 0.005$) their association with the *P. aeruginosa* biofilms and glass substratum, when compared to both uncharged RAMBs and NOMBs. The average decrease in non-selective NOMBs$^+$ binding of 7% compared to RAMBs$^+$, but an average increase in NOMBs$^+$ interaction of 16% and 24% respectively over uncharged RAMBs and NOMBs (**Figure 39**).

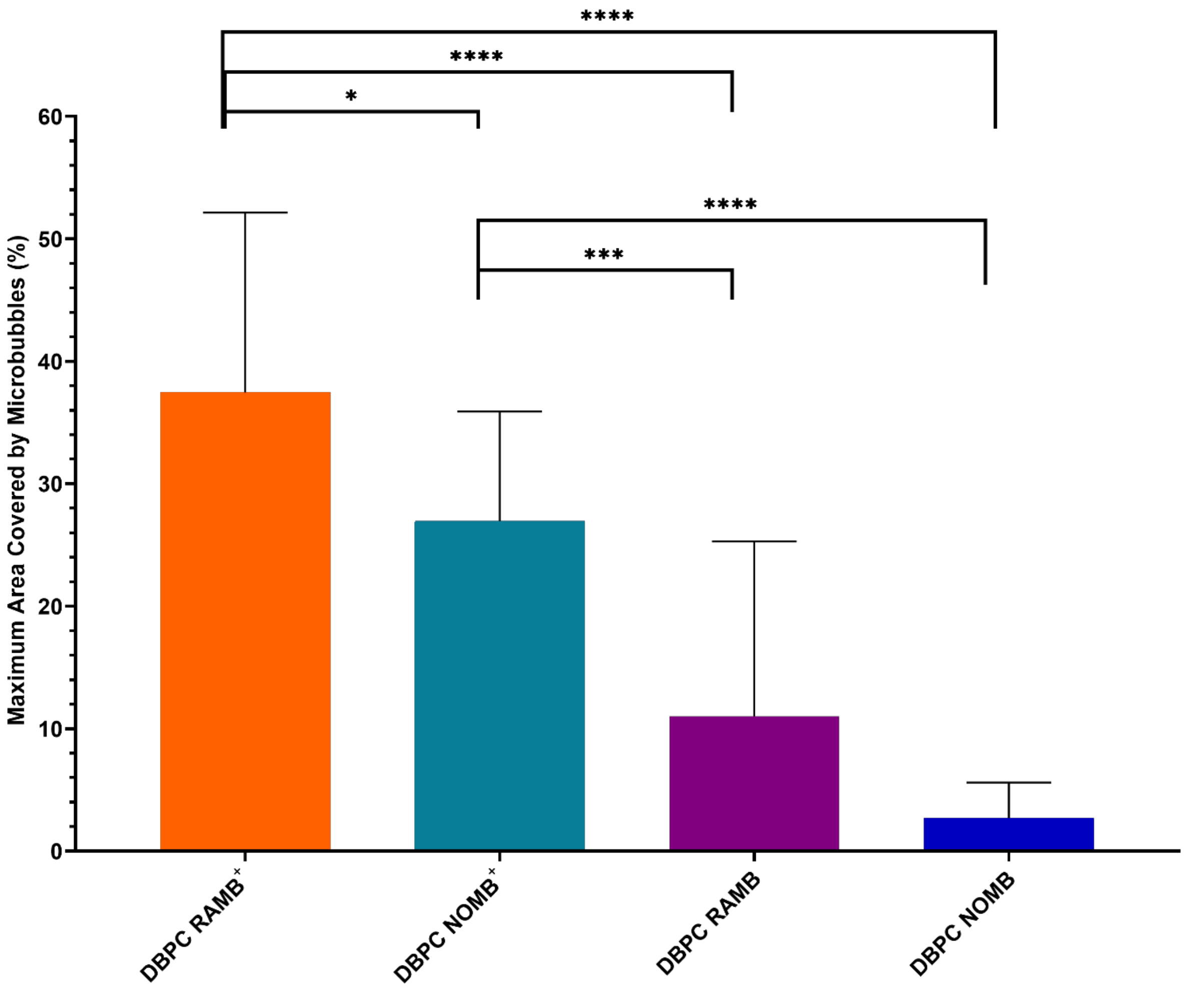

Figure 39 The maximum average percentage area covered by each MB formulation, assessed by analysing three independent biofilm samples for each of the four MB formulations tested. After administration of MBs to biofilms and subsequent washing to remove all MBs with a weak or no association to the biofilms, the average percentage coverage of the remaining MBs was 37% for RAMBs$^+$, 27% for NOMBs$^+$, 11% for uncharged RAMBs and 3% in uncharged NOMB suspensions; error bars report the standard deviation. Quantification of MB coverage was assessed by determining the percentage area that MB formulations covered in each image, which incorporated both MB association to the *P. aeruginosa* biofilms and glass substratum of the Ibidi® dish growth area.

3.5 Discussion

As outlined in Chapter 1 (Section 1.1.3), biofilms present a multifaceted challenge to achieving a positive therapeutic outcome in chronic infections, principally due to their competency as a physicochemical barrier to treatment (Ciofu *et al.*, 2017; Carniello *et al.*, 2018). Growing research suggests that the targeted delivery of antimicrobial agents to biofilms may increase their therapeutic potential (Palmioli *et al.*, 2019; Sharma *et al.*, 2019; Meiers *et al.*, 2020), by increasing their local concentration to overcome the biofilms innate tolerance and reducing the negative peripheral side-effects of antimicrobial therapy (De Gunzburg *et al.*, 2018; Heta and Robo, 2018). However, due to the heterogeneity of the EPS that constitutes the extracellular matrix of the biofilm, the identification of an appropriate, commonly expressed target receptor has proved challenging (Palmioli *et al.*, 2019). One potential ligand target present in the biofilm matrix of clinically significant biofilms such as *P. aeruginosa* are lectins (Sommer *et al.*, 2017); lectins play an important role in mediating initial bacterial adhesion to surfaces for biofilm formation, and subsequent polysaccharide cross-linking in the extracellular matrix of biofilms (Johansson *et al.*, 2008). A significant limitation of this method of biofilm targeting however, is that lectin receptors have a very weak natural affinity for their natural carbohydrate ligands; making them a difficult target in an already impervious structure (Wagner *et al.*, 2017; Meiers *et al.*, 2020). The affinity that a ligand has for the intended receptor suffers from high variability across biological systems, this is therefore a widespread issue for ligand-receptor mediated specific targeting (Takalkar *et al.*, 2004). Due to the challenges in current research on specific ligand-receptor mediated targeting of bacterial biofilms, it was the aim of this research to validate the use of a non-selective means of targeting the bacterial biofilm. The ubiquitous presence of negatively charged extracellular DNA and polysaccharide constituents of the biofilm extracellular matrix and highly negatively charged bacterial cell components such as teichoic acids and lipopolysaccharides (Renner and Weibel, 2011; Harper *et al.*, 2019), confer a net negative charge upon bacterial biofilms. It has been demonstrated that *P. aeruginosa* biofilms have a zeta potential in the range of -20 mV (Khelissa *et al.*, 2019). We hypothesised that cationic MBs could therefore be utilised as a non-selective means of targeting bacterial biofilms, to achieve greater local concentrations of MBs associated with and proximal to the biofilm to increase the efficacy of the proposed ultrasound mediated therapy.

In order to assess this research aim, a flow cell was designed where a glass or quartz surface could be bonded to an acrylic manifold (**Figure 28**). To provide an effective level of support to the fragile (170 µm) glass surfaces used in these experiments required to allow microscopy, the manifold selected was 6 mm thick clear acrylic. This allowed each flow cell to be optically transparent, produced rapidly and precisely by laser cutting and cost effective at £0.83 per flow cell. Aqueous solutions in contact with a solid surface can create charge on the solid surface, depending on the composition of the solid material and chemical properties of the solution; zeta potential can be used as a measure of the relative charge created at this surface (Ginés *et al.*, 2017). Borosilicate glass coverslips bonded to the acrylic manifold created a surface that does not create or sustain a charge, made them a suitable representation of a neutrally charged surface. A quartz surface in contact with PBS at pH 7.4 has been shown to create a zeta potential in the range of -40 mV (Abaka-Wood *et al.*, 2017), which provides a valuable artificial control for an surface with a negative electrostatic charge.

The artificially anionic and neutral environments that were created in the flow cells, formed an essential proof of concept to determine the baseline ability of cationic MBs to interact with a negatively charged surface. It was important to first characterise this interaction in an environment that is static and can be controlled, to best establish if there could be an effect before moving into more complex biological testing on biofilms. This characterisation of interaction focused on inducing contact between RAMBs$^+$, RAMBs, NOMBs$^+$ and NOMBs and either a negatively charged or uncharged surface, then by inverting the device creating ideal conditions for weakly associated MBs to passively float away from the surface. As this method is carried out using smooth surfaces with augmented charge, it strictly accounts for the MB association induced by electrostatic forces only. This is an important assessment as it provides a baseline for the efficacy of incorporating charge as a means of non-selective targeting, without overestimation in the data caused by MB trapping at the surface due to variations in topography intrinsic to biological samples. It is a limitation of this research that the zeta potential of the cationic MB suspensions were not assessed, as this would directly determine the relative charge associated with the MB. However, highly comparable research that has produced MBs with the same sonication method, lipid composition and molar ratios utilised in this work, assessed their cationic MBs had a zeta potential of approximately +25 mV (Owen *et al.*, 2018). An indicative assessment of cationic MB charge was carried out by Delalande *et al.,* (2017); the most frequently reported range of MB charge was +15 mV to +40 mV, however the highest reported charge of +60 mV was also for a DSTAP:DSPC:PEG40s lipid shelled MB used in gene delivery to skeletal muscle.

The flow cell was tested for any potential leakage, with both the quartz and borosilicate glass cover slip bonded to the acrylic manifold. Our assessment verified that the flow cells could maintain the integrity of the fluid channels i.e. did not leak, up to volumetric flow rates of 25 mL/min. This provided confidence that the flow cells could be sustain continuous flow over time, given that the typical flow rates used in these experiments were a maximum of 1 mL/min. As the biocompatibility of the flow cells was assessed for the growth of *P. aeruginosa* biofilms, the leakage tests also verified that there was very little risk of biohazardous material escaping from the flow cell. Due to the limitations of the microscope used in the initial phase of this research, simultaneous visualisation of MBs and biofilms was not possible. Therefore, the flow cell was only utilised as a means of providing a smooth surface with a neutral or anionic charge, for the investigation of cationic MB interaction under i) static conditions to assess the level of passive electrostatic induced and ii) flow to determine relative binding strength of the interaction.

The data for static interaction of RAMBs$^+$ provide an excellent insight into the efficacy of charge as a means of non-selective binding; there is a significant increase of > 40% in RAMBs$^+$ associated with the negatively charged surface compared to the uncharged surface, which affirms that the observed effect is due to interaction of the cationic MB and anionic surface (**Figure 35**). Uncharged RAMBs display no significant percentage increase in MBs associated with the charged surface compared to the uncharged surface. This provides evidence that the non-selective binding effect is explicitly caused by the incorporation of DSEPC in the MB^+ shell. Given this evidence that DSEPC cationic MBs promote electrostatic interactions with anionic surfaces, it appears anomalous that there should be a greater loss of $NOMBs^+$ from the negatively charged surface compared to the uncharged surface. It was hypothesised than an NO specific mediated interaction was causing interference with the charged interactions, consequently reducing the binding efficacy of the charged MBs, as discussed below. Evidence for this effect is abundantly clear in the data for the interaction of uncharged NOMBs with negatively charged surfaces; there is a highly statistically significant difference between the number of $NOMBs^+$ lost from the negatively charged surface compared to the uncharged surface. It would therefore appear that the presence of DSEPC effectively mitigates the repulsive effect seen in MBs with an NO core from anionic surfaces, since 40% more DSPC $NOMBs^+$ remain in contact with the charged surface than DSPC NOMBs (**Figure 34**).

The relative strength of the electrostatic interaction between cationic MBs and an anionic surface, was assessed by exposing MBs in a flow channel to increasing levels of wall shear stress from 0.1 to 1 Pa by altering the volumetric flow rate through the channel (**Table 5**). Takalkar *et al*. (2004) demonstrated that wall shear stress values up to 0.06 Pa could promote binding, however there is a decline in attachment after this point. We hypothesised that in a similar manner, we would observe a decline in surface associated MBs in response to increasing shear stress. It was confirmed that the dissociation of MBs from both charged and neutral surfaces was less pronounced at shear stress values up to 0.5 Pa, but occurred more rapidly from 0.5 Pa to 1 Pa for all formulations (**Figure 36**, **Figure 37**). In our investigation, both $RAMBs^+$ and $NOMBs^+$ were able to remain in contact or continue accumulating on the negatively charged surface up to shear stress values of 0.2 Pa and 0.5 Pa respectively. This result would suggest that in comparison to studies that have assessed the binding strength of ligand-targeted MBs under increasing wall shear stress, the electrostatic interaction induced here can withstand a greater level of wall shear stress before initial detachment begins (Rodgers *et al.*, 2000; Takalkar *et al.*, 2004). These findings are directly concurrent with work carried out by Edgeworth *et al.*, (2010), who demonstrated that MBs electrostatically attached to a surface remained up to wall shear stress values of 0.66 Pa. However, in these experiments RAMBs$^+$ and NOMBs$^+$ were reduced by approximately 90% and 30% respectively of their maximum coverage surface at a wall shear stress of 1 Pa (**Figure 36**, **Figure 37**), whereas ligand-receptor targeted MBs have been shown to withstand wall shear stress conditions up to 50 Pa (Edgeworth *et al.*, 2010). It is important to note however, that this may not be an accurate representation of the MB binding and detachment kinetics that would occur *in vivo.* As most studies can only estimate the local site density of the target receptor, there may be a significant over or under-estimation in the data. For example, Takalkar *et al.,* (2004) who modelled their ligand-binding

In both static interaction testing RAMBs$^+$ were able to bind most consistently to negatively charged surfaces compared to all other formulations, as there was a consistent net loss of NOMB$^+$ from negatively charged surfaces. In all experiments carried out in this research involving the NOMBs and negatively charged surfaces, there has been a clear repulsion effect of the MB from the surface compared to RAMBs. Although NO is a highly reactive molecule due to the presence of an unpaired electron, is not an anionic molecule in either the gas or solution phase (Chacko and Wenthold, 2006). However, under physiological and environmental conditions the bioactivity of NO is limited by its oxidation to the stable anionic products nitrite (NO^{2-}) and nitrate (NO^{3-}), with nitrate being the prevailing oxidation product formed (Weitzberg *et al.*, 2010). As demonstrated in other research it is highly likely that the repulsion of NOMBs from negatively charged surfaces seen in these experiments, is caused by the accumulation of the anionic products NO^{2-} and NO^{3-} in solution (Choi *et al.*, 2001; Mautner *et al.*, 2017; John *et al.*, 2018). The exception to this effect seen in experiments conducted under flow to assess NOMB binding strength (**Figure 37**), is likely due to the flow of PBS facilitating removal of oxidised products of NO; thereby reducing the concentration of negative ions in the fluid and mitigating their interference with binding. Building on this assumption, it would seem plausible that the loss of NO from NOMBs by oxidation would render their utility as a means of inducing dispersal in biofilms is invalidated. However, in delivering a solution that invariably contains the oxidative products of NO, we provide bacterial cells within the biofilm with an important source of nitrate that can be recycled to form NO via bacterial nitrate reductases (Lundberg *et al.*, 2008).

Research in this area has explored the inherent antimicrobial effects of nitrite in solution (Weitzberg *et al.*, 2010); this has been demonstrated in cystic fibrosis models of *P. aeruginosa* infection, where a 3-log reduction in bacteria was seen after a four-day prolonged exposure to 15 mM nitrite (Sang *et al.*, 2006). Further research *in vitro* has shown that the conversion of nitrite to NO is potentiated in the presence of ascorbic acid, which is produced by clinically important species of bacteria such as *P. aeruginosa* and *S. aureus* and results in enhance bactericidal activity (Carlsson *et al.*, 2003; Bremus *et al.*, 2006). Importantly, the impact of providing bacterial biofilms with sources NO^{3-} that can be reduced endogenously to NO by aerobically grown *P. aeruginosa* biofilms has been characterised by Barraud *et al.,* (2006)*,* who have shown that low concentrations (100 nM to 1 µM) of endogenous NO can induce biofilm dispersal. The presence of nitrite and nitrate in the effluent of biofilms is usually only present in mature biofilms > 5 days old, at which point the endogenous production of NO induces dispersal of the biofilm architecture (Barraud *et al.*, 2006). Therefore, by providing biofilms with an abundant source of nitrite and nitrate in the NOMB solution, there will be a corresponding upregulation in denitrification and endogenous production of NO to more rapidly induce a major biofilm dispersal event. The expedited endogenous production of NO in biofilms for dispersal, may prove to be an interesting avenue of exploration for future work in this area.

Though the flow cells provided a valid and essential initial assessment of cationic MB interactions with charged surfaces, to be able understand the interaction between cationic MBs and biofilms more comprehensively they were not fit for purpose. Due to the difficulty in analysing biofilm architecture and MBs simultaneously and a lack of translational applicability in terms of how MB suspensions would be applied clinically, biofilms were instead grown in Ibidi® micro dishes that feature a 170 µm thick glass coverslip growth area. This provided a means to grow biofilms on a surface where MB suspensions could be applied topically, under clinically relevant conditions. It should be noted that there is a change in MB formulation used in these experiments from DSPC:PEG40s:DSEPC to

DBPC:PEG40s:DSEPC; this decision was made based on information gathered on the stability of different MB formulations (Chapter 2, Section 2.3.1.3), which was not available during initial testing of cationic MBs. DBPC shelled MBs were identified as the most stable formulation for the delivery of NO in this research, it was therefore most appropriate to assess the non-selective interaction between cationic MBs and biofilms with this formulation.

The data presents the percentage area occupied by MBs in microscopy images (**Figure 39**), which were retained after a three step washing process to remove all weakly associated MBs. This data was averaged across three independent biofilms, to demonstrate consistency in MB binding regardless of biofilm topography. The data shares a strong correlation with the effects observed in flow cell experiments; RAMBs$^+$ exhibit a significantly ($P < 0.001$) increased level of non-selective association with the biofilm (38%) compared to all other formulations, with NOMBs$^+$ second most effective (28%) (**Figure 39**). The assessment of MB coverage as a proportion of the total area in the image was assessed, as opposed to limiting the analysis to only the percentage area of the biofilm covered by MBs. Though this includes MBs non-selectively interacting with the glass surface of the growth area, it provides a more accurate presentation of what is likely to occur *in vitro*. By not eliminating MBs that were peripheral to the biofilm but not directly associated, we gain a better understanding of the innate level of MB retention due to varied surface topography. Moreover, even though they are not directly associated with the biofilm, proximal MBs may still have a significant impact on the overall efficacy of treatment due to the cavitation regimes induced upon administration of ultrasound (Ferrara *et al.*, 2007; Stride and Coussios, 2009; Kooiman *et al.*, 2014). Specifically, microstreaming velocity fields induced by cavitation may potentiate local drug delivery by imparting greater shear stress on the biofilm, to increase permeability and induce mixing of the fluid (Leighton, 2007; Pereno *et al.*, 2020). As demonstrated by Pereno *et al.*, (2018), microstreaming velocities can peak in the order of 1000 µm/s and be maintained at 100 µm/s, at distances > 1 mm from the source MBs cavitating in response to a 1 MHz ultrasound stimulus. It is important to note that the reduced number of surface associated NOMBs in this experiment, provides further support to the hypothesis developed in flow cell experiments; that there is a net repulsion between MBs with a NO core and surfaces with a net negative charge i.e. biofilms in this experiment. Evidence to support this can be seen in the significant increase ($P = <0.0001$) in NOMB$^+$ binding to biofilms compared to their uncharged counterparts; it can thus be hypothesised that the positive charge of the lipid in this instance is aiding the MB in overcoming the effect of NOMB repulsion from the biofilm. There is still a significant change amount of NOMBs$^+$ bound to biofilms when compared to uncharged RAMBs ($P = <0.0005$) and NOMBs ($P = <0.0001$), which only cover a maximum surface area of 10% and 2% respectively (**Figure 39**). This data coupled with the significant difference ($P = <0.05$) between NOMBs$^+$ and RAMBs$^+$, adds credence to the claim that the cause of this apparent repulsion is NO or more specifically its anionic oxidised products.

3.6 Conclusion

The aim of this phase of the study was to investigate the feasibility of using cationic MBs to induce non-selective targeting of RAMBs and NOMBs to bacterial biofilms. This work is to the best of the authors' knowledge, the first to consider the use of cationic MBs as a means of non-selective targeting of bacterial biofilms. The research aims were achieved by assessing the binding affinity and strength of cationic MBs to neutral and artificially charged surfaces under static and dynamic conditions, within a flow cell capable of augmenting surface charge that was developed in this research to facilitate the study of these interactions in a controlled manner. Subsequent testing demonstrated the efficacy of cationic MBs in significantly enhancing MB contact, when applied directly to a *P. aeruginosa* biofilm.

The use of electrostatic interactions for facilitating targeted drug delivery has been considered successful in other research, with the principal aim of creating a 'reservoir' of drug carriers proximal to the target area (Bajpayee and Grodzinsky, 2017). As the topical application of MBs is the principal means of administration considered by this research, it can be concluded that cationic MBs have the ability to increase proximity, promote and sustain contact with negatively charged substrates such as biofilms.

An unexpected effect observed throughout these experiments was that NOMB suspensions exhibit an innate level of repulsion from both artificial and biological anionic surface; cited research on the physiochemical interactions of NO and its oxidised products NO^{2-} and NO^{3-} in solution has provided an insight into most probable cause of this effect. The use of a cationic lipid in the shell of $NOMBs^{+}$, appears to have a significant mitigating effect on the repulsion between the anionic products of NO oxidation and negatively charged surfaces.

CHAPTER IV

4 PASSIVE INTERACTION AND ACTIVE ULTRASOUND STIMULATION OF BIOACTIVE MICROBUBBLES FOR THE DISPERSAL AND TREATMENT OF BACTERIAL BIOFILMS

4.1 Introduction

Bacterial biofilms are an ever-growing concern for public health, featuring both inherited genetic resistance and a conferred innate tolerance to traditional antibiotic therapies. Consequently, there is a growing interest in novel methods of drug delivery, in order to increase the efficacy of antimicrobial agents. One such method is the use of acoustically activated MBs, which undergo volumetric oscillations and collapse upon exposure to an ultrasound field. This facilitates physical perturbation of the biofilm and provides the means to control drug delivery both temporally and spatially. Consequently, acoustically stimulated MBs may have the capacity to enhance the efficacy of antibiotics, reducing the dosage required to achieve successful treatment. This work specifically seeks to evaluate the therapeutic efficacy, of the novel ultrasound responsive agents developed as part of the wider scope of this research. The anti-biofilm and bactericidal effects of neutral RAMBs and NOMBs as well as cationic RAMBs$^+$ and NOMBs$^+$, are evaluated with cell viability assessments and fluorescence imaging techniques using relevant pathophysiological models of biofilm infection. Recent research has begun to characterise the bactericidal efficacy of NOMBs in planktonic bacterial suspensions (Lafond *et al.* (2020), however to the best of our knowledge, there are currently no acoustically stimulated NOMBs that have been applied to the treatment of biofilms *in vitro* or *in vivo.* Consequently, there is currently no evidence on the efficacy of NOMBs as a means of inducing biofilm dispersal or potentiating bactericidal activity in biofilms.

The experimental work on biofilms in this research has been carried out using *P. aeruginosa* (PA01), principally because it is used extensively as a model organism of opportunistic Gram-negative infection (LaBauve and Wargo, 2012). It is particularly relevant to this research, as *P. aeruginosa* and *S. aureus* are the most commonly isolated biofilm-forming pathogens from chronic wounds (Banu *et* *al.*, 2015; Bessa *et al.*, 2015). As *P. aeruginosa* exhibits a range of virulent phenotypes and is subject to rapid growth over a period of 24 hours, it is a dynamic and representative single-species biofilm model of infection. Previous studies have shown that *P. aeruginosa* responds well to NO induced dispersal (Howlin *et al.*, 2017), making it a useful model to validate the utility of NOMBs. This is an important step in achieving one of this project's aims; i.e. to validate the therapeutic potential of NOMBs in a complex model of chronic infection. By first establishing how NOMBs interact with single species biofilms, the formulation of the ultrasound responsive NOMBs can be refined to ensure it is as efficacious as possible. The optimised NOMB can then be applied in testing more complex, multi-species biofilm models of chronic wound infection, to bring this work closer to a clinically relevant application. One prospective model incorporates the most commonly pathogenic species of bacteria isolated from chronic wounds, such as *Klebsiella pneumoniae*, *P. aeruginosa, S. aureus* and *Enterococcus faecalis* (Touzel *et al.*, 2016). Whilst this is an established multi-species biofilm model, there is no model that can fully incorporate the dynamic and complex interactions within the microenvironments and functional equivalent pathogroups of a polymicrobial biofilm.

4.2 Statement of objectives

This chapter will investigate the therapeutic efficacy of the ultrasound responsive agents developed in Chapters 2 and 3, to determine the potential and efficacy of their associated anti-biofilm and bactericidal effects. This chapter will outline the development and importance of implementing a pathophysiologically relevant wound constituent medium, for *in vitro* growth of biofilms with morphological and phenotypic characteristics comparable to *in vivo* wound biofilms.

4.3 Materials and methods

4.3.1 *Method's rationale*

The interaction between RAMBs and NOMBs and *P. aeruginosa* biofilms in this study has been assessed in a number of ways, including the application of MBs to biofilms in the presence and absence of ultrasound (hereby referred to as 'active' and 'passive' testing, respectively). In order to characterise the biological effect of NOMBs in passive testing, biofilms were grown in a microtiter plate for quantification by crystal violet biomass staining (O'Toole, 2011). This is perhaps the most extensively used high-throughput observational method of biofilm formation, especially for the simultaneous and rapid testing of various treatments (Coffey and Anderson, 2014; Ommen *et al.*, 2017). Crystal violet was used to determine early biofilm biomass, as it remains one of the most simple but reliable methods of total biomass quantification *in vitro* (Stiefel *et al.*, 2016). Crystal violet binds to negative charges, as such it binds to both bacterial cells and the EPS of the biofilm providing an indication of biomass (Kwasny and Opperman, 2010). Unlike fluorescent live/dead stains, such as SYTO9 and propidium iodide, crystal violet is not capable of differentiating between viable and dead bacteria (Beveridge, 2001). Consequently, this would suggest that values attained by this staining method, are potentially an overestimation of total biofilm biomass (Stiefel *et al.*, 2016).

Active testing to obtain preliminary data on the efficacy of different RAMB and NOMB formulations was carried out the purpose built 'biofilm on a coupon sonication' (BOCS) system (Appendix A – Supplementary experimental material 6.1.7), the device design and manufacturing is described in paragraph 6.1.7.1 and acoustic calibration is outlined in Appendix A, paragraph 6.1.5. Although the BOCS system was fully characterised and fit for its intended purpose and very economical to fabricate, however the handling of samples, device set-up and ease of use were labour intensive and time consuming tasks. In preliminary active testing biofilms were grown in a Centre for Disease Control (CDC) bioreactor in a nutrient broth, though this is a well-established and reliable method of growing biofilms *in vitro* it was not the most applicable to this research. Wound constituent media (WCM) was developed to more accurately reflect the pathophysiological conditions of a chronic wound, biofilms were grown in static conditions to more accurately simulate the stagnant environment of a wound. Another development from BOCS preliminary testing to SAT testing, was the refinement of the MB administration process and acoustic parameters used. A summary of parameters assessed in preliminary experiment, which lead to the ultrasound stimulation methodology assessed here is shown in **Table 7** (Appendix A – Supplementary experimental material, paragraph 6.1.8). Due to the development of NOMBs in this research and refinement of the MB composition key developments include: a reduction in passive incubation period of MBs in a volumetric ratio of 1:5 from 15 minutes to 60 seconds, and reduction in ultrasound exposure time from 5 minutes (1 MHz, 25% duty cycle, 100 kHz PRF, 0.5 MPa) to 40 seconds (0.9 MHz, 20% duty cycle, 500 Hz PRF and 0.5 MPa). The increase in PRF in these experiments can be linked to the suspected increase in the proportion of inertial cavitation and microbubble collapse, and a decrease in the stable cavitation likely to be present and sustained over a longer period of time in preliminary experiments. To facilitate both visualisation of biofilms by fluorescence microscopy and physical enumeration of culturable cells by CFU quantification, biofilms were grown in Ibidi® dishes using the refined WCM. This was also a necessary transition into using a newly developed ultrasound stimulation system for acoustic transfection (SAT), which is a highly simplified means of stimulating MBs for biofilm treatment as there is a single removable component for loading sampled. The design of this device and acoustic characterisation are fully defined in paragraph 4.2.4 and Appendix A, paragraph 6.1.6 respectively.

4.3.2 *Crystal violet biomass stain to assess the passive effect of MBs on a P. aeruginosa biofilm*

A sterile inoculating loop was used to select three identical colonies of *P. aeruginosa* (PA01), grown on *Pseudomonas* isolation agar (17208, Sigma-Aldrich). The colonies were inoculated into 5 mL of tryptone-soy broth (22092, Sigma-Aldrich), and incubated at 37 °C overnight. A *P. aeruginosa* (PA01) biofilm was formed on a 96-well microtiter plate (12088528, Fisher Scientific) by diluting the overnight culture to 1:100 (v/v), and transferring a 150 µL aliquot into each well before incubating at 37 °C for

24 hours. In this experiment the average of six wells was used to constitute one replicate, peripheral wells that did not contain culture were filled with 200 µL of sterile deionised water. The planktonic suspension was aspirated from each well after 24 hours, each well was then washed twice with 200 µL of sterile PBS to remove any remaining unadhered cells. A 200 µL suspension of RAMBs, NOMBs or sterile PBS (control) was added to wells containing biofilm, after one hour each well was washed again with 200 µL of sterile PBS. A 200 µL solution of 1% (v/v) aqueous crystal violet was applied to each well for 15 minutes; excess stain was removed by washing all wells three times with sterile water. Once dry, a 30% (v/v) acetic acid solution (11463473, Fisher Scientific) was applied to each well for 30 minutes, to solubilise the bound crystal violet (Pro-Lab Diagnostics™, PL8000). A 100 µL sample was taken from each well containing solubilised crystal violet and transferred to a new 96-well plate, 100 µL of 30% acetic acid was also added to six wells to act as a blank. The absorbance of the solubilised crystal violet was measured at 584 nm using a plate reader (FLUOstar Omega, BMG Labtech), this data was analysed and plotted using Prism7 (GraphPad).

4.3.3 *Development of an artificial wound constituent medium for growth of P. aeruginosa biofilms*

Planktonic growth and biofilm development of *P. aeruginosa* was assessed with the base media Bolton broth (BB) (67454, Millipore), Lysogeny broth (LB) (L3152, Supelco) or TSB, supplemented with laked horse blood (LHB) (SR0048C, Oxoid) and plasma (P4639, Bovine Plasma, Sigma-Aldrich). Each base media was prepared to 2X concentration, which was supplemented with 10% (v/v) LHB. Citrated plasma was rehydrated in sterile water, standard concentrations of 100%, 80%, 60%, 40%, and 20% were prepared by subsequent dilution in sterile water. For each base media BB, LHB or TSB supplemented with LHB, 75 µL was combined 1:1 with a plasma standard on a 96-well plate, for a total volume in each well of 150 µL. The addition of plasma to each LHB supplemented media provided the final concentrations per well of 5% LHB and 10% - 50% plasma in BB, LHB or TSB. Control wells consisted of LHB alone, plasma alone and BB, LB or TSB alone; with additional controls for each base media supplemented with 5% LHB only (plasma negative control), or supplemented with 10% - 50% plasma only (blood negative control).

To assess growth in each media and control an overnight culture of *P. aeruginosa* was adjusted to an optical density of 0.1 determined by absorbance of 600 nm; 1 µL of the adjusted inoculum was pipetted into each well. The plate was incubated in a plate reader at 37°C with optical density readings taken at an absorbance of 600 nm every 60 minutes for 18 hours. The early biofilm development in each media and control was assessed by crystal violet staining as outlined in 4.2.2. Briefly, the planktonic suspension was aspirated from all wells before each well was washed thrice with sterile PBS to remove any non-adherent material, the biomass within each well was stained with 1% (aq) crystal violet for 15 minutes and solubilised in 30% acetic acid for 30 minutes before the absorbance was measured at 580 nm blanked against the absorbance of 30% acetic acid alone. All growth and biomass analysis was conducted in triplicate.

4.3.4 *Ultrasound stimulation of NOMB and RAMB formulations for P. aeruginosa biofilm treatment with SAT*

Building on the work carried out as part of preliminary investigations on the effect of RAMB and NOMBs on *P. aeruginosa* biofilms, this section of work oversaw the development of a number of methodological approaches. This includes the implementation of WCM for physiologically representative biofilm growth, ultrasound stimulation with SAT and the assessment of both cationic and neutral MBs effect on biofilm surface area coverage by fluorescence microscopy and cell death assessed by viable cell counts.

4.3.4.1 **Growth of *P. aeruginosa* biofilms for SAT ultrasound stimulation**

P. aeruginosa biofilms were grown in Ibidi® dishes (ibiTreat, µ-Dish 35 mm, Polymer coverslip bottom, Thistle Scientific) containing 1500 µL of WCM, by inoculating the centre of a 1 cm^2 area previously coated in a 50 µg/mL fibronectin (F1141-1MG, Fibronectin from Bovine Plasma, Sigma Aldrich) with 10 µL of an overnight suspension of *P. aeruginosa* diluted 1:100 (**Figure 40**). After growth and biofilm development over 48 hours in at 37 °C as described in section 4.2.3, the WCM was aspirated from the Ibidi® dish and biofilms were washed three times with sterile PBS, to remove any planktonic or weakly attached cells from growth area.

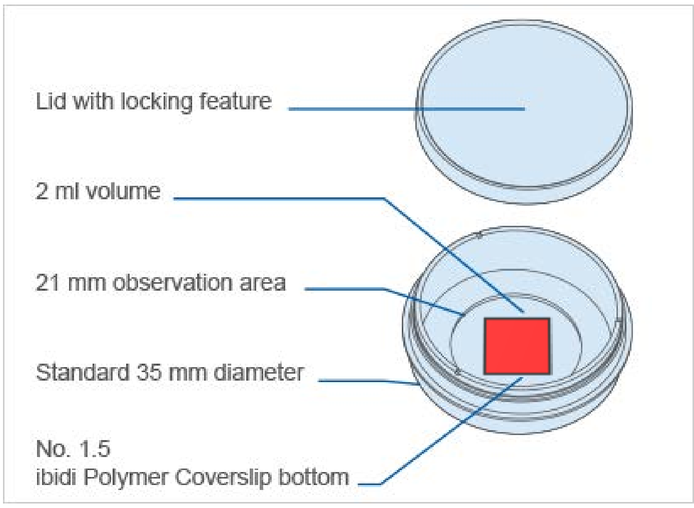

Figure 40 Technical specifications of the Ibidi® dish used for growth of biofilms in SAT experiments, adapted from Ibidi.com. The red box indicates a 1 cm^2 area around the centre point of the growth area; this was used to ensure pre- and post-treatment fluorescence microscopy images were captured at identical positions.

4.3.4.2 MB fabrication

Four MB formulations were assessed in this research; DBPC:PEG40s shelled RAMB and NOMBs, and DBPC:PEG40s:DSEPC shelled $RAMB^+$ and $NOMBs^+$. The specific fabrication of these MBs is fully outlined in Chapter 2, sections 2.2.2 and 2.2.3 respectively.

4.3.4.3 Treatment parameters assessed

P. aeruginosa biofilms were exposed to two principal treatment conditions: i) Ultrasound stimulated MBs only, and ii) Ultrasound stimulated MBs with a 4 µg/mL sub-inhibitory concentration of the antibiotic gentamicin (G1397, Gentamicin solution, Sigma Aldrich). For application to biofilms all MB formulations were diluted in a 1:5 volumetric ratio with either i) sterile PBS, for ultrasound stimulated MBs only tests, or ii) 1:5 in sterile PBS containing 5 µg/mL gentamicin; resulting in a final antibiotic concentration of 4 µg/mL once combined with MB suspension.

4.3.4.4 SAT set-up for ultrasound stimulation testing

The ultrasound mediated treatment of *P. aeruginosa* biofilms in this research was carried out using the SAT chamber manufactured by the BUBBL group (Institute of Biomedical Engineering, University of Oxford), which is a modified version of the one utilised in other research to assess ultrasound-activated microbubbles as an intracellular drug delivery system for urinary tract infections (**Figure 41**) (Horsley *et al.*, 2019). MB suspensions applied topically to biofilms grown in Ibidi® dishes were contained by the friction fit sonolid (**Figure 74**); the fabrication and ultrasound performance of the sonolid have been fully characterised elsewhere (Carug*o et al.*, 2015). Each MB suspension assessed was diluted 1:5 in sterile PBS, a total of 10 mL was applied to each biofilm in two stages. Firstly, 6 mL of the 1:5 MB suspension was gently pipetted onto the biofilm; the sonolid assembly was then sealed onto the dish and held at a 45° angle, whilst the remaining 4 mL was slowly injected through the lid ensuring no air pockets formed. The sonolid was held in the SAT by a circular bracket in the pre-focal region of a 40 mm radius, 120 mm radius of curvature, 1.1 MHz centre frequency ultrasound transducer (Sonic Concepts, Inc. Bothell, Washington, USA), such that the incident pressure field was focused on the biofilm growth surface (**Figure 42**). The transducer drive signal path consisted of an oscilloscope (Handyscope HS3, TiePie Engineering, Netherlands), direct digital synthesis function generator (TG2000, 20 MHz, AimTTi, UK), power amplifier (1040L, 400W RF power, E&I Ltd., New York, USA) and impedance matching network (H151-013, Sonic Concepts, Inc.). The SAT was filled with degassed water up to the cover plate, 30 minutes prior to intended use. After administration of the MB suspension the sonolid and dish assemble held by the circular bracket was lowered into the water-filled SAT chamber; this was oriented with the surface of the sonolid facing the transducer so MBs could float upwards towards the biofilm sample (**Figure 41**). The total treatment time was 100 seconds, divided into a 60 second passive interaction period prior to 40 second ultrasound stimulation; each MB formulation was tested in triplicate. Control tests for the MB administration process were carried out in triplicate for every MB formulation; 10 mL of each neutral or cationic RAMB and NOMB suspension was diluted 1:5, in either sterile PBS with 5 μg/mL gentamicin for a final sub-inhibitory concentration of 4 µg/mL or sterile PBS only. Each MB suspension was applied to biofilms for a duration of 100 s; the sonolid assembly was inverted after the application of MBs, but no ultrasound stimulation was carried out.

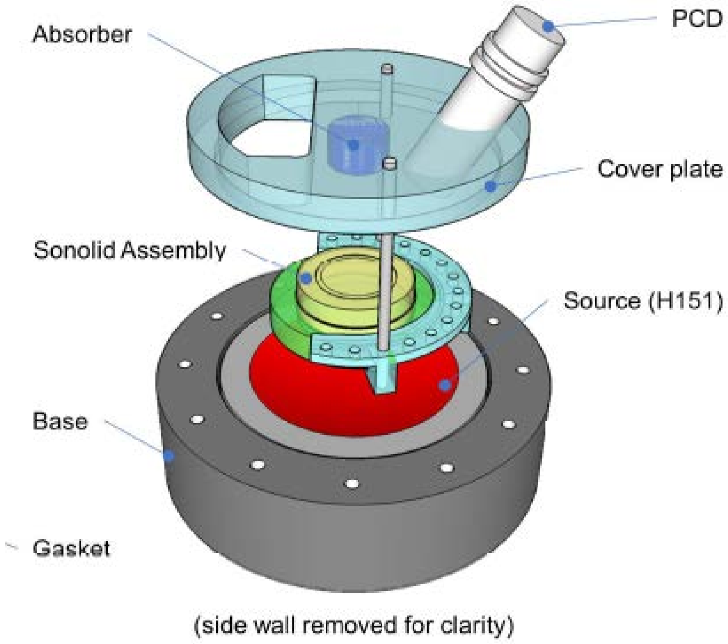

Figure 41 A schematic characterisation of the SAT ultrasound stimulation setup (image courtesy of Dr Michael Gray, University of Oxford), with key features labelled. The PCD identified here was utilised in testing outlined in 4.2.4.7, but was not present during any other experiments. The sonolid assembly orientation during experiments can be seen, where the Ibidi® dish (yellow) is held in place by the sonolid (green) inserted into the circular bracket attached to the cover plate.

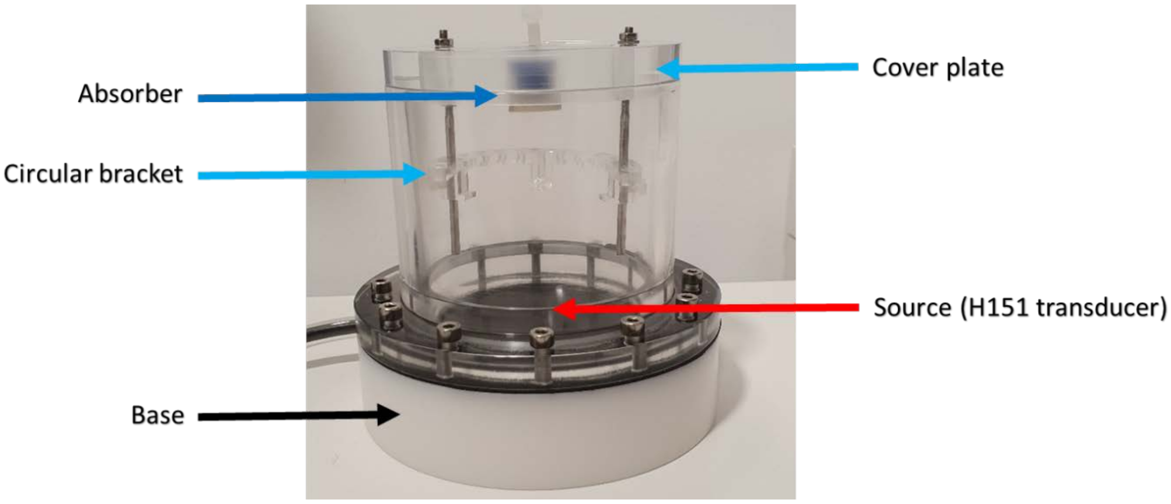

Figure 42 An *in situ* photograph of the SAT ultrasound stimulation device, with key features from the schematic diagram labelled.

4.3.4.5 Ultrasound exposure conditions

Ultrasound stimulation was carried out at 0.9 MHz, 20% duty cycle and a 500 Hz PRF; 45 V_{pp} was applied to the transducer to reach an acoustic pressure of 0.5 MPa at the target site, for 40 s. These ultrasound conditions were kept constant throughout the experimental series. The ultrasound conditions examined in this research were based on parameters considered in our preliminary experiments (Paragraph 6.1.7.3), as well as comparable research in this area (Han *et al.*, 2005, 2007; Ikeda-Dantsuji *et al.*, 2011; Lattwein *et al.*, 2018; Horsley *et al.*, 2019).

4.3.4.6 Assessment of ultrasound stimulated MBs impact on *P. aeruginosa* biofilms

In order to assess the change in surface area coverage due to treatment; biofilms were live/dead stained with 2.5 µM Syto9 (S34854, Invitrogen™, ThermoFisher Scientific) and 9 µM propidium iodide (P3566, Invitrogen™, ThermoFisher Scientific) for 15 minutes, and stored under foil to prevent exposure to light. Excess stain was removed by washing the biofilm once with sterile PBS. Prior to the application of any treatment, live/dead stained images of the biofilm over a defined 1 cm^2 growth area on the Ibidi® dish were captured with fluorescence microscopy. Each treatment condition assessed i.e. ultrasound stimulated RAMBs, $RAMBs^+$, NOMBs and $NOMBs^+$ with or without antibiotic, was tested in triplicate using three independent biofilms. All images were acquired using a gain of 150, light source intensity of 1.8, brightness of 0.5 and an exposure time of 90 ms, with the EVOS M5000 (Invitrogen™, ThermoFisher Scientific) and a 2x objective (EVOS plan fluor AMEP4931, Invitrogen™, ThermoFisher Scientific). An emission wavelength of 498 nm (GFP LED cube, AMEP4653, Invitrogen™, ThermoFisher Scientific), was used to capture images of the green fluorescent Syto9 stained proportion of the biofilm. Images of the red fluorescent propidium iodide stained proportion of the biofilm, were acquired with an emission of 617 nm (RFP LED cube, AMEP4653, Invitrogen™, ThermoFisher Scientific). After ultrasound stimulation, the treatment supernatant was removed from the Ibidi® dish. Fluorescence microscopy was used again to acquire post-treatment images of the biofilm, at identical positions over the same 1 cm^2 area observed in pre-treatment images (**Figure 40**).

Post-treatment images were acquired using the same live/dead staining methodology and microscope settings used to acquire pre-treatment images. Images were imported into ImageJ and the minimum cross-entropy Li threshold was applied (Terheyden *et al.*, 2020), to reliably differentiate between the bright fluorescence of the biofilm in the foreground and the dark underlying surface of the Ibidi® dish. The thresholded image was used to determine the surface area covered by the biofilm, the change in surface area between pre- and post-treatment images could then be calculated.

After ultrasound stimulation, the 10 mL treatment supernatant was aspirated from the Ibidi® dish with a 10 mL Luer lock syringe and placed into a 50 mL sterile centrifuge tube (Nunc™, 50mL Conical Sterile Polypropylene Centrifuge Tubes, ThermoFisher Scientific™). To enumerate the number of viable cells, the treatment supernatant was centrifuged (Eppendorf, 5702R, FisherScientific) at 4000 rpm for 10 minutes to form a pellet of all cellular material, the subsequent centrifuged supernatant was poured off carefully to avoid disturbing the pelleted material. The pellet was re-suspended in 5 mL sterile LB and agitated on a vortex mixer (UY-04726-01, Cole-Parmer, 0 to 3400 rpm, 115 vac), at 3400 rpm for 15 minutes to ensure homogenisation of biofilm aggregates into the fluid. Viable cells from the biofilm were enumerated using the Miles-Misra method (Miles *et al.*, 1938). Three 10 µL samples of the LB containing homogenised biofilm were taken for each Ibidi® dish, this was placed into 90 µL of sterile LB on a 96-well plate and serially diluted to 10^{-9}. Serial dilutions were performed with a multichannel pipette, ensuring each 10 µL transfer into 90 µL of sterile TSB was mixed well. For each serial dilution three 10 µL droplets were dispensed onto a sterile tryptone soy agar plate, the droplets were allowed to dry before the plate was inverted and incubated overnight at 37 °C. After incubation all clearly visible individual colonies were counted for each dilution, the number of visible colonies was multiplied by the dilution factor to gain an assessment of the number of CFU/mL.

4.3.4.7 Passive cavitation detection of DBPC:PEG40s shelled MBs

The dynamic behaviour of microbubbles was assessed by PCD, in response to the ultrasound stimulation parameters considered by this research (outlined in 4.2.4.5). The placement of the PCD is demonstrated in **Figure 41**. PCD testing and post-processing of the data was carried out with the support of Dr Sara Ferri, Faculty of Engineering and Physical Sciences, University of Southampton. The signal recorded by the PCD was processed with an FFT algorithm in MATLAB, the script of which is reported in Appendix A, 6.1.7. The Welch method was applied to determine the power density of the signal over the 30 seconds of stimulation. Power spectral density describes the power present in the signal as a function of frequency.

4.3.5 *Statistical analysis*

All data were assessed for normal distribution; for normally distributed data both paired and independent t-tests have been used to compare data. For multiple treatment conditions, a one-way ANOVA was used to identify any significant difference between different treatment groups. All data was analysed and plotted using Prism 8.4.3 (GraphPad), with a threshold value for significance of < 0.05; where * = P < 0.05, ** = P < 0.005, *** = P < 0.0005 and **** = P < 0.0001.

4.4 Results

4.4.1 *Passive interaction testing without ultrasound of MB formulations on P. aeruginosa biofilms in microtiter plates*

As demonstrated by **Figure 43**, biofilms of *P. aeruginosa* (PA01) formed after 24 hours, predominantly at the fluid-air interface within wells on a microtiter plate. Biomass was defined as the quantity of viable and dead cellular biofilm and extracellular matrix material adhered to the well and stained with 1% aqueous crystal violet, after any planktonic suspension had been aspirated and remaining non-adhered cells removed by subsequent washing steps.

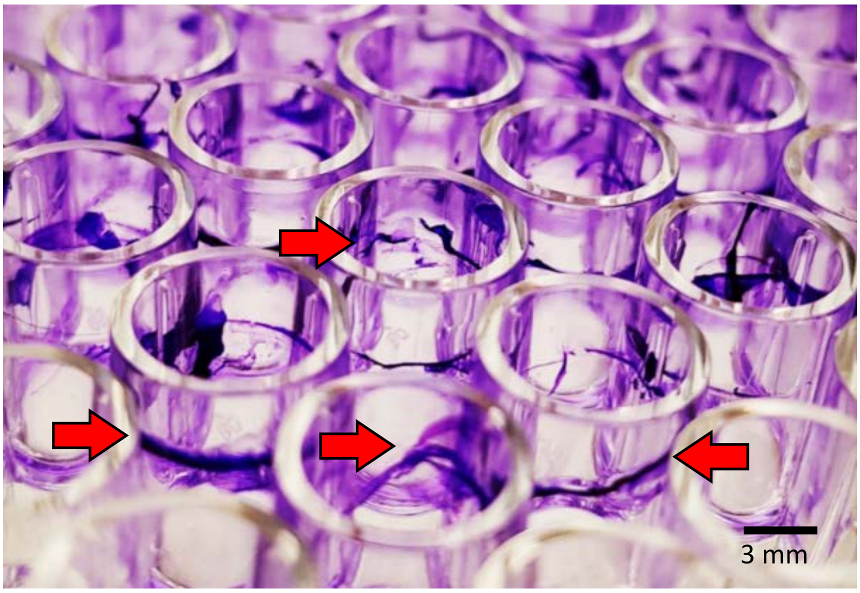

Figure 43 *Pseudomonas aeruginosa* biofilms formed after 24 hours at the media-air interface within a 96-well plate, stained with 1% aqueous crystal violet for 15 minutes and air dried. The presence of biofilms at the media-air interface has been indicated with arrows.

A mean value for each replicate consisting of 6 wells was taken, this established an overall mean value for the crystal violet stained biomass after each treatment. The data was normalised to the control to provide a baseline biomass of 100%, to which the application of air MBs and NOMBs could be compared (**Figure 44**). The experiment only assessed the ability of each MB formulation to potentiate a reduction in biomass, therefore no antibiotic or ultrasound was applied in this test. There was no significant difference in the biomass change achieved by each MB formulation; out of all MB formulations tested the largest reduction in biomass attained was 63.28% by DBPC NOMBs over three biological replicates (**Figure 44**). A consistent feature of this test was that RAMBs incubated with sessile cells, caused an apparent increase in the biomass later stained with crystal violet of over 9% compared to untreated controls (**Figure 44**).

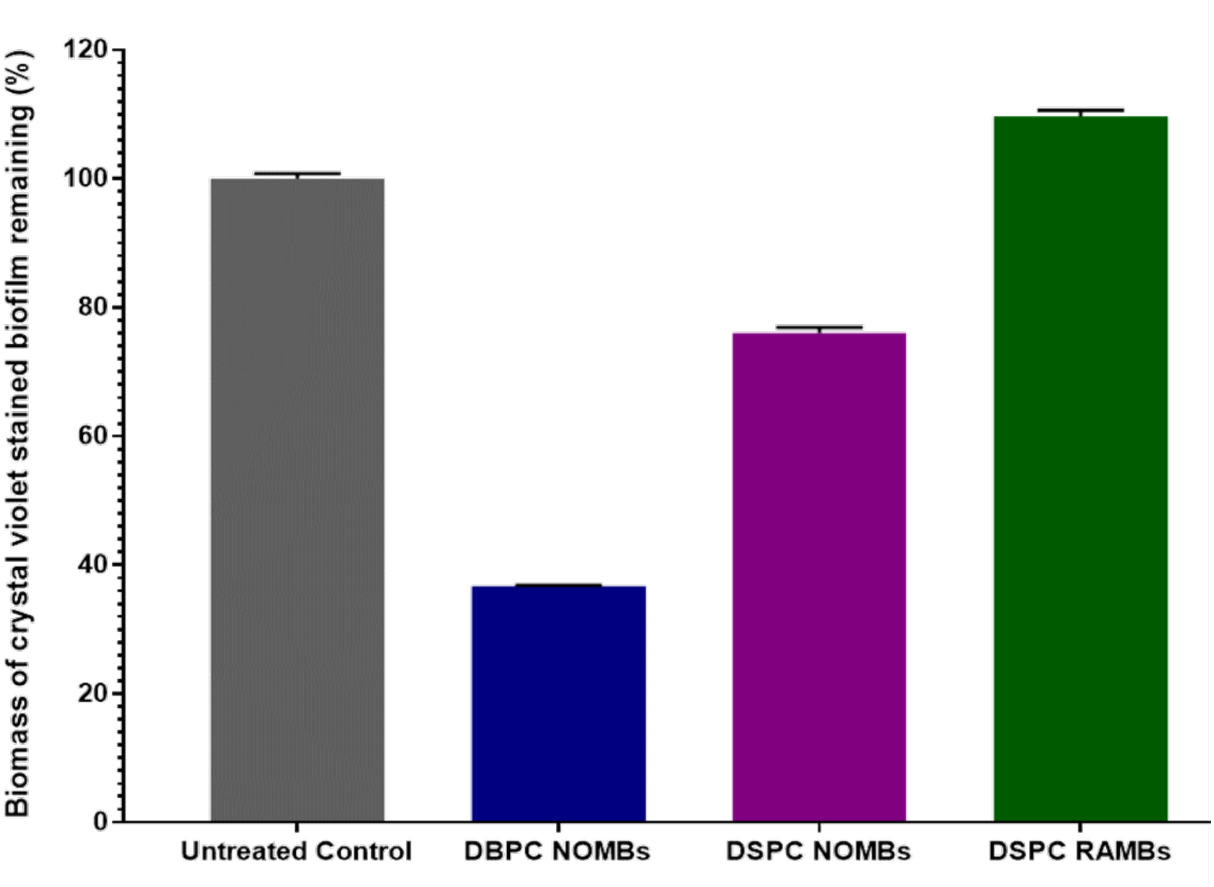

Figure 44 MBs composed of DSPC or DBPC with an air or NO core were incubated with 24 hour old biofilms for one hour, the remaining adherent biomass after treatment was stained with 1% (aq) crystal violet and the relative change in biomass was compared control wells exposed only to PBS. The static incubation of DSPC NOMBs achieved an average reduction of 23.96% in biomass, whereas DSPC RAMBs caused an apparent increase in biomass of 9.71% compared to the biomass of untreated control biofilms. There was no statistically significant difference observed in the data. The largest change in biomass was achieved by DBPC NOMBs, where a 63.28% reduction in adherent biomass was observed compared to controls. The data shown is the mean of three biological replicates, with error bars to show the standard error of the mean.

4.4.2 *Assessment of P. aeruginosa growth and biofilm development in WCM*

The growth of *P. aeruginosa* was assessed in three base media: BB, LB and TSB, by measuring the optical density of the media at 600 nm every hour over a total period of 18 hours. The growth in each media was highly comparable over the period assessed, and demonstrated very good congruency over biological replicates (**Figure 45**). Though no statistical significance in growth was observed between the three base media, BB was the optimal medium based on highest optical density achieved.

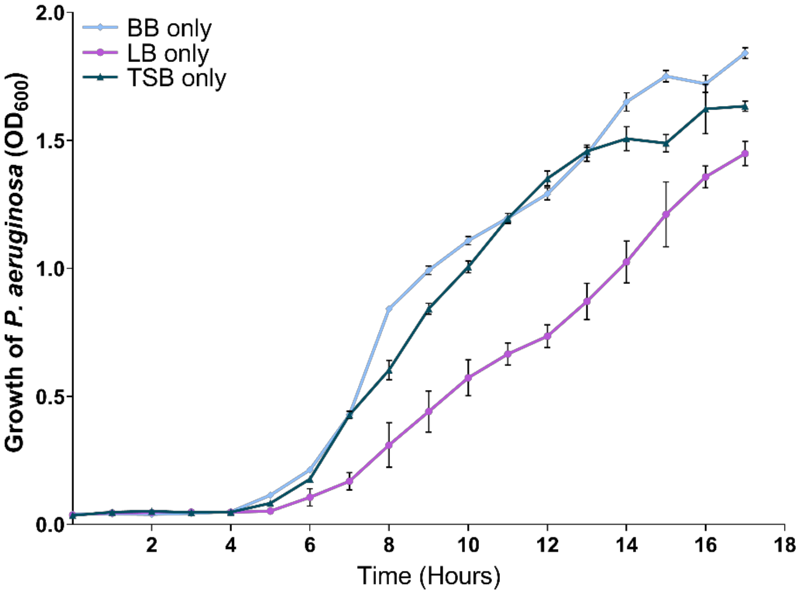

Figure 45 The growth of *P. aeruginosa* was assessed in each base media alone by measuring the optical density of the media at 600 nm at intervals of one hour for 18 hours, each media was blanked against the absorbance of sterile control at 600 nm and the data averaged across three biological replicates. Growth was successful in all media and largely consistent across biological replicates as demonstrated by error bars for standard deviation; growth was most proficient in BB, but there was no statistically significant difference between the three base media.

The early biofilm development in wells was assessed by crystal violet biomass staining after aspiration of the planktonic suspension, both BB and LB demonstrated a consistent and significantly higher ($P < 0.0001$) average biomass than TSB (**Figure 46**). The assessment of growth and biofilm development in the three base media alone, demonstrated that BB was the optimal choice as a growth-medium that balances *P. aeruginosa* planktonic growth with biofilm development.

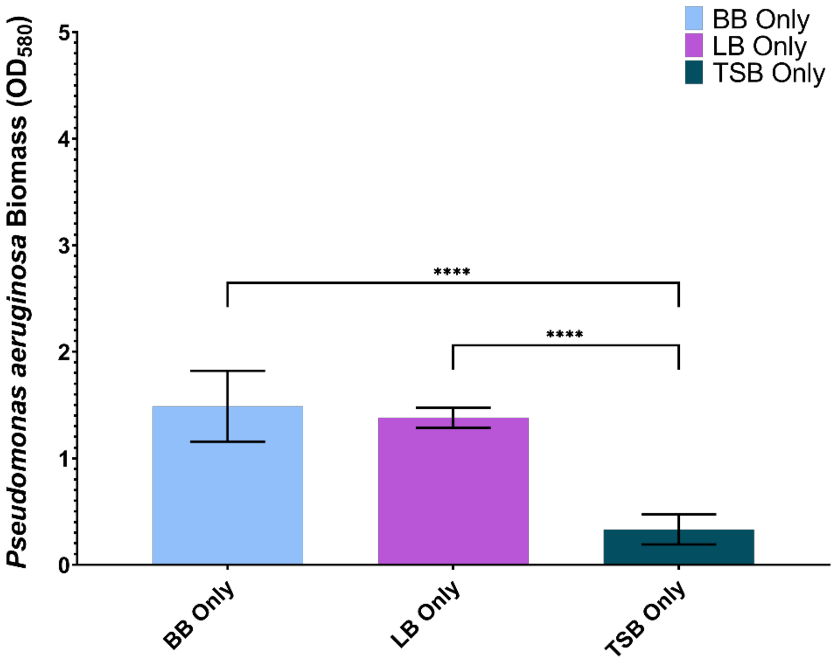

Figure 46 Biofilm biomass in wells were stained with 1% aqueous crystal violet to assess the total biomass of biofilms that formed on the walls of each individual well. The crystal violet stained biofilms were solubilised in 30% acetic acid, the absorbance of the crystal violet solution was blanked against 30% acetic acid alone and measured at 580 nm to quantify total biomass per well. The data is averaged across three biological replicates, with error bars for standard deviation. There was a significant difference between the total biomass present in both BB and LB alone compared to TSB alone ($P < 0.0001$), this demonstrated an inherently greater level of biofilm development in BB and LB than TSB. The biomass quantified in LB appears marginally less variable across repeats, however there was no statistically significant difference between the total biomass measured in BB and LB only.

Utilising BB as the base medium with a fixed quantity of LHB (5%), a range of plasma concentrations (10% - 50%) were assessed to determine how it affected *P. aeruginosa* planktonic growth and biofilm development. The addition of plasma caused an apparent reduction in the growth rate of *P. aeruginosa* at all concentrations (**Figure 47**); this effect was not present in BB alone or supplemented with 5% LHB only. The reduction in growth rate was not found to be significantly different from BB alone, but the impact of this effect was mitigated in the presence of lower plasma concentrations (< 20%) (**Figure 47**).

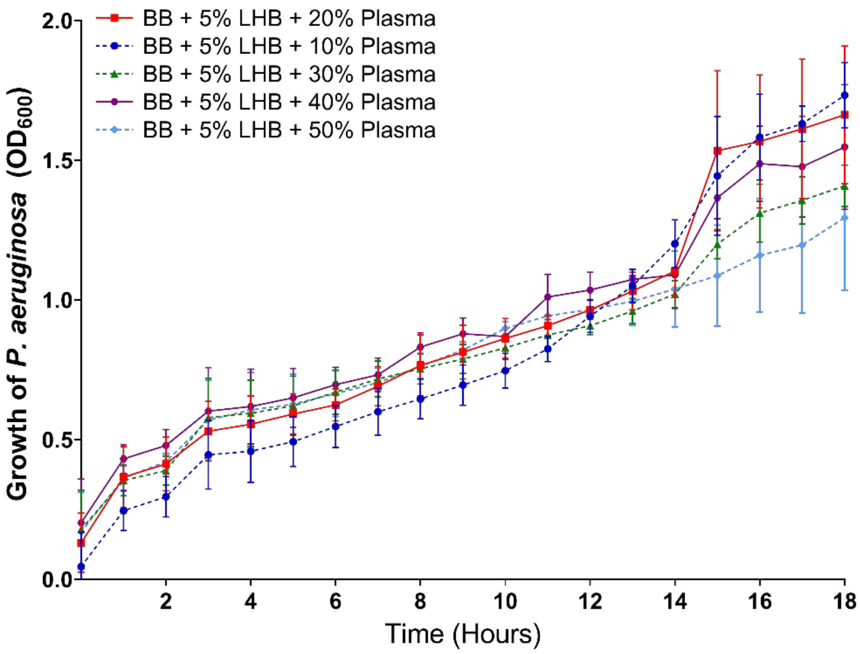

Figure 47 After assessment of *P. aeruginosa* growth in each base media alone, it was determined that BB was the optimal base medium in which to assess the effect of medium supplementation with blood and plasma. Growth of *P. aeruginosa* was reassessed in BB supplemented with 10% - 50% plasma and 5% LHB, by measuring the optical density at 600 nm at intervals of one hour over a total of 18 hours. The data is an average of three biological replicates that have been blanked against non-inoculated wells, which contained BB, LHB and respective concentrations of plasma (10% - 50%). In supplemented media there is still suitable growth of *P. aeruginosa,* however it suffers an apparent lag and overall reduction in growth compared to BB alone. There was no significant difference in this between BB alone and the supplemented BB, importantly growth was not observed to decline at any point over time.

Despite the impact of plasma on planktonic growth, this did not translate into diminished biofilm development. In contrast, there was a significant increase in biofilm development at all plasma concentrations compared to BB alone (**Figure 48**). There was no significant difference between any of the plasma concentrations compared to one another, however it can be observed that biofilm development was hindered at plasma concentrations > 40% (**Figure 48**). The optimal range for plasma concentration was found between 20% and 30%, there was no discernible difference in the biofilm development observed across multiple replicates between these concentrations (**Figure 48**).

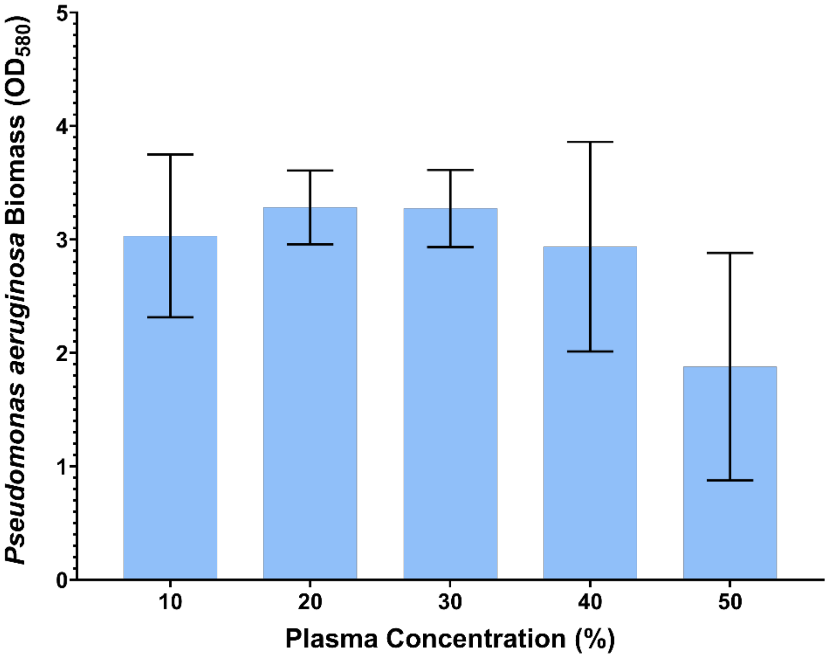

Figure 48 After the assessment of *P. aeruginosa* growth in LHB and plasma supplemented BB, all wells were stained with 1% aqueous crystal violet to assess the total biomass of biofilms that formed on the walls of each individual well. The crystal violet stained biofilms were solubilised in 30% acetic acid, the absorbance of the crystal violet solution was blanked against 30% acetic acid alone and measured at 580 nm to quantify total biomass per well. The data is averaged across three biological replicates, with error bars for standard deviation. There was a visibly discernible difference in the data showing that plasma concentrations > 30% result in a decreased biofilm formation, but there was no statistically significant difference between any of the plasma concentrations assessed. Optimal biofilm formation appears to occur between plasma concentrations of 20% and 30%, indicated by congruous and consistent total biomass stained across replicates.

The refined WCM that resulted from these investigations, was shown to exhibit analogous features to *in vivo* samples of biofilms taken from debrided chronic wounds (**Figure 49**). The figure demonstrates the homogeneity between *in vitro* biofilms grown in WCM and clinical biofilm samples; specifically, regarding the ability of *in vitro* biofilms grown in WCM to accurately reproduce the complex morphological features of *in vivo* biofilms, such as the extensive production of fibrous extracellular matrix.

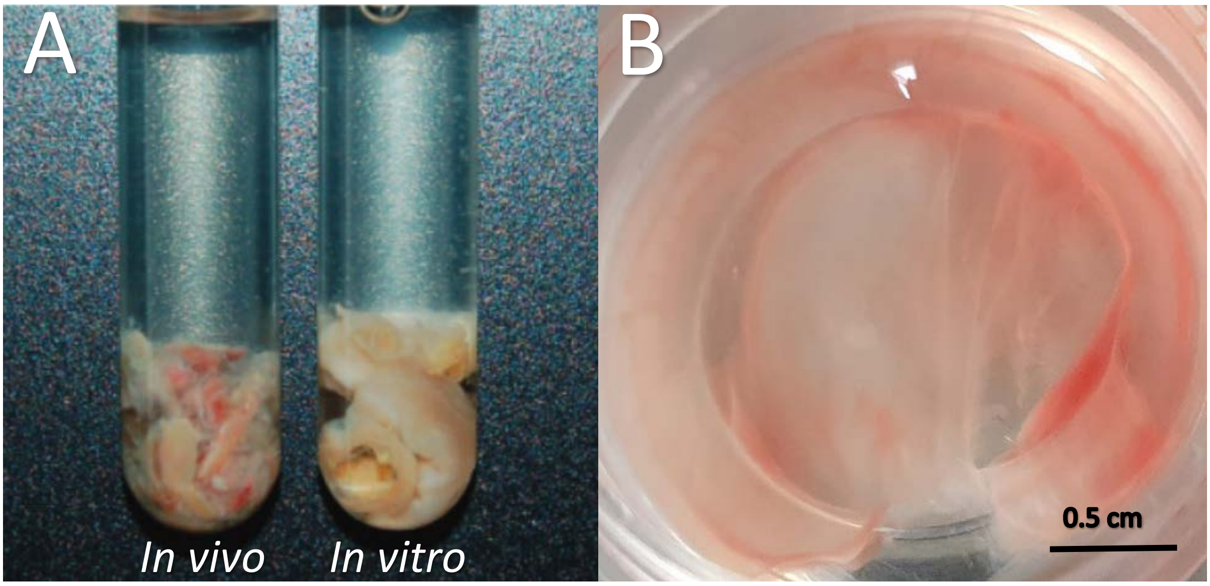

Figure 49 Adapted with permission from Sun *et al.,* (2008); this figure demonstrates a visual representation of (A) an *in vivo* debridement sample (left) taken from a chronic wound biofilm, and the *in vitro* Lubbock chronic wound biofilm grown in WCM (right). For comparison, (B) depicts the *P. aeruginosa* biofilms grown on Ibidi® dishes *in vitro* using WCM (BB, 5% LHB, 20% plasma) in this research.

4.4.3 *Ultrasound stimulated MBs for P. aeruginosa biofilm treatment using the SAT device*

The efficacy of ultrasound-mediated *P. aeruginosa* biofilm treatment was assessed in these experiments, with the MB formulations DBPC:PEG40s RAMBs and NOMBs and DBPC:PEG40s:DSEPC cationic RAMBs$^+$ and NOMBs$^+$ developed at the outset of this research. Their anti-biofilm capacity was determined by assessing reduction in biofilm biomass as a percentage of a 1 cm^2 surface area, whilst their bactericidal activity was quantified by comparing the reduction in culturable cells (CFU/mL) recovered from treated biofilms.

4.4.3.1 Ultrasound stimulated MBs without antibiotic

In order to ascertain the impact of MB administration on biofilm detachment during the treatment process, the reduction in surface area of biofilms that were not treated with ultrasound acted as a control. The average reduction in surface area for the no ultrasound control biofilms was 11.3% (**Figure 50**), this corresponded to relatively minor observable changes in the biofilm morphology assessed by fluorescence microscopy (**Figure 51**). Uncharged RAMBs and NOMBs had the most significant ($P = < 0.0001$) reduction in biofilm biomass compared to the no ultrasound control, corresponding to a 93.3 and 94.0% change respectively. NOMBs were very marginally more successful than RAMBs, though as shown in **Figure 52** there is still biofilm present over the 1 cm^2 area. This would correspond to the biofilm still occupying 6 mm^2 of the total area assessed, which is proportionally still a very large area for the micrometre sized bacteria to occupy and re-colonise.

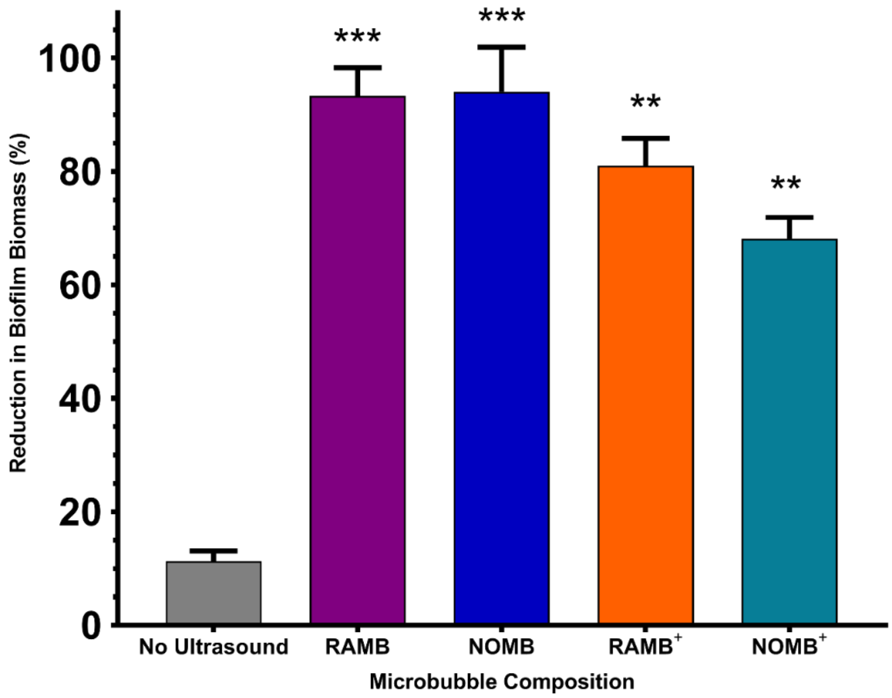

Figure 50 The percentage reduction in *P. aeruginosa* biofilm surface area reported here, was determined by calculating the change in surface area of the live/dead stained biofilm before and after treatment in a 1 cm^2 area. The four principal MB formulations: uncharged RAMBs and NOMBs and cationic RAMBs+ and NOMBs+ were stimulated without antibiotic using an ultrasound driving frequency of 0.9 MHz, duty cycle of 20% and a 500 Hz PRF; 45 V_{pp} was applied to the transducer to reach an acoustic pressure of 0.5 MPa at the target site for 40 s. The change in surface area induced by the application of MBs in the absence of ultrasound was 11.3%, this provided a control for baseline level of biofilm detachment due to the method of MB administration. In these experiments, uncharged RAMBs and NOMBs were the most efficacious in biofilm detachment from the surface with a 93.3% and 94.0% reduction in surface area respectively. Cationic MBs consistently performed worse than their uncharged counterparts; $RAMBs^+$ achieved an average reduction in biofilm surface area of 80.9%, whilst $NOMBs^+$ only attained an average reduction of 68.2%. Error bars indicate standard deviation of the mean; significant differences in the reduction of surface area between each MB formulation and the unstimulated control, are indicated as ** P = < 0.0005 and *** P = < 0.0001 above the relevant bar.

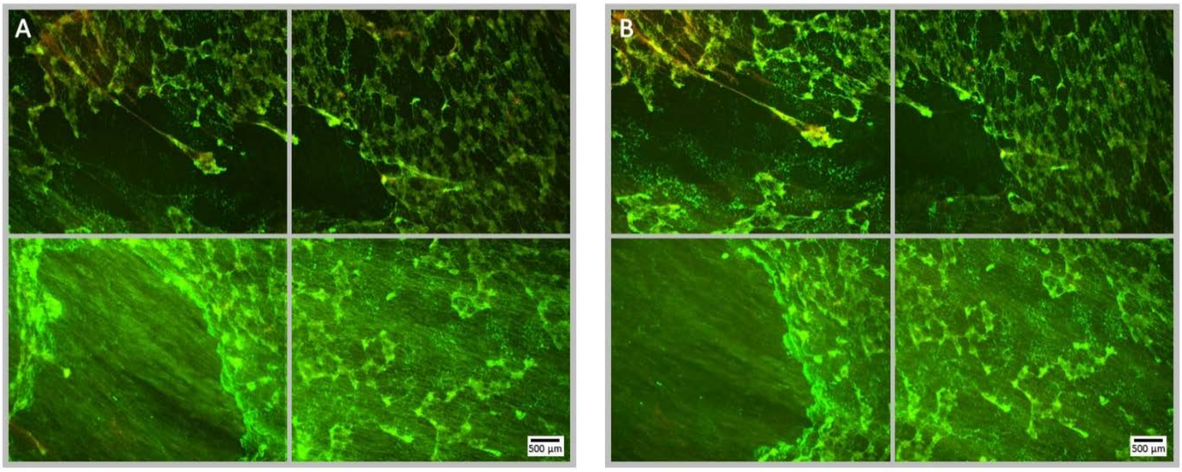

Figure 51 Fluorescence microscopy images of a Syto9 (green) and PI (red) stained *P. aeruginosa* biofilm; the images are representative of a no ultrasound, no antibiotic control where MBs were applied, but not stimulated with ultrasound. Each panel is comprised of four images, which provide an overview of the biofilms gross architecture in a 1 cm^2 area at the centre of the Ibidi® dish. Panel A, depicts the pre-treatment images of the 1 cm^2 area of biofilm, captured prior to the administration of the MB suspension; scale bar is equal to 500 µm. Panel B, depicts the post-treatment images of the same 1 cm^2 area of biofilm, captured after the administration and removal of MBs from the Ibidi® dish. The average reduction in biofilm biomass due to the administration of MBs alone was 11.3%, the observed changes between panel A and B here visually confirm that there are very minor alterations to the biofilms gross architecture after the administration of MBs. Based on the visual analysis undertaken, the reduction in biomass can mostly be attributed to the observed movement of the biofilms extracellular matrix.

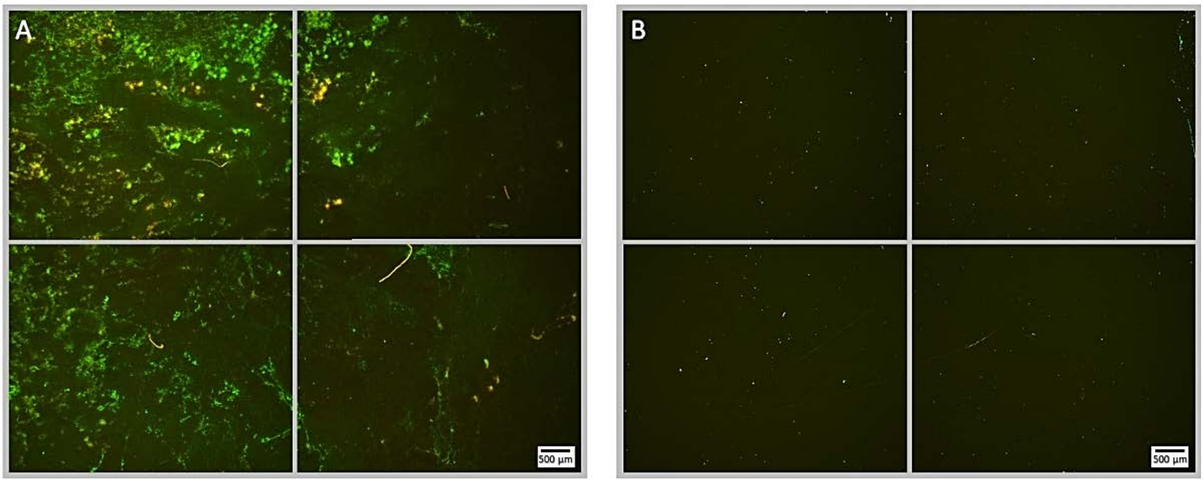

Figure 52 Fluorescence microscopy images of *P. aeruginosa* biofilm stained with Syto9 (green) and PI (red); Panel A images depict the pre-treatment morphology of the biofilm over a 1 cm^2 area. Panel B images show the changes in attached biomass after ultrasound stimulation of a NOMB suspension without antibiotic; 45 V_{pp} was applied to the transducer to reach an acoustic pressure of 0.5 MPa at the target site for 40 s, with a driving frequency of 0.9 MHz, duty cycle of 20% and a 500 Hz PRF. Ultrasound stimulated NOMB alone were able to significantly (P = < 0.0005) reduce the surface area of biofilm coverage by 94.0%, compared to controls where MBs were not stimulated by ultrasound. Though a considerable proportion of the biofilm has been removed, there is clear evidence of both residual MBs and biofilm still associated with the surface.

Both cationic RAMBs$^+$ and NOMBs$^+$ were less efficacious at biofilm detachment than their uncharged counterparts, achieving an 80.9% and 68.2% reduction in surface area respectively (**Figure 50**). Further image analysis of NOMB$^+$ treated biofilms confirmed that there was a large proportion of biofilm left attached to the surface (**Figure 53**), however there was also a potential over-estimation in the surface area this corresponded to due to a high number of residual MBs still non-selectively bound to the biofilm by electrostatic forces (**Figure 54**). Despite less attachment being induced by NOMBs$^+$ a large portion of biofilm was comprised of dead cells, as indicated by an increased proportion of PI stained cells (**Figure 53**).

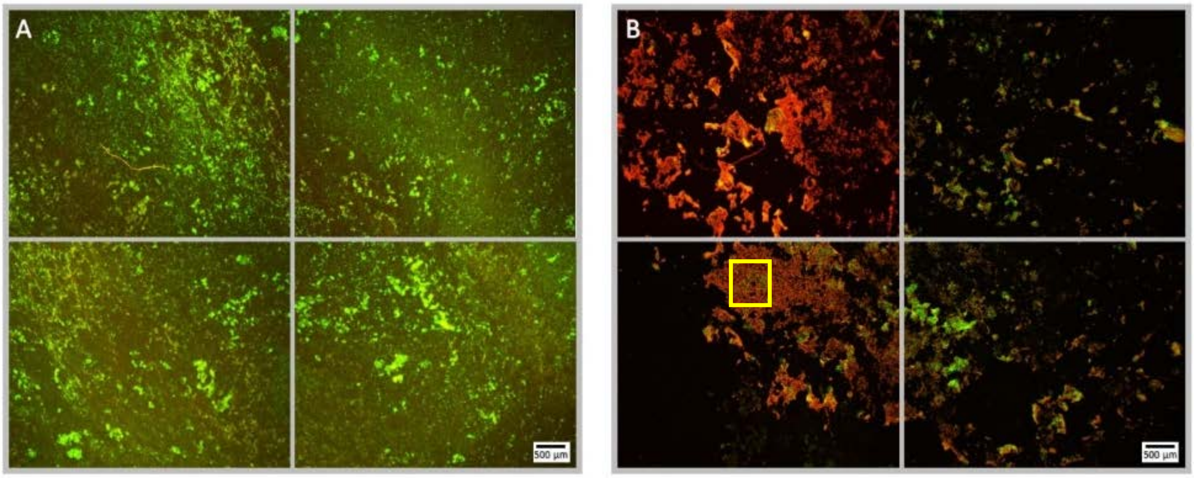

Figure 53 Fluorescence microscopy images of *P. aeruginosa* biofilm stained with Syto9 (green) and PI (red); Panel A images depict the pre-treatment morphology of the biofilm over a 1 cm^2 area. Panel B images show the changes in morphology after ultrasound stimulation of a NOMB$^+$ suspension without antibiotic; 45 V_{pp} was applied to the transducer to reach an acoustic pressure of 0.5 MPa at the target site for 40 s, with a driving frequency of 0.9 MHz, duty cycle of 20% and a 500 Hz PRF. After ultrasound stimulation NOMBs$^+$ achieved a reduction in biofilm surface area of 68.2%, making NOMBs$^+$ on average 26% less efficacious than their uncharged counterpart NOMBs. It is demonstrated in Panel B that though there is a higher proportion of biomass still attached to the surface, the majority of this appears to consist of PI stained dead cells. A yellow box has been added in the lower left image of panel B, to indicate the location at which **Figure 54** was viewed at 20x magnification.

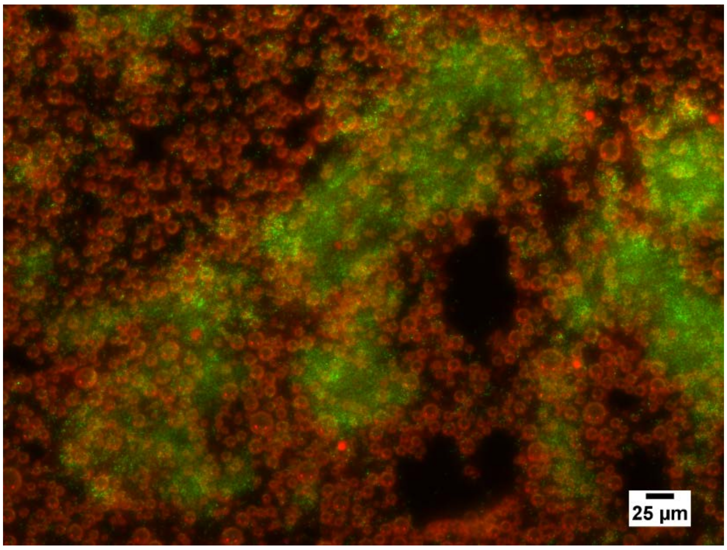

Figure 54 A closer inspection of the area indicated in panel B of **Figure 53** by a yellow box, showing NOMBs$^+$ treated biofilm after ultrasound exposure where *P. aeruginosa* biofilm was stained with Syto9 (green) and PI (red). As observed in electrostatic binding assessments carried out on biofilms in Chapter 3, Paragraph 3.3.5, there is considerable proportion of cationic MBs clustering in contact with and proximal to the biofilm. It is important to note here that MBs (red) were not fluorescently labelled in any way, but it has been shown that MBs can create a distorted ring peripheral to the gas core due to the change in refractive index as light is transmitted through the gas-filled MB and surrounding fluid (Ibsen *et al.*, 2013; Leung *et al.*, 2013).

Biofilm dispersal from the surface achieved by each MB formulation was only one aspect assessed in this research, as it was also important to determine if the dispersed biofilms contained culturable cells. This was assessed by quantifying the culturable cells recovered from the treated biofilm in CFU/mL, this ultimately showed that enhanced biofilm detachment is not always conducive to bactericidal activity. Despite NOMBs$^+$ being the least efficacious in biofilm detachment they demonstrated the highest bactericidal activity, reducing the number of culturable cells after treatment by 86.1% compared to the CFU recovered from the no ultrasound control biofilms. Similarly, the bactericidal activity of RAMBs$^+$ was greater than their anti-biofilm activity, decreasing the proportion of culturable cells by 84.7%. Despite RAMBs and NOMBs demonstrating the ability to induce > 90% biofilm detachment, their subsequent bactericidal activity was comparatively weak with only a 26.9%

and 65.3% reduction in culturable cells respectively (**Figure 55**). None of the MB formulations evaluated in these test attained a reduction in culturable cells > 90% (1-log reduction), therefore the ability of MBs to work synergistically to potentiate sub-inhibitory concentrations of antibiotic was assessed.

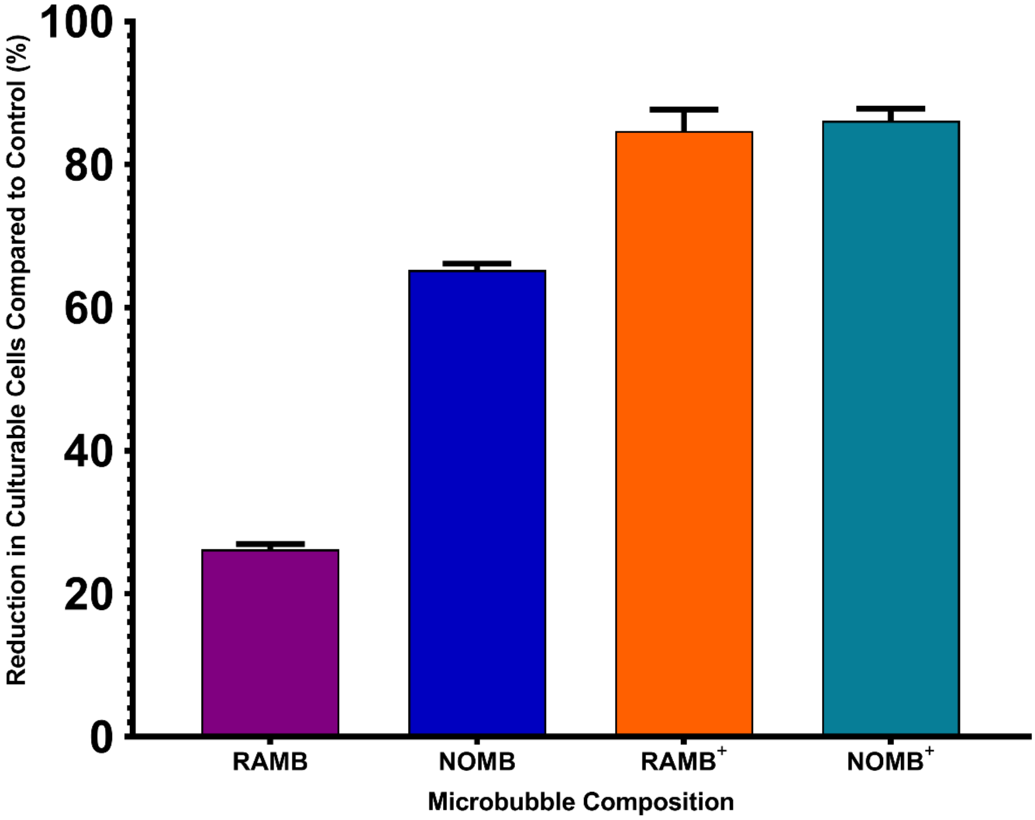

Figure 55 The viability of the total biofilm biomass detached during ultrasound stimulation of MBs, was assessed by quantifying the average reduction in CFU/mL compared to an untreated control; error bars indicate standard deviation of the mean. The untreated control biofilms were exposed to the MB application process, but not stimulated with ultrasound. No antibiotic was applied during the treatment process at any stage, the results therefore represent only the efficacy of the ultrasound stimulated MB formulation. In these experiments uncharged RAMBs and NOMBs showed less bactericidal activity than their cationic counterparts, attaining a reduction in culturable cells of just 26.9% and 65.3% respectively. RAMBs$^+$ were able to achieve a reduction of 84.7%, the largest reduction in culturable cells was achieved by NOMBs$^+$ at 86.1%. No significant difference in the reduction of culturable cells was shown between any of the formulations.

4.4.3.2 Ultrasound stimulated MBs with sub-inhibitory antibiotic (4 µg/mL) gentamicin

Although ultrasound stimulated MBs alone demonstrate a substantial capacity for biofilm detachment and reducing the proportion of culturable cells, no single formulation tested was able to achieve concurrent high levels of biofilm perturbation and bactericidal activity. Therefore, in line with preliminary data achieved in BOCS testing, each MB formulation was tested with the addition of a 4 µg/mL sub-inhibitory concentration of gentamicin in the MB suspension as a free-drug. In order to define the impact that sub-inhibitory gentamicin and MBs had on biofilm detachment during the administration process, the reduction in surface area of biofilms that were not treated with ultrasound acted as a control. The average reduction in surface area for the no ultrasound control biofilms was 11.1% (**Figure 56**), this corresponded to relatively minor observable changes in the biofilm morphology assessed by fluorescence microscopy. Importantly, there was no detectable decrease the in viability of the biofilm assessed by fluorescence microscopy, which provided a visual confirmation that the antibiotic concentration was indeed sub-inhibitory. All MB formulations assessed in conjunction with gentamicin, exhibited a highly statistically significant ($P = < 0.0001$) reduction in biofilm biomass; compared to the no ultrasound control (**Figure 56**). NOMBs and NOMBs$^+$ had the most significant reduction in biofilm biomass compared to the no ultrasound control, corresponding to a 99.9% and 93.9% change respectively. RAMBs$^+$ had a comparable efficacy to NOMBs$^+$, eliciting a surface area reduction in biofilm of 92.5%. Contrary to the substantial reduction of biomass attained by RAMBs stimulated with ultrasound in the absence of antibiotic (**Figure 50**), in these experiments RAMBs only achieve a maximum reduction in biomass of 81.3% (**Figure 56**).

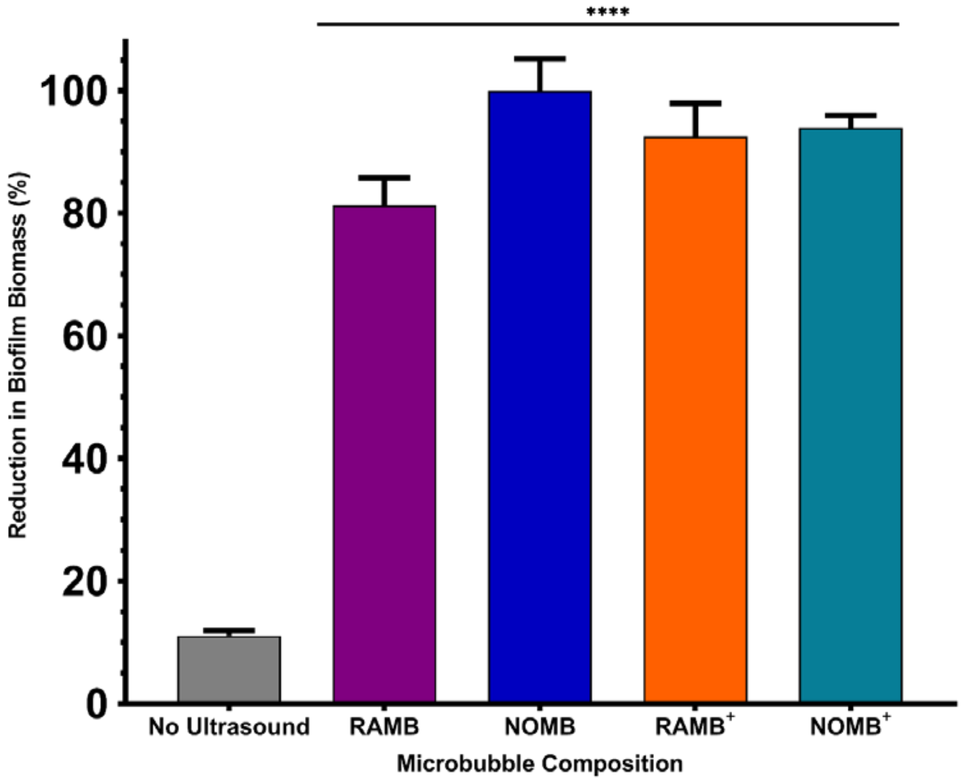

Figure 56 The percentage reduction in *P. aeruginosa* biofilm surface area reported here, was determined by calculating the change in surface area of the live/dead stained biofilm before and after treatment in a 1 cm^2 area. Each MB composition was diluted 1:5 in PBS containing 4 µg/mL gentamicin, were stimulated with using an ultrasound driving frequency of 0.9 MHz, duty cycle of 20% and a 500 Hz PRF. 45 V_{pp} was applied to the transducer, to reach an acoustic pressure of 0.5 MPa at the target site for 40 s. The change in surface area induced by the application of MBs in the absence of ultrasound was 11.1%, this provided a control for baseline level of biofilm detachment due to the method of MB-antibiotic suspension administration. The data demonstrated that uncharged NOMBs were consistently the most efficacious in biofilm detachment from the surface, eliciting a 99.9% reduction in biofilm surface area. Cationic NOMBs$^+$ were somewhat less effective than uncharged NOMBs, achieving an average reduction in biomass of 93.9%. RAMBs and RAMBs$^+$ performed consistently worse than their NOMB analogues, achieving an average reduction in biofilm surface area of 81.3% and 92.5% respectively. Significant difference in the reduction of surface area between all MB formulation and the unstimulated control, are indicated as **** P = < 0.0001, error bars indicate standard deviation.

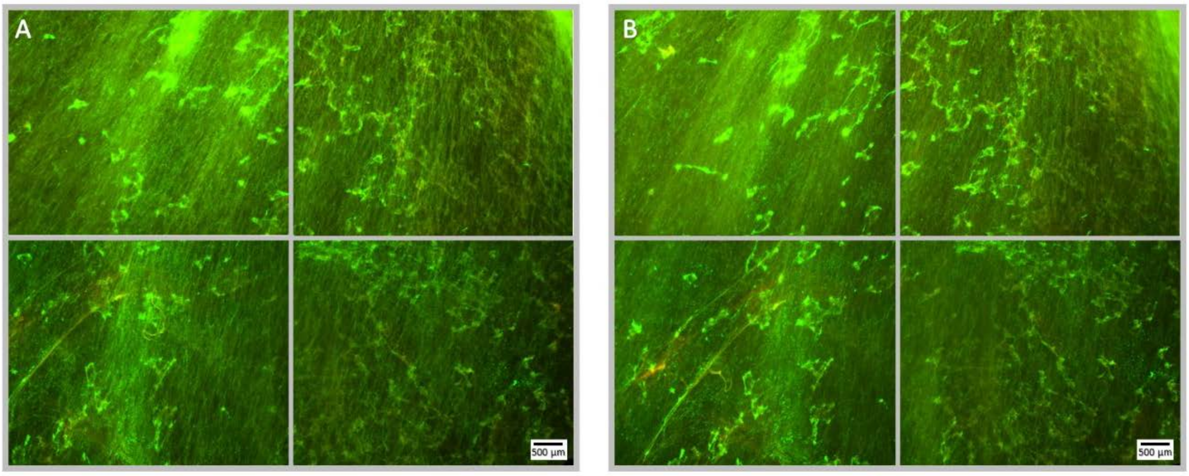

Figure 57 Fluorescence microscopy images of a Syto9 (green) and PI (red) stained *P. aeruginosa* biofilm; the images are representative of a no ultrasound treatment control where MBs were applied with 4 µg/mL sub-inhibitory gentamicin, but not stimulated with ultrasound. Each panel is comprised of four images, which provide an overview of the biofilms gross architecture in a 1 cm^2 area at the centre of the Ibidi® dish. Panel A, depicts the pre-treatment images of the 1 cm^2 area of biofilm, captured prior to the administration of the MB-antibiotic suspension; scale bar is equal to 500 µm. Panel B, depicts the post-treatment images of the same 1 cm^2 area of biofilm, captured after the administration and removal of the MBs-antibiotic suspension from the Ibidi® dish. The average reduction in biofilm biomass due to the administration of MBs alone was 11.1%, the observed changes between panel A and B here visually confirm that there are very minor alterations to the biofilms gross architecture after the administration of MBs. Based on the visual analysis undertaken, the reduction in biomass can mostly be attributed to the observed movement of the biofilms extracellular matrix. There is no visibly discernible decrease in cell viability assessed by PI, subsequent to the administration of gentamicin at 4 µg/mL; this further validates that the concentration used is sub-inhibitory.

Fluorescence microscopy images of *P. aeruginosa* biofilms captured after ultrasound stimulation with NOMBs, visually demonstrate the highly efficacious level of MB detachment observed upon their co-administration with gentamicin at 4 µg/mL (**Figure 58**). Despite being the second most efficacious formulation tested with sub-inhibitory antibiotic, NOMBs$^+$ still exhibit a number of MB clusters bound to the Ibidi® surface (**Figure 59**).

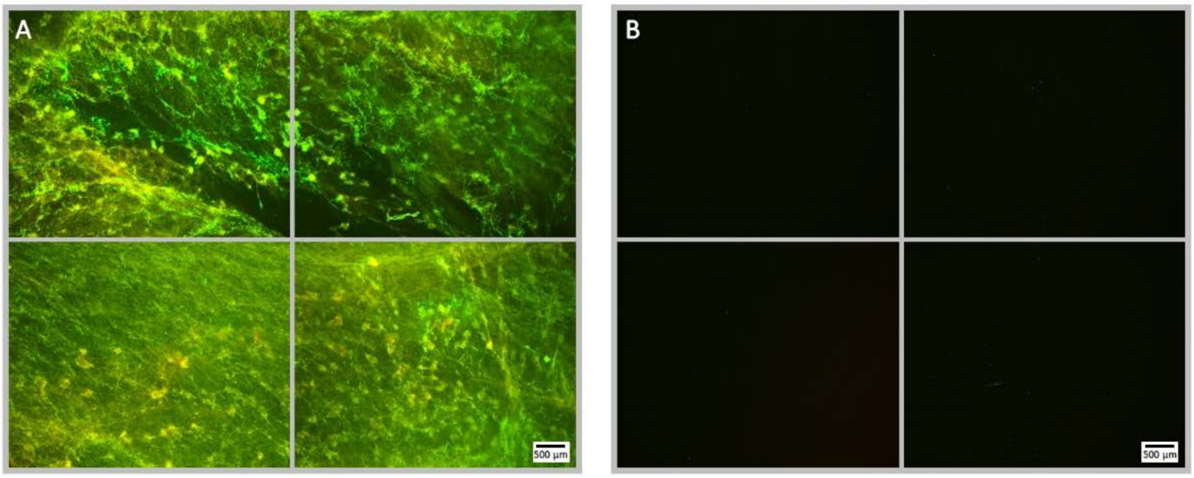

Figure 58 Fluorescence microscopy images of *P. aeruginosa* biofilm stained with Syto9 (green) and PI (red); Panel A images depict the pre-treatment morphology of the biofilm over a 1 cm^2 area. Panel B images show the changes in attached biomass after ultrasound stimulation of a NOMB suspension without antibiotic; 45 V_{pp} was applied to the transducer to reach an acoustic pressure of 0.5 MPa at the target site for 40 s, with a driving frequency of 0.9 MHz, duty cycle of 20% and a 500 Hz PRF. Ultrasound stimulated NOMB and sub-inhibitory gentamicin were able to significantly (P = < 0.0001) reduce the surface area of biofilm biomass by 99.9%, compared to controls where MBs were not stimulated by ultrasound. There are inevitably some residual cells and microbubbles still present on the surface of the Ibidi® dish, however the significance of the reduction in biomass observed is made abundantly clear in these images.

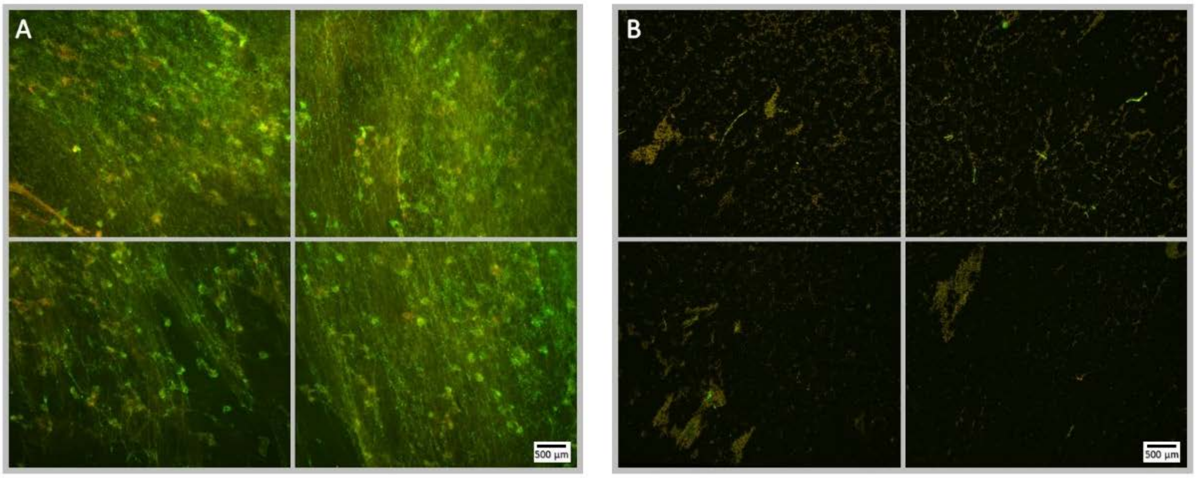

Figure 59 Fluorescence microscopy images of *P. aeruginosa* biofilm stained with Syto9 (green) and PI (red); Panel A images depict the pre-treatment morphology of the biofilm over a 1 cm^2 area. Panel B images show the changes in morphology after ultrasound stimulation of a NOMB$^+$ suspension with sub-inhibitory gentamicin; 45 V_{pp} was applied to the transducer to reach an acoustic pressure of 0.5 MPa at the target site for 40 s, with a driving frequency of 0.9 MHz, duty cycle of 20% and a 500 Hz PRF. After ultrasound stimulation NOMBs$^+$ achieved a reduction in biofilm surface area of 93.9%, making NOMBs$^+$ on average only 6% less efficacious than their uncharged counterpart NOMBs. It is demonstrated in Panel B that though there is a higher proportion of biomass still attached to the surface, the majority of this appears to consist of PI stained dead cells as seen in earlier examples of an NOMB$^+$ treated biofilm.

Biofilm dispersal from the surface achieved by each MB formulation without antibiotic, was limited to < 1-log reduction in culturable cells (**Figure 55**). The reduction in culturable cells was re-assessed by quantifying the CFU/mL recovered from detached biofilm, after the ultrasound stimulation of MBs with sub-inhibitory (4 µg/mL) gentamicin (**Figure 60**). The relationship between biofilm detachments by the MB-antibiotic suspensions, was highly congruent with the data observed for bactericidal activity. In addition to achieving a 99.9% reduction in biofilm surface area coverage, NOMBs were also able to attain an important 99.9% (3-log) reduction in culturable cells. All formulations tested performed significantly better than in previous tests conducted without sub-inhibitory gentamicin (**Figure 55**); the testing of each MB formulation with gentamicin showed NOMBs and both cationic RAMBs$^+$ and NOMBs$^+$ were significantly (** P = < 0.005 and * < 0.05 respectively) more effective than RAMBs. Despite this other formulations performing significantly better RAMBs still performed better when administered with gentamicin than without, achieving a 99.4% (2-log) reduction in culturable cells. RAMBs$^+$ and NOMBs$^+$ equally attained a 99.8% (2.5-log) reduction in culturable cells, further validating the efficacy and consistency of MB-antibiotic suspensions.

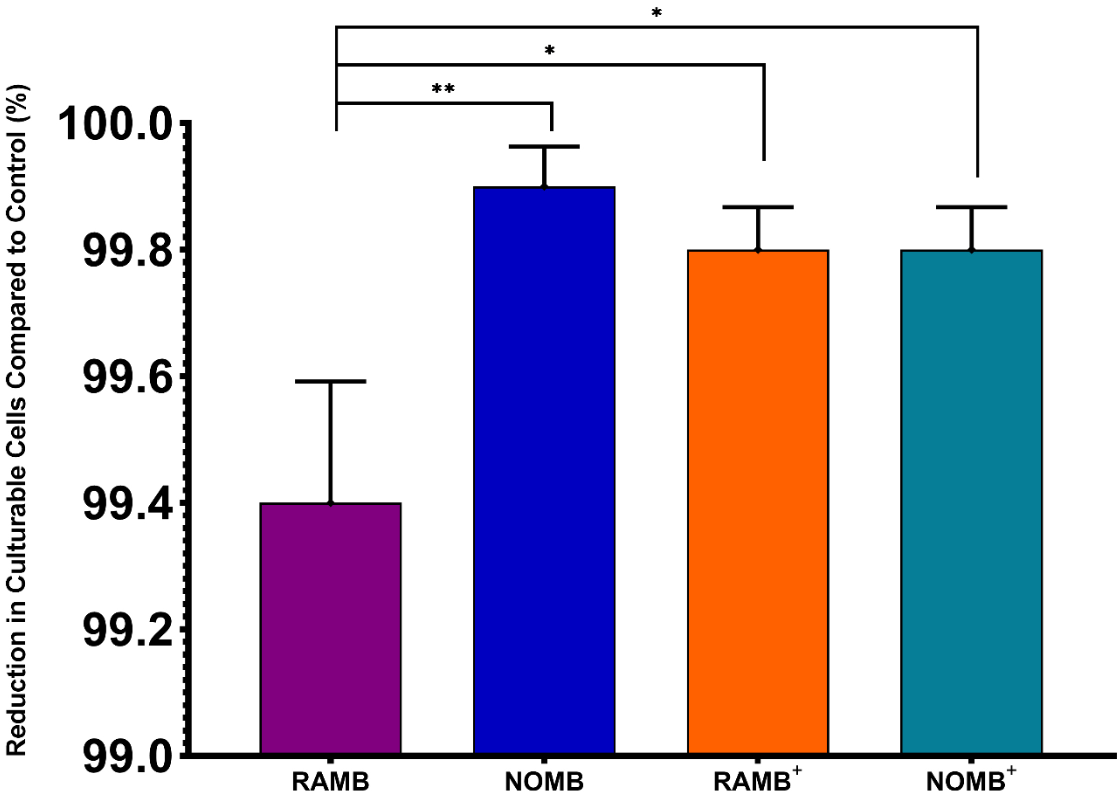

Figure 60 The viability of the total biofilm biomass detached during ultrasound stimulation of MBs, was assessed by quantifying the average reduction in CFU/mL compared to a control biofilm. Error bars indicate standard deviation of the mean. The control biofilms were exposed to the MB application process and sub-inhibitory gentamicin, but not stimulated with ultrasound. The results represent the combined efficacy of each ultrasound stimulated MB formulation co-administered with 4 µg/mL sub-inhibitory gentamicin. Of particular significance, is that all microbubble formulations tested appear to have potentiated the gentamicin. This has resulted in a significantly increased efficacy of the treatment, compared to the ultrasound stimulation of the MBs without antibiotic. Firstly, NOMBs achieved a critical 99.9% (3-log) reduction in culturable cells and were significantly (** P = < 0.005) more efficacious than RAMBs, which achieved a 99.4% (2-log) reduction in culturable cells. Cationic RAMBs$^+$ and NOMBs$^+$ attained an equal 99.8% (2.5-log) reduction in culturable cells, which was also significantly (* P = < 0.05) better than RAMBs.

4.4.3.3 Passive cavitation detection of DBPC:PEG40s shelled MBs

In order characterise the behaviour of MBs in response to ultrasound stimulation, PCD testing was carried out using the ultrasound stimulation settings applied to MBs in the presence of *P. aeruginosa* biofilms. The ultrasound stimulation was carried out at 0.9 MHz, 20% duty cycle and a 500 Hz PRF; 45 V_{pp} was applied to the transducer to reach an acoustic pressure of 0.5 MPa at the target site for 40 s. The first assessment carried out was in the absence of MBs, where the sonolid assembly contained only PBS. The data confirmed that with no MBs present in the fluid, there was no cavitation apparent in the fluid (**Figure 61**).

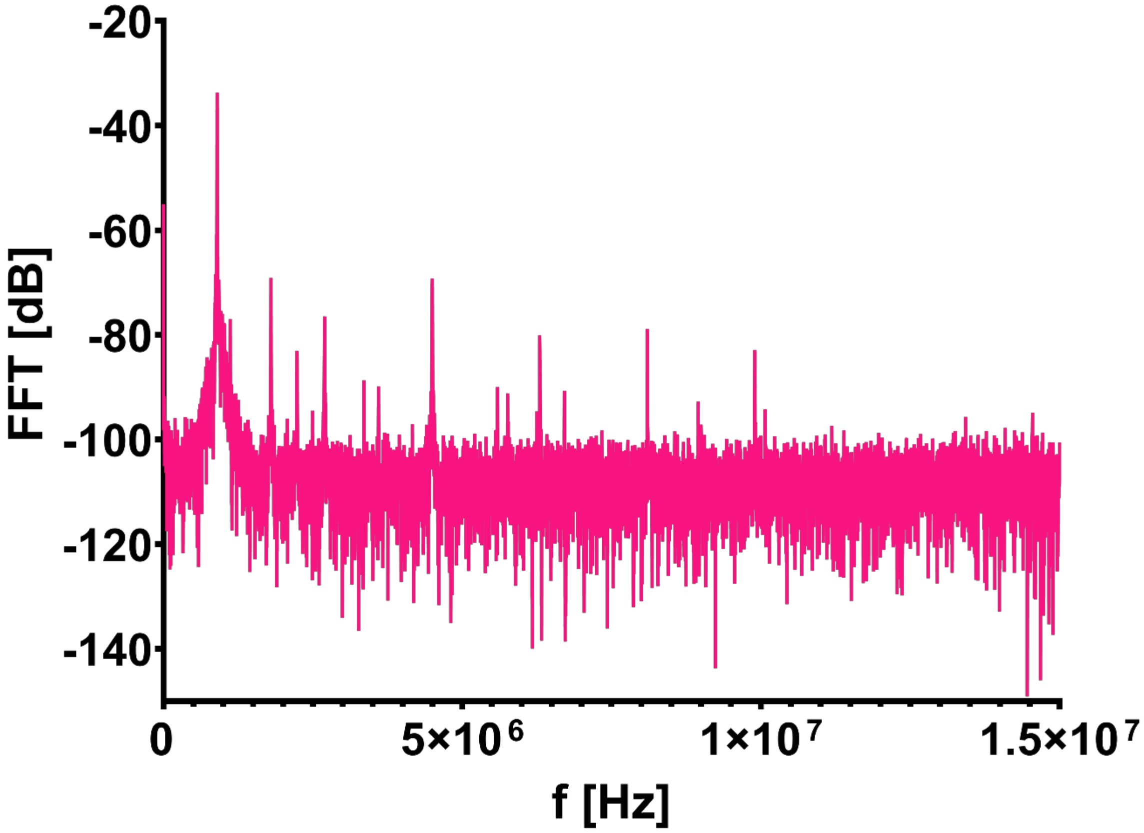

Figure 61 Logarithmic FFT of the signal recorded by the PCD when the Ibidi® dish contained only PBS, where the *y*-axis shows the amplitude of the FFT (dB). Ultrasound stimulation was carried out at 0.9 MHz, 20% duty cycle and a 500 Hz PRF; 45 V_{pp} was applied to the transducer to reach an acoustic pressure of 0.5 MPa at the target site for 40 s. The graph shows a peak registered at the driving frequency; there are no sub- or ultra-harmonics or broadband noise evident which confirms that there was no detectable cavitation in the fluid.

Subsequently, PCD was carried out on a 10 mL suspension of DBPC:PEG40s shelled MBs diluted 1:5 in PBS; the FFT of the MBs acoustic response demonstrates features consistent with the detection of stable and inertial cavitation of MBs (**Figure 62**). However, this does not provide spatiotemporal information on the acoustic behaviour of cavitating MBs, so a spectral power density graph was produced (**Figure 63**). This indicated substantial broadband noise (i.e. potentially indicative of inertial cavitation and MB collapse) within the first few seconds of exposure, followed by distinctive presence of ultra-/sub-harmonics and a lower level of broadband noise (i.e. potentially indicative of both stable and inertial cavitation).

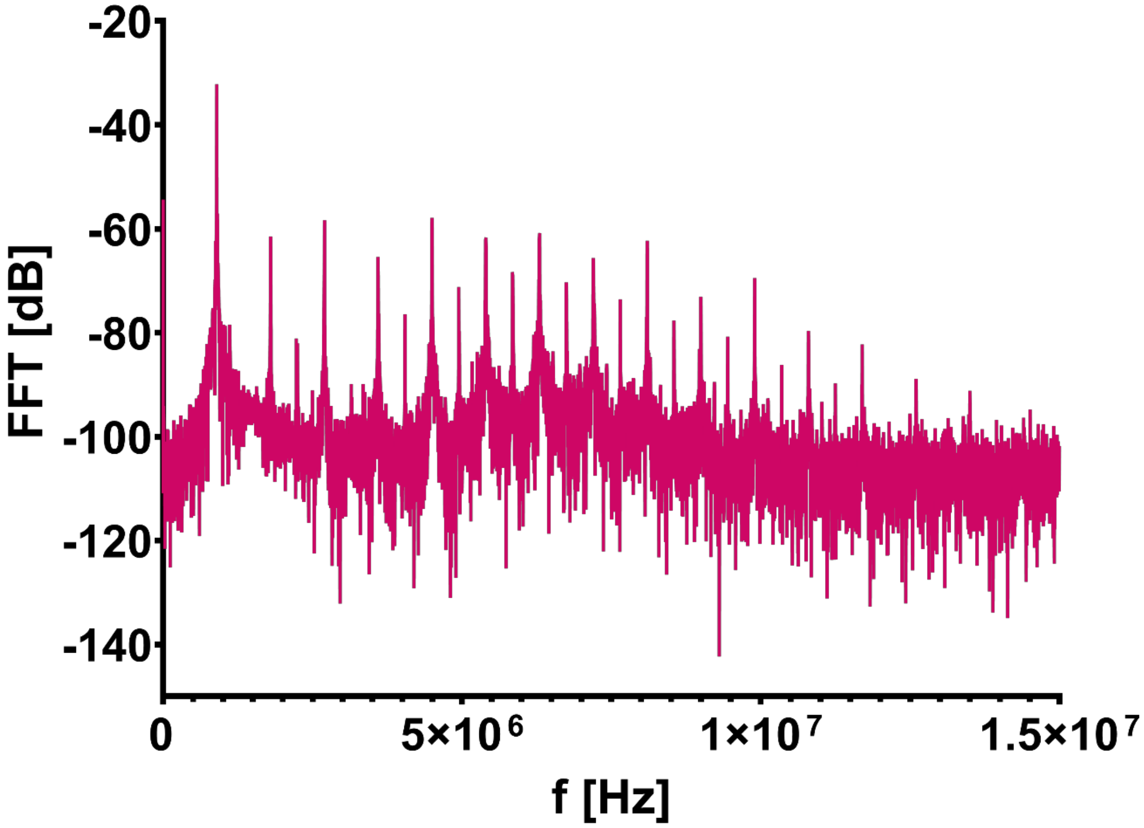

Figure 62 Logarithmic FFT of the signal recorded by the PCD when the Ibidi® dish contained a 1:5 dilution of DBPC:PEG40s MBs in PBS, where the *y*-axis shows the amplitude of the FFT (dB). Ultrasound stimulation was carried out at 0.9 MHz, 20% duty cycle and a 500 Hz PRF; 45 V_{pp} was applied to the transducer to reach an acoustic pressure of 0.5 MPa at the target site for 40 s. The presence of MBs is confirmed due to the appearance of sub- and ultra-harmonics; some level of broadband noise is also evident. The features of this FFT are a potential indication of stable and inertial cavitation occurring.

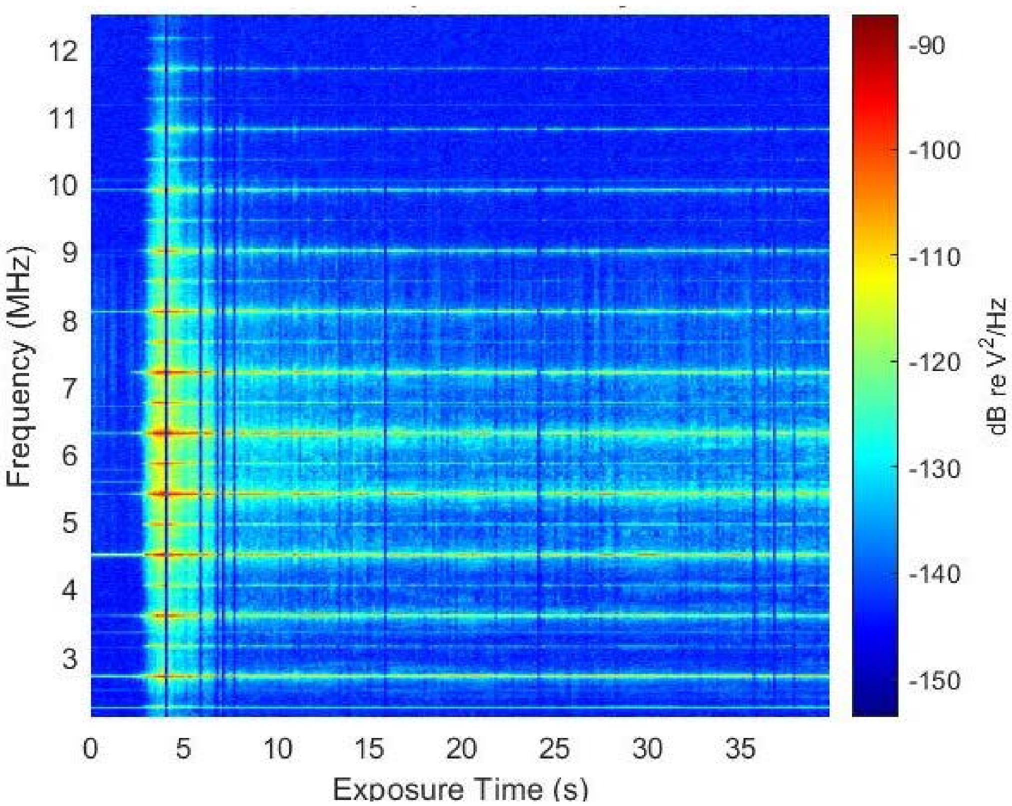

Figure 63 Time dependant acoustic response spectrogram of a 1:5 dilution of DBPC:PEG40s MBs in PBS. Ultrasound stimulation was carried out at 0.9 MHz, 20% duty cycle and a 500 Hz PRF; 45 V_{pp} was applied to the transducer to reach an acoustic pressure of 0.5 MPa at the target site for 40 s. The *x*-axis shows the 40 s duration of ultrasound stimulation, frequency in MHz is shown on the left *y*-axis and the colour-bar (right *y*-axis) indicates the power spectral density. There is evidence of a significant level of inertial cavitation and MB destruction, occurring over the initial few seconds of the 40 s exposure. After this initial phase there is a lower level of residual inertial cavitation, but the greater proportion of the remaining MB population appears to undergo stable cavitation for the remaining duration of the 40 s exposure period.

4.5 Discussion

This work sought to evaluate the therapeutic efficacy of neutral RAMBs and NOMBs as well as cationic RAMBs$^+$ and NOMBs$^+$, in terms of their passive interaction and ultrasound stimulation induced effects on *P. aeruginosa* biofilms. A range of techniques have been used with relevant pathophysiological models of biofilm infection to assess their anti-biofilm and bactericidal activity; including high-throughput biofilm straining techniques, fluorescence microscopy and direct quantification of cell viability. There have been relatively few studies to date that have characterised and implemented the use of an ultrasound responsive carrier of NO for biofilm treatment; research carried out by Hetrick *et al.* (2009) investigated the use of NO-releasing silica nanoparticles, however it focused only on the bactericidal efficacy of the NO and not on biofilm dispersal. Similarly, in recent work carried out by Choi *et al.* (2019) on NO delivery by perfluorocarbon micro-emulsion, only its antibacterial efficacy was assessed. This work importantly showed the effect that different NO concentrations can have on bacterial activity; using NO concentrations of 0.175 – 2.622 µM a 50% decrease in bacterial viability was observed in planktonic suspensions of *S. aureus*, however no discernible bactericidal activity was seen in planktonic suspensions of *P. aeruginosa* (Choi *et al.*, 2019). More recently the innate bactericidal activity of NOMBs has been demonstrated; using planktonic *S. aureus* suspensions NOMBs showed a statistically significant decrease in CFU compared to MBs containing air; however the observed reduction in CFU was < 1 Log (< 90%)(Lafond *et al.*, 2020).

4.5.1 *Passive MB interaction testing on P. aeruginosa biofilms*

Initial data from the incubation of RAMBs and NOMBs with 24-hour old *P. aeruginosa* biofilms was promising; though no significant difference was observed for the change in biomass due to passive application of MBs, NOMB formulations did reduce biomass more than RAMBs (**Figure 44**). The biofilms within wells that were suffused with DSPC NOMBs saw an average decrease in biomass of 23.96%, compared to an untreated control (**Figure 44**). In experiments conducted under flow, it has been reported that dispersal induced by the NO donor SNP reduced biofilm surface coverage by 80%

(Barraud *et al.*, 2006). DBPC NOMBs achieved a biomass reduction of 63.28%, which despite this test being conducted in static conditions is close to the results seen in the Barraud *et al.* (2006) study. Due to the longer hydrocarbon chain of DBPC the MB shell is comparatively thicker than DSPC MBs (paragraph 1.1.4), consequently the passive diffusion of NO from the MB would be slower and thus more sustained over time. The incubation of air filled MBs with biofilms increased the relative biomass compared to controls by 9.75% (**Figure 44**); this is an interesting observation that is potentially linked to the composition of the gaseous core. Although constituents of the MB used in these experiments such as PEG40s are reported to possess innate bactericidal properties (Park *et al.*, 1998; Nalawade *et al.*, 2015), it is possible that the relative increase in biomass here is the result of intercalation of lipids from the MB into the biofilm (Owen *et al.*, 2018a). Crystal violet binds specifically to the negatively charged components of bacterial cell membranes such as lipopolysaccharides and teichoic acids; the relative increase crystal violet stained biomass here therefore may be a result of crystal violet binding to negatively charged residues of oxidised MB shell constituents present in the well or shed from MBs. One of the potential issues of working with MBs in a microtiter plate, is that due to their low density they naturally rise to the surface out of suspension. However in this microtiter plate assay this was an advantage, as MBs pipetted into the well occupied the same 150 µL volume as the initial growth media; as such when MBs float to the surface contact will be induced with the pellicle. It could further be speculated that there is a relative increase in local oxygen, due to the diffusion of air from the MBs. In close proximity to the biofilm, this may potentiate the metabolic activity of dormant cells resulting in an increased biomass

The use of a microtiter plate for establishing naïve biofilms for high throughput assessment, is perhaps the most commonly used method in research today. It is a simple, inexpensive, high-throughput means to obtain data on anti-biofilm treatments, but does have some limitations (Coffey and Anderson, 2014). During the washing steps to remove planktonic cells and excess crystal violet, it is easy to disturb the pellicle formed at the fluid-air interface and detach loosely adhered cells (Azeredo *et al.*, 2017). Perhaps the biggest issues associated with this method is reproducibility, interpersonal difference in methodology or lab practices that can be detrimental to the comparability of tests (Kwasny and Opperman, 2010). A useful alternative to the flat bottom microtiter plate is the Calgary biofilm device, which allows biofilm to grow on pegs affixed to the lid that are immersed in the wells (Macia *et al.*, 2014). This ensures that biofilm formation occurs by a phase shift from planktonic to sessile, as opposed to sedimentation. Using a consistent method and exercising caution whilst pipetting, can mitigate some of the issues associated with the microtiter plate assay. By filling all peripheral wells with sterile water on the microtiter plate, fluid loss by evaporation is mitigated which aids the uniform development of biofilms and binding of crystal violet. Furthermore, careful placement of the pipette at the same point in each well to aspirate fluid can prevent disturbing the pellicle, which is formed at the medium-air interface (**Figure 43**).

As discussed in paragraph 1.1.4, the composition of the MB is important for the determination of biophysical effects in response to stimulation by ultrasound. It is perhaps just as important to account for the physicochemical interactions between the MB and the environment, caused by the composition of the MB. It is important to be able to balance the suitability of the MB composition for its intended application, with its efficacy to perform the assigned task. Recent studies have shown that PEG has anti-biofouling properties, though the exact mechanism by which this occurs is not clear (Shi *et al.*, 2016). The efficacy of antibiotic tobramycin was successfully enhanced against *P. aeruginosa* biofilms by conjugation with PEG, however in planktonic cells the conjugated antibiotic was reduced 10-fold (Du *et al.*, 2015). Therefore, in order to explain any relative increase in biomass it should be considered that constituents of the MB may be intercalating with bacterial membranes (**Figure 44**). Alternatively, if MBs constituents become electrostatically or covalently associated with the biofilm and take up the crystal violet stain, this could also result in the increase in biomass seen in this experiment (Zhang *et al.*, 2017). This effect could potentially be mitigated by centrifuging the MB suspension to remove any unincorporated lipids, but this may induce collapse of MBs and reduce their concentration.

4.5.2 *Development of a pathophysiologically relevant artificial WCM*

A significant development since the preliminary investigations carried out with the BOCS system, has been the implementation of a pathophysiologically relevant WCM; this has been an important step in ensuring the data gathered *in vitro* is as applicable as possible to what might be seen *in vivo*. To the best of the author's knowledge this work is the first to use a complex pathophysiologically relevant growth-medium, for the study of ultrasound-mediated therapies on clinically relevant biofilms. This research utilised and refined the basic media constituents present in the highly regarded Lubbock wound model developed by Sun *et al.* (2008), who have demonstrated the production of biofilms *in vitro* that exhibit morphological and functional characteristics that are analogous with *in vivo* wound biofilms (**Figure 49**). As a chronic wound is a nutritionally rich environment for bacterial growth and biofilm development, this needed to be accurately reflected in the media used for *in vitro* biofilm growth. The media explored in this research was specifically designed to contain the three most dominant pathophysiological factors present in the wound bed: damaged tissue, red blood cells and plasma. Firstly, BB is a complex desiccated-meat based growth-medium, which contains a high proportion of essential factors that would be present under normal physiological conditions (Seliwiorstow *et al.*, 2016). This importantly includes meat peptones, essential amino acids, salts and ketones such as sodium pyruvate and alpha-ketoglutaric acid, which have important regulatory functions in cellular metabolic activity and host immunocompetence (Mathioudakis *et al.*, 2011; Glasser *et al.*, 2017). Although *P. aeruginosa* is innately beta haemolytic (an organism capable of carrying out complete lysis of red blood cells), LHB was used to provide bacteria with immediate access to the nutritionally important components of red blood cells such as iron from haemoglobin (Reyes *et al.*, 1981; Pishchany and Skaar, 2012). The presence of plasma *in vivo* has been shown to significantly enhance adhesion of bacteria, which subsequently facilitates biofilm development in environments like the wound bed and on implanted medical devices (Wagner *et al.*, 2011; She *et al.*, 2016).

Therefore, it can be well reasoned that the WCM considered here provided *in vitro* environmental conditions, which are nutritionally analogous to those observed in a chronic wound *in vivo*.

For specific applicability to this research further optimisation from the Sun *et al.* Lubbock model was required, specifically to define the proportion of plasma required to balance sufficient planktonic growth with consistent biofilm development. The concentration of BB was fixed in accordance with the manufacturers recommended preparation of the medium, the concentration of LHB was fixed at 5% in line with the general recommendation for the concentration of blood used in diagnostic microbiology culture (Yeh *et al.*, 2009). A significant finding of this research was that TSB as a base medium facilitated good planktonic growth, however it allowed significantly less biofilm formation in the conditions assessed here (**Figure 47**). This difference is most likely due to the addition of essential amino acids (leucine, proline, serine and aspartate) in more complex media such as BB, which drive the production of important adhesion factors such as fibronectin binding protein that promotes bacterial adhesion (Singh *et al.*, 2017). In order to achieve an optimal balance between growth of planktonic phase and biofilm development, a concentration of 20% plasma was accepted as the most appropriate. Biofilms of *P. aeruginosa* grown in this optimised final wound constituent media (WCM) of BB, 5% LHB and 20% plasma, exhibited concurrent validity with the morphology of *in vitro* biofilms derived from debrided tissue chronic wound (**Figure 49**).

4.5.3 *Active testing of consolidated MB formulations on P. aeruginosa biofilms*

This work oversaw the implementation of four principal ultrasound responsive MB formulations: RAMBs, NOMBs, RAMBs$^+$ and NOMBs$^+$, which have been developed and characterised as part of the wider scope of this research. In order to assess the efficacy of each microbubble formulation in terms of their anti-biofilm and bactericidal activity, 40-second ultrasound stimulation was carried out at 0.9 MHz with a 20% duty cycle and 500 Hz PRF, at an acoustic pressure of 0.5 MPa at the target site. Initial experiments were carried out to assess the ability of each formulation to induce biofilm detachment without antibiotic (**Figure 50**), therefore the reduction in biomass observed can be attributed solely to the mechanical action of cavitating MBs and the specific MB composition. In these experiments, it was noted that there was a lack of congruity between the propensity of each MB formulation to induce detachment of the biofilm and exhibit biocidal activity. For example, NOMBs achieved the highest reduction in biofilm biomass of 94% and NOMBs$^+$ the lowest at 68.2% (**Figure 50**), however viability data indicated that their efficacy killing biofilm cells during treatment was 65.5% and 86.1% respectively (**Figure 55**). Whilst achieving a high level of biofilm detachment is desirable, this cannot supersede the bactericidal efficacy of the ultrasound stimulated MB formulation. This is principally because a high level of biofilm detachment in conjunction with a low level reduction in viability *in vitro*, would mean dissemination of live biofilm aggregates across a larger area of exposed and susceptible wound bed (Guilhen *et al.*, 2017). Due to the complex architecture of the biofilm and the innate tolerance to antimicrobial treatment that is imposed by the presence of the encasing extracellular matrix, it is perhaps unsurprising that each ultrasound stimulated MB formulation applied without antibiotic failed to attain even a 1-log (90%) reduction in culturable cells compared to untreated controls (**Figure 55**). However, this did establish an important baseline level of treatment efficacy, which can be solely attributed to the MB composition and cavitation. It is interesting to note that NOMBs and NOMBs$^+$ achieved a greater reduction in viability than their RAMB equivalents (**Figure 55**), it can be speculated that this is achieved specifically by an NO mediated interaction with the biofilm such as dispersal. The efficacy of sub-micromolar concentration of NO in mediating biofilm dispersal are now well established, even if the mechanism of action is not yet fully understood (Barraud *et al.*, 2006; Ren *et al.*, 2016; Howlin *et al.*, 2017). Research has shown that the dispersed cells are considerably more susceptible to antimicrobial treatments; it can therefore be inferred that adjuvant NO can potentiate antibiotics against biofilms (Howlin *et al.*, 2017).

Subsequent to testing each MB formulation alone, they were assessed again under the same conditions except for the addition of sub-inhibitory (4 µg/mL) gentamicin. This concentration of gentamicin was selected in line with preliminary experiments carried out using the BOCS system (paragraph 6.1.7.4), in order to assess whether the ultrasound stimulation of MBs could potentiate the effect of the antibiotic. In control biofilms that did not receive ultrasound stimulation, but had 4 µg/mL gentamicin applied for the same 100 second total treatment time as sonicated biofilms; there was no detectable reduction in biofilm biomass (**Figure 56**) or viability assessed by live/dead fluorescence microscopy (**Figure 57**). This is concurrent with both the literature in this area and the reduction in culturable biofilm cells seen in preliminary experiments carried out in this research (**Figure 76**); the application of 4 µg/mL can achieve a maximum 1-log (90%) sub-inhibitory reduction in culturable cells during exposure period > 1 hour (VanCleave *et al.*, 2017; Durham, 2018). It is first important to note, that consistent with efficacy of NOMBs alone in reducing total biofilm biomass; in tests carried out with 4 µg/mL gentamicin NOMBs were again the most effective combination, attaining a clinically significant 3-log (99.9%) reduction in total biofilm biomass (**Figure 56**). As observed in representative fluorescence microscopy images of an ultrasound stimulated NOMB-antibiotic suspension, this substantial reduction in attached biofilm is visibly palpable (**Figure 58**). The NO mediated impact of biomass reduction observed is compounded in these experiments, as the second highest reduction of 93.9% was achieved by NOMBs$^+$ (**Figure 56**). RAMBs and RAMBs$^+$ were consistently less efficacious than their NO analogues, achieving an average reduction in attached biofilm of 81.3% and 92.5% respectively. Though the addition of gentamicin has improved the potency of NOMB$^+$ treatment, as observed in previous experiments NOMBs$^+$ appear to suffer from pervasive retention of non-selectively bound MBs after treatment (**Figure 59**); with underlying areas of untreated, unperturbed biofilm (**Figure 54**).

Due to the presence of high numbers of residual MBs that remained non-selectively bound to the Ibidi® dish and biofilm surface after treatment (**Figure 54**, **Figure 59**), it is possible that the percentage surface area reduction achieved by NOMBs$^+$ in these experiments was underestimated. The SAT device is calibrated to expose the surface of the sonolid assembly (20 mm) to the administered pressure (0.5 MPa), consequently clustered MBs in close proximity can cause distortion of the ultrasound field and thereby reduce the efficacy of the treatment (Schutt *et al.*, 2014; Lazarus *et al.*, 2017). Due to the enhanced non-selective binding of cationic MBs to biofilms used in this research, the tight clustering of MBs is very evident from visual analysis of the post-treatment biofilm sample (**Figure 54**). Therefore, as cationic MBs are subject to physical greater physical constraints than uncharged MBs in contact with the biofilm, they may exhibit modified acoustic behaviour during cavitation. It has been shown that in MBs of a clinically relevant size (1 – 10 µM), that inter-MB distances of less than 37 µM can facilitate interactions between adjacent MBs that results in MB cloud collective behaviour (Schutt *et al.*, 2014). MB clouds can experience lower volume changes during oscillation and therefore reduce the impact of the local effect induced by the cavitating MB such as microstreaming (Lazarus *et al.*, 2017), this in turn would result in a lower shear stress imparted on the biofilm and reduced efficacy of the MB treatment. Moreover, though MB clouds will invariable still respond to ultrasound stimulation, the outer layer of shelled MBs in the cloud, may confer a shielding effect that prevents MBs at the core of the cloud from oscillating (Brennen, 2013; Schutt *et al.*, 2014). It may be possible to increase the efficacy of cationic MBs by lowering the concentration that is administered, this can be achieved by optimising the volumetric ratio used to dilute MB suspensions. Interestingly, the addition of the antibiotic gentamicin appeared to mitigate this issue somewhat (**Figure 56**), this is potentially due to cationic sites present on the gentamicin molecule acting as a buffer between the MB in solution; by creating greater distance between MBs due to the repulsion between like-charged molecules (Khan and Alden, 2002).

Perhaps the most important observation this work has made is that ultrasound stimulated NOMBs, have been shown to significantly potentiate the efficacy of sub-inhibitory concentrations of gentamicin (**Figure 60**). Compared to the number of culturable cells recovered from control biofilms, NOMBs achieved a 99.9% reduction in culturable cells that corresponds to a clinically significant 3-log (1000 fold) decrease in cells. Cationic RAMBs$^+$ and NOMBs$^+$ were equally as effective in terms of their bactericidal ability, with both formulations reducing the number of recoverable culturable cells by 99.8% (**Figure 60**). As cationic MBs have demonstrated the ability to non-selectively bind to biofilms (**Figure 39**), it was hoped that increasing the proximity of NOMBs to the biofilm would enhance the delivery of the NO released from the MB to biofilms; which would results in more efficacious treatment. It is important to note that in the investigations carried out in the SAT device, MB contact with the biofilm was artificially induced due to the orientation of the sonolid assembly. Therefore, the enhanced anti-biofilm and bactericidal activity of uncharged NOMBs observed in these experiments, may in itself demonstrate that NO release from MBs in closer proximity to biofilms can enhances its efficacy. Given that the sole difference between RAMBs and NOMBs in these experiments is the gas content of MB core, the significantly enhanced efficacy of NOMBs over RAMBs can only be attributed to NO-specific mediated effects (**Figure 60**). NOMBs were the only formulation to attain both a 99.9% reduction in attached biofilm biomass and culturable cells; these experiments can be used reliably validate the utility of ultrasound stimulated NOMBs, to potentiate sub-inhibitory concentrations of antibiotics as a means of inducing dispersal and killing of *P. aeruginosa* biofilms. Consistent with the data in this research, it has shown that NO-antibiotic combination therapy results in more substantial anti-biofilm effects than NO or antibiotic alone (Soren *et al.*, 2020). The research carried out by Soren *et al.* (2020) showed a maximum reduction of NO-colisitin treated biofilms biomass of 97.8%, the incomplete reduction in biomass has been attributed to the presence of populations of biofilm persister cells. Due to the mechanical perturbation of biofilms and antibiotic uptake induced by cavitating MBs (He *et al.*, 2011; Agarwal *et al.*, 2012; Rmaile *et al.*, 2014), these NO-mediated anti-biofilm effects such as dispersal and antibiotic potentiation can be further enhanced.

All biofilms were live/dead stained with Syto9 and PI to allow visualisation of the biofilm with fluorescence microscopy, this was principally to be able to track changes in surface area coverage. As one of the principal aspect this research assessed was biofilm dispersal and surface detachment, fluorescence staining could not be used to directly quantify the relative proportions of live and dead cells. Consequently, the culturability of the detached biofilm was assessed by quantitative CFU analysis, based on the Miles-Misra method of serial dilution and culturable colony counting (Jenkins and Maddocks, 2019). Culture-based enumeration of cells is one of the most commonly used methods in bacteriology, however under environmental stresses such as antimicrobial treatment some pathogens have been noted to enter a viable but non-culturable (VBNC) state (Highmore *et al.*, 2018;

Truchado *et al.*, 2020). As this can invariable result in an overestimate of treatment efficacy, direct viable counts can be performed on live/dead stained samples (Wilks *et al.*, 2020). Due to the efficacy of biofilm removal in this research, this direct quantification could not be reliably implemented on biofilms post-treatment (Appendix A – Supplementary experimental material, paragraph 6.1.9). Moreover, the persistence of residual MBs in the fluid scattering transmitted light predominantly in the red, would have significantly impacted on the reliability of this method (**Figure 54**). However, it has been noted that VBNC populations are less likely to develop, if the method of treatment is competently bactericidal (Kumar and Ghosh, 2019; Wilks *et al.*, 2020). As the peak treatment efficacy of NOMB-antibiotic suspensions was determined to be 99.9% by viable colony counting, it could be hypothesised that the potential development of VBNC populations would be minimalised substantially. As previously described in Chapter 1, persister cells represent a distinct, dormant sub-population of cells within the biofilm, typically found at the lowest layers of the biofilm where oxygen and nutrient depletion are prominent (Miyaue *et al.*, 2018). Metabolic activity such as cellular proliferation provide site of action for antibiotics; due to the lack of cellular activity within this sub-population of persister cells they are highly tolerant to antimicrobial therapies, which is why they are strongly implicated in the persistence of recalcitrant biofilm infections (Wood *et al.*, 2013; Chihara *et al.*, 2015). Therefore, it was important that research was able to confidently ascertain the extent to which the treatment modality was able to remove biofilms, but also be able to exert bactericidal activity in these highly tolerant sub-populations of biofilm cells.

Recent research has shown that release of NO from lipid-shelled MBs can occur rapidly within approximately 7 minutes of administration (Lafond *et al.*, 2020), it was therefore an important development in testing that NOMBs administered in SAT testing were applied immediately after production. Whereas, NOMBs utilised in preliminary testing in the BOCS system could not be applied to biofilms until > 90 minutes after production, though they were transported in ice the NO-linked interactions observed in SAT experiments are likely to have been acutely limited. An important step taken in this research was to verify the inclusion of NO within the MB (paragraph 2.4.3), though it is a limitation of the current research that the concentration of NO encapsulated by MBs could not be reliably assessed directly. NOMBs with a comparable lipid-shell formulation utilised by Lafond *et al.,* (2020) also describe the difficulties associated with determining the precise passive release profile of NOMBs, they attained a quantification of NO concentration by amperometric sensor that showed an average concentration in the suspension of 5 mM. The biofilm dispersal effects of nitric oxide and its innate antimicrobial ability due to antibiotic interactions, have been shown to be dose dependant in the range of 0.025 – 2500 nM (Arora *et al.*, 2015). With the number of similarities in MB production and NO loading methodology in this research compared to Lafond *et al.,* (2020), we can make the relative assumption that NOMBs utilised in this research are likely to contain a comparable concentration and release profile.

The success of low frequency ultrasound (20–100 kHz) in facilitating the uptake of systemic antibiotics by biofilms has been variable, therefore the use of ultrasound responsive MBs in light of their controllable physical response may be viewed as an evolution in antimicrobial drug delivery (Kooiman *et al.*, 2020). These effects have been demonstrated in physiologically relevant *in vitro* biofilm models of *S. aureus* infective endocarditis; Lattwein *et al.* (2018) showed that infected thrombi treated with combinations of MBs, plasma, thrombolytic, antibiotic and low frequency ultrasound (120-kHz, 0.44 MPa peak-to-peak pressure) could reduce infected clot mass by 99.3% (± 1.7%), this was termed a 'sonobactericidal' effect by the authors; as the treatment was signifcantly better than any other combination of the treatment agents. However, it is important to note that this study measured treatment efficacy by reduction in thrombi size. The study did not conduct a direct assessment of bactericidal or bacterostatic activity of the treatment, therefore there is no conclusive evidence from this study that cell death of bacteria within biofilm was achieved (Lattwein *et al.*, 2018). Consequently, viable biofilm-residing bacteria may become disseminated upon destruction of the thrombi, which would facilitate redevelopment of biofilms elsewhere (Müsken *et al.*, 2018). Research carried out by Hetrick *et al.* (2009) investigated the use of NO-releasing silica nanoparticles, however it focused only on the bactericidal efficacy of the NO and not on biofilm dispersal. Similarly, in recent work carried out by Choi *et al.* (2019) on NO delivery by perfluorocarbon micro-emulsion, only its antibacterial efficacy was assessed. This work importantly showed the effect that different NO concentrations can have on bacterial activity; using NO concentrations of 0.175 – 2.622 µM a 50% decrease in bacterial viability was observed in planktonic suspensions of *S. aureus*, however no discernible bactericidal activity was seen in planktonic suspensions of *P. aeruginosa* (Choi *et al.*, 2019). There is an exciting body of research investigating the potential of ultrasound responsive carriers of nitric oxide, however until this research only the bactericidal efficacy of NO carriers on planktonic bacterial suspensions has been demonstrated.

4.5.4 *Passive cavitation detection of DBPC:PEG40s shelled MBs*

In order to better understand the mechanisms by which MBs in this research initiate perturbation of the biofilm and potentiate antibiotic delivery, the acoustic behaviour of the primary DBPC:PEG40s shelled MB formulations was assessed by PCD. Testing was carried out at the relevant acoustic parameters administered to biofilms treated with MBs in SAT experiments, corresponding to 0.9 MHz, 20% duty cycle and a 500 Hz PRF; 45 V_{pp} was applied to the transducer to reach an acoustic pressure of 0.5 MPa at the target site for 40 s. An FFT showed that MBs in the sonolid assembly were responsive to the ultrasound stimulation, exhibiting both stable and inertial cavitation **Figure 62**. In order to more fully understand the acoustic behaviour of MBs, their time dependant response over the 40 s treatment period was investigated. It was shown that within the first few seconds of treatment the bulk volume of MBs seems to experience inertial cavitation and collapse, succeeded by stable cavitation of the remaining MBs and a residual low-level of inertial cavitation for the remainder of the treatment period **Figure 63**. Micro-jet formation and shockwaves are more transient biophysical effects attributed to the collapse of MBs in inertial cavitation, which can respectively puncture proximal membranes and increase membrane permeability through imparted mechanical stress (Yu *et al.*, 2014; Leow *et al.*, 2015). It can be hypothesised that in the treatment process tested here, that the 60 second passive interaction of NOMB may prime the biofilm for biological dispersal and potentiate antimicrobial efficacy. Subsequently, the initiation of ultrasound stimulation and inertial cavitation proximal to the biofilm (potentially in the form of shockwaves), actively drives the antibiotic deeper into the biofilm architecture and facilitates removal from the surface by mechanical perturbation (Dong *et al.*, 2013; Lentacker *et al.*, 2014; Rmaile *et al.*, 2014; Carugo *et al.*, 2015; X. Chen *et al.*, 2016).

4.6 Conclusion

This research is the first of its kind to report the efficacy of NO-loaded, ultrasound-responsive MBs, for the elimination of biofilms with a sub-inhibitory concentration of gentamicin. Preliminary data investigating the use of NOMBs for the elimination of biofilms, has been invaluable in providing direction in this project. One notable difference observed between active and passive testing, is the effect of NOMB composition on the efficacy of treatment. In passive testing, DSPC shelled NOMBs achieved the highest reduction in biomass (**Figure 44**). In contrast, DBPC NOMBs were substantially more effective than DSPC NOMBs during active testing (**Figure 76**). This can be explained in terms of the MB shell properties; due to the shorter hydrocarbon chains associated with DSPC phospholipids, the shell is comparatively thinner than DBPC MBs. In static tests this is an advantage as the NO may diffuse out of the DSPC MB more rapidly, whereas the thicker DBPC shell would demonstrate a slower and more sustained passive release over time. The advantage of DBPC shelled NOMBs is their utility in active testing, as DBPC MBs are likely to maintain their integrity for a longer period of time, this would result in more cycles of oscillation and subsequently more mechanical perturbation of the biofilm subsequent to NO release. PCD of DBPC:PEG40s shelled MBs used in this research confirmed that at the ultrasound stimulation settings used (0.9 MHz, 500 Hz PRF, 20% duty cycle, 0.5 MPa), MBs undergo an initial period of inertial cavitation, after the first few seconds of exposure the remaining MBs appear to undergo stable cavitation with a low-level of residual inertial cavitation over the remaining 40 s exposure time (**Figure 63**). The administration of DBPC NOMBs and sub-inhibitory concentrations of gentamicin to *P. aeruginosa* biofilms, was shown in preliminary BOCS testing to capable of attaining a greater reduction in culturable cells than DSPC NOMBs and RAMBS (**Figure 44**). However, the results were not able to demonstrate a consistent 99.9% clinically relevant reduction in culturable cells (**Figure 76**). The ultrasound stimulation parameters were refined and MB delivery method optimised for subsequent testing in the SAT device; it was shown that the administration of NOMBs alone could achieve a substantial reduction in attached biofilm and culturable cells without antibiotic, however a 3-log reduction was not shown (**Figure 50**, **Figure 55**). The addition of 4 µg/mL gentamicin to MB suspensions showed an overwhelmingly positive benefit, in particular in NOMBs where a 99.9% reduction in attached biofilm and culturable cells was consistently achieved (**Figure 56**, **Figure 60**); demonstrating the ability of NOMBs to potentiate antibiotic efficacy for the efficacious treatment of *P. aeruginosa* biofilms. Critically, this research remains the only work to have characterised and comprehensively demonstrate the efficacy of NO encapsulating ultrasound responsive agents, which have proven highly efficacious in the treatment and dispersal of bacterial biofilms. Furthermore, the development and implementation of WCM in this research also makes it the first to investigate ultrasound-mediated therapies, using *in vitro* biofilms that share morphological features analogous with *in vivo* biofilm samples. The contribution of a complex growth-medium to facilitate representative *in vivo* growth of *in vitro* biofilms should not be overlooked; going forward the use of this growth-medium could make a significant novel contribution, in the development of more complex multispecies models of biofilm infection.

CHAPTER V

5 PROJECT DEVELOPMENT AND FUTURE WORK

5.1 Introduction

The data collected so far in this research has provided significant groundwork on which this project can build, and enable greater understanding of the mechanisms behind the activity of ultrasound responsive NOMB for the dispersal and elimination of biofilms. In line with the aims of this project, the future work set out in this chapter seeks to further expand the available knowledge of bioactive microbubbles. Despite the efficacy demonstrated by NOMBs and the verification of significantly higher concentrations oxidised the products of NO in solution, there is presently no definitive value for the concentration of NO encapsulated by NOMBs in this research. Therefore a logical first step would be robust quantification of nitric oxide encapsulation and release kinetics, which will actively drive refinement of the NOMB gas loading fabrication methodology. The use of model *P. aeruginosa* biofilms in this research, provided an excellent means of assessing the fundamental efficacy and potential of ultrasound stimulated MBs for biofilm treatment. An important next step in this research will be to move into trials using more complex multi-species models of biofilms. One of the important mechanisms in this research that is not fully understood is the specific interaction of the ultrasound–responsive agent with the biofilm, which has potential to be evaluated by established high-speed imaging and microscopy techniques. Finally, this research has excellent translational features, which may be readily adapted for clinical implementation of ultrasound-mediated therapies for biofilms in chronic wounds.

5.2 Quantification of nitric oxide encapsulation and characterisation of active and passive release

Now that the stability of NOMBs has been characterised it will be important to establish the release kinetics of NO gas from the MB; to date this has only been carried out in one study *(Chapter 1, 6.2.2)*. This research previously attempted to use Greiss reagent to detect the final products of nitric oxide

(NO) oxidation, such as nitrate and nitrite (Giustarini *et al.*, 2008). Due to the slow kinetics of the reaction and a small NO volume, the data produced was unreliable and lacked repeatability. There are a number of options that can be explored for measuring the level of NO in solution, including chemiluminescence and electrochemical detection (Woldman *et al.*, 2009; Privett *et al.*, 2010). Chemiluminescence is considered the standard for measuring NO levels in solution, NO is detected by reaction with ozone to form NO_2 in a state of excitation, which emits a photon upon returning to ground state (Hunter *et al.*, 2013). The light emission is detected by a photomultiplier and is directly proportional to the NO present in the sample; the reaction is highly specific to NO and produces highly accurate results (Hetrick and Schoenfisch, 2009). Electrochemical detection of NO is somewhat more diverse than chemiluminescence, it can be used to measure NO in most biological systems with high precision and accuracy (Hunter *et al.*, 2013). The use of electrochemical sensors has been very successful in detecting NO in oxygenated PBS, which is usually achieved by electro-oxidation of NO by applying potential current (Ho *et al.*, 2003). Electrochemical detection of NO was attempted with a nitric oxide Sensor (NO-100 microsensor, Unisense) in this research, prior to the use of DHR fluorescence detection of oxidised NO products (paragraph 2.2.5). It was not possible to quantify NO release with the electrochemical sensor as expected, principally because NO standards to plot a calibration curve for NO concentration could not be reliably established. However, recent research on comparable a comparable NOMB formulation showed that MBs co-loaded with octafluoropropane and nitric oxide, contained an NO concentration 2-5 mM in an undiluted suspension with rapid release over 340 seconds. In line with aforementioned studies, a 1:5 diluted suspension of NOMBs used in this research would be within the range of 450 nM shown to induce biofilm dispersal. Though the release of NO from MBs over time was also characterised by Grishnkov *et al.* (2015), they did not quantify the NO loading concentration. It will be important to establish the release of NO over time of the specific NOMB formulation used in this research, for both cationic and neutral MB suspensions. It will also be important to determine how long NO remains in solution and at what concentration; this can in turn be used to determine the bioavailability of NO, which will induce dispersal upon release from NOMBs.

Passive diffusion of NO from the MB may have a valuable priming effect on the biofilm, before the application of ultrasound. This may dictate changes in the MB priming time before ultrasound stimulation, which was set to 60 seconds in the current research. In conclusion, the quantification of nitric oxide by MBs is a crucial factor in determining the progression of this research for two reasons: i) the dose-dependent effects of NO on biofilms is a key determining factor in the efficacy of its administration (Arora *et al.*, 2015); ii) NO is known to interact with aminoglycoside antibiotics such as gentamicin; i.e. in high concentrations NO acts as a competitive inhibitor of the antibiotic (Howlin *et al.*, 2017). Future work on the development of ultrasound-responsive carriers of NO should aim to identify and identify means of reliably controlling the concentration of encapsulated NO. The use of perfluorocarbon nanodroplets is one potential modification that could improve NO loading and retention. This is principally as nanodroplets contain a liquid perfluorocarbon core into which NO can be effectively solubilised (Ortiz *et al.*, 2013); upon application later of ultrasound the liquid core can be vaporised into a gas phase (X. Xu *et al.*, 2017). The use of nanodroplets that are generally more concentrated and smaller than MBs, would confer a greater control over the retention and delivery of NO.

5.3 Development of a clinically relevant wound model

One of the primary concerns of current *in vitro* models of biofilms, is their comparatively poor translation to real world scenarios. A significant proportion of research focuses exclusively on single species biofilms grown for 24 hours (Dong *et al.*, 2017), which distinctly lack the characteristics of biofilms that are be found *in vivo*. This research utilised the basic media constituents present in the highly regarded Lubbock wound model developed by Sun *et al.* (2008), who have demonstrated the production of biofilms *in vitro* that exhibit morphological and functional characteristics that are analogous with *in vivo* wound biofilms. As a chronic wound is a nutritionally rich environment for bacterial growth and biofilm development, this needed to be accurately reflected in the media used for *in vitro* biofilm growth. The media explored in this research was specifically designed to contain the three most dominant pathophysiological factors present in the wound bed: damaged tissue, red blood cells and plasma. To build on this further as the role of NOMBs in the resolution of biofilm infections is refined, the use of more complex multi-species models of wound infection could be considered. An established model of chronic wound infection by Touzel *et al.* (2016), utilised a Centres for Disease Control and Prevention bioreactor to incorporate *Klebsiella pneumoniae*, *P. aeruginosa, S. aureus* and *Enterococcus faecalis*. Whilst this model is representative of species most commonly isolated from chronic wounds, the biofilm itself is relatively naïve at only 30 hours old. It would be beneficial to develop a model of chronic wound infection that also considers the normal microflora of the diabetic foot, to provide representative microbial interactions of ordinarily commensal bacteria in the chronic wound. Studies have shown that specifically in DFU; *P. aeruginosa, S. aureus* and the fungus *Candida albicans* are the most commonly isolated organisms (Bansal *et al.*, 2008). A significant progression in this research was the development of WCM, in which *P. aeruginosa* biofilms were grown for 48 hours. This resulted in the development of more complex biofilms, which have been shown to exhibit key morphological characteristics associated with biofilm samples derived from wounds *in vivo*. There is vast potential for this research to contribute to a successful clinical application, by bringing together the various facets of this interdisciplinary project. It will be especially important to consider the role of the niche microbiome of the diabetic foot and how the complex inter-species interactions impact the proposed NOMB treatment modality (Jneid *et al.*, 2017). The Touzel *et al.* multi-species biofilm model will provide a good starting point for future testing of NOMB efficacy in a complex biofilm model, however this could be adapted to account for further inter-species and commensal microorganism interactions.

5.4 Closing remarks

Over the last decade research focus has seen a transition in focus from acute infection to multi-drug resistant (MDR) organisms and biofilms, which mediate over 90% of chronic wound infections (Attinger and Wolcott, 2012; Bjarnsholt, 2013). The augmented persistence of biofilms can be attributed in part to inherited genetic antibiotic resistance traits, which actively reduce the efficacy of an administered antimicrobial agent. However, studies of the biofilm life cycle have shown that the use of NO in the sub-micromolar range, is able to stimulate endogenous mechanisms of biofilm dispersal (Barraud *et al.*, 2015). By inducing dispersal of the biofilm with NO, the physical barrier imposed by the EPS matrix can be negated entirely. The major problem with the delivery of NO in a gaseous form is that it is highly reactive, which translates to a half-life of only seconds (Thomas *et al.*, 2001). A solution to this challenge is to utilise an ultrasound responsive agent such as the MB, which could provide the means to successfully control the delivery and release of NO. Very few studies have utilised NO as the core of gas microbubbles; until this research no one has reported on the anti-biofilm effects of a NOMB formulation, as other research has exclusively focused on the utility of NO releasing agents to induce direct bactericidal effects (Hetrick *et al.*, 2009; Lattwein *et al.*, 2018; Choi *et al.*, 2019; Lafond *et al.*, 2020)

The principal aim of this research was to develop an ultrasound-responsive agent that could be utilised in the treatment of biofilms in chronic wounds. The first objective was therefore to characterise an ultrasound-responsive agent capable of delivering nitric oxide contained in MBs; which can be administered with free antimicrobial compounds, for dispersal and elimination of biofilms respectively. Through theoretical evaluation and robust practical assessment, we successfully demonstrated the utility of sonication as a means of producing NOMB suspensions. Importantly, the NOMBs produced in this manner composed of a DBPC:PEG40s lipid shell in a 9:1 molar ratio, were both stable and responsive to ultrasound stimulation with an average post-production diameter of 3.3 µm (SD ±1.9). With supporting evidence from comparable MB formulations in the literature, we have verified that the MBs produced were sufficiently stable for current *in vitro* and prospective downstream *in vivo* applications. Research released since the production of lipid-shelled NOMBs in this research by Lafond *et al.,* (2020), has cited this research as a source of information for the development of their own lipid-shelled NOMB formulation. A significant challenge within this work was establishing an accurate assessment of nitric oxide concentration and release kinetics, the use of fluorescence detection methods demonstrated that NOMB suspensions contain a highly significant quantity of peroxynitrite; which can only occur as a direct result of oxidation of NO in solution over time.

The second objective of this research was to assess the utility of electrostatic interaction as a means of non-selective biofilm targeting, by modifying the engineered NOMB to contain a cationic lipid. The use of electrostatic interactions for facilitating targeted drug delivery has been considered successful in other research, with the principal aim of creating a ‘reservoir’ of drug carriers proximal to the target area (Bajpayee and Grodzinsky, 2017). In this research cationic microbubbles demonstrated the ability enhance microbubble-biofilm contact by up to 37%, with a binding strength comparable to that seen in specific ligand-receptor targeting of biofilm extracellular matrix constituents. The use of electrostatic interaction as a means of facilitating drug delivery is by no means a novel concept in itself, however the development of cationic NOMBs and their subsequent application to biofilms in this research has not previously been characterised. The novel application of cationic NOMBs to biofilms facilitates the delivery of NO from the MB, by reducing the diffusion distance between the MB and the biofilm. However, further research that specifically investigated the efficacy of cationic NOMBs stimulated by ultrasound, showed that the benefit of creating a cloud of NOMB to utilise their passive anti-biofilm effects unfortunately impacts upon their acoustic response.

It was the third objective of this research to fully assess the therapeutic efficacy of the developed ultrasound responsive agents, in terms of their anti-biofilm and bactericidal effects. This research is consequently the first of its kind to report the efficacy of NO-loaded, ultrasound-responsive MBs, for the elimination of biofilms with a sub-inhibitory concentration of gentamicin. To facilitate growth of *in vitro* biofilms that shared comparable structural and functional characteristics of *in* vivo chronic wound biofilms, a wound constituent media featuring key pathophysiological components of the wound environment *in vivo* was developed. It was successfully demonstrated that insonified DBPC nitric oxide microbubbles could reliably elicit a clinically significant 99.9% (3-log reduction) in culturable cells recovered from treated biofilms, by enhancing the efficacy of sub-inhibitory (4 µg/mL) concentrations of the antibiotic gentamicin. Moreover, the combination of the nitric oxide and the ultrasound mediated physical perturbation of biofilms by microbubbles, was also shown to elicit a significant 99.9% reduction in surface area covered by *P. aeruginosa* biofilms.

With the development of a novel NOMB that exhibits potent anti-biofilm and bactericidal effects, the final objective of this research was to assess the feasibility of implementing a clinically viable translation. This work provided the principal design and methodology to develop the simple and cost-effective system for ultrasound mediated interventional therapy (SUMIT), for delivering ultrasound and MBs to a superficial wound area. The system functioned by injecting a suspension of bubbles onto a contained area over the wound which allowed a 1 MHz ultrasound stimulation to be applied. The use of 3D-printed components contributed to easy manufacturing with fast throughput. The selection of soft and pliable PDMS for the treatment area was ideal for creating a watertight interface with the foot, because it was able to conform to the uneven surface geometry. Acoustic pressure field variances within the 1 cm fluid cavity were quantified by a coefficient of variance of 0.162. Although this work provides a successful proof of concept for delivering ultrasound-mediated microbubbles to a surface wound, there are invariably still improvements that are required for future use in clinical applications.

To conclude, this research has met its defined objectives in the development, characterisation, targeting and application of a novel ultrasound-responsive carrier of nitric oxide; for the dispersal and elimination of biofilms with translational applicability in chronic wounds. Importantly, this has also lead to us breaking ground on the overarching aim of this research; to develop an ultrasound-mediated therapy for the treatment of biofilms in chronic wounds. Whilst there are inevitably further avenues to explore in this area, the significance, novelty and scope for impact of this project has become evident. The data presented in this thesis demonstrates; the reliable generation of stable NOMB, the efficacy of electrostatic charge as a means of non-selective targeting of biofilms, the ability of NOMBs to facilitate biofilm removal from surfaces and potentiate sub-inhibitory concentrations of antibiotic and the feasibility of a viable clinical translation with SUMIT. The further refinement and exploration of this area can only lead to a better understanding of at least one new way, with which the global issue of antibiotic resistance and bacterial biofilms can be overcome. In order to achieve fundamental change in healthcare practices such as the treatment of chronic wounds, we believe this research exemplifies the need for collaborative and interdisciplinary research to potentiate existing therapies and develop novel treatment modalities.

6 APPENDICES

6.1 Appendix A – Supplementary experimental material

6.1.1 *Determining the fit of 4 mm tubing into acrylic holes*

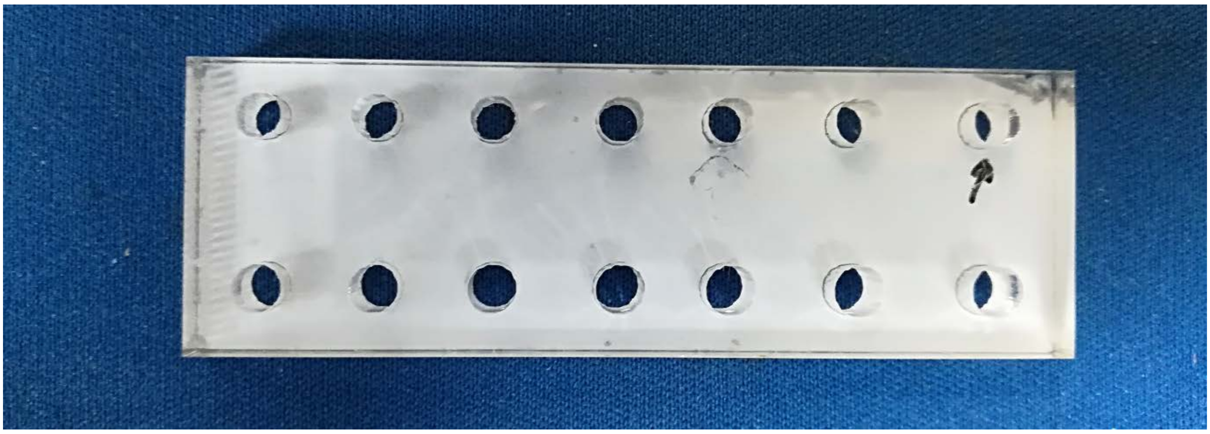

Figure 64 Test holes laser cut into acrylic to determine inlet and outlet diameter. The 4 mm tubing was inserted into each hole of different diameter and the diameter 3.5 mm (indicated by the arrow) was chosen that offered a balance between a secure tight fit and ease of insertion.

6.1.2 *Biofilm development within 24 hours in flow cells*

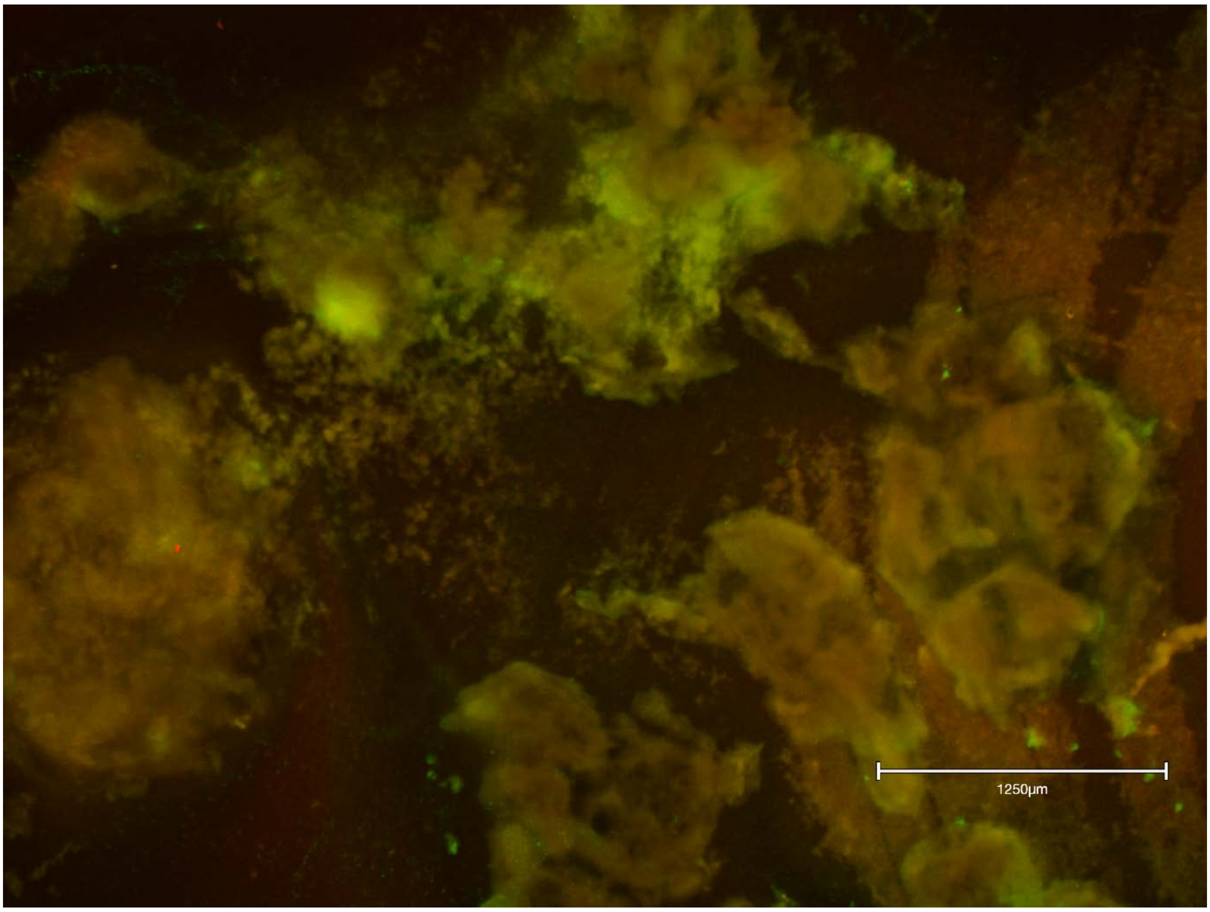

Figure 65 Example of biofilm growth after 24 hours in flow cells captured using a gain of 150, light source intensity of 1.8, brightness of 0.5 and an exposure time of 90 ms, with the EVOS M5000 (Invitrogen™, ThermoFisher Scientific) and a 2x objective (EVOS plan fluor AMEP4931, Invitrogen™, ThermoFisher Scientific). An emission wavelength of 498 nm (GFP LED cube, AMEP4653, Invitrogen™, ThermoFisher Scientific), was used to capture images of the green fluorescent Syto9 stained proportion of the biofilm. Images of the red fluorescent propidium iodide stained proportion of the biofilm, were acquired with an emission of 617 nm (RFP LED cube, AMEP4653, Invitrogen™, ThermoFisher Scientific). Scale bar represents 1250 µM.

6.1.3 *Cationic MBs with increased molar ratio of DSEPC*

MB concentration increased after static interaction with neutral and anionic glass for MBs with 9:0.5:2 DSPC:PEG40s:DSEPC molar ratio. A higher proportion of cationic lipids (DSEPC) resulted in the 9:0.5:2 molar ratio MB having a more positive charge relative to the 9:0.5:1 molar ratio MBs. Non-selective binding of the 9:0.5:2 DSPC:PEG40s:DSEPC molar ratio MBs to the neutral glass could have occurred, this may have been due to moisture retention in the device trapping some bubbles by hydrostatic rather than electrostatic forces. It was decided that subsequent experiments would exclude the 9:0.5:2 molar ratio composition. This was principally due to the potential that the high level of non-selective binding to uncharged surfaces translated *in vivo*, could pose a potential barrier to effective delivery of MBs that become trapped away from the treatment target.

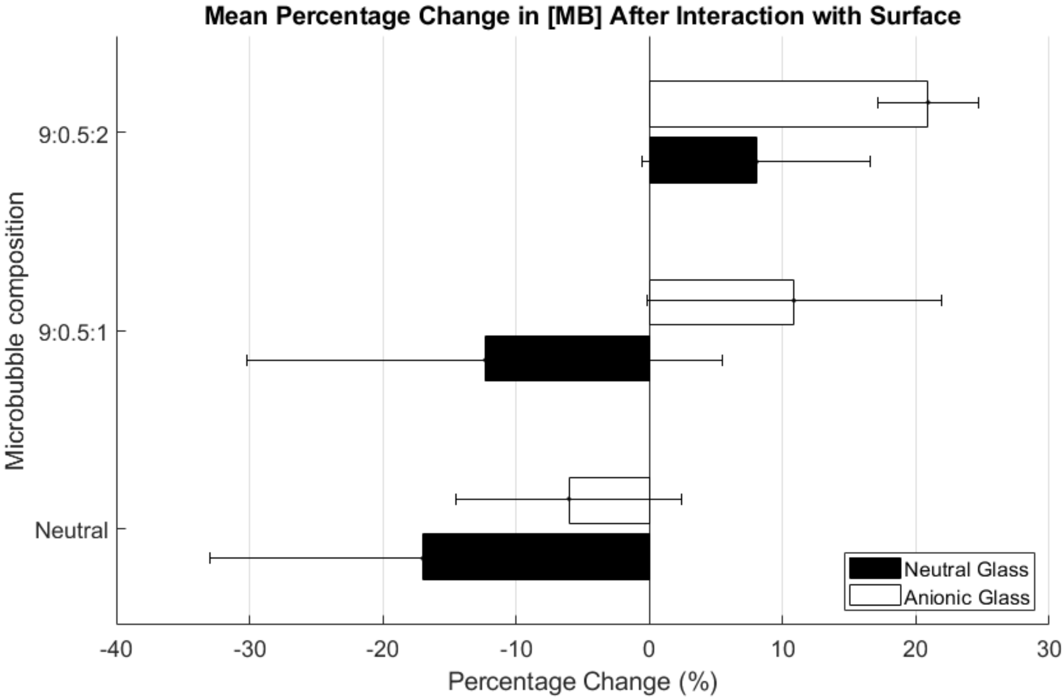

Figure 66 Mean percentage change in MB concentration after interaction with flow cell glass surface for 1 min. Error bars represent the standard error of the mean. Neutral MB concentration fell after interaction with both neutral and anionic glass. MB concentration of 9:0.5:1 DSPC:PEG40s:DSEPC molar ratio MBs increased after interaction with anionic glass, but decreased with neutral glass. 9:0.5:2 DSPC:PEG40s:DSEPC molar ratio MBs increased after interaction with both neutral and anionic

glass. Significant overlap in error bars also made the data from this experiment less reliable, thus all experiments with charged MBs were repeated in full. The origin of this error is thought to be caused by changes in pH of the MB solution before administration to the flow cell, future experiments measured pH before proceeding.

6.1.4 *Flow cell visualisation of biofilm-MB interaction optimisation*

A challenge in assessing the interaction between cationic MBs and biofilms the flow cell designed in this research was visualisation; as the presence of a biofilm on the glass surface prevented simultaneous visualisation of the MBs and biofilm. This was principally due to MBs being in phase closest to the glass surface, effectively obscuring all the underlying biofilm architecture with the exception of the most superficial residual planktonic phase (**Figure 34**). The converse was true if the biofilm was grown on the acrylic manifold of the device, as the MBs could be visualised effectively but the biofilm could not. To overcome this issue initiative was taken to develop a second generation flow cell to include a glass-glass interface, so that the channel in which the biofilm is grown can be viewed from both sides (**Figure 67**). A window was created in the acrylic backing of the flow cell, however the dimensions of this were limited by the need to maintain the structural integrity of the flow cell, which consequently limits the area of the channel that can be viewed. Due to the reduction in flow cell stability the dimensions of the cavity in the acrylic manifold to allow a microscope objective lens to reach the glass surface, could not be made large enough to incorporate a range of objective sizes which reduced the utility of the device. The second generation of the flow cell was also designed to facilitate the application of ultrasound; an ultrasonic transducer can be adhered to one of the glass surfaces to perform acoustic studies on MBs under flow, given the efficient coupling between the ultrasound transducer and glass. However, this design has not yet been used in any tests.

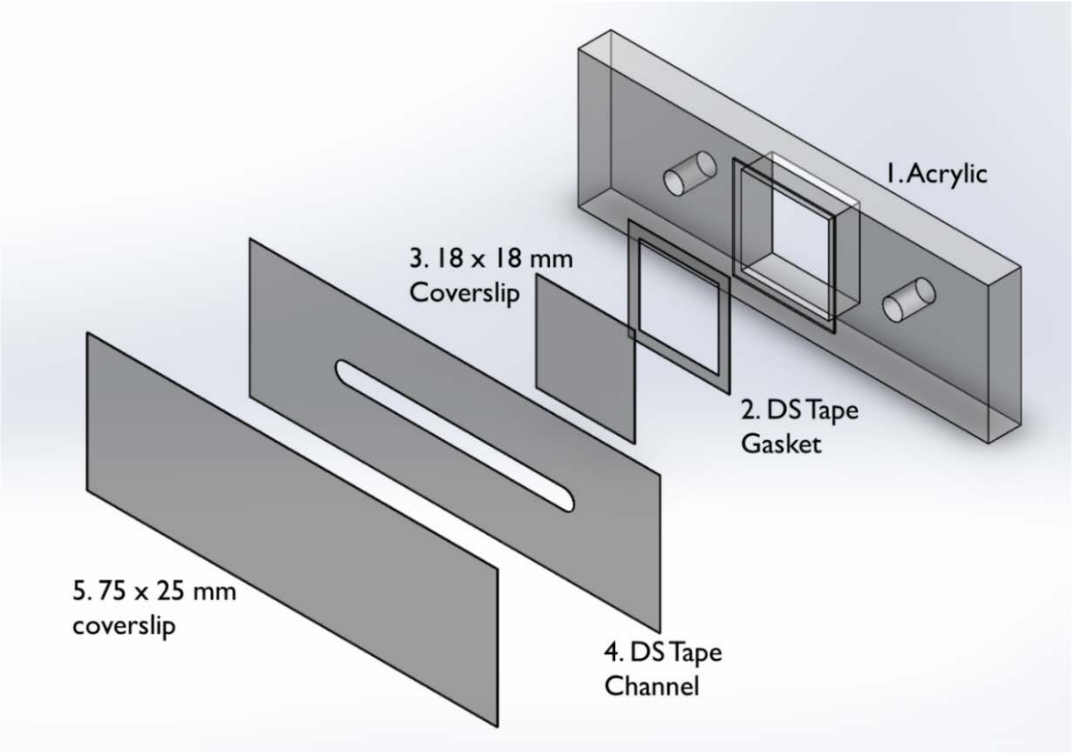

Figure 67 Glass-on-glass flow cell: exploded view with parts labelled. The acrylic, double-sided tape gasket and double-sided tape channel were laser cut. DS Tape – Double-sided tape. Firstly, the window, inlet and outlet holes were laser cut from 6 mm acrylic cut to 75 mm by 25 mm. A lip was engraved around the window to a depth of 0.31 mm to counter-sink the glass window (Speed 400, 25% power, 1-2 repeats or until depth was achieved). Next, a small piece of double-sided tape was placed over the window and the lip, and laser cut to form a gasket that fit in the lip. An 18 x 18 mm glass coverslip was adhered to the double sided tape to form the small glass window. Double-sided tape was taped down to a piece of acrylic (without removing the paper backing) and the channels were laser cut before adhering the double-sided tape to the flow cell. A 75 x 25 mm glass coverslip was fitted onto the double-sided tape to complete the flow cell.

In an additional effort to overcome the issue of visualising MBs and biofilms in the first generation flow cell, the lipophilic stain DiI was instead incorporated into the MB shell (**Figure 68**). This allowed the MBs and Syto9 stained biofilm to be visualised simultaneously using fluorescence microscopy, as the two fluorophores can be viewed under independent fluorescence channels. The limitation of fluorescently labelled MBs is that the altered composition can impact upon their stability, however at the concentration of dye used the effects should be minimal (Kooiman *et al.*, 2017). Though this method seemed initially effective, there was a considerable amount of light scattering caused by the presence of MBs. It has been shown that MBs can behave like individual optical lenses and created a distorted ring peripheral to the gas core, due to the change in refractive index as light is transmitted through the gas-filled MB and surrounding fluid (Ibsen *et al.*, 2013; Leung *et al.*, 2013). This optical distortion caused by the light scattering MB is clearly evident in this work (**Figure 69**); to overcome this challenge in imaging MBs and biofilms simultaneously imaging was carried out using the EVOS M5000. With the EVOS microscope separate images from fluorescent and bright field channels could be captured, these can later be overlaid in post-processing to provide an accurate reconstruction of biofilm architecture and MB positioning (**Figure 38**). This would mean that biofilms can be fluorescently labelled and MBs can be visualised in bright field, mitigating the need to fluorescently label the MB.

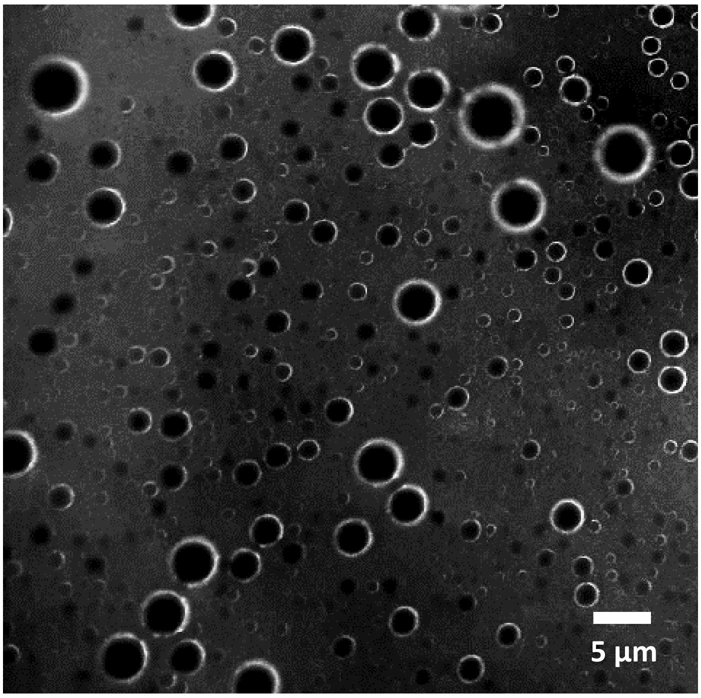

Figure 68 The inclusion of fluorescent stain DiI into the MB shell allows simultaneous visualisation of MBs and biofilm in the acrylic-on-glass flow cell. Images were taken using a x50 objective, using the uncharged borosilicate flow cell.

Figure 69 Biofilm grown in acrylic-on-glass flow cell stained with green fluorescent Syto9, MBs were stained with DiI that has an emission wavelength of 565 nm (red). The red box indicates MBs present in proximity to sessile bacterial cells scattering light creating a ring distortion around the gas core of the MB, scale bar indicates 10 µm.

6.1.5 *Calibration of BOCS system used in preliminary ultrasound stimulation investigations*

The acoustic pressure field was characterised using a needle hydrophone (200 m diameter needle, Precision Acoustics, Dorchester, UK), with the ultrasound stimulation setup submerged in a tank filled with filtered and degassed water. All tests were performed at the location where biofilms sit in the device; a distance of 14.5 mm from the transducer. The transducer had a peak output, at 200 V_{pp}, 0.5 MPa.

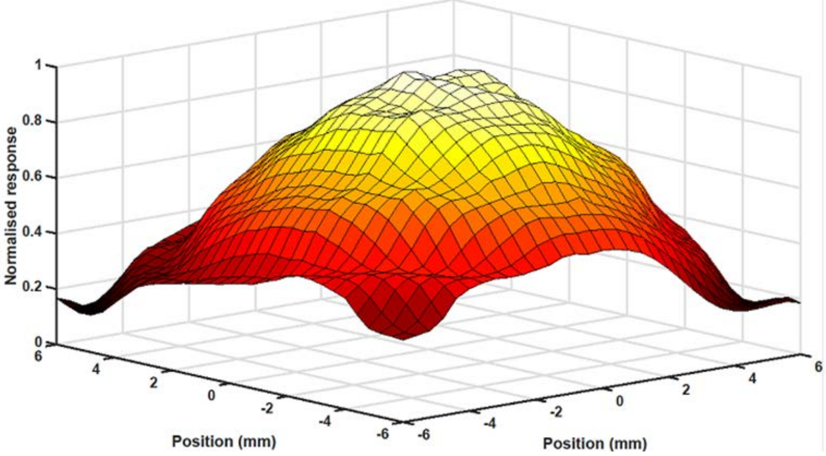

Figure 70 The BOCS system was calibrated with an input voltage was 200 Vpp which produced a maximum peak-to-peak pressure of 0.5 MPa at the biofilm on the surface of a polypropylene coupon. The frequency of the ultrasound was 1 MHz and every exposure was 5 minutes long. In experiments with pulsed ultrasound a 25% duty cycle with a 100 kHz PRF was used.

6.1.6 *Calibration of SAT device used in ultrasound stimulation investigations*

The SAT used in this work was calibrated by Dr Michael Gray (Institute of Biomedical Engineering, University of Oxford), with the system fully assembled using a fibre optic hydrophone inserted through the D-shaped hole in the cover plate (**Figure 71**). Using these results, the required drive voltages to produce a spatially averaged pressure of 1.0 MPa peak to peak is shown in **Table 7**. The spatial average was calculated over the width of the Ibidi® dish membrane (~20mm). Note that the required voltage is frequency dependent, and all calibrations have an uncertainty of 13%, corresponding to the value given by the hydrophone manufacturer. Power amplifier gains have been observed to drift significantly during their warmup, so the amplifier was run for at least 15 minutes prior to starting cell exposure experiments. It was strongly advised that power amp output voltage be verified as part of each experiment.

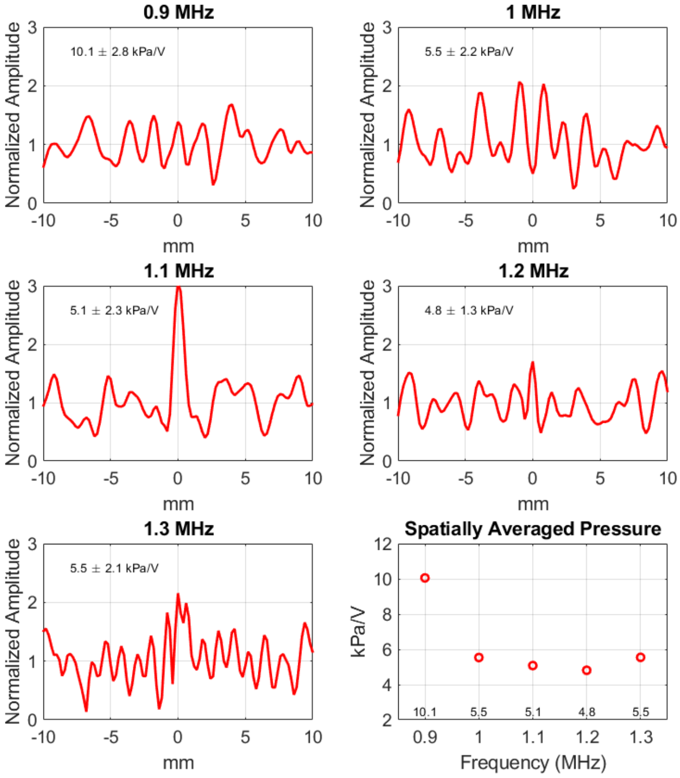

Figure 71 Calibration plots of SAT demonstrate that 0.9 MHz and 1.2 MHz driving frequencies create the most uniform field of pressure at the target treatment site, however the spatially averaged pressure showed that 0.9 MHz was the most efficient. At 0.9 MHz there is a greater pressure obtained at lower applied voltage to the transducer, therefore this frequency was selected to prolong the lifetime of the SAT transducer, provide efficient delivery of ultrasound with minimal or no heating, and achieve a uniform pressure over the treatment area defined.

Table 6 Drive voltages for 1 MPa peak-peak spatially averaged pressure

Frequency (MHz)	Vpower amp (V_{pp})
0.9	100
1.0	181
1.1	197
1.2	208
1.3	180

6.1.7 *MATLAB code used for analysis of MB PCD data*

6.1.7.1 Energy

```
% process_pcd_06Nov2020.m
% Example script for processing pcd data from SAT-D
% MDG, 06Nov2020

for i=1:6


%% 1. SETUP: set paths and basic processing parameters
datadir = 'F:\Southampton - 2020_12_19 TUTTO\BioLab\...
3 - Acoustic characterization\2020_12_17 - PFB NDs...
  Qiang 1 MHz focused\N6\Processati Matlab\';

% filename front, used for file loading
if i == 1
  nmfrnt = '10mV';
elseif i == 2
  nmfrnt = '20mV';
elseif i == 3
  nmfrnt = '50mV';
elseif i == 4
  nmfrnt = '100mV';
elseif i == 5
  nmfrnt = '150mV';
elseif i == 6
  nmfrnt = '200mV';
end

% pcd preamp gain, if any.
gain = 1;
```

```
% file list
dd = dir([datadir,nmfrnt,'*.txt']);
% number of files
Nfiles = length(dd);

% FUS drive frequency, Hz
f0 = 1.0e6;
% spectrum bin width: 1/50th of f0, Hz
bin = f0/100;
% pulse repetition frequency
prf = 1;


%% 2. PROCESSING Loop
for qd = 1:Nfiles
  tmp = importdata([datadir,nmfrnt,num2str(qd),'.txt'],';',9)
  % columns are semicolon delimited, 9 header lines

  % extract data parameters needed for spectrum processing
  if qd==1
    % sample rate, Hz
    fs = 1/diff(tmp.data(1:2,1));
    % file length
    Npts = length(tmp.data(:,1));
    % number of fft points
    Nfft = round(fs/bin);
    % overlap size in pwelch
    Novr = round(Nfft/2);
    Nfrq = round(Nfft/2)+1;
    % number of points in pwelch spectrum (one-sided)
    P = zeros(Nfrq,Nfiles);
    % presize power spectral density matrix

    fharm = f0:f0:floor(0.9*fs/2);
    % drive harmonics below Nyquist
    % indices of harmonics
    iharm = round(fharm/bin) + 1;
    iharmselected = [iharm(1,3:11)];
    %nharm = length(iharm);
    nharm = length(iharmselected);

    fuhrm = f0/2:f0:floor(0.9*fs/2);
    % ultraharmonics below Nyquist
    % indices of harmonics
    iuhrm = round(fuhrm/bin) + 1;
    iuhrmselected = [iuhrm(1,3:11)];
    %nuhrm = length(iuhrm);
    nuhrm = length(iuhrmselected);

    % Presize harmonic data
```

```
    Pharm = zeros(nharm,Nfiles);
    % Presize ultraharmonic data
    Puhrm = zeros(nuhrm,Nfiles);
  end

  [P(:,qd),F] = pwelch(tmp.data(:,2)/gain,Nfft,Novr,Nfft,fs);
  % run pwelch, P is units of V^2 / Hz

  Pharm(:,qd) = P(iharmselected,qd)+P(iharmselected+1,qd)+...
     P(iharmselected+2,qd)+P(iharmselected-1,qd)+ ...
     P(iharmselected-2,qd);
  % Harmonic power
  Puhrm(:,qd) = P(iuhrmselected,qd)+P(iuhrmselected+1,qd)+...
     P(iuhrmselected+2,qd)+P(iuhrmselected-1,qd)+...
     P(iuhrmselected-2,qd);
  % Ultraharmonic power

end

% Total power by signal type, units are V^2
Pwr(:,1) = sum(P,1)*bin;                % total
Pwr(:,2) = sum(Pharm,1)*bin;            % harmonic
Pwr(:,3) = sum(Puhrm,1)*bin;            % ultraharmonic
Pwr(:,4) = Pwr(:,1) - sum(Pwr(:,2:3),2);   % broadband

% Energy: sum the powers and multiply by the record time
Trec = diff(tmp.data([1 end],1));       % data record length
E = sum(Pwr,1)*Trec;                    % energies (V^2*s)

if i == 1
  E10 = E;
elseif i == 2
  E20 = E;
elseif i == 3
  E50 = E;
elseif i == 4
  E100 = E;
elseif i == 5
  E150 = E;
elseif i == 6
  E200 = E;
end




%% 3. PLOT
t = (0:Nfiles-1)/prf;

if i == 1
  figure(1)
```

```
elseif i == 2
    figure(2)
elseif i == 3
    figure(3)
elseif i == 4
    figure(4)
elseif i == 5
    figure(5)
elseif i == 6
    figure(6)
end

limits = [-142 -100];

set(gcf,'position',[100 200 1200 400])
subplot(1,2,1)
    pcolor(t, F(211:1251,1)*1e-6, 0.5*db(P(211:1251,:))),...
        shading flat, ...
        h=colorbar('vert');
    caxis(limits);
    h.Label.String = 'dB re V^2/Hz'; colormap jet
    xlabel('Exposure Time (s)'), ylabel('Frequency (MHz)')
    title('Power Spectral Density')

subplot(1,2,2)
    plot(t, 0.5*db(Pwr))
    xlabel('Exposure Time (s)'), ylabel('Power, dB re V^2',...
        'interpreter','tex')
    title('Power By Signal Type')
    legend({['Total, ', num2str(0.5*db(E(1)),3),...
        ' dB re V^2 \bullet s'],...
            ['Harmonic, ', num2str(0.5*db(E(2)),3),...
            ' dB re V^2 \bullet s'],...
            ['Ultraharmonic, ', num2str(0.5*db(E(3)),3),...
            ' dB re V^2 \bullet s'],...
            ['Broadband ', num2str(0.5*db(E(4)),3),...
            ' dB re V^2 \bullet s']},...
            'location','se','fontsize',10)
    ylim([round(min(min(0.5*db(Pwr))))...
        -20 round(max(max(0.5*db(Pwr))))+10 ])

end

Etot = [E10; E20; E50; E100; E150; E200];
%Etotdb = 0.5*db*Etot;

% end mfile
```

6.1.7.2 **FFT**

```
%% Import the data
```

```
[~, ~, raw] = xlsread('\\filestore.soton.ac.uk\users...
\sf2e17\mydocuments\Southampton\BioLab\3 - Acoustic...
   characterization\2018_12_04 - TESTS - BOX+ ...
   absorbing mat 50,100,150,200\1_50mV, no MBs,...
   no abs\ALL0000\Sample0.xlsx','A0000CH1','C17:C4016');

%% Create output variable
WaveformData = reshape([raw{:}],size(raw));
%% Clear temporary variables
clearvars raw;

figure(1);
plot(Times,WaveformData);
title('Wave Signal');
xlabel('Time (s)');
ylabel('Amplitude (V)');

%%
Y = fft(WaveformData);
L = length(Y);
P2 = abs(Y/L);
P1 = P2(1:L/2+1);
P1(2:end-1) = 2*P1(2:end-1);
Fs = 1/0.000000005;
f = Fs*(0:(L/2))/L;

figure(2);
plot(f,20*log10(P1))
title('Single-Sided Amplitude Spectrum - FFT')
xlabel('f (Hz)')
ylabel('log(|P1(f)|)')

figure(3);
plot(f,P1)
title('Single-Sided Amplitude Spectrum - FFT')
xlabel('f (Hz)')
ylabel('|P1(f)|')
```

6.1.8 *Preliminary testing of ultrasound and MB conditions in BOCS system*

Table 7 Summary of preliminary experimental parameters assessed, which informed the development of the experimental parameters ultimately assessed in this research.

Parameter Assessed	Summary
Ultrasound Exposure	Both continuous and pulsed ultrasound exposures were created using a signal generator (Rigol, DG1022A); The signal was fed to a power amplifier (55 dB gain, T&C Power Conversion Inc., AG1020), which then output the signal to the transducer at 200 Vpp to create 0.5 MPa acoustic pressure amplitude at 1 MHz. Exposure time was 5 mins, and for the pulsed exposures there was a 100 kHz pulse repetition frequency (PRF) at 25% duty cycle.
Microbubble Concentration	All microbubbles used in preliminary testing were RAMBs, all MB formulations were assessed against the efficacy of a sub-inhibitory concentration of gentamicin at < 8 µg/mL. MB concentrations in volumetric ratios of 1:1, 1:5 and 1:10 were assessed for their bactericidal efficacy against *P. aeruginosa* biofilms, grown on CDC bioreactor coupons as outlined in paragraph 6.1.8. This preliminary investigation showed that over shorter time frames the 1:10 concentration was the most successful (80% reduction in culturable cells), however due to the dissolution, coalescence and potential collapse of MBs over time the concentration of MBs was insufficient for repeated ultrasound exposures after a rest period or for the use of an increased PRF. At 1:1 the concentration of MBs had a negative impact on the treatment, this was potentially due to the crowding of MBs limiting their response to the ultrasound stimulation. Therefore, to balance the need for

	suitably high concentration of MBs over time with responsiveness to ultrasound a 1:5 concentration of MBs was thought to be optimal.
Pulsed vs Continuous Wave Ultrasound	Using continuous wave ultrasound achieved negligible positive effects with a 1:5 MB concentration (i.e. very small reduction in biofilm cells), and a detrimental effect at 1:1 and 1:10 (i.e. increased biofilm growth). It was speculated that continuous wave ultrasound caused clustering or trapping of microbubbles, which significantly reduced the area over which they may exert an effect. In contrast, pulsed wave consistently achieved a reduction in culturable biofilm cells, with the best result observed for 1:10 MB concentration (0.7 log or 80% reduction in biofilm cells compared to antibiotic alone).
MB Priming Time	The introduction of a rest period of between pulsed wave ultrasound exposures was explored, which clearly showed that resting enhanced antibiotic activity between exposures and promoted greater biofilm eradication compared to other MB concentrations. For a 1:5 concentration of MBs a 15 minutes rest period between a first and second sonication periods (so that the bubbles, and bubble constituents, have time interact with the biofilm), resulted in a reduction in culturable biofilm cells of 0.6 log (76%). With a 60 minute rest period between exposures, this increased to 0.76 log (an 83% reduction).

6.1.8.1 BOCS system design and manufacturing protocol

In order to expose biofilms to ultrasound within the confines of a microbiological safety cabinet for active testing, the biofilm BOCS system was fabricated to allow controlled ultrasound delivery on a smaller scale and budget (**Figure 72**).

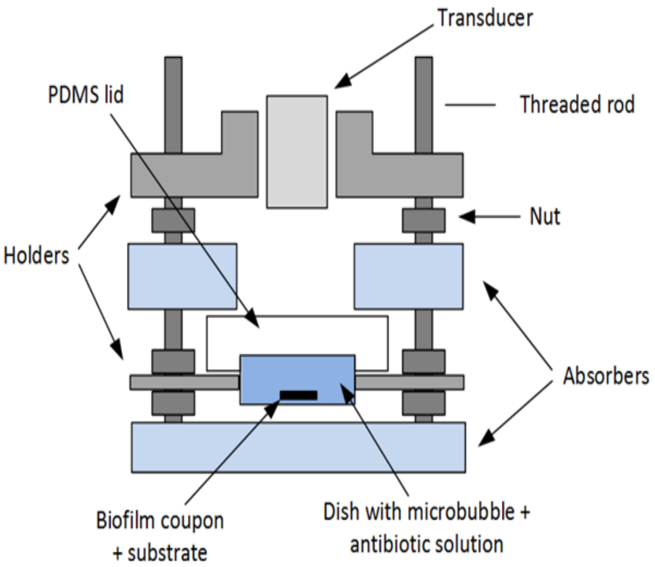

Figure 72 A schematic model of the BOCS device used to deliver ultrasound to a MB-antibiotic suspension, proximal to a biofilm grown in a CDC bioreactor on a polypropylene coupon. The transducer and PDMS capsule are shown being held in place by 3D printed components, with polyurethane ultrasound absorbing material lateral to the transducer and basal to the sample to prevent reflection of sound waves. The device components are held in place at set distances by steel rods and nuts.

Polyurethane acoustic absorbers (Aptflex F48, 10 mm, Precision Acoustics, Dorchester, UK) placed lateral to a transducer and at the base of the container, prevented the transmitted acoustic wave from being reflected, causing a spatial distortion of the acoustic field. Biofilms grown on standard 12.7 mm polypropylene coupons were placed inside a polydimethylsiloxane (PDMS) capsule, which was suspended 2.5 cm under the transducer (1 MHz, 15 mm diameter active area, Camasonics, Wiltshire, UK). PDMS (SYLGARD™ 184, Dow Corning Corporation, UK) was prepared by vigorously mixing silicone elastomer base with silicone elastomer curing agent in a disposable plastic cup, in a weight ratio of 10:1. The mixture was allowed to settle for 10 minutes and then poured into the assembled mould. The filled mould was placed into a vacuum chamber to remove all the air bubbles. The mould was removed from the chamber and left to cure at room temperature for 48 hours, then carefully removed using a thin spatula and scalpel. The PDMS capsule had an acoustic impedance comparable to water, which allows the ultrasound to travel directly to the sample. Both the transducer and biofilm capsule were held in place by 3D printed components, which created a direct line between the transducer and the sample.

6.1.8.2 Growth of biofilms for BOCS system active testing

Biofilms for active testing in the BOCS system were grown on coupons using a CDC bioreactor (**Figure 73**); an advantage of this method of growing biofilms is that whilst growing they are exposed to a consistent shear stress field (Azeredo *et al.*, 2017). The presence of fluid shear stress emulates the mechanism of adherence and formation of biofilms at certain locations *in vivo*; this is an advantage over microtiter plate biofilms in which biofilms may be more loosely attached, easily disturbed and subject to sedimentation (Kwasny and Opperman, 2010). However, this may not be the most representative mode of growth for biofilms intended to emulate the environment of a chronic wound. Polypropylene was chosen as the biofilm coupon substrate, as it best replicated soft tissue in terms of acoustic interaction. Soft tissue has a mean value for acoustic impedance of 1.63 MRayl, with the sound velocity of 1540 m/s, and density of 1.06 g/cm3; polypropylene has an acoustic impedance of 2.36 MRayl, with the sound velocity of 2660 m/s, and density of 0.89 g/cm3 (George and Ludwig, 2004; Lochab and Singh, 2004).

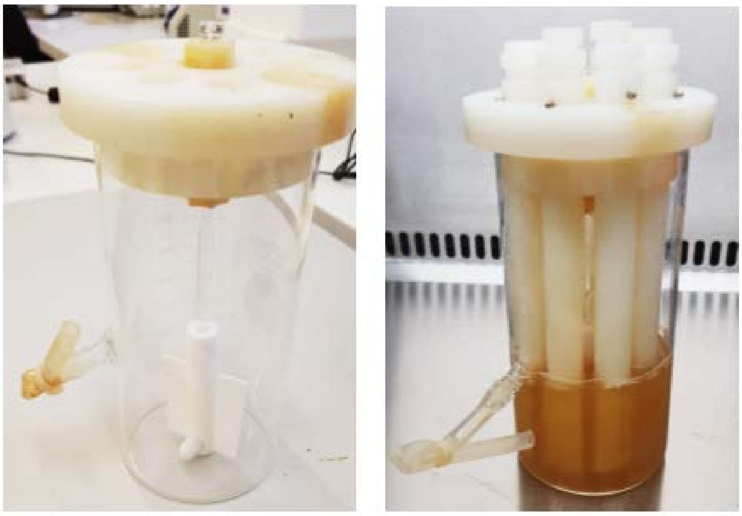

(a) Empty bioreactor *(b) Full bioreactor*

(c) Empty rod

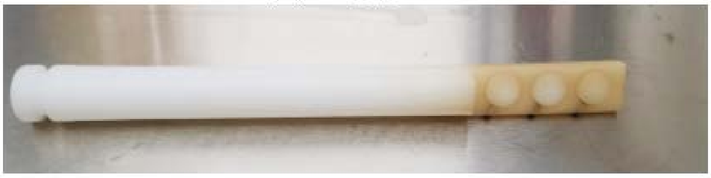

(d) Full rod

Figure 73 Reference images of a complete CDC bioreactor and its relative components, (a) a sterile empty bioreactor, (b) inoculated bioreactor, (c) rods for holding coupons within the bioreactor, (d) coupons loaded into a rod.

6.1.8.3 Preliminary Testing: Ultrasound stimulation of a MB-antibiotic suspension on *P. aeruginosa* biofilms using BOCS device

An overnight culture of *P. aeruginosa* was prepared by inoculating three identical colonies into 3 mL of tryptone soy broth (TSB), this was grown at 37 °C. The optical density overnight culture was adjusted to a 0.5 McFarland standard (Zapata and Ramirez-Arcos, 2015), with a final volume of 2 mL. The 2 mL of adjusted culture was used to inoculate 400 mL of sterile TSB, this was then added to a sterile CDC bioreactor containing an appropriate number of rods that each hold three coupons (**Figure 73**). The top of the bioreactor was covered with foil, then placed on a stirring hotplate (Fisherbrand™, Isotemp™) at 37 °C and 200 rpm for 24 hours, to allow biofilm formation on the coupons. Each biofilm covered coupon was placed individually into the bottom of a PDMS capsule using tweezers; the untreated control was handled in the same way but not exposed to MBs, antibiotic or ultrasound. The MBs used in this experiment were DSPC or DBPC NOMBs and DSPC RAMBs, the MB suspension was combined in a 1:10 volumetric ratio with gentamicin (4 µg/mL final concentration). A 3 mL syringe (Thermo Scientific™ S7510-3) was used to draw up 2 mL of the MB-antibiotic solution, this was injected into the PDMS capsule slowly until no air spaces were visible before the inlet and outlet holes were sealed (**Figure 74**). The PDMS capsule was loaded into the ultrasound tank and submerged under water (**Figure 75**), the MB-antibiotic solution was left to interface with the biofilm for 15 minutes. A signal generator (Rigol, DG1022A) was then used to emit a 1 MHz signal at 0.5 MPa, with a 100 kHz pulse repetition frequency (PRF), at 25% duty cycle for 5 minutes. The signal was fed to a power amplifier (55 dB gain, T&C Power Conversion Inc., AG1020), which then output the signal to the transducer at 200 V_{pp}. This process was repeated once for each side of the coupon; upon completion of the ultrasound exposure the coupon was removed from the disk and placed into a sterile bioreactor rod. The rods containing post-treatment coupons were stored in Falcon tubes containing 50 mL of sterile TSB with 4 µg/mL gentamicin, the coupons were incubated at 37°C for 24 hours.

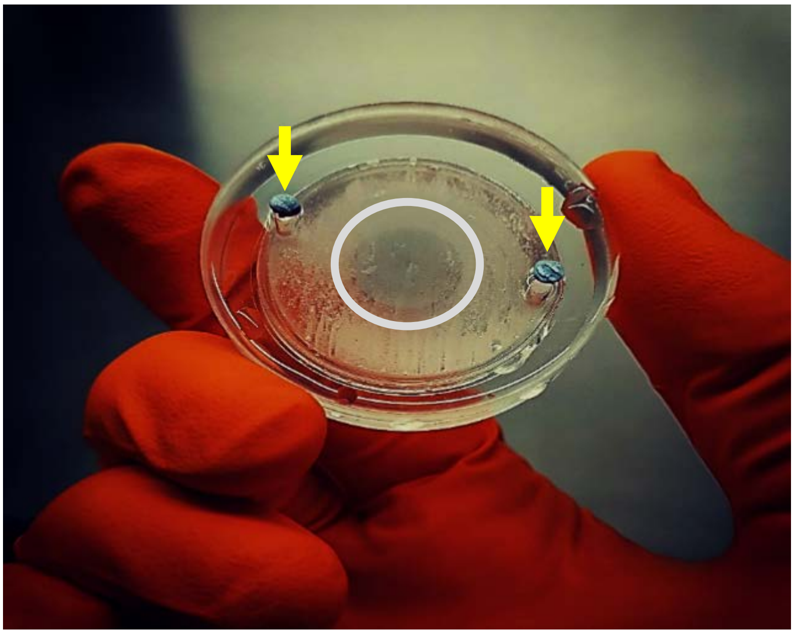

Figure 74 Image of biofilm covered coupon held in a PDMS capsule (i.e. ‘sonolid’), into which a suspension of MBs and antibiotics has been injected prior to the capsule inlet and outlet being sealed. The inlet and outlet ports have been indicated with yellow arrows, whilst the placement of the coupon has been indicated with a white circle.

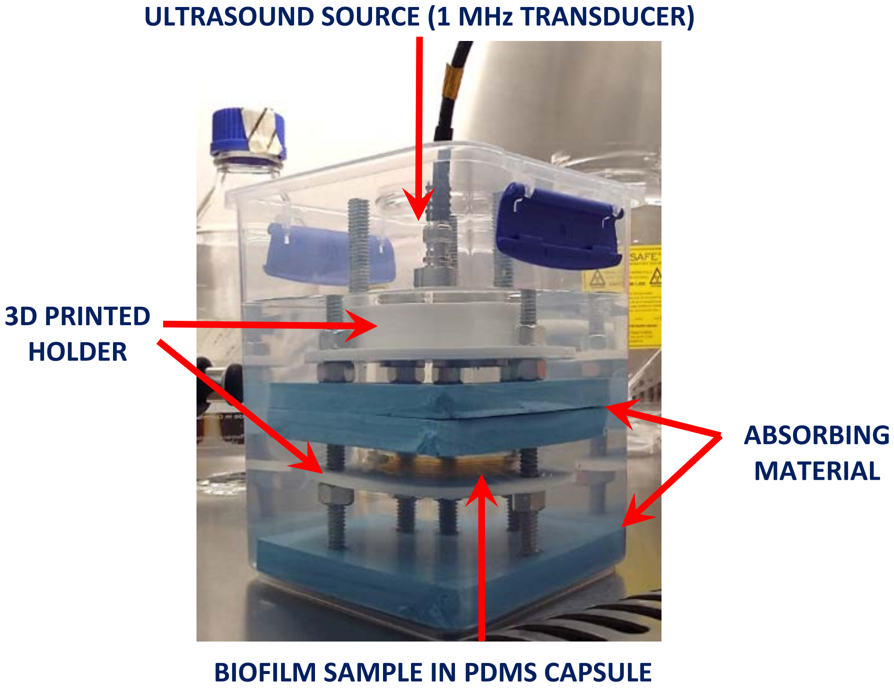

Figure 75 *In situ* photograph of the BOCS system, used for the insonification of MBs proximal to a biofilm grown on a CDC bioreactor coupon.

After incubation the culturable cells from the biofilm were enumerated using the Miles-Misra method (Miles *et al.*, 1938). To remove any unadhered cells from the coupons, each rod was washed by being placed into a Falcon tube half containing 50 mL of sterile PBS. The coupons were then removed from the rod and individually placed Falcon tubes containing 10 mL of sterile TSB. The tubes were sealed and agitated at 2000 rpm for 10 minutes on a shaker, to detach the biofilm from the coupon. Three 10 µL samples of the TSB containing dislodged biofilm were taken for each coupon, this was placed into 90 µL of sterile TSB on a 96-well plate and serially diluted to 10^{-8}. Serial dilutions were performed with a multichannel pipette, ensuring each 10 µL transfer into 90 µL of sterile TSB was mixed well. For each serial dilution three 10 µL droplets were dispensed onto a sterile tryptone soy agar plate, the droplets were allowed to dry before the plate was inverted and incubated overnight at 37◦C. After incubation all clearly visible individual colonies were counted for each dilution, one dilution factor was selected and the number of visible colonies was multiplied to gain an estimate of the number of colonies present per coupon.

6.1.8.4 Preliminary data on ultrasound stimulation of MBs with *P. aeruginosa* biofilms grown on polypropylene coupons using the BOCS device

It has been shown that the combination of NOMBs with ultrasound (1 MHz, 0.5 MPa, PRF of 100 kHz, 25% duty cycle, 5 minutes exposure) and a sub-inhibitory (4 µg/mL) dose of gentamicin, are capable of inducing a significant 3 log reduction in the number of culturable cells recovered from biofilms compared to untreated controls (**Figure 76**). Although a significant difference was not observed for the reduction in culturable cells achieved by MBs compared to sub-inhibitory gentamicin alone, the reduction in culturable cells was still substantial. In the initial test represented by the data, DSPC NOMBs appeared to be the most successful in eradicating biofilm.

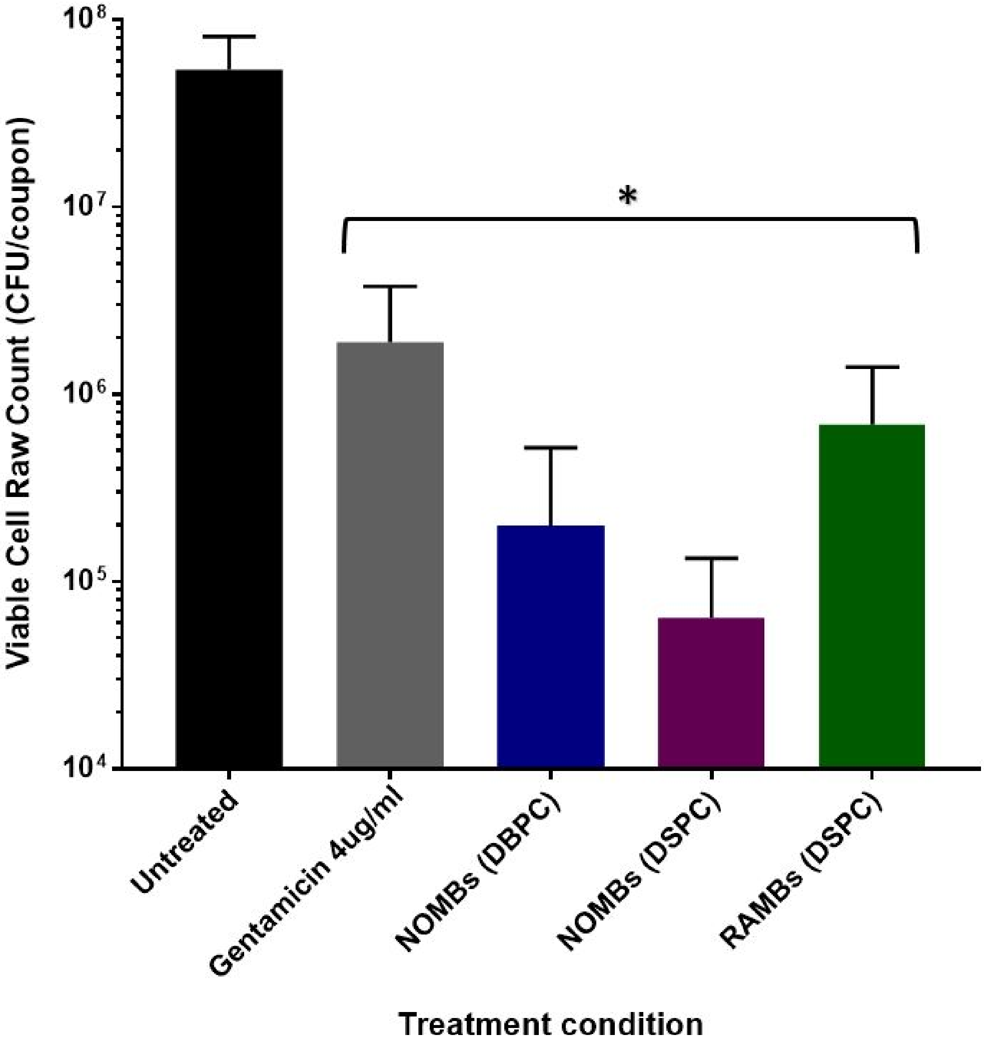

Figure 76 Biofilms grown on polypropylene coupons were exposed to a MB suspension containing a sub-inhibitory concentration (4 µg/mL) of the antibiotic gentamicin, the suspension was passively incubated with the biofilm for 15 minutes before pulsed ultrasound was applied (1 MHz, 0.5 MPa, PRF of 100 kHz, 25% duty cycle, 5 minutes exposure). The untreated control coupon was not exposed to ultrasound or antibiotic, but was handled in the same manner as all other coupons. All other conditions were exposed to both ultrasound and 4 µg/mL gentamicin. The data presented represent the average number of culturable cell recovered from three coupons, constituting one biological replicate of each treatment group. There was a significant difference between all treatment groups and an untreated control * $P < 0.05$; for two 10 µL droplets taken from a DBPC NOMB treated coupon no culturable cells were recovered, indicating a 3-log reduction in culturable cells may have been achieved.

Subsequent testing demonstrated that DBPC NOMBs were able to achieve a consistent reduction of 99.68% over three biological replicates, approximately equivalent to a 2.5 log reduction in culturable cells recovered from biofilms (**Figure 76**). Though not statistically significant, this is a substantial improvement over the < 1 log reduction achieved by a sub-inhibitory concentration of gentamicin. Though not as effective as DBPC NOMBs, DSPC shelled NOMBs were still more efficacious than their RAMB equivalent (**Figure 77**).

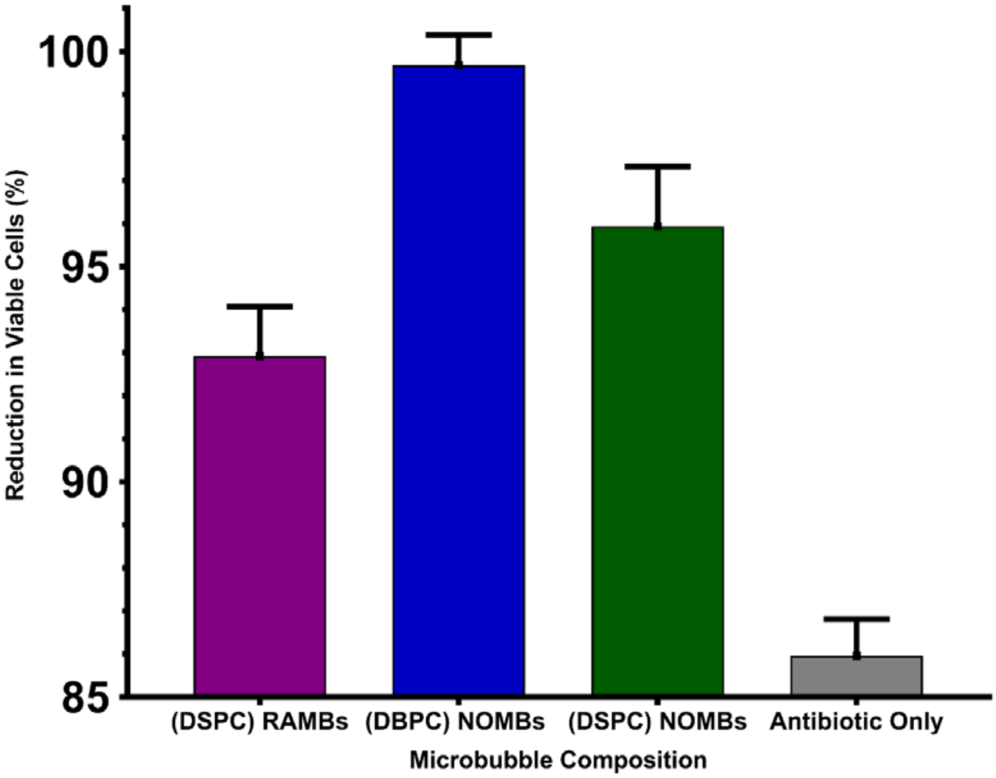

Figure 77 Biofilms grown on polypropylene coupons were exposed to a MB suspension containing a sub-inhibitory concentration (4 μg/mL) of the antibiotic gentamicin, the suspension was passively incubated with the biofilm for 15 minutes before pulsed ultrasound was applied (1 MHz, 0.5 MPa, PRF of 100 kHz, 25% duty cycle, 5 minutes exposure). The data depict the percentage reduction in culturable cells for each treatment condition, data is derived from three biological replicates totalling nine coupons. DBPC and DSPC NOMBs achieved a 99.68% and 95.93% reduction in culturable cells respectively, compared to 92.92% reduction by DSPC RAMBs. DBPC NOMBs attained > 2.5 log reduction than gentamicin used alone at a sub-inhibitory concentration of 4 μg/mL. There was no statistically significant difference for MB treatment conditions compared to gentamicin alone.

6.1.9 *Preliminary active testing of MBs on P. aeruginosa biofilms with BOCS system*

The preliminary active testing of RAMBs and NOMBs in the BOCS system was carried out using *P. aeruginosa* biofilms grown on coupons using a (Centre for Disease Control) CDC bioreactor (**Figure 73**); an advantage of this method of growing biofilms compared to microtiter plates is that whilst growing they are exposed to a consistent shear stress field (Azeredo *et al.*, 2017). The presence of fluid shear stress can emulate the mechanism of adherence and formation of biofilms seen at specific sites *in vivo*; this is a potential advantage over microtiter plate biofilms in which biofilms can be more loosely attached and therefore easily disturbed (Kwasny and Opperman, 2010). However, as the intended application of this research is biofilms in chronic wounds that would not be subjected to any significant fluid shear stress level, this mode of growth is potentially less applicable for this research (Omar *et al.*, 2017). Importantly, later developments in this research led to the characterisation of a pathophysiologically representative WCM (Paragraph 4.4.2), for biofilm growth under conditions that are more closely related to those seen *in vivo.*

Polypropylene was chosen as the biofilm coupon substrate, as it best replicated soft tissue in terms of acoustic interaction. Soft tissue has a mean value for acoustic impedance of 1.63 MRayl, with the sound velocity of 1540 m/s, and density of 1.06 g/cm^3; polypropylene has an acoustic impedance of 2.36 MRayl, with the sound velocity of 2660 m/s, and density of 0.89 g/cm^3 (George and Ludwig, 2004; Lochab and Singh, 2004). The initial tests therefore provided a valuable insight into the mechanical interaction of an oscillating MB on a biofilm (**Figure 76**), data showed that MBs were capable of enhancing the efficacy of sub-inhibitory concentrations of gentamicin (**Figure 76**). The aminoglycoside gentamicin was selected as the antibiotic in these experiments, this is due to gentamicin being the most widely selected broad spectrum antibiotic used in chronic infections of *P. aeruginosa* (Van Stormbroek *et al.*, 2019). The first experiment to use DSPC and DBPC shelled NOMBs demonstrated that the mechanical effect of the MB oscillating in response to ultrasound, can be effectively augmented by the biological effect of NO being delivered to the biofilm. Initial testing showed that DSPC NOMBs were able to reduce biofilm from 4 x10^7 to 6 x 10^4 CFU/coupon, when compared to an untreated control (**Figure 76**). All untreated coupons were subject to the same amount of handing as coupons in treatment conditions, this was an important control to account for loss of biofilm due to handling of the coupon. The reduction in culturable cells recovered from coupons was significantly reduced in all treatment groups (* $P < 0.05$), when compared to the untreated control coupons. Over three biological replicates, there was no significant difference observed between the use of antibiotic alone and the combined use of MBs, gentamicin and ultrasound (**Figure 77**). Despite the lack of significant difference due to a small sample size and variation in success of experimental repeats, NOMBs with DSPC and DBPC shells consistently reduced the biofilm mass associated with a coupon. DBPC NOMBs demonstrated the greatest efficacy over three biological replicates (**Figure 77**), achieving up to a 4-log reduction in the number of culturable cells in some tests and a cumulative average reduction of 99.68% equivalent to a 2.5 log reduction (**Figure 77**). A sub-inhibitory concentration of gentamicin alone, was unable to achieve a log reduction greater than 1. In perspective, this demonstrates that the synergistic effect of biologically active NO and cavitating MBs, can effectively increase the efficacy of sub-inhibitory concentrations of gentamicin by over 90% (**Figure 76**).

6.1.10 *Fluorescence microscopy examples of direct viable counts attempted on ultrasound-MB-antibiotic treated biofilm samples*

Direct viable counts of fluorescently stained bacterial cells allow the reliable quantification of viable cells affected by treatment conditions, this has the distinct advantage over culture based methods of differentiating VBNC from dead cells that can lead to an over-estimation of treatment efficacy. This method of direct quantification described by Wilks *et al.* (2020), was attempted in this research on biofilms treated with ultrasound, sub-inhibitory concentrations of gentamicin and MBs. Directly after insonification the treated supernatant was withdrawn and the Ibidi™ dish washed gently with PBS 3 times, the dish containing any residual Syto9/PI stained biofilm/cells was then observed with the EVOS M5000 fluorescence microscope. Due to the persistence of insonified MBs the reliability of this method was compromised. **Figure 78**A shows one example of a biofilm treated with NOMBs$^+$, where the trapping of MBs bound electrostatically to the biofilm has reduced the efficacy of dispersal. This exemplified one of the limitations of applying this method to biofilms treated with MBs; as the residual MBs are able to very effectively scatter the transmitted light, post-processing to quantify the number of live/dead cells would have poor accuracy. In **Figure 78**B that shows an example of the planktonic cells remaining after the most efficacious treatment with NOMBs, the ability to differentiate between live/dead cells is more clear. However, though this image appears to offer support of the 99.9% anti-biofilm and bactericidal efficacy of the treatment modality, true direct quantification is again unreliable. Firstly, as with samples where residual biofilm has remained attached to the growth surface, MBs were still present in the sample and predominantly scattering red light. This would have directly skewed the results artificially in favour of a higher proportion of dead cells, moreover a further complication seen in NOMB treated samples was that 99.9% of the biofilm was disrupted and removed with the end result of planktonic cells being present in multiple phases of the residual fluid. The end result of utilising direct viable counts in this research would therefore be subject the same potential overestimation in the number of dead cells, which is an artefact of the VBNC phenomenon in culture methods.

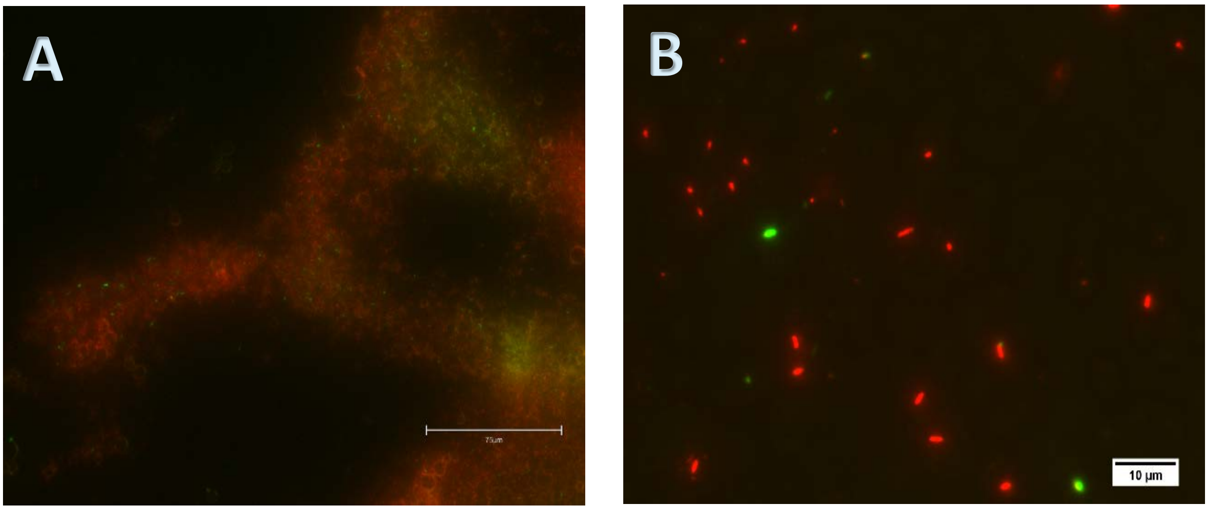

Figure 78 To support the data on bactericidal efficacy of ultrasound-mediated treatment of biofilms with NOMBs gathered by culture methods, direct quantification of live/dead cells was attempted using. Image A shows an NOMB$^+$ treated biofilm and image B shows a NOMB treated biofilm sample; both samples were prepared in the same manner, where after insonification the treatment supernatant was carefully withdrawn and the culture surface was gently washed 3 times with PBS. An emission wavelength of 498 nm (GFP LED cube, AMEP4653, Invitrogen™, ThermoFisher Scientific), was used to capture images of the green fluorescent Syto9 stained proportion of the insonified biofilm or planktonic cells. Images of the red fluorescent propidium iodide stained proportion of the insonified biofilm or planktonic cells, were acquired with an emission of 617 nm (RFP LED cube, AMEP4653, Invitrogen™, ThermoFisher Scientific). Scale bar in A represents 75 µM, whilst the scale bar in B represents 10 µM.

Due to severe constraints on time and resources placed upon this research by the COVID-19 pandemic, this method of direct viable counts could not be refined and explored further in this research. However, it would be an important recommendation in future work in this area that the quantificaiton of treatment efficacy be investigated thoroughly, both by more traditional culture methods such as Miles-Misra as well as new techniques for direct quantification to ensure validity of the data in light of the VBNC phenomenon.

6.2 Appendix B – Design, fabrication and characterisation of a proof of concept System for Ultrasound Mediated Interventional Therapy (SUMIT)

6.2.1 *Introduction*

Bacterial infection and subsequent development of biofilms in open wounds, poses a significant risk to human health. Due to their increased resistance to traditional antimicrobial therapies and non-selective drug delivery, interdisciplinary techniques are being explored as novel treatment methods. Ultrasound responsive drug delivery vehicles provide a dynamic means of delivering therapeutic agents, with high temporal and spatial specificity. Ongoing research has shown that ultrasound responsive agents can facilitate drug delivery, utilising both bioactive compounds and mechanical stimulation to eliminate biofilms. However, at present there is no clinically viable translation of this treatment modality as a therapeutic approach against infected superficial wounds. This phase of the study aimed to develop a device that can (i) be placed onto the skin and loaded with an ultrasound-responsive liquid suspension, (ii) deliver ultrasound to an affected area at relevant acoustic pressures, (iii) be easy to use without specialist training, (iv) offer affordable fabrication or opportunity for re-use. Both computational and experimental methods will be required for the design and development process. Due to the lack of congruity in size, shape and depth of wounds, it is likely that a successful design would be primarily targeted at early stages of DFU development with small lesions. This would then have the potential to either prevent or limit biofilm development, in addition to dispersing and treating any adherent cells present in the wound bed. For primary *in vitro* testing it will be possible to use epithelial tissue models, on which biofilms can be established to study the impact of treatment on wound healing (Gonzalez-Andrades *et al.*, 2016)

6.2.2 *Design objectives*

The first objective was to design a device that provides the integration of a liquid media delivery system and an ultrasound pressure field to a superficial wound. The design objective will be completed by addressing the following sub-design objectives.

6.2.2.1 Injection of MBs

An integral part of the proposed treatment procedure is the action of the MBs. As a result, the device must include a method for the injection of MBs to the wound area to perform its function. The device is not required to generate the MBs, but it must be able to deliver a premade solution to the skin. The method of the injection of the bubbles should not compromise the integrity of the bubble shell or induce their premature destruction. In addition, bubbles must be delivered to the skin and contained on the surface for the duration of the treatment period. This means that there must be a water tight seal at the point of contact with the skin.

6.2.2.2 Delivery of an acoustic field to MBs

The driving feature of the device is the acoustic field, provided by the ultrasound transducer. The device must be able to deliver ultrasound waves to the MBs at the wound surface. For greater predictability of the results stable cavitation of the bubbles may preferable for *in vitro* applications, however this research has shown excellent efficacy of MBs that undergo inertial cavitation in response to ultrasound. Acoustic reflections in the system need to be minimized to reduce unwanted formation of ultrasonic standing waves, which may influence the spatial and temporal behaviour of microbubbles in suspension.

6.2.2.3 Extraction of treated solution

After injection, a given volume of fluid is expected to be contained on the surface of the skin. This indicates that before removal of the device, the fluid must be extracted from the system to prevent spillages. The device is required to be placed on the surface of an open wound. Once the solution is injected into the system and interacts with the wound, it has been directly exposed to bacterial cells. The extraction process must therefore be conducted in a closed system to avoid exposure to the environment and must facilitate the sterile disposal of the extracted MB solution.

6.2.2.4 Characterisation the ultrasound field

The delivery of the ultrasound field to the treatment area must be characterised to evaluate its uniformity and behaviour within the device, which will in turn provide a validation of the proposed design and material selection. The characterisation of the field must be conducted before a prototype is developed.

6.2.2.5 Manufacturing of a prototype

Developing a prototype system not only involves a conceptual design, but also manufacturing a functional device. The objective is to use the selected materials in conjunction with appropriate manufacturing techniques to produce a physical project result. Since the intention of the project is to create a system that can be translated to a clinical environment, the features and functions of the device must be verified. An important component to the manufacturing process is to perform a functional verification to prove that the device features work as intended without failures.

6.2.2.6 Validation of the ultrasound delivery of the device

The novel aspect of this project is the ability of the resulting device to deliver an ultrasound field through a suspension of microbubbles to a chronic wound. This objective is to provide evidence that the device prototype can successfully do this by validating the ultrasound field delivery through the device to the treatment area.

6.2.3 *Materials and methods*

6.2.3.1 Component selection and concept testing features for SUMIT

The component selected for injection of the MBs was a syringe. A container called a coupon was designed for enclosing the bubbles on the skin. The coupon size was determined using ultrasound field characterization and the size of the volume of the syringe was selected accordingly. Inlet and outlet ports were constructed and added to the coupon design. For the delivery of an acoustic field to MBs a 1 1 MHz transducer was selected, to provide a driving frequency close to the resonant frequency of the MBs utilised in this research that are typically (1 – 10 µm). The shape and dimensions of the transducer were measured and used to determine the size of other designed components. A syringe was also selected to extract the post-treated fluid and incorporated into the cover piece design.

Table 8 Summary of design features and testing of the appropriateness of materials

Design Features	Areas of Concern	Feasibility Testing
Injection of bubbles	Failure to deliver bubbles Potential leaking before and during injection	Water stained with red food dye was injected into the assembled system. The external surface of the injection port was observed during filling to ensure all the water was being delivered directly into the coupon without external leakages around the port.
Water-tight seal	Leakages around the skin-device interface	The device was strapped to a waterproof block and filled with red coloured water using the device's injection mechanism (syringe). The interface between the coupon and the block was inspected for the presence of red fluid around the outside of the device on the surface of the block to ensure there were no leakages.
Air bubble removal	A layer of exogenous air remains inside the coupon	The coupon material was translucent therefore red coloured water allowed clear distinction between fluid and air layers. After complete filling, the treatment area was viewed from the top to inspect for colour differences indicative of the presence of air bubbles
Fluid extraction	Fluid is not completely removed from the coupon	The device was strapped on to a waterproof block and filled to maximum capacity with red coloured water. The water was

		then extracted using the syringe and the device was unstrapped and removed to view the remnants on the surface.
Secure placement	Device & components fall out of place in alternative orientations Coupon is unevenly compressed onto the surface of the foot Features don't work in specific orientations	A model foot was used to attach the device in multiple orientations and the components were observed for loosening or detachment. The compressed coupon base was observed for shape deformities resulting in obvious spaces at the coupon/foot interface. To evaluate the features in multiple orientations, the device was attached to a waterproof block and the entire fluid delivery process conducted in all orientations and observed for failed or altered actions.

6.2.3.2 Computational modelling of the acoustic field

The delivery of an ultrasound field was simulated using COMSOL Multiphysics 5.4 (COMSOL Ltd., Cambridge, UK), based on the device geometry shown in **Figure 79**. The proposed design was simulated with different volumetric capacities within the coupon (3.5, 7, 10, and 14 mL) corresponding to heights of the fluid layer of 0.5 to 2 cm. The boundary material was selected as polydimethylsiloxane (PDMS) due to the ease of moulding the material, and the similarities in the acoustic impedance values of 1.1 MRayl and 1.5 MRayl between PDMS and water that facilitates > 97% acoustic transmission (Rahman *et al.*, 2012; Guillermic *et al.*, 2019).The target wound area would be comprised of soft tissue, which has a mean value for acoustic impedance of 1.63 MRayl that is not significantly different to water (Alkins and Hynynen, 2014).·The interaction between the delivered field and boundary material was assessed using a frequency domain acoustic pressure study, and the model geometry was discretised with COMSOL free triangular predefined extra fine mesh element size ranging from 0.8 µm – 0.4 mm.

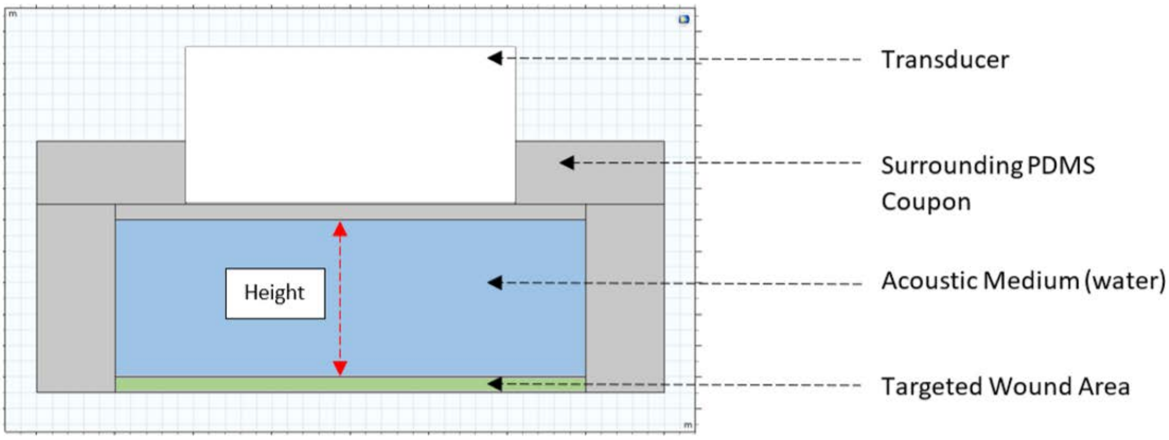

Figure 79 A 2D representation of the COMSOL coupon geometry. The materials are colour coded to show the defined acoustic zones. The acoustic medium was chosen to be water and the target wound area was simulated as a skin layer. The coupon height is represented by the red arrow. This distance was adjusted to alter the coupon's volumetric capacity.

The software was used to verify interactions between the delivered field (blue line on **Figure 80**) and the boundary material (PDMS), to ensure that the field was sufficiently uniform at the target. The COMSOL simulation incorporated the properties of the materials used to validate the use of PDMS for the coupon. The applied boundary conditions are illustrated in **Figure 80**. A plot of the absolute pressure values at the skin layer across the whole treatment diameter (red line on **Figure 80**) was produced for each simulated coupon height. A statistical analysis of the pressure values was conducted to determine the mean and standard deviation of the acoustic pressures along the skin layer.

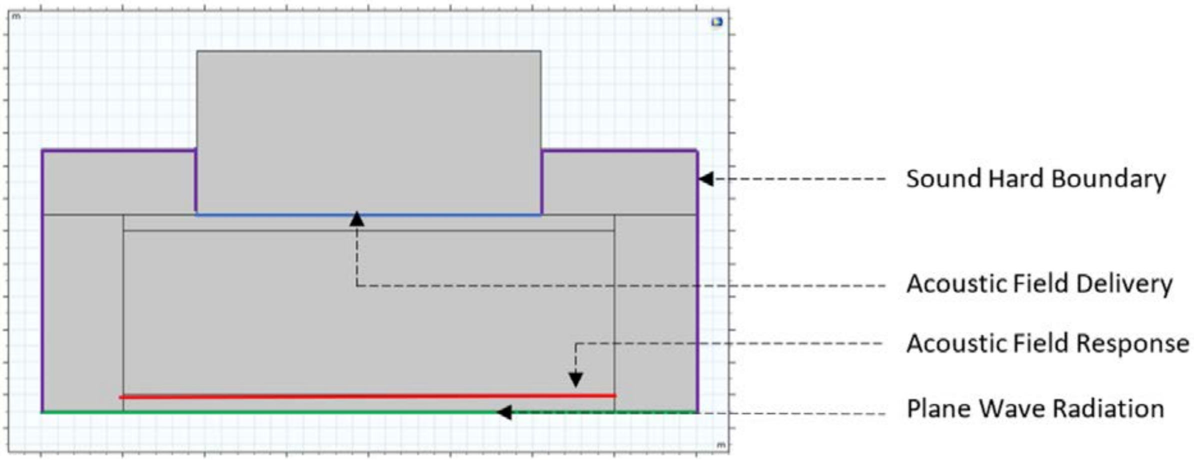

Figure 80 A 2D representation of the COMSOL coupon boundary conditions. The boundary walls were placed around the walls of the coupon represented by the purple lines. The blue and red lines were the parallel delivery and targeted response zones respectively. At the base of the coupon was a plane wave radiation boundary line represented in green.

6.2.3.3 **Manufacturing of coupon for MB containment**

A mould was designed in SOLIDWORKS using the dimensions from the simulations and 3D printed with PLA. The mould consisted of four individual detachable components to facilitate removal of the cured PDMS coupon (**Figure 81**). PDMS (SYLGARD™ 184, Dow Corning Corporation, UK) was prepared by vigorously mixing silicone elastomer base with curing agent in a disposable plastic cup, in a weight ratio of 10:1. The mixture was allowed to settle for 10 minutes and then poured into the assembled 3D printed mould. The filled mould was placed into a vacuum chamber to remove all the air bubbles. The mould was removed from the chamber and left to cure at room temperature for 48 hours, then carefully removed using a thin spatula and scalpel.

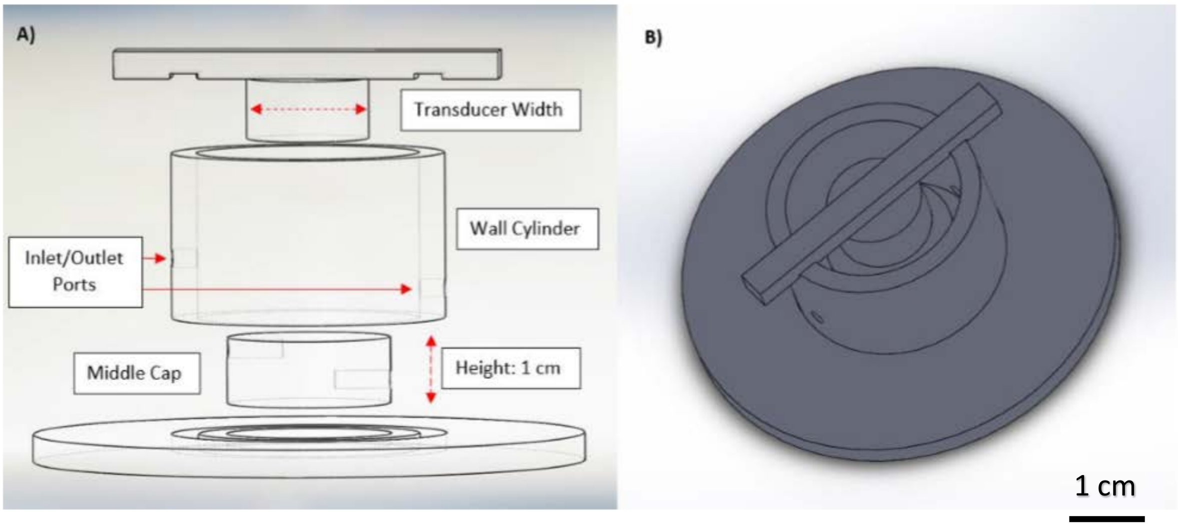

Figure 81 Printed negative mould for coupon. A) Exploded view of the individual pieces of the coupon mould showing the main components in the design. The ports were used as inlet and outlet for the fluid, the middle cap controlled the height of the treatment area, the wall cylinder determined the diameter of the coupon and the top plunger created a slot for the transducer. B) The full assembly of the four components

6.2.3.4 **Manufacturing of a rigid coupon cover piece**

An RS PRO digital calliper (RS Components Ltd., Northants, UK) was used to collect the measurements of components required, which included the syringe diameter, transducer diameter and transducer length to fit the design of the cover piece. A model was created using SOLIDWORKS 2018 (Dassault Systèmes, France) using the cover piece design and the specified dimensions. An Ultimaker S5 (Ultimaker B.V., Netherlands) 3D printer was used to print models with PLA (RS Components Ltd, Northlands, UK) using a layer height of 0.2 mm and an infill of 20%.

6.2.4 ***Results***

The principal outcome of this work was a functioning proof of concept device: SUMIT, for application to superficial chronic wounds. The final device consisted of a re-usable central structure (cover piece) with several disposable or reusable functional components. A key elements included: a soft cylindrical PDMS coupon that incorporated inlet and outlet ports, a 10 mL Luer lock syringe connected to a 15G

(1.83 mm) 1 cm blunt needle, a 3-way Luer lock valve and a 0.22-µm sterile syringe filter with PES membrane. The design of the cover piece incorporated a slot for the application of a transducer and an adjustable Velcro strap for secure fastening to patient limbs. The fully assembled system is shown in **Figure 82**. To use the device, it was first placed over the targeted area and securely tightened onto the treatment surface. The 10 mL syringe was loaded with a pre-made suspension of MBs (1:5 v/v ratio of MBs to PBS) and connected to the inlet port. The 3-way valve was adjusted to ensure the connections to the outlet port and filter were opened and the MBs were then delivered to the coupon via the syringe. Once the coupon was filled, the 3-way valve was adjusted to lock the outlet port to prevent air from flowing back into the system. The target area was primed with bubbles and ready for the application of ultrasound. After the ultrasound delivery period was completed, the 3-way valve was adjusted once more to open the outlet port. This allowed the same syringe to be used to withdraw the fluid that had been in contact with the wound area.

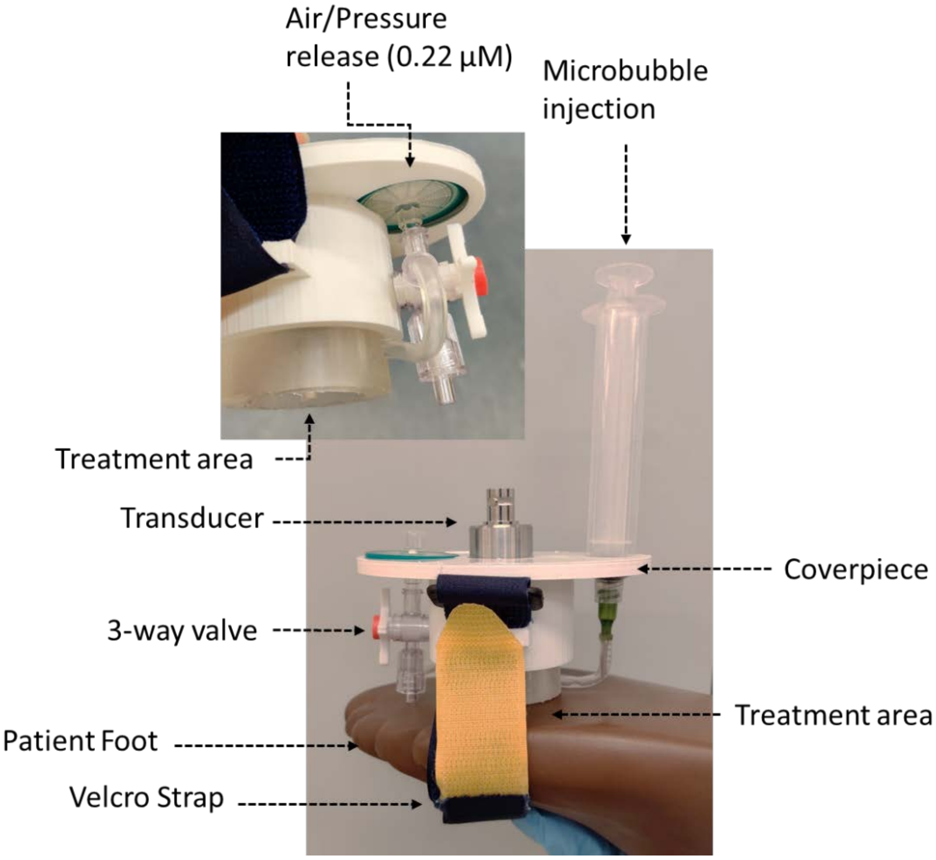

Figure 82 Final SUMIT design. The fully assembled system is shown with the locations of the inserted transducer; attached syringe, filter, 3-way valve, air filter, coupon, cover piece and Velcro strap.

6.2.4.1 Computational modelling of acoustic environment within the treatment coupon

Numerical simulations carried out using COMSOL provided a characterisation of the acoustic field within the fluid cavity of the device. The spatial distribution of the absolute pressure is shown in **Figure 83**; the results clearly show that there were minimal reflections present from the PDMS coupon walls of the device, in comparison to the direct sound pathway of the transducer field projection.

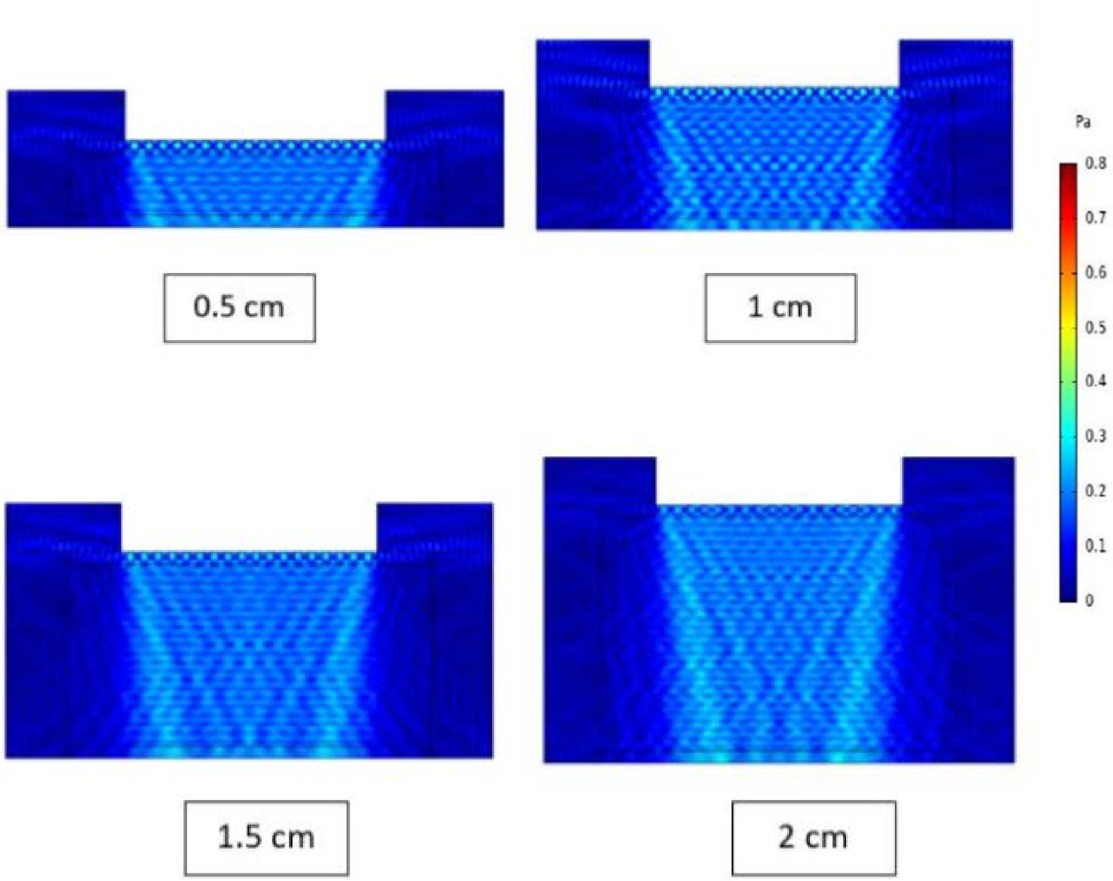

Figure 83 Absolute acoustic pressure field determined numerically. The responses at each coupon height (0.5 cm to 2 cm) corresponding to different volumetric capacities are shown and the colour bar represents the relative pressure levels from low (dark blue) to high (dark red). As the field delivery distance is increased, there is a decrease in the lateral uniformity of the pressure field in the coupon cavity.

The mean values indicated in **Table 9** of absolute acoustic pressure show that the optimal coupon height was 1 cm, due to the lowest standard deviation (0.33) and coefficient of variance of pressure (0.174) at the target site (skin layer). The largest mean pressure (0.212 Pa) and standard deviation (0.046) corresponded to a coupon height of 2 cm. The values for 0.5 cm and 1.5 cm were comparable to those at 1 cm, with an increase in variance of 7.27% and 13.8%, respectively. The similarities between the performance of the 0.5, 1 and 1.5 cm coupon designs made them all viable options. However, the smaller volume (7 mL) associated with the 1 cm height was better suited for the selection of a 10 mL standard clinical syringe, and reduced the cost of manufacturing.

Table 9 Summary of mean and standard deviation values for acoustic pressures observed for different coupon heights assessed along the skin layer, derived from the values for absolute acoustic pressures

Height (cm)	Mean Pressure (Pa)	Standard Deviation (Pa)	Coefficient of Variance
0.5	0.208	0.036	0.174
1	0.203	0.033	0.162
1.5	0.203	0.038	0.185
2	0.212	0.046	0.219

6.2.4.2 **Fabrication of SUMIT component parts**

The fabrication of the SUMIT device was based on the dimensions and material properties of the computationally optimised design. The filling procedure utilised an overflow system, which was achieved by placing the inlet and outlet ports at different heights in the wall of the coupon. The outlet port was placed as close to the surface as possible to facilitate complete filling, whilst limiting the formation of air pockets within the coupon (**Figure 84**).

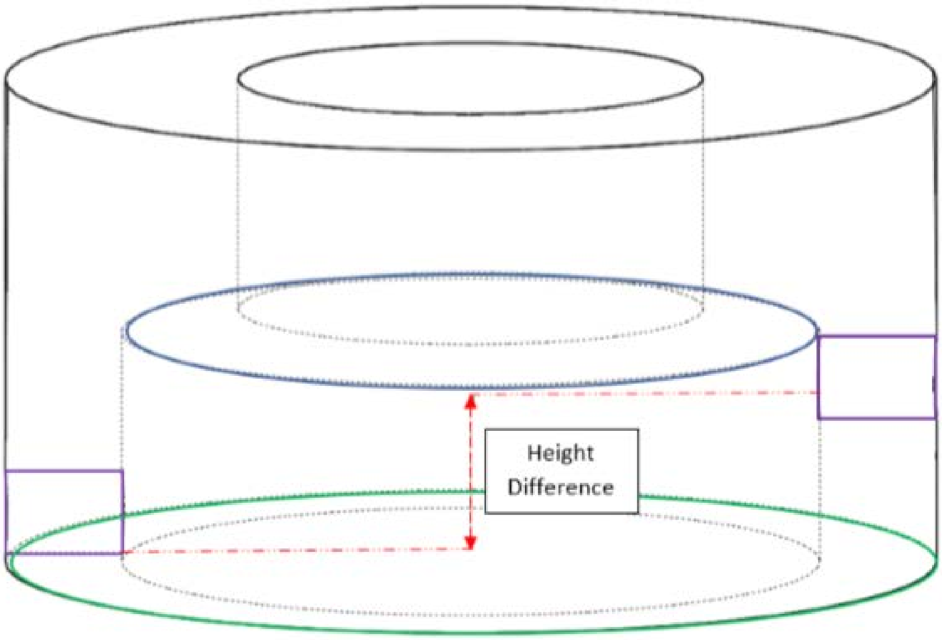

Figure 84 A schematic of the front view of the coupon. The purple regions indicate the locations of the inlet and outlet ports separated spatially by a height difference. The inlet port is located close to the base of the coupon (green circle) and the outlet port is located at the surface (blue circle).

To reduce hydraulic resistance at the outlet an open flow system was created, using a 0.22 µm sterile syringe filter connected to a 3-way Luer lock valve. A closed system was initially proposed to prevent biohazardous material exiting the coupon area after treatment, however this additional hydraulic resistance in the system that increased the risk of leakage and the formation of air pockets. To prevent leakage of any biohazardous fluid, the installation of a 0.22 µm filter ensured any fluid ejected was acellular and thus sterile. When wet the filter no longer allows air to flow freely and therefore during extraction air cannot re-enter the system to replace the removed fluid. The 3-way valve provided a second pathway for an open-air flow back into the system, or allow faster extraction of fluid from the coupon if required.

The cover piece was designed to provide a frame for connection of all the functional components. In addition to this, it was also responsible for translating the compressive force evenly around the coupon when attached to a limb by Velcro straps. The initial positioning of the straps resulted in unbalanced strapping to the foot model, due to the angle of application of the resultant forces and moments (**Figure 85**). The longer distance from the pivot point (coupon base) caused a larger twisting moment and therefore the coupon was not evenly compressed onto the foot. This resulted in uneven curvatures at the foot/coupon interface and some sections around the circumference of the coupon were not in contact with the foot. The cover design was revised as seen in the final design so the straps could be attached closer to the base of the coupon, decreasing the pivot distance (**Figure 86**).

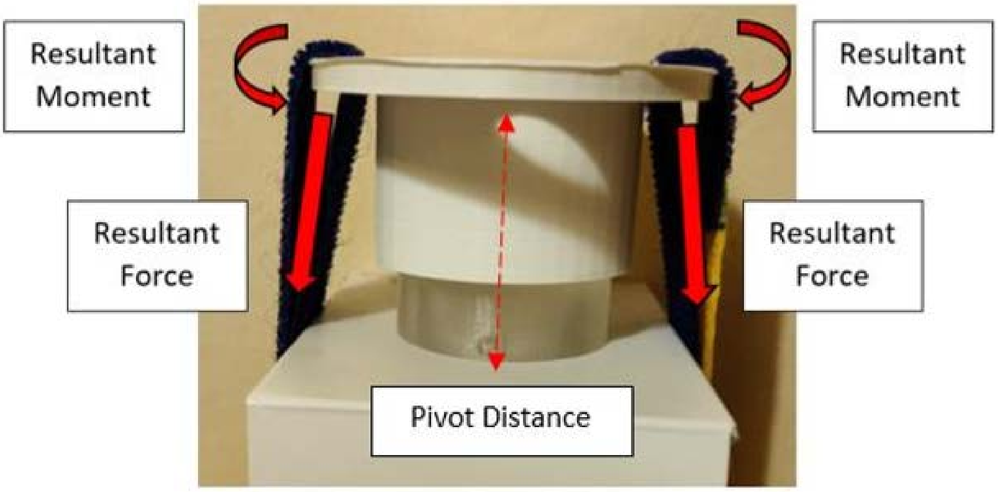

Figure 85 Resultant forces and moments. Forces from the straps are applied to the coupon from the top of the cover piece. A longer pivot distance resulted in greater twisting moments leading to uneven compressions.

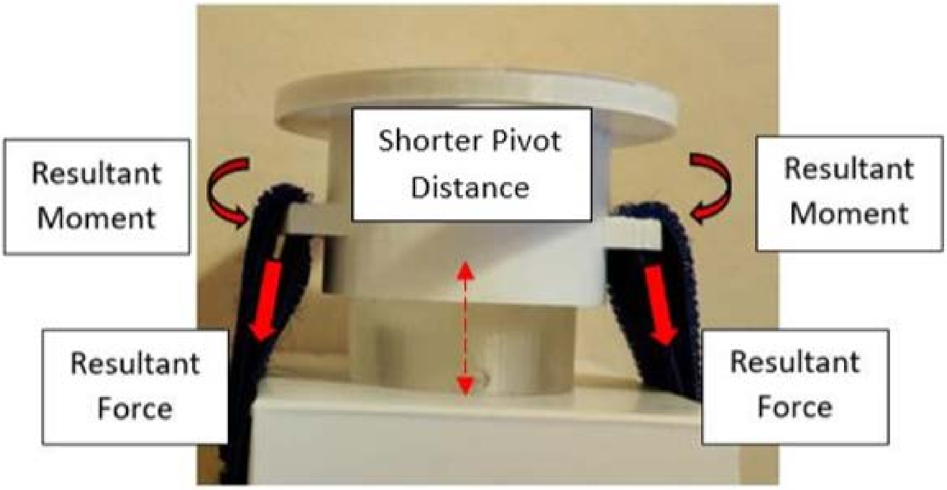

Figure 86 Resultant forces and moments. Resultant forces are applied at a shorter distance away from the coupon resulting in lower twisting moments

During testing, it was found that the coupon was not securely fastened into the cover piece, which presented challenges in re-creating the expected treatment procedure. The cover piece was modified to incorporate a ridge that fit into a groove on the coupon (**Figure 87**a), this provided a secure fit but the insertion of the coupon into the cover piece became challenging. The proposed alternative in the final cover piece design was to reduce the diameter of the coupon slot, this created a friction fit between the cover and the coupon that made insertion of the coupon easy and secure (**Figure 87**b).

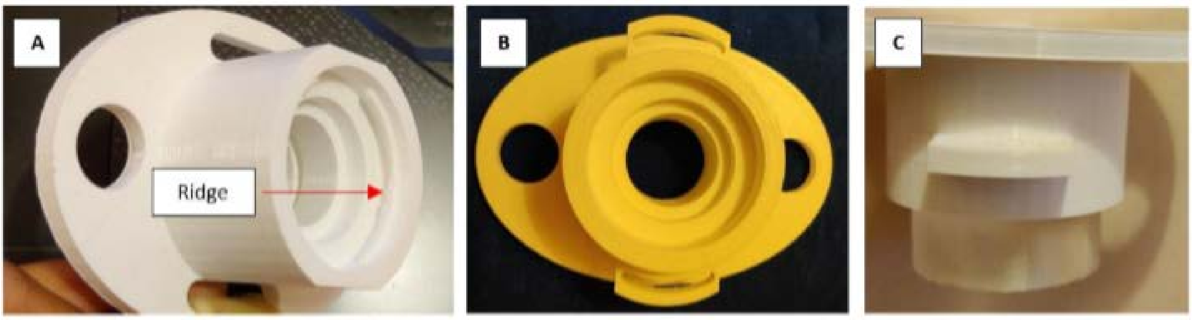

Figure 87 Coupon attachment design revisions. A) A built-in ridge was designed to slot in to a matching groove around the coupon, B) The inner diameter of the coupon cavity in the cover piece was reduced to the size of the coupon to allow a ‘friction fit’ attachment, C) The securely fastened coupon in the cover piece.

6.2.4.3 **Functional testing of assembled SUMIT**

Initial leakage testing based was on the coupon geometry of the computationally optimised design; breach points at the interface of the coupon with a waterproof block were noted, this was potentially due to minor variances in the smoothness of the PDMS coupon surface (**Figure 88**). To counteract this issue an oil-based gel (petroleum jelly) was applied around edges between the interface of the device and the testing surface, to provide and additional barrier to leakage. The test was conducted once again and the previously observed pools of liquid around the edges of the coupon were eliminated (**Figure 89**). This indicated that the petroleum jelly provided an adequate seal to prevent leaking and maintain a watertight treatment area. The filled device was fully rotated 90° to ensure that fluid remained contained, and no leakage was observed after this manipulation.

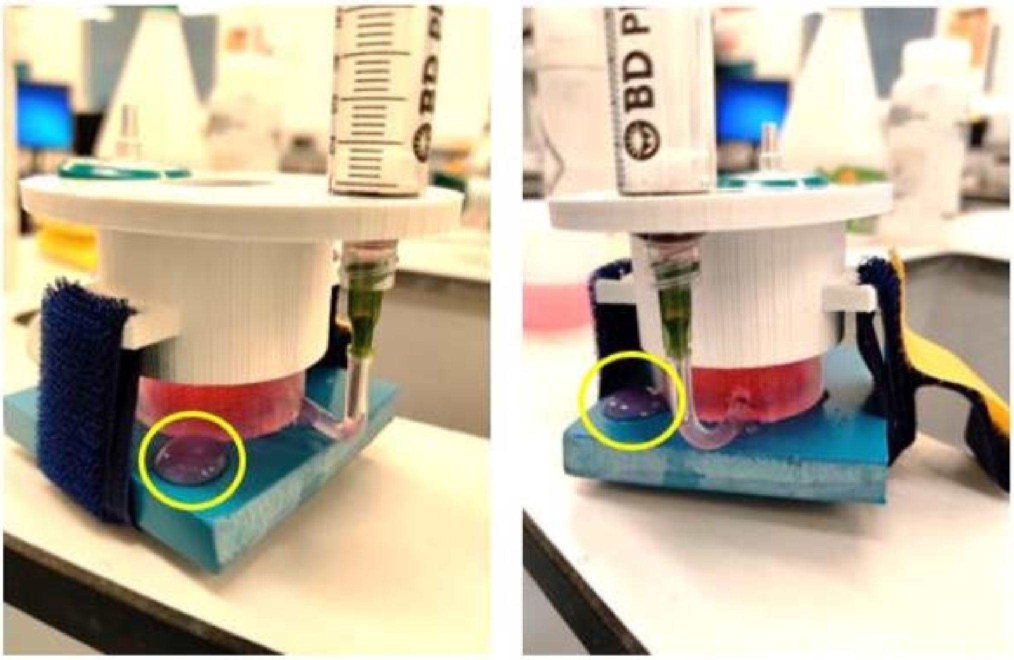

Figure 88 Results of first leakage test show small pools of coloured fluid around the outer edges of the coupon highlighted by the yellow circles. This represented the weakly sealed locations around the interface, allowing fluid to escape.

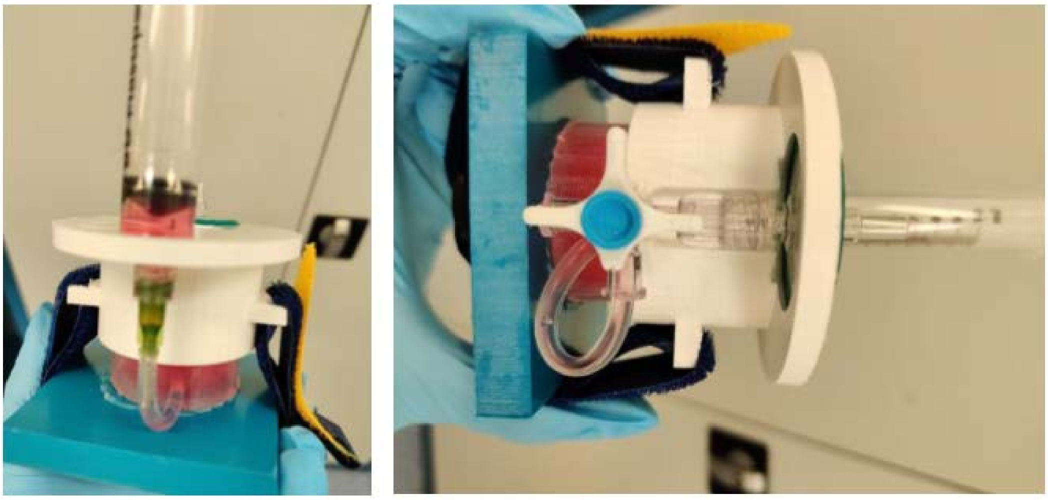

Figure 89 Results of second leakage test. The absence of liquid around the edges of the coupon when horizontal and at 90 degrees, demonstrated the efficacy of petroleum jelly as a means of creating a watertight seal to prevent leakage.

Extraction of the fluid contents from the coupon was achieved using the syringe; removal of the device from the surface after fluid extraction revealed the remnants of liquid (< 1 mL) inferred from the extracted volume present in the syringe. Although the ideal result was to remove all the fluid to have a clear surface, the remaining volume of fluid was not considered significant enough to be hazardous or challenging to handle in a normal clinical setting to require further refinement of the fluid extraction process. Since the wound area will be cleaned post-treatment to remove the residual petroleum jelly and prepare the area for dressing, the remaining fluid will also be cleared in this step.

A prosthetic foot was used in order to assess the effectiveness of SUMIT attachment to the geometry; whilst this did not provide an anatomically relevant topography of the plantar surface, it did reliably demonstrate how robust the attachment of the device was to the general shape of the foot. Using the Velcro straps and positioning the model foot in multiple orientations, showed that the components remained securely in place (**Figure 90**); this also demonstrated the clinical utility of the design since the foot can be placed in various orientations, whilst the attachment of the device remains secure.

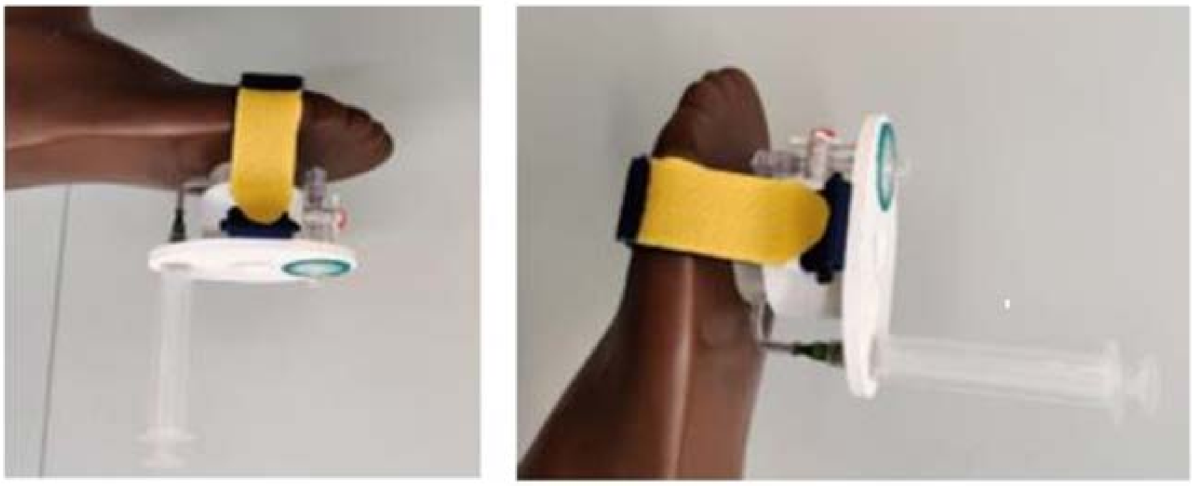

Figure 90 The device is shown attached to the model foot whilst pronated (facing downwards) and supinated (facing upwards) to demonstrate the versatility of the device. All components remained securely positioned within the cover piece, and no leakage from the coupon was seen. The coupon in these experiments was filled with water, to prevent damage or staining of the loaned prosthetic foot.

6.2.5 *Discussion*

The purpose of this work was to develop a proof of concept device (SUMIT), to assess the viability of a clinical translation of ultrasound mediated MB delivery to biofilms in chronic wounds. With the intention to utilise such a system in a clinical environment, the design was developed to include standard clinical components where possible (syringe fitted with a blunt needle, sterile filter and 3-way Luer valve). This was intended to facilitate the utility and integration, since the primary users (surgical and nursing staff) would already be familiar with and trained in the use of these components. However, it should be noted that without specific guidance general medical staff may not be familiar with the electronic ultrasound components of the device. The optimisation of the ultrasound delivery system has not been completed in this set up, which should comprise of a simple interface that allows users to attach and activate the device without the need for programming acoustic parameters. The added clinical benefit of incorporating these components was that they were also cost effective, detachable and disposable, eliminating the need for sterilization and cleaning before re-use. The combined system was small and light (~72 g), which ensured that it was easily manipulated for use by a single person. Another important clinical aspect was the versatility in the application of the device; the successful results of testing the device on multiple orientations of an artificial foot provided clinical versatility for both the user and the patient. Additionally, although the device was designed with intended use on a foot, the final product contains a non-geometry-specific design and can potentially be used at various other locations on the human body.

Careful consideration was taken in selecting appropriate materials for the construction of the device; this was important to ensure uniformity in the delivered ultrasound field whilst maintaining some compressibility of the coupon material, for patient comfort and moulding to the geometry of the treatment area. PDMS has an acoustic impedance similar to water, which reduces reflections at the water-PDMS interfaces (Rahman *et al.*, 2012; Guillermic *et al.*, 2019). However, the ultrasound wave that travels through PDMS will eventually encounter the PDMS-air interface, where it will be reflected backwards. The use of PDMS was justified by the association with a high attenuation coefficient (>2 dB/cm). The attenuation levels at 10:1 w/w ratio at 1 MHz have been reported around 2.35 dB/cm (Cafarelli *et al.*, 2017). The hypothesis was that the PDMS would attenuate the ultrasound wave to the point that the reflected component is very week. The COMSOL simulation incorporated the properties of the chosen material and validated the use of PDMS; minimal lateral reflections observed at the air-PDMS interface (**Figure 80**) in the results (**Figure 83**) suggested that PDMS does in fact attenuate the signal and would not contribute to non-uniform field delivery to the wound area. Moreover, the ability of the PDMS to be compressed, allowed the generation of a sealed environment around the treatment area. It also showed promising surface conformity results when tested on an artificial foot model, indicating that it has great potential to conform to the uneven plantar surface of a human foot. Therefore, the soft and pliable nature of the PDMS proved to be quite beneficial for the applications of this device.

Selecting a material for the cover piece did not carry as many restrictions as the previously described coupon. The main concern of this component was its ability to withstand the tensile forces applied by the Velcro straps. The use of 3D printing was fast and cost-effective (~£30 per kg), however the large variance in the tolerances often caused unforeseen failures in the prototypes. Nevertheless, PLA was strong enough to withstand the forces applied from repeated strapping on to a variety of surfaces. Furthermore, commonly used medical grade plastics such as polypropylene and polycarbonate have densities of 1.22 g/cm^3 and 0.95 g/cm^3 respectively. The light weight (density = 1.25 g/cm^3) of PLA proved to be comparable to current clinical plastics, thereby contributing to the transferability into a clinical environment.

The reasoning behind developing this device was to fill a clinical gap in the currently available systems. There are many currently available products which possess the ability to individually deliver either ultrasound or drugs to the surface of the skin, however none possess the ability to combine the delivery of ultrasound with a fluid. For example, the availability of transdermal patches allows the controlled delivery of pre-loaded drugs to a confined area (Amjadi *et al.*, 2018). There have also been FDA approved ultrasound patches which deliver an ultrasound field to the skin through a coupling bandage (Best *et al.*, 2015; Draper *et al.*, 2018). The issue with these is that they lack the necessary combined treatments, such as ultrasound mediated therapies utilising MBs and antibiotic, that have been proven to be more effective on bacterial biofilms (He *et al.*, 2011; Dong *et al.*, 2017). The trans dermal drug loaded patches fail to provide the mechanical stimulation required to detach the biofilms from the surface (Agarwal *et al.*, 2012). On the other hand, while the ultrasound alone has the potential to deliver the mechanical activity for detachment, studies have shown that its bactericidal effects are limited in the absence of a drug (Pitt *et al.*, 1994), or in combination with an acoustically active agent (Dong *et al.*, 2017; LuTheryn *et al.*, 2019; Kooiman *et al.*, 2020). Although bandages offer a simple clinical solution and are easily manufactured and applied to a wound, the problem lies in the integration of a MB solution. Containing a premade liquid capsule or a solution to which the MBs must be added is a challenging feature to add to a bandage and the bubbles would also be constrained in a thin and/or viscous layer, which may limit their degree of oscillation upon ultrasound exposure. Additionally, MBs possess a relatively short shelf life that depends heavily on composition and storage conditions (Talu *et al.*, 2006; Mulvana *et al.*, 2010; Lee *et al.*, 2015a; Owen, Kamila, *et al.*, 2018; Ojha *et al.*, 2019). Incorporating this directly onto a patch or bandage is challenging since microbubbles dissolve at a faster rate if stored at room temperature, which significantly limits the viable period of the treatment modality. The advantage of the system developed in this project is that the microbubbles are not directly integrated into the physical design and can therefore be stored externally (~ 4 °C) or produced and injected when required.

The utility of ultrasound-stimulated MBs for the treatment of biofilms, has been conclusively demonstrated in this research and elsewhere to be highly efficacious in facilitating the removal and killing of biofilms (paragraph 4.4.3). It has been shown that the *in vitro* application of 0.08 MHz, 1.0 W/cm^{-2}, 50% duty cycle, and 10-min duration ultrasound, MBs and vancomycin can significantly decrease the number of viable cells (7.17 $\log_{10}$ CFU/mL) from *S. epidermidis* biofilms compared to an untreated control (10.51 $\log_{10}$ CFU/mL) (He *et al.*, 2011). It is important to note however, that this study could not demonstrate a significant difference between these groups using an *in vivo* rabbit model, in which *S. epidermidis* biofilms grown on polyethylene disks were subcutaneously implanted bilateral to the vertebral column. The work carried out by He *et al.* (2011), demonstrated that ultrasound activated sulphur hexafluoride MBs with a mean diameter of 2.5 µm and vancomycin create micro-pores within the biofilm architecture (0.08 MHz, 1.0 W/cm^{-2}, 50% duty cycle, and 10-min duration), which does support the hypothesis of facilitated uptake mediated by membrane/EPS disruption. An interesting point is that not only does the membrane disruption facilitates antibiotic uptake, but the influx of nutrients may induce a phase of active growing in deeper layers of the biofilm, potentiating the efficacy of the antibiotic (Dong *et al.*, 2013). The utility of the coupon in this project is that it provides a means of translating this *in vitro* work, into a physical device for *in vivo* ultrasound stimulation within the confined treatment area of a wound. The design of the proof of concept device in this research, allows the bubbles to be applied between the wound surface and the acoustic field in a similar manner to which *in vitro* tests have been carried out. An important aspect to consider in the implementation of a clinical translation, is that microbubbles will invariable rise to the top of the fluid suspension. Therefore, the orientation of the foot during treatment would dictate which surface the MBs passively rise towards. A pronated foot will allow MBs to passively rise in the fluid to interact with the wound; this orientation can be achieved with the patient in a sitting position, which should be feasible for the vast majority of patients. However, the device can be applied in multiple orientations to facilitate clinical manipulation suitable for the patients mobility needs. If MB interaction cannot be achieved passively due to device orientation; the use of targeted MBs can be used artificially increase MB proximity to the wound surface, and ensure the bubbles remain in contact with the wound surface during treatment (Ye *et al.*, 2013; Owen *et al.*, 2015c).

6.2.6 *Device design limitations and recommendations for future work*

The project resulted in the development of a system capable of delivering ultrasound to a superficial wound through a suspension of acoustically active microbubbles. Although the overall system could be successfully manufactured and tested, there are some limitations to the current design that could be improved upon for future use. A common symptom of chronic wounds is the presence of persistent pain surrounding the wound area. The method of creating a watertight seal with the device involves applying a compressive force at the interface between the device and the treatment surface. Applying this to an already painful wound area can result in and uncomfortable treatment process for the patient. For this reason, the current attachment methods and subsequent fluid containment are not ideal for these situations without the administration of a local anaesthetic. In diabetic foot nephropathy, it is common for patients to have little to no feeling and this device is well suited for that application, however it limits the translation to chronic wounds located elsewhere. A further solution to this potential issue in application, is that the implementation of the device could be specifically targeted to the early stages of chronic wound development.

For the scope of this project, the device was fabricated to target early stage wounds and therefore the treatment area of the coupon was limited to a 3 cm diameter. With a growing need for personalised therapies this would invariably not be suitable for all chronic wound applications, however the fabrication methods used to rapidly develop this prototype device have a significant capacity for adaptation. Since the sizes of chronic wounds vary significantly from patient to patient, it is necessary to include management strategies to counteract these variances such as larger coupon sizes or multiple treatment zones. At the start of this project, acoustic behaviour of the skin layers within a chronic wound were not well defined. The assumption made was that the 1MHz frequency signal was attenuated beyond the wound. However, the location and depth of the wound can cause interactions between the delivered ultrasound signal and the acoustically reflective bone tissue. Depending on the location and position of the bone tissue relative to the skin surface, if the previously made assumption was incorrect and the ultrasound waves can travel to the bone, this can potentially have an adverse effect on the field delivered to the microbubbles. The bubbles can effectively be manipulated at specific locations of an ultrasonic standing wave field and do not remain in contact with the wound surface (Vohra and Jasuja, 2016; Guillermic *et al.*, 2019). The oscillatory effects are therefore inhibited and proposes a major challenge to the functioning of the device. The future application of this device will benefit from an acoustic characterization of a skin model and should therefore be explored moving forward. This research attempted to carry out PCD of the microbubble response within the SUMIT, however there were a number of irregularities perhaps derived from the experimental set-up that made the preliminary data unreliable. There was an apparent suppression of sub- and ultra-harmonics in the FFT of the original data, which would perhaps be indicative of inertial cavitation of the MBs present. However, this was incongruous with the simulated data that demonstrated the peak pressure in the system was 0.2 MPa. However, this would be potentially beneficial given the success of inertial cavitation seen in earlier experiments in this research at 0.5 MPa(paragraph 4.3.3.3). With an expanded body of research carried out in Chapter 4 on the ultrasound stimulation and response of MBs, it would be possible to more accurately test representative acoustic regimes in the future. This will be an important step in verifying the utility of the SUMIT for clinical application.

To properly characterize the effectiveness of the ultrasound targeted microbubble system provided by the device, the results of its action on bacterial biofilms must be observed. An attempt was made to apply the system to biofilms grown on a glass coverslip, however the visualization of these results proved to be a challenge. Due to the time restrictions placed on this work, further bacterial characterization could not be completed. The results of testing on bacterial biofilms are an important form of validation for this device. As a result, it is highly recommended that these tests are repeated using different methods to produce quantifiable results. Testing on large animals such as pigs provide the greatest congruency with therapeutic effects seen in clinical trials, as such this research could first consider the use of a porcine skin model for biological proof of concept trials of the SUMIT (Gordillo *et al.*, 2013). As clearly highlighted in the current literature, there is a growing body of research aimed at developing experimental procedures for investigating the effect of ultrasound-mediated therapies on biofilms. However, there is yet very little exploration on how these treatment modalities might be implemented clinically; the developments of the SUMIT described here bring us a step closer to filling this gap.

6.2.7 *Conclusion*

This work provided the principal design and methodology to develop the simple and cost-effective SUMIT, for delivering ultrasound and MBs to a superficial wound area. The system functioned by injecting a suspension of bubbles onto a contained area over the wound which allowed a 1 MHz ultrasound stimulation to be applied. The use of 3D-printed components contributed to easy manufacturing with fast throughput. The selection of soft and pliable PDMS for the treatment area was ideal for creating a watertight interface with the foot, because it was able to conform to the uneven surface geometry. Acoustic pressure field variances within the 1 cm fluid cavity were quantified by a coefficient of variance of 0.162. Although this work provides a successful proof of concept for delivering ultrasound-mediated microbubbles to a surface wound, there are invariably still improvements that are required for future use in clinical applications.

6.3 *Appendix C* – Conference and events attended

Name	Location	Date/Type	Work presented
BioMedEng18	Imperial College, London	September, 2018 Oral presentation	https://www.researchgate.net/publication/330485109_Ultrasound_responsive_microbubbles_enhance_the_activity_of_sub-inhibitory_concentrations_of_gentamicin_in_the_treatment_of_Pseudomonas_aeruginosa_biofilms
Leeds Microbubble Symposium	Weetwood Hall, Leeds	July, 2018 Oral presentation	(As above)
The 24th European symposium on Ultrasound Contrast Imaging	Hilton Hotel, Rotterdam	January, 2019 5 minute talk and poster	DOI: 10.13140/RG.2.2.29250.84169

6.4 Appendix D – Additional responsibilities

Activity	Main Responsibilities
Brilliant Club PhD tutor	Design of a KS4/5 course to engage students from under-represented background to enable them to progress to highly selective universities
Faculty of Life Sciences, Microbiology BIOL2038 Demonstrator	Supervision of second year microbiology students, providing practical assistance and advice on laboratory practice
Faculty of Engineering and Physical Sciences, AER Exam Invigilator	Invigilation of exams for students with additional needs
Co-supervision of Masters students	I have completed the co-supervision of one MSc student who attained a high first in their dissertation, I am currently co-supervising two MSc students.
Microbiology project support	Microbiology training and support on post-doc project investigating the effect of biofilms and encrustation on urinary catheters
Reviewer, Journal of Wound Care	I have successfully peer-reviewed three publications to date for the Journal of Wound Care

BIBLIOGRAPHY

Abaka-Wood, G. B., Addai-Mensah, J. and Skinner, W. (2017) 'A study of flotation characteristics of monazite, hematite, and quartz using anionic collectors', *International Journal of Mineral Processing*. Elsevier B.V., 158, pp. 55–62. doi: 10.1016/j.minpro.2016.11.012.

Abou-Saleh, R. H., Swain, M., Evans, S. D. and Thomson, N. H. (2014) 'Poly(ethylene glycol) Lipid-Shelled Microbubbles: Abundance, Stability, and Mechanical Properties', *Langmuir*. American Chemical Society, 30(19), pp. 5557–5563. doi: 10.1021/la404804u.

Abu-Zidan, F. M., Hefny, A. F. and Corr, P. (2011) 'Clinical ultrasound physics.', *Journal of emergencies, trauma, and shock*. Wolters Kluwer -- Medknow Publications, 4(4), pp. 501–3. doi: 10.4103/0974-2700.86646.

Agarwal, A., Xu, H., Ng, W. J. and Liu, Y. (2012) 'Biofilm detachment by self-collapsing air microbubbles: A potential chemical-free cleaning technology for membrane biofouling', *Journal of Materials Chemistry*. The Royal Society of Chemistry, 22(5), pp. 2203–2207. doi: 10.1039/c1jm14439a.

Ahmadi, F., Mcloughlin, I. V., Chauhan, S. and Ter-Haar, G. (2012) *Bio-effects and safety of low intensity, low frequency ultrasonic exposure*, *Progress in Biophysics and Molecular Biology*. Prog Biophys Mol Biol. doi: 10.1016/j.pbiomolbio.2012.01.004.

Alexiadou, K. and Doupis, J. (2012) 'Management of diabetic foot ulcers.', *Diabetes therapy : research, treatment and education of diabetes and related disorders*. Springer, 3(1), p. 4. doi: 10.1007/s13300-012-0004-9.

Algburi, A., Comito, N., Kashtanov, D., Dicks, L. M. T. and Chikindas, M. L. (2017) 'Control of Biofilm Formation: Antibiotics and Beyond.', *Applied and environmental microbiology*. American Society for Microbiology, 83(3), pp. e02508-16. doi: 10.1128/AEM.02508-16.

Alkins, R. and Hynynen, K. (2014) 'Ultrasound Therapy', in *Comprehensive Biomedical Physics*. Elsevier, pp. 153–168. doi: 10.1016/B978-0-444-53632-7.01010-8.

Allison, L., Walker, L., Sanders, B., Yang, Z., Eckert, G. and Gregory, R. (2015) 'Effect of Human Milk and its Components on Streptococcus Mutans Biofilm Formation', *Journal of Clinical Pediatric Dentistry*. Clinical Pediatric Dentistry , 39(3), pp. 255–261. doi: 10.17796/1053-4628-39.3.255.

Almeida, A. C., Gomes, T., Habuda-Stanić, M., Lomba, J. A. B., Romić, Ž., Turkalj, J. V. and Lillicrap, A. (2019) 'Characterization of multiple biomarker responses using flow cytometry to improve environmental hazard assessment with the green microalgae Raphidocelis subcapitata', *Science of the Total Environment*. Elsevier B.V., 687, pp. 827–838. doi: 10.1016/j.scitotenv.2019.06.124.

Amjadi, M., Sheykhansari, S., Nelson, B. J. and Sitti, M. (2018) 'Recent Advances in Wearable Transdermal Delivery Systems', *Advanced Materials*. Wiley-VCH Verlag, 30(7), p. 1704530. doi: 10.1002/adma.201704530.

Ammons, M. C. B., Ward, L. S., Dowd, S. and James, G. A. (2011) 'Combined treatment of Pseudomonas aeruginosa biofilm with lactoferrin and xylitol inhibits the ability of bacteria to respond to damage resulting from lactoferrin iron chelation.', *International journal of antimicrobial agents*. Elsevier, 37(4), pp. 316–23. doi: 10.1016/j.ijantimicag.2010.12.019.

Ammons, M. C. B., Ward, L. S. and James, G. A. (2011) 'Anti-biofilm efficacy of a lactoferrin/xylitol wound hydrogel used in combination with silver wound dressings', *International Wound Journal*. Wiley/Blackwell

(10.1111), 8(3), pp. 268–273. doi: 10.1111/j.1742-481X.2011.00781.x.

Andrews, J. M. (2001) ‘Determination of minimum inhibitory concentrations.’, *The Journal of antimicrobial chemotherapy*, 48 Suppl 1, pp. 5–16. Available at: http://www.ncbi.nlm.nih.gov/pubmed/11420333 (Accessed: 24 March 2019).

Appis, A. W., Tracy, M. J. and Feinstein, S. B. (2015) ‘Update on the safety and efficacy of commercial ultrasound contrast agents in cardiac applications’, *Echo Research and Practice*. BioScientifica Ltd., pp. R55–R62. doi: 10.1530/ERP-15-0018.

Arora, D. P., Hossain, S., Xu, Y. and Boon, E. M. (2015) ‘Nitric Oxide Regulation of Bacterial Biofilms’, *Biochemistry*, 54(24), pp. 3717–3728. doi: 10.1021/bi501476n.

Attinger, C. and Wolcott, R. (2012) ‘Clinically Addressing Biofilm in Chronic Wounds.’, *Advances in wound care*. Mary Ann Liebert, Inc., 1(3), pp. 127–132. doi: 10.1089/wound.2011.0333.

Aubry, A. and Derode, A. (2011) ‘Multiple scattering of ultrasound in weakly inhomogeneous media: Application to human soft tissues’, *The Journal of the Acoustical Society of America*. Acoustical Society of America (ASA), 129(1), pp. 225–233. doi: 10.1121/1.3506343.

Ayala, A., Muñoz, M. F. and Argüelles, S. (2014) ‘Lipid peroxidation: Production, metabolism, and signaling mechanisms of malondialdehyde and 4-hydroxy-2-nonenal’, *Oxidative Medicine and Cellular Longevity*. Landes Bioscience. doi: 10.1155/2014/360438.

Azarov, I., Huang, K. T., Basu, S., Gladwin, M. T., Hogg, N. and Kim-Shapiro, D. B. (2005) ‘Nitric Oxide Scavenging by Red Blood Cells as a Function of Hematocrit and Oxygenation’, *Journal of Biological Chemistry*, 280(47), pp. 39024–39032. doi: 10.1074/jbc.M509045200.

Azeredo, J., Azevedo, N. F., Briandet, R., Cerca, N., Coenye, T., Costa, A. R., Desvaux, M., Di Bonaventura, G., Hébraud, M., Jaglic, Z., Kačániová, M., Knøchel, S., Lourenço, A., Mergulhão, F., Meyer, R. L., Nychas, G., Simões, M., Tresse, O. and Sternberg, C. (2017) ‘Critical review on biofilm methods’, *Critical Reviews in Microbiology*, 43(3), pp. 313–351. doi: 10.1080/1040841X.2016.1208146.

Bajpayee, A. G. and Grodzinsky, A. J. (2017) ‘Cartilage-targeting drug delivery: Can electrostatic interactions help?’, *Nature Reviews Rheumatology*. Nature Publishing Group, pp. 183–193. doi: 10.1038/nrrheum.2016.210.

Bansal, E., Garg, A., Bhatia, S., Attri, A. K. and Chander, J. (2008) ‘Spectrum of microbial flora in diabetic foot ulcers.’, *Indian journal of pathology & microbiology*, 51(2), pp. 204–8. Available at: http://www.ncbi.nlm.nih.gov/pubmed/18603682 (Accessed: 25 June 2018).

Banu, A., Noorul Hassan, M. M., Rajkumar, J. and Srinivasa, S. (2015) ‘Spectrum of bacteria associated with diabetic foot ulcer and biofilm formation: A prospective study.’, *The Australasian medical journal*. Australasian Medical Journal, 8(9), pp. 280–5. doi: 10.4066/AMJ.2015.2422.

Barraud, N., Hassett, D. J., Hwang, S.-H., Rice, S. A., Kjelleberg, S. and Webb, J. S. (2006) ‘Involvement of nitric oxide in biofilm dispersal of Pseudomonas aeruginosa.’, *Journal of bacteriology*. American Society for Microbiology, 188(21), pp. 7344–53. doi: 10.1128/JB.00779-06.

Barraud, N., Kelso, M. J., Rice, S. A. and Kjelleberg, S. (2015) ‘Nitric oxide: a key mediator of biofilm dispersal with applications in infectious diseases.’, *Current pharmaceutical design*, 21(1), pp. 31–42. Available at: http://www.ncbi.nlm.nih.gov/pubmed/25189865 (Accessed: 30 November 2017).

Barraud, N., Storey, M. V., Moore, Z. P., Webb, J. S., Rice, S. A. and Kjelleberg, S. (2009) 'Nitric oxide-mediated dispersal in single- and multi-species biofilms of clinically and industrially relevant microorganisms', *Microbial Biotechnology*. Wiley/Blackwell (10.1111), 2(3), pp. 370–378. doi: 10.1111/j.1751-7915.2009.00098.x.

Bartell, J. A., Sommer, L. M., Haagensen, J. A., Loch, A., Espinosa, R., Molin, S. and Johansen, H. K. (2018) 'Evolutionary highways to persistent infection by Pseudomonas aeruginosa', *bioRxiv*. Cold Spring Harbor Laboratory, p. 326025. doi: 10.1101/326025.

Basudhar, D., Ridnour, L. A., Cheng, R., Kesarwala, A. H., Heinecke, J. and Wink, D. A. (2016) 'Biological signaling by small inorganic molecules', *Coordination Chemistry Reviews*. Elsevier, 306, pp. 708–723. doi: 10.1016/J.CCR.2015.06.001.

Bessa, L. J., Fazii, P., Di Giulio, M. and Cellini, L. (2015) 'Bacterial isolates from infected wounds and their antibiotic susceptibility pattern: some remarks about wound infection', *International Wound Journal*, 12(1), pp. 47–52. doi: 10.1111/iwj.12049.

Best, T. M., Moore, B., Jarit, P., Moorman, C. T. and Lewis, G. K. (2015) 'Sustained acoustic medicine: Wearable, long duration ultrasonic therapy for the treatment of tendinopathy', *Physician and Sportsmedicine*. Taylor and Francis Ltd., 43(4), pp. 366–374. doi: 10.1080/00913847.2015.1095617.

Beveridge, T. (2001) 'Use of the Gram stain in microbiology', *Biotechnic & Histochemistry*. Taylor & Francis, 76(3), pp. 111–118. doi: 10.1080/bih.76.3.111.118.

Birkin, P. R., Offin, D. G. and Leighton, T. G. (2016) 'An activated fluid stream - New techniques for cold water cleaning'. doi: 10.1016/j.ultsonch.2015.10.001.

Birkin, P. R., Offin, D. G., Vian, C. J. B., Howlin, R. P., Dawson, J. I., Secker, T. J., Hervé, R. C., Stoodley, P., Oreffo, R. O. C., Keevil, C. W. and Leighton, T. G. (2015) 'Cold water cleaning of brain proteins, biofilm and bone – harnessing an ultrasonically activated stream', *Physical Chemistry Chemical Physics*. Royal Society of Chemistry, 17(32), pp. 20574–20579. doi: 10.1039/C5CP02406D.

Bjarnsholt, T. (2013) 'The role of bacterial biofilms in chronic infections', *APMIS*, 121(136), pp. 1–58. doi: 10.1111/apm.12099.

Borden, M. A. (2016) 'Lipid-Coated Nanodrops and Microbubbles', in *Handbook of Ultrasonics and Sonochemistry*. Singapore: Springer Singapore, pp. 1075–1100. doi: 10.1007/978-981-287-278-4_26.

Borden, M. A., Kruse, D. E., Caskey, C. F., Zhao, S., Dayton, P. A. and Ferrara, K. W. (2005) 'Influence of lipid shell physicochemical properties on ultrasound-induced microbubble destruction.', *IEEE transactions on ultrasonics, ferroelectrics, and frequency control*. NIH Public Access, 52(11), pp. 1992–2002. doi: 10.1109/TUFFC.2005.1561668.

Borden, M. A. and Song, K. H. (2018) 'Reverse engineering the ultrasound contrast agent', *Advances in Colloid and Interface Science*. Elsevier B.V., pp. 39–49. doi: 10.1016/j.cis.2018.10.004.

Bowler, P. G., Duerden, B. I. and Armstrong, D. G. (2001) 'Wound microbiology and associated approaches to wound management.', *Clinical microbiology reviews*. American Society for Microbiology (ASM), 14(2), pp. 244–69. doi: 10.1128/CMR.14.2.244-269.2001.

Bremus, C., Herrmann, U., Bringer-Meyer, S. and Sahm, H. (2006) 'The use of microorganisms in l-ascorbic acid production', *Journal of Biotechnology*. Elsevier, pp. 196–205. doi: 10.1016/j.jbiotec.2006.01.010.

Brennen, C. E. (2013) *Cavitation and bubble dynamics*, *Cavitation and Bubble Dynamics*. doi: 10.1017/CBO9781107338760.

Browning, R. J., Aron, M., Booth, A., Rademeyer, P., Wing, S., Brans, V., Shrivastava, S., Carugo, D. and Stride, E. (2020) 'Spectral Imaging for Microbubble Characterization', *Langmuir*. American Chemical Society, 36(2), pp. 609–617. doi: 10.1021/acs.langmuir.9b03828.

Cafarelli, A., Verbeni, A., Poliziani, A., Dario, P., Menciassi, A. and Ricotti, L. (2017) 'Tuning acoustic and mechanical properties of materials for ultrasound phantoms and smart substrates for cell cultures', *Acta Biomaterialia*. Elsevier Ltd, 49, pp. 368–378. doi: 10.1016/j.actbio.2016.11.049.

Cai, Y., Wang, J., Liu, X., Wang, R. and Xia, L. (2017) 'A Review of the Combination Therapy of Low Frequency Ultrasound with Antibiotics', *BioMed Research International*. Hindawi, 2017, pp. 1–14. doi: 10.1155/2017/2317846.

Cardinal, M., Eisenbud, D. E., Armstrong, D. G., Zelen, C., Driver, V., Attinger, C., Phillips, T. and Harding, K. (2009) 'Serial surgical debridement: A retrospective study on clinical outcomes in chronic lower extremity wounds', *Wound Repair and Regeneration*, 17(3), pp. 306–311. doi: 10.1111/j.1524-475X.2009.00485.x.

Carding, S., Verbeke, K., Vipond, D. T., Corfe, B. M. and Owen, L. J. (2015) 'Dysbiosis of the gut microbiota in disease.', *Microbial ecology in health and disease*. Taylor & Francis, 26, p. 26191. doi: 10.3402/MEHD.V26.26191.

Carlsson, S., Govoni, M., Wiklund, N. P., Weitzberg, E. and Lundberg, J. O. (2003) 'In Vitro Evaluation of a New Treatment for Urinary Tract Infections Caused by Nitrate-Reducing Bacteria', *Antimicrobial Agents and Chemotherapy*. American Society for Microbiology (ASM), 47(12), pp. 3713–3718. doi: 10.1128/AAC.47.12.3713-3718.2003.

Carniello, V., Peterson, B. W., van der Mei, H. C. and Busscher, H. J. (2018) 'Physico-chemistry from initial bacterial adhesion to surface-programmed biofilm growth', *Advances in Colloid and Interface Science*. Elsevier B.V., pp. 1–14. doi: 10.1016/j.cis.2018.10.005.

Carugo, D., Aron, M., Sezgin, E., Bernardino de la Serna, J., Kuimova, M. K., Eggeling, C. and Stride, E. (2017) 'Modulation of the molecular arrangement in artificial and biological membranes by phospholipid-shelled microbubbles', *Biomaterials*. Elsevier, 113, pp. 105–117. doi: 10.1016/J.BIOMATERIALS.2016.10.034.

Carugo, D., Owen, J., Crake, C., Lee, J. Y. and Stride, E. (2015) 'Biologicallyand acoustically compatible chamber for studying ultrasound-mediated delivery of therapeutic compounds', *Ultrasound in Medicine and Biology*. Elsevier USA, 41(7), pp. 1927–1937. doi: 10.1016/j.ultrasmedbio.2015.03.020.

Casini, G., Loiudice, P., De Cillà, S., Radice, P. and Nardi, M. (2016) 'Sulfur hexafluoride (SF6) versus perfluoropropane (C3F8) tamponade and short term face-down position for macular hole repair: a randomized prospective study', *International Journal of Retina and Vitreous*. BioMed Central, 2(1), p. 10. doi: 10.1186/s40942-016-0036-9.

Cavalieri, F., Finelli, I., Tortora, M., Mozetic, P., Chiessi, E., Polizio, F., Brismar, T. B. and Paradossi, G. (2008) 'Polymer Microbubbles As Diagnostic and Therapeutic Gas Delivery Device', *Chemistry of Materials*. American Chemical Society, 20(10), pp. 3254–3258. doi: 10.1021/cm703702d.

Caveney, N. A., Li, F. K. and Strynadka, N. C. (2018) 'Enzyme structures of the bacterial peptidoglycan and wall teichoic acid biogenesis pathways', *Current Opinion in Structural Biology*. Elsevier Current Trends, 53, pp. 45–58.

doi: 10.1016/J.SBI.2018.05.002.

Chacko, S. A. and Wenthold, P. G. (2006) ‘The negative ion chemistry of nitric oxide in the gas phase’, *Mass Spectrometry Reviews*. Mass Spectrom Rev, 25(1), pp. 112–126. doi: 10.1002/mas.20060.

Chen, T., Shin, J. and Huang, L. (2016) ‘Ultrasound transmission attenuation tomography using energy-scaled amplitude ratios’, in Duric, N. and Heyde, B. (eds) *Medical Imaging 2016: Ultrasonic Imaging and Tomography*. SPIE, p. 979016. doi: 10.1117/12.2216412.

Chen, X., Wang, J., Pacella, J. J. and Villanueva, F. S. (2016) ‘Dynamic Behavior of Microbubbles during Long Ultrasound Tone-Burst Excitation: Mechanistic Insights into Ultrasound-Microbubble Mediated Therapeutics Using High-Speed Imaging and Cavitation Detection.’, *Ultrasound in medicine & biology*. NIH Public Access, 42(2), pp. 528–538. doi: 10.1016/j.ultrasmedbio.2015.09.017.

Chihara, K., Matsumoto, S., Kagawa, Y. and Tsuneda, S. (2015) ‘Mathematical modeling of dormant cell formation in growing biofilm’, *Frontiers in Microbiology*. Frontiers Research Foundation, 6(MAY), p. 534. doi: 10.3389/fmicb.2015.00534.

Choi, J. J., Carlisle, R. C., Coviello, C., Seymour, L. and Coussios, C.-C. (2014) ‘Non-invasive and real-time passive acoustic mapping of ultrasound-mediated drug delivery’, *Physics in Medicine and Biology*. IOP Publishing, 59(17), pp. 4861–4877. doi: 10.1088/0031-9155/59/17/4861.

Choi, M., Park, S., Park, K., Jeong, H. and Hong, J. (2019) ‘Nitric Oxide Delivery Using Biocompatible Perfluorocarbon Microemulsion for Antibacterial Effect’, *ACS Biomaterials Science and Engineering*. American Chemical Society, 5(3), pp. 1378–1383. doi: 10.1021/acsbiomaterials.9b00016.

Choi, S., Yun, Z., Hong, S. and Ahn, K. (2001) ‘The effect of co-existing ions and surface characteristics of nanomembranes of the removal of nitrate and fluoride’, *Desalination*. Elsevier, 133(1), pp. 53–64. doi: 10.1016/S0011-9164(01)00082-0.

Chua, S. L., Liu, Y., Yam, J. K. H., Chen, Y., Vejborg, R. M., Tan, B. G. C., Kjelleberg, S., Tolker-Nielsen, T., Givskov, M. and Yang, L. (2014) ‘Dispersed cells represent a distinct stage in the transition from bacterial biofilm to planktonic lifestyles’, *Nature Communications*. Nature Publishing Group, 5(1), p. 4462. doi: 10.1038/ncomms5462.

Ciofu, O., Rojo-Molinero, E., Macià, M. D. and Oliver, A. (2017) ‘Antibiotic treatment of biofilm infections’, *APMIS*. Blackwell Munksgaard, pp. 304–319. doi: 10.1111/apm.12673.

Clark, R. A. F. (1993) ‘Biology of Dermal Wound Repair’, *Dermatologic Clinics*. Elsevier, 11(4), pp. 647–666. doi: 10.1016/S0733-8635(18)30218-3.

Cochain, C., Channon, K. M. and Silvestre, J.-S. (2013) ‘Angiogenesis in the Infarcted Myocardium’, *Antioxidants & Redox Signaling*, 18(9), pp. 1100–1113. doi: 10.1089/ars.2012.4849.

Coffey, B. M. and Anderson, G. G. (2014) ‘Biofilm Formation in the 96-Well Microtiter Plate’, in *Methods in molecular biology (Clifton, N.J.)*, pp. 631–641. doi: 10.1007/978-1-4939-0473-0_48.

Collis, J., Manasseh, R., Liovic, P., Tho, P., Ooi, A., Petkovic-Duran, K. and Zhu, Y. (2010) ‘Cavitation microstreaming and stress fields created by microbubbles’, *Ultrasonics*, 50(2), pp. 273–279. Available at: https://www.sciencedirect.com/science/article/pii/S0041624X09001395 (Accessed: 8 June 2018).

Cooper, R. A., Bjarnsholt, T. and Alhede, M. (2014) ‘Biofilms in wounds: a review of present knowledge’, *Journal* *of Wound Care*, 23(11), pp. 570–582. doi: 10.12968/jowc.2014.23.11.570.

Costa, R. H. R., Cardoso, N. A., Procópio, R. J., Navarro, T. P., Dardik, A. and de Loiola Cisneros, L. (2017) ‘Diabetic foot ulcer carries high amputation and mortality rates, particularly in the presence of advanced age, peripheral artery disease and anemia’, *Diabetes & Metabolic Syndrome: Clinical Research & Reviews*. Elsevier, 11, pp. S583–S587. doi: 10.1016/J.DSX.2017.04.008.

Cowan, T. (2011) ‘Biofilms and their management: from concept to clinical reality’, *Journal of Wound Care*, 20(5), pp. 220–226. doi: 10.12968/jowc.2011.20.5.220.

Crum, L. A. (1984) ‘Acoustic cavitation series: part five rectified diffusion’, *Ultrasonics*. Elsevier, 22(5), pp. 215–223. doi: 10.1016/0041-624X(84)90016-7.

Damianou, C., Christofi, C. and Mylonas, N. (2015) ‘Removing atherosclerotic plaque created using high cholesterol diet in rabbit using ultrasound.’, *Journal of therapeutic ultrasound*. BioMed Central, 3(1), p. 3. doi: 10.1186/s40349-015-0025-8.

Daneman, R. and Prat, A. (2015) ‘The blood-brain barrier.’, *Cold Spring Harbor perspectives in biology*. Cold Spring Harbor Laboratory Press, 7(1), p. a020412. doi: 10.1101/cshperspect.a020412.

Datta, S., Coussios, C.-C., McAdory, L. E., Tan, J., Porter, T., De Courten-Myers, G. and Holland, C. K. (2006) ‘Correlation of cavitation with ultrasound enhancement of thrombolysis’, *Ultrasound in Medicine & Biology*. Elsevier, 32(8), pp. 1257–1267. doi: 10.1016/J.ULTRASMEDBIO.2006.04.008.

Delalande, A., Bastié, C., Pigeon, L., Manta, S., Lebertre, M., Mignet, N., Midoux, P. and Pichon, C. (2017) ‘Cationic gas-filled microbubbles for ultrasound-based nucleic acids delivery.’, *Bioscience reports*. Portland Press Ltd, 37(6), p. 20160619. doi: 10.1042/BSR20160619.

Demidova-Rice, T. N., Hamblin, M. R. and Herman, I. M. (2012) ‘Acute and impaired wound healing: pathophysiology and current methods for drug delivery, part 1: normal and chronic wounds: biology, causes, and approaches to care.’, *Advances in skin & wound care*. NIH Public Access, 25(7), pp. 304–14. doi: 10.1097/01.ASW.0000416006.55218.d0.

Dhall, S., Do, D., Garcia, M., Wijesinghe, D. S., Brandon, A., Kim, J., Sanchez, A., Lyubovitsky, J., Gallagher, S., Nothnagel, E. A., Chalfant, C. E., Patel, R. P., Schiller, N. and Martins-Green, M. (2014) ‘A Novel Model of Chronic Wounds: Importance of Redox Imbalance and Biofilm-Forming Bacteria for Establishment of Chronicity’, *PLoS ONE*. Edited by V. D. Appanna. Public Library of Science, 9(10), p. e109848. doi: 10.1371/journal.pone.0109848.

Dhanaliwala, A. H., Dixon, A. J., Lin, D., Chen, J. L., Klibanov, A. L. and Hossack, J. A. (2015) ‘In vivo imaging of microfluidic-produced microbubbles’, *Biomedical Microdevices*, 17(1), p. 23. doi: 10.1007/s10544-014-9914-9.

Dinarello, C. A. (2000) ‘Proinflammatory cytokines.’, *Chest*, 118(2), pp. 503–8. Available at: http://www.ncbi.nlm.nih.gov/pubmed/10936147 (Accessed: 23 January 2017).

Dini, V., Salvo, P., Janowska, A., Di Francesco, F., Barbini, A. and Romanelli, M. (2015) ‘Correlation Between Wound Temperature Obtained With an Infrared Camera and Clinical Wound Bed Score in Venous Leg Ulcers.’, *Wounds : a compendium of clinical research and practice*, 27(10), pp. 274–8. Available at: http://www.ncbi.nlm.nih.gov/pubmed/26479211 (Accessed: 21 June 2018).

Doinikov, A. A., Haac, J. F. and Dayton, P. A. (2009) ‘Resonance frequencies of lipid-shelled microbubbles in the regime of nonlinear oscillations’, *Ultrasonics*. NIH Public Access, 49(2), pp. 263–268. doi:

10.1016/j.ultras.2008.09.006.

Dong, Y., Chen, S., Wang, Z., Peng, N. and Yu, J. (2013) ‘Synergy of ultrasound microbubbles and vancomycin against Staphylococcus epidermidis biofilm’, *Journal of Antimicrobial Chemotherapy*. Oxford University Press, 68(4), pp. 816–826. doi: 10.1093/jac/dks490.

Dong, Y., Xu, Y., Li, P., Wang, C., Cao, Y. and Yu, J. (2017) ‘Antibiofilm effect of ultrasound combined with microbubbles against Staphylococcus epidermidis biofilm’, *International Journal of Medical Microbiology*. Urban & Fischer, 307(6), pp. 321–328. doi: 10.1016/j.ijmm.2017.06.001.

Donlan, R. M. (2002) ‘Biofilms: microbial life on surfaces.’, *Emerging infectious diseases*. Centers for Disease Control and Prevention, 8(9), pp. 881–90. doi: 10.3201/eid0809.020063.

Draper, D. O., Klyve, D., Ortiz, R. and Best, T. M. (2018) ‘Effect of low-intensity long-duration ultrasound on the symptomatic relief of knee osteoarthritis: A randomized, placebo-controlled double-blind study’, *Journal of Orthopaedic Surgery and Research*. BioMed Central Ltd., 13(1), pp. 1–9. doi: 10.1186/s13018-018-0965-0.

Dronkers, C. E. A., Ende-Verhaar, Y. M., Kyrle, P. A., Righini, M., Cannegieter, S. C., Huisman, M. V. and Klok, F. A. (2017) ‘Disease prevalence dependent failure rate in diagnostic management studies on suspected deep vein thrombosis: communication from the SSC of the ISTH’, *Journal of Thrombosis and Haemostasis*. Wiley/Blackwell (10.1111), 15(11), pp. 2270–2273. doi: 10.1111/jth.13805.

Du, J., Bandara, H. M. H. N., Du, P., Huang, H., Hoang, K., Nguyen, D., Mogarala, S. V. and Smyth, H. D. C. (2015) ‘Improved Biofilm Antimicrobial Activity of Polyethylene Glycol Conjugated Tobramycin Compared to Tobramycin in *Pseudomonas aeruginosa* Biofilms’, *Molecular Pharmaceutics*. American Chemical Society, 12(5), pp. 1544–1553. doi: 10.1021/mp500846u.

Durham, A. E. (2018) ‘An evaluation of serum gentamicin concentrations and bacterial susceptibility to gentamicin in equine practice’, *Journal of Veterinary Internal Medicine*. Blackwell Publishing Inc., 32(3), pp. 1194–1201. doi: 10.1111/jvim.15078.

Edgeworth, A., Ross, J. A., Anderson, T., Butler, M., McDicken, W. N. and Moran, C. (2010) ‘Novel flow chamber to investigate binding strength of a lipid-based, high-frequency, ultrasonic contrast agent’, *Ultrasound*. SAGE PublicationsSage UK: London, England, 18(3), pp. 130–139. doi: 10.1258/ult.2010.010008.

Efthymiou, K., Pelekasis, N., Butler, M. B., Thomas, D. H. and Sboros, V. (2018) ‘The effect of resonance on transient microbubble acoustic response: Experimental observations and numerical simulations’, *The Journal of the Acoustical Society of America*. Acoustical Society of America (ASA), 143(3), pp. 1392–1406. doi: 10.1121/1.5026021.

Elsayed, M., Kothandaraman, A., Edirisinghe, M. and Huang, J. (2016) ‘Porous Polymeric Films from Microbubbles Generated Using a T-Junction Microfluidic Device’, *Langmuir*. American Chemical Society, 32(50), pp. 13377–13385. doi: 10.1021/acs.langmuir.6b02890.

Emerich, D. F., Snodgrass, P., Lafreniere, D., Dean, R. L., Salzberg, H., Marsh, J., Perdomo, B., Arastu, M., Winn, S. R. and Bartus, R. T. (2002) ‘Sustained Release Chemotherapeutic Microspheres Provide Superior Efficacy over Systemic Therapy and Local Bolus Infusions’, *Pharmaceutical Research*. Kluwer Academic Publishers-Plenum Publishers, 19(7), pp. 1052–1060. doi: 10.1023/A:1016434926649.

Fabiilli, M. L., Haworth, K. J., Fakhri, N. H., Kripfgans, O. D., Carson, P. L. and Fowlkes, J. B. (2009) ‘The role of inertial cavitation in acoustic droplet vaporization', *IEEE Transactions on Ultrasonics, Ferroelectrics, and Frequency Control*. Institute of Electrical and Electronics Engineers Inc., 56(5), pp. 1006–1017. doi: 10.1109/TUFFC.2009.1132.

Fan, Z., Kumon, R. E. and Deng, C. X. (2014) 'Mechanisms of microbubble-facilitated sonoporation for drug and gene delivery', *Therapeutic Delivery*, 5(4), pp. 467–486. doi: 10.4155/tde.14.10.

Ferrara, K., Pollard, R. and Borden, M. (2007) 'Ultrasound Microbubble Contrast Agents: Fundamentals and Application to Gene and Drug Delivery', *Annual Review of Biomedical Engineering*. Annual Reviews, 9(1), pp. 415–447. doi: 10.1146/annurev.bioeng.8.061505.095852.

Feshitan, J. A., Chen, C. C., Kwan, J. J. and Borden, M. A. (2009) 'Microbubble size isolation by differential centrifugation', *Journal of Colloid and Interface Science*. Elsevier Inc., 329(2), pp. 316–324. doi: 10.1016/j.jcis.2008.09.066.

Fiabane, J., Prentice, P. and Pancholi, K. (2016) 'High Yielding Microbubble Production Method', *BioMed Research International*. Hindawi, 2016, pp. 1–9. doi: 10.1155/2016/3572827.

Figueiredo, A. M. S., Ferreira, F. A., Beltrame, C. O. and Côrtes, M. F. (2017) 'The role of biofilms in persistent infections and factors involved in *ica* -independent biofilm development and gene regulation in *Staphylococcus aureus*', *Critical Reviews in Microbiology*. Taylor & Francis, 43(5), pp. 602–620. doi: 10.1080/1040841X.2017.1282941.

Findlay, M. W. and Gurtner, G. C. (2017) 'Engineering Niches for Skin and Wound Healing', in *Biology and Engineering of Stem Cell Niches*. Elsevier Inc., pp. 559–579. doi: 10.1016/B978-0-12-802734-9.00035-4.

Fix, S. M., Borden, M. A., Dayton, P. A., Samantha M. Fix, Mark A. Borden, P. A. D., Fix, S. M., Borden, M. A. and Dayton, P. A. (2015) 'Therapeutic gas delivery via microbubbles and liposomes', *Journal of Controlled Release*. Elsevier B.V., 209, pp. 139–149. doi: 10.1016/j.jconrel.2015.04.027.

Flemming, H.-C., Neu, T. R. and Wozniak, D. J. (2007) 'The EPS Matrix: The "House of Biofilm Cells"', *Journal of bacteriology*. American Society for Microbiology, 189(22), pp. 7945–7. doi: 10.1128/JB.00858-07.

Flemming, H.-C., Wingender, J., Szewzyk, U., Steinberg, P., Rice, S. A. and Kjelleberg, S. (2016) 'Biofilms: an emergent form of bacterial life', *Nature Reviews Microbiology*. Nature Publishing Group, 14(9), pp. 563–575. doi: 10.1038/nrmicro.2016.94.

Fujii, H., Matkar, P., Liao, C., Rudenko, D., Lee, P. J., Kuliszewski, M. A., Prud'homme, G. J. and Leong-Poi, H. (2013) 'Optimization of Ultrasound-mediated Anti-angiogenic Cancer Gene Therapy', *Molecular Therapy - Nucleic Acids*. Elsevier, 2(Fujii, H., Matkar, P., Liao, C., Rudenko, D., Lee, P. J., Kuliszewski, M. A., Prud'homme, G. J. and Leong-Poi, H. (2013) 'Optimization of Ultrasound-mediated Anti-angiogenic Cancer Gene Therapy', Molecular Therapy-Nucleic Acids. Elsevier, 2, p. e94. doi), p. e94. doi: 10.1038/mtna.2013.20.

García-Montoya, I. A., Cendón, T. S., Arévalo-Gallegos, S. and Rascón-Cruz, Q. (2012) 'Lactoferrin a multiple bioactive protein: An overview', *Biochimica et Biophysica Acta (BBA) - General Subjects*. Elsevier, 1820(3), pp. 226–236. doi: 10.1016/J.BBAGEN.2011.06.018.

Gardner, S. E., Hillis, S. L., Heilmann, K., Segre, J. A. and Grice, E. A. (2013) 'The neuropathic diabetic foot ulcer microbiome is associated with clinical factors.', *Diabetes*. American Diabetes Association, 62(3), pp. 923–30. doi: 10.2337/db12-0771.

Garg, S., Thomas, A. A. and Borden, M. A. (2013) 'The effect of lipid monolayer in-plane rigidity on in vivo microbubble circulation persistence.', *Biomaterials*. NIH Public Access, 34(28), pp. 6862–70. doi: 10.1016/j.biomaterials.2013.05.053.

Geisinger, E. and Isberg, R. R. (2017) 'Interplay Between Antibiotic Resistance and Virulence During Disease Promoted by Multidrug-Resistant Bacteria', *The Journal of Infectious Diseases*. Oxford University Press, 215(suppl_1), pp. S9–S17. doi: 10.1093/infdis/jiw402.

George, D. L. and Ludwig, C. (2004) 'The Velocity of Sound through Tissues and the Acoustic Impedance of Tissues'. Available at: https://www.semanticscholar.org/paper/The-Velocity-of-Sound-through-Tissues-and-the-of-George-Ludwig/e18337bf9dcf5dba99e397cda7674db0e5df1304 (Accessed: 17 March 2019).

Ginés, L., Mandal, S., Ashek-I-Ahmed, Cheng, C. L., Sow, M. and Williams, O. A. (2017) 'Positive zeta potential of nanodiamonds', *Nanoscale*. Royal Society of Chemistry, 9(34), pp. 12549–12555. doi: 10.1039/c7nr03200e.

Giustarini, D., Rossi, R., Milzani, A. and Dalle-Donne, I. (2008) 'Nitrite and Nitrate Measurement by Griess Reagent in Human Plasma: Evaluation of Interferences and Standardization', in *Methods in enzymology*, pp. 361–380. doi: 10.1016/S0076-6879(07)00823-3.

Glasser, N. R., Wang, B. X., Hoy, J. A. and Newman, D. K. (2017) 'The pyruvate and α-ketoglutarate dehydrogenase complexes of pseudomonas aeruginosa catalyze pyocyanin and phenazine-1-carboxylic acid reduction via the subunit dihydrolipoamide dehydrogenase', *Journal of Biological Chemistry*. American Society for Biochemistry and Molecular Biology Inc., 292(13), pp. 5593–5607. doi: 10.1074/jbc.M116.772848.

Gong, Y., Cabodi, M. and Porter, T. M. (2014) 'Acoustic investigation of pressure-dependent resonance and shell elasticity of lipid-coated monodisperse microbubbles', *Applied Physics Letters*. American Institute of Physics, 104(7), p. 074103. doi: 10.1063/1.4865805.

Gonzalez-Andrades, M., Alonso-Pastor, L., Mauris, J., Cruzat, A., Dohlman, C. H. and Argüeso, P. (2016) 'Establishment of a novel in vitro model of stratified epithelial wound healing with barrier function', *Scientific Reports*. Nature Publishing Group, 6(1), p. 19395. doi: 10.1038/srep19395.

Gordillo, G. M., Bernatchez, S. F., Diegelmann, R., Di Pietro, L. A., Eriksson, E., Hinz, B., Hopf, H. W., Kirsner, R., Liu, P., Parnell, L. K. S., Sandusky, G. E., Sen, C. K., Tomic-Canic, M., Volk, S. W. and Baird for the Wound Healing Society, A. (2013) 'Preclinical Models of Wound Healing: Is Man the Model? Proceedings of the Wound Healing Society Symposium', *Advances in Wound Care*, 2(1), pp. 1–4. doi: 10.1089/wound.2012.0367.

Grishenkov, D., Gonon, A., Weitzberg, E., Lundberg, J. O., Harmark, J., Cerroni, B., Paradossi, G. and Janerot-Sjoberg, B. (2015) 'Ultrasound contrast agent loaded with nitric oxide as a theranostic microdevice.', *Drug design, development and therapy*. Dove Press, 9, pp. 2409–19. doi: 10.2147/DDDT.S77790.

Gu, Y. and Chen, C. C. (2008) 'Eliminating the interference of oxygen for sensing hydrogen peroxide with the polyaniline modified electrode', *Sensors*. Multidisciplinary Digital Publishing Institute (MDPI), 8(12), pp. 8237–8247. doi: 10.3390/s8128237.

Gu, Y., Chen, C., Tu, J., Guo, X., Wu, H. and Zhang, D. (2016) 'Harmonic responses and cavitation activity of encapsulated microbubbles coupled with magnetic nanoparticles', *Ultrasonics Sonochemistry*. Elsevier B.V., 29, pp. 309–316. doi: 10.1016/j.ultsonch.2015.10.006.

Guilhen, C., Forestier, C. and Balestrino, D. (2017) 'Biofilm dispersal: multiple elaborate strategies for dissemination of bacteria with unique properties', *Molecular Microbiology*, 105(2), pp. 188–210. doi: 10.1111/mmi.13698.

Guillermic, R. M., Lanoy, M., Strybulevych, A. and Page, J. H. (2019) 'A PDMS-based broadband acoustic impedance matched material for underwater applications', *Ultrasonics*. Elsevier B.V., 94, pp. 152–157. doi: 10.1016/j.ultras.2018.10.002.

De Gunzburg, J., Ghozlane, A., Ducher, A., Le Chatelier, E., Duval, X., Ruppé, E., Armand-Lefevre, L., Sablier-Gallis, F., Burdet, C., Alavoine, L., Chachaty, E., Augustin, V., Varastet, M., Levenez, F., Kennedy, S., Pons, N., Mentré, F. and Andremont, A. (2018) 'Protection of the human gut microbiome from antibiotics', *Journal of Infectious Diseases*. Oxford University Press, 217(4), pp. 628–636. doi: 10.1093/infdis/jix604.

Guo, S. and DiPietro, L. A. (2010) 'Factors Affecting Wound Healing', *Journal of Dental Research*. SAGE Publications, 89(3), pp. 219–229. doi: 10.1177/0022034509359125.

Gurtner, G. C., Werner, S., Barrandon, Y. and Longaker, M. T. (2008) 'Wound repair and regeneration', *Nature*, 453(7193), pp. 314–321. doi: 10.1038/nature07039.

Gyöngy, M. and Coussios, C.-C. (2010) 'Passive cavitation mapping for localization and tracking of bubble dynamics', *The Journal of the Acoustical Society of America*. Acoustical Society of America (ASA), 128(4), pp. EL175–EL180. doi: 10.1121/1.3467491.

H Yu, A. C., Chen, X., Shan Leow, R., Hu, Y. and F Wan, J. M. (2014) 'Single-site sonoporation disrupts actin cytoskeleton organization'. doi: 10.1098/rsif.2014.0071.

ter Haar, G. (2007) *Therapeutic applications of ultrasound*, *Progress in Biophysics and Molecular Biology*. Pergamon. Available at: https://www.sciencedirect.com/science/article/pii/S0079610706000836?via%3Dihub (Accessed: 12 April 2019).

Hall-Stoodley, L., Costerton, J. W. and Stoodley, P. (2004) 'Bacterial biofilms: from the Natural environment to infectious diseases', *Nature Reviews Microbiology*. Nature Publishing Group, 2(2), pp. 95–108. doi: 10.1038/nrmicro821.

Hall, C. W. and Mah, T.-F. (2017) 'Molecular mechanisms of biofilm-based antibiotic resistance and tolerance in pathogenic bacteria', *FEMS Microbiology Reviews*. Oxford University Press, 41(3), pp. 276–301. doi: 10.1093/femsre/fux010.

Han, G. and Ceilley, R. (2017) 'Chronic Wound Healing: A Review of Current Management and Treatments.', *Advances in therapy*. Springer, 34(3), pp. 599–610. doi: 10.1007/s12325-017-0478-y.

Han, Y. W., Ikegami, A., Chung, P., Zhang, L. and Deng, C. X. (2007) 'Sonoporation is an efficient tool for intracellular fluorescent dextran delivery and one-step double-crossover mutant construction in Fusobactenum nucleatum', *Applied and Environmental Microbiology*, 73(11), pp. 3677–3683. doi: 10.1128/AEM.00428-07.

Han, Y. W., Ikegami, A., Rajanna, C., Kawsar, H. I., Zhou, Y., Li, M., Sojar, H. T., Genco, R. J., Kuramitsu, H. K. and Deng, C. X. (2005) 'Identification and characterization of a novel adhesin unique to oral fusobacteria', *Journal of Bacteriology*, 187(15), pp. 5330–5340. doi: 10.1128/JB.187.15.5330-5340.2005.

Harper, R. A., Carpenter, G. H., Proctor, G. B., Harvey, R. D., Gambogi, R. J., Geonnotti, A. R., Hider, R. and Jones, S. A. (2019) 'Diminishing biofilm resistance to antimicrobial nanomaterials through electrolyte screening of electrostatic interactions', *Colloids and Surfaces B: Biointerfaces*. Elsevier B.V., 173, pp. 392–399. doi:

10.1016/j.colsurfb.2018.09.018.

He, N., Hu, J., Liu, H., Zhu, T., Huang, B., Wang, X., Wu, Y., Wang, W. and Qu, D. (2011) 'Enhancement of vancomycin activity against biofilms by using ultrasound-targeted microbubble destruction', *Antimicrobial Agents and Chemotherapy*. American Society for Microbiology, 55(11), pp. 5331–5337. doi: 10.1128/AAC.00542-11.

Helfield, B. L., Cherin, E., Foster, F. S. and Goertz, D. E. (2012) 'Investigating the Subharmonic Response of Individual Phospholipid Encapsulated Microbubbles at High Frequencies: A Comparative Study of Five Agents', *Ultrasound in Medicine & Biology*. Elsevier, 38(5), pp. 846–863. doi: 10.1016/J.ULTRASMEDBIO.2012.01.011.

Hengzhuang, W., Wu, H., Ciofu, O., Song, Z. and Høiby, N. (2012) '*In Vivo* Pharmacokinetics/Pharmacodynamics of Colistin and Imipenem in Pseudomonas aeruginosa Biofilm Infection', *Antimicrobial Agents and Chemotherapy*, 56(5), pp. 2683–2690. doi: 10.1128/AAC.06486-11.

Heta, S. and Robo, I. (2018) 'The Side Effects of the Most Commonly Used Group of Antibiotics in Periodontal Treatments', *Medical Sciences*. MDPI AG, 6(1), p. 6. doi: 10.3390/medsci6010006.

Hetrick, E. M. and Schoenfisch, M. H. (2009) 'Analytical chemistry of nitric oxide.', *Annual review of analytical chemistry (Palo Alto, Calif.)*. NIH Public Access, 2, pp. 409–33. doi: 10.1146/annurev-anchem-060908-155146.

Hetrick, E. M., Shin, J. H., Paul, H. S. and Schoenfisch, M. H. (2009) 'Anti-biofilm efficacy of nitric oxide-releasing silica nanoparticles', *Biomaterials*. Elsevier, 30(14), pp. 2782–2789. doi: 10.1016/J.BIOMATERIALS.2009.01.052.

Highmore, C. J., Warner, J. C., Rothwell, S. D., Wilks, S. A. and Keevil, C. W. (2018) 'Viable-but-nonculturable Listeria monocytogenes and Salmonella enterica serovar thompson induced by chlorine stress remain infectious', *mBio*. American Society for Microbiology, 9(2). doi: 10.1128/mBio.00540-18.

Ho, K.-C., Hung, W.-T. and Yang, J.-C. (2003) 'On the Electrooxidation and Amperometric Detection of NO Gas at the Pt/Nafion® Electrode', *Sensors*. Molecular Diversity Preservation International, 3(8), pp. 290–303. doi: 10.3390/s30800290.

Høiby, N., Ciofu, O., Johansen, H. K., Song, Z., Moser, C., Jensen, P. Ø., Molin, S., Givskov, M., Tolker-Nielsen, T. and Bjarnsholt, T. (2011) 'The clinical impact of bacterial biofilms', *International Journal of Oral Science*, 3(2), pp. 55–65. doi: 10.4248/IJOS11026.

Holt, J. E., Houston, A., Adams, C., Edwards, S. and Kjellerup, B. V. (2017) 'Role of extracellular polymeric substances in polymicrobial biofilm infections of Staphylococcus epidermidis and Candida albicans modelled in the nematode Caenorhabditis elegans', *Pathogens and Disease*. Oxford University Press, 75(5). doi: 10.1093/femspd/ftx052.

Horsley, H., Owen, J., Browning, R., Carugo, D., Malone-Lee, J., Stride, E. and Rohn, J. L. L. (2019) 'Ultrasound-activated microbubbles as a novel intracellular drug delivery system for urinary tract infection', *Journal of Controlled Release*. Elsevier, 301, pp. 166–175. doi: 10.1016/J.JCONREL.2019.03.017.

Hosny, N. A., Mohamedi, G., Rademeyer, P., Owen, J., Wu, Y., Tang, M.-X., Eckersley, R. J., Stride, E. and Kuimova, M. K. (2013) 'Mapping microbubble viscosity using fluorescence lifetime imaging of molecular rotors.', *Proceedings of the National Academy of Sciences of the United States of America*. National Academy of Sciences, 110(23), pp. 9225–30. doi: 10.1073/pnas.1301479110.

Howlin, R. P., Cathie, K., Hall-Stoodley, L., Cornelius, V., Duignan, C., Allan, R. N., Fernandez, B. O., Barraud, N., Bruce, K. D., Jefferies, J., Kelso, M., Kjelleberg, S., Rice, S. A., Rogers, G. B., Pink, S., Smith, C., Sukhtankar, P. S., Salib, R., Legg, J., Carroll, M., Daniels, T., Feelisch, M., Stoodley, P., Clarke, S. C., Connett, G., Faust, S. N. and Webb, J. S. (2017) 'Low-Dose Nitric Oxide as Targeted Anti-biofilm Adjunctive Therapy to Treat Chronic Pseudomonas aeruginosa Infection in Cystic Fibrosis', *Molecular Therapy*. Cell Press, 25(9), pp. 2104–2116. doi: 10.1016/J.YMTHE.2017.06.021.

Hu, J., Zhang, N., Li, L., Zhang, N., Ma, Y., Zhao, C., Wu, Q., Li, Y., He, N. and Wang, X. (2018) 'The synergistic bactericidal effect of vancomycin on UTMD treated biofilm involves damage to bacterial cells and enhancement of metabolic activities', *Scientific Reports*. Nature Publishing Group, 8(1), p. 192. doi: 10.1038/s41598-017-18496-3.

Huang, C., Zhang, H. and Bai, R. (2017) 'Advances in ultrasound-targeted microbubble-mediated gene therapy for liver fibrosis.', *Acta pharmaceutica Sinica. B*. Elsevier, 7(4), pp. 447–452. doi: 10.1016/j.apsb.2017.02.004.

Hunter, R. A., Storm, W. L., Coneski, P. N. and Schoenfisch, M. H. (2013) 'Inaccuracies of nitric oxide measurement methods in biological media.', *Analytical chemistry*. NIH Public Access, 85(3), pp. 1957–63. doi: 10.1021/ac303787p.

Ibsen, S., Schutt, C. E. and Esener, S. (2013) *Microbubble-mediated ultrasound therapy: A review of its potential in cancer treatment*, *Drug Design, Development and Therapy*. Dove Press. doi: 10.2147/DDDT.S31564.

Ikeda-Dantsuji, Y., Feril, L. B., Tachibana, K., Ogawa, K., Endo, H., Harada, Y., Suzuki, R. and Maruyama, K. (2011) 'Synergistic effect of ultrasound and antibiotics against Chlamydia trachomatis-infected human epithelial cells in vitro', *Ultrasonics Sonochemistry*. Elsevier B.V., 18(1), pp. 425–430. doi: 10.1016/j.ultsonch.2010.07.015.

Jain, R., Jordan, N., Weiss, S., Foerstendorf, H., Heim, K., Kacker, R., Hübner, R., Kramer, H., van Hullebusch, E. D., Farges, F. and Lens, P. N. L. (2015) 'Extracellular Polymeric Substances Govern the Surface Charge of Biogenic Elemental Selenium Nanoparticles', *Environmental Science & Technology*, 49(3), pp. 1713–1720. doi: 10.1021/es5043063.

Jakobsen, T. H., Alhede, M., Hultqvist, L. D., Bjarnsholt, T. and Givskov, M. (2018) 'Qualitative and Quantitative Determination of Quorum Sensing Inhibition In Vitro', in *Methods in molecular biology (Clifton, N.J.)*. Humana Press, New York, NY, pp. 275–285. doi: 10.1007/978-1-4939-7309-5_21.

Jamal, M., Ahmad, W., Andleeb, S., Jalil, F., Imran, M., Nawaz, M. A., Hussain, T., Ali, M., Rafiq, M. and Kamil, M. A. (2018) 'Bacterial biofilm and associated infections', *Journal of the Chinese Medical Association*. Elsevier, 81(1), pp. 7–11. doi: 10.1016/J.JCMA.2017.07.012.

Jamal, M., Tasneem, U., Hussain, T. and Andleeb, S. (2015) 'Bacterial Biofilm: Its Composition, Formation and Role in Human Infections', *Research & Reviews: Journal of Microbiology and Biotechnology*. Research and Reviews, 4(3). Available at: http://www.rroij.com/open-access/bacterial-biofilm-its-composition-formation-and-role-in-human-infections.php?aid=61426 (Accessed: 28 May 2018).

Jang, H., Rusconi, R. and Stocker, R. (2017) 'Biofilm disruption by an air bubble reveals heterogeneous age-dependent detachment patterns dictated by initial extracellular matrix distribution', *npj Biofilms and Microbiomes*. Nature Publishing Group, 3(1), p. 6. doi: 10.1038/s41522-017-0014-5.

Jenkins, R. and Maddocks, S. (2019) *Bacteriology methods for the study of infectious diseases*, *Bacteriology Methods for the Study of Infectious Diseases*. Elsevier. doi: 10.1016/C2017-0-02665-4.

Jiang, B., Gao, C. and Shen, J. (2006) ‘Polylactide hollow spheres fabricated by interfacial polymerization in an oil-in-water emulsion system’, *Colloid and Polymer Science*. Springer-Verlag, 284(5), pp. 513–519. doi: 10.1007/s00396-005-1415-1.

Jiang, W., Wang, Yuexiang, Tang, J., Peng, J., Wang, Yu, Guo, Q., Guo, Z., Li, P., Xiao, B. and Zhang, J. (2016) ‘Low-intensity pulsed ultrasound treatment improved the rate of autograft peripheral nerve regeneration in rat.’, *Scientific reports*. Nature Publishing Group, 6, p. 22773. doi: 10.1038/srep22773.

Jneid, J., Lavigne, J. P., La Scola, B. and Cassir, N. (2017) ‘The diabetic foot microbiota: A review’, *Human Microbiome Journal*. Elsevier, 5–6, pp. 1–6. doi: 10.1016/J.HUMIC.2017.09.002.

Johansson, E. M. V., Crusz, S. A., Kolomiets, E., Buts, L., Kadam, R. U., Cacciarini, M., Bartels, K. M., Diggle, S. P., Cámara, M., Williams, P., Loris, R., Nativi, C., Rosenau, F., Jaeger, K. E., Darbre, T. and Reymond, J. L. (2008) ‘Inhibition and Dispersion of Pseudomonas aeruginosa Biofilms by Glycopeptide Dendrimers Targeting the Fucose-Specific Lectin LecB’, *Chemistry and Biology*. Cell Press, 15(12), pp. 1249–1257. doi: 10.1016/j.chembiol.2008.10.009.

John, Y., David, V. E. and Mmereki, D. (2018) ‘A Comparative Study on Removal of Hazardous Anions from Water by Adsorption: A Review’, *International Journal of Chemical Engineering*, 2018, pp. 1–21. doi: 10.1155/2018/3975948.

De Jong, N., Bouakaz, A. and Frinking, P. (2002) *Basic acoustic properties of microbubbles*, *Echocardiography*. doi: 10.1046/j.1540-8175.2002.00229.x.

Karwowska, M. and Kononiuk, A. (2020) ‘Nitrates/nitrites in food—risk for nitrosative stress and benefits’, *Antioxidants*. MDPI AG. doi: 10.3390/antiox9030241.

Kasimanickam, R. K., Ranjan, A., Asokan, G. V, Kasimanickam, V. R. and Kastelic, J. P. (2013) ‘Prevention and treatment of biofilms by hybrid- and nanotechnologies.’, *International journal of nanomedicine*. Dove Press, 8, pp. 2809–19. doi: 10.2147/IJN.S44100.

Kelm, M. (1999) ‘Nitric oxide metabolism and breakdown’, *Biochimica et Biophysica Acta - Bioenergetics*. Elsevier, pp. 273–289. doi: 10.1016/S0005-2728(99)00020-1.

Khan, K. and Alden, C. (2002) ‘Kidney’, in *Handbook of Toxicologic Pathology*. Elsevier, pp. 255–336. doi: 10.1016/B978-012330215-1/50034-X.

Khanum, R. and Thevanayagam, H. (2017) ‘Lipid peroxidation: Its effects on the formulation and use of pharmaceutical emulsions’, *Asian Journal of Pharmaceutical Sciences*. Shenyang Pharmaceutical University, pp. 401–411. doi: 10.1016/j.ajps.2017.05.003.

Khelissa, S. O., Abdallah, M., Jama, C., Barras, A. and Chihib, N. E. (2019) ‘Comparative study on the impact of growth conditions on the physiology and the virulence of pseudomonas aeruginosa biofilm and planktonic cells’, *Journal of Food Protection*. International Association for Food Protection, 82(8), pp. 1357–1363. doi: 10.4315/0362-028X.JFP-18-565.

Khmel, I. A. (2006) ‘Quorum-sensing regulation of gene expression: Fundamental and applied aspects and the role in bacterial communication’, *Microbiology*. Nauka/Interperiodica, 75(4), pp. 390–397. doi: 10.1134/S0026261706040047.

Kim, D., Namen Ii, W., Moore, J., Buchanan, M., Hayes, V., Myntti, M. F. and Hakaim, A. (2018) ‘Clinical

Assessment of a Biofilm-disrupting Agent for the Management of Chronic Wounds Compared With Standard of Care: A Therapeutic Approach.', *Wounds : a compendium of clinical research and practice*, 30(5), pp. 120–130. Available at: http://www.ncbi.nlm.nih.gov/pubmed/29521641 (Accessed: 10 June 2018).

Koh, T. J. and DiPietro, L. A. (2011) 'Inflammation and wound healing: the role of the macrophage.', *Expert reviews in molecular medicine*. NIH Public Access, 13, p. e23. doi: 10.1017/S1462399411001943.

Kooiman, K., van Rooij, T., Qin, B., Mastik, F., Vos, H. J., Versluis, M., Klibanov, A. L., de Jong, N., Villanueva, F. S. and Chen, X. (2017) 'Focal areas of increased lipid concentration on the coating of microbubbles during short tone-burst ultrasound insonification', *PLOS ONE*. Edited by J. TU. Public Library of Science, 12(7), p. e0180747. doi: 10.1371/journal.pone.0180747.

Kooiman, K., Roovers, S., Langeveld, S. A. G., Kleven, R. T., Dewitte, H., O'Reilly, M. A., Escoffre, J. M., Bouakaz, A., Verweij, M. D., Hynynen, K., Lentacker, I., Stride, E. and Holland, C. K. (2020) 'Ultrasound-Responsive Cavitation Nuclei for Therapy and Drug Delivery', *Ultrasound in Medicine and Biology*. Elsevier USA, pp. 1296–1325. doi: 10.1016/j.ultrasmedbio.2020.01.002.

Kooiman, K., Vos, H. J., Versluis, M. and de Jong, N. (2014) 'Acoustic behavior of microbubbles and implications for drug delivery', *Advanced Drug Delivery Reviews*. Elsevier B.V., 72, pp. 28–48. doi: 10.1016/j.addr.2014.03.003.

Kuliasha, C. A., Finlay, J. A., Franco, S. C., Clare, A. S., Stafslien, S. J. and Brennan, A. B. (2017) 'Marine anti-biofouling efficacy of amphiphilic poly(coacrylate) grafted PDMSe: effect of graft molecular weight', *Biofouling*. Taylor & Francis, 33(3), pp. 252–267. doi: 10.1080/08927014.2017.1288807.

Kumar, A., Alam, A., Rani, M., Ehtesham, N. Z. and Hasnain, S. E. (2017) 'Biofilms: Survival and defense strategy for pathogens', *International Journal of Medical Microbiology*. Urban & Fischer, 307(8), pp. 481–489. doi: 10.1016/J.IJMM.2017.09.016.

Kumar, S. S. and Ghosh, A. R. (2019) 'Assessment of bacterial viability: A comprehensive review on recent advances and challenges', *Microbiology (United Kingdom)*. Microbiology Society, pp. 593–610. doi: 10.1099/mic.0.000786.

Kwan, P., Desmoulière, A. and Tredget, E. E. (2018) 'Molecular and cellular basis of hypertrophic scarring', in *Total Burn Care: Fifth Edition*. Elsevier Inc., pp. 455-465.e4. doi: 10.1016/B978-0-323-47661-4.00045-9.

Kwasny, S. M. and Opperman, T. J. (2010) 'Static biofilm cultures of Gram-positive pathogens grown in a microtiter format used for anti-biofilm drug discovery.', *Current protocols in pharmacology*. NIH Public Access, Chapter 13, p. Unit 13A.8. doi: 10.1002/0471141755.ph13a08s50.

LaBauve, A. E. and Wargo, M. J. (2012) 'Growth and laboratory maintenance of Pseudomonas aeruginosa.', *Current protocols in microbiology*. NIH Public Access, Chapter 6, p. Unit 6E.1. doi: 10.1002/9780471729259.mc06e01s25.

Lafond, M., Shekhar, H., Panmanee, W., Collins, S. D., Palaniappan, A., McDaniel, C. T., Hassett, D. J. and Holland, C. K. (2020) 'Bactericidal activity of lipid-shelled nitric oxide-loaded microbubbles', *Frontiers in Pharmacology*. Frontiers Media S.A., 10. doi: 10.3389/fphar.2019.01540.

Laganenka, L. and Sourjik, V. (2017) 'Autoinducer 2-dependent Escherichia coli biofilm formation is enhanced in a dual-species co-culture.', *Applied and environmental microbiology*. American Society for Microbiology, p.

AEM.02638-17. doi: 10.1128/AEM.02638-17.

LaSarre, B. and Federle, M. J. (2013) 'Exploiting quorum sensing to confuse bacterial pathogens.', *Microbiology and molecular biology reviews : MMBR*. American Society for Microbiology (ASM), 77(1), pp. 73–111. doi: 10.1128/MMBR.00046-12.

Lattwein, K. R., Shekhar, H., Van Wamel, W. J. B., Gonzalez, T., Herr, A. B., Holland, C. K. and Kooiman, K. (2018) 'An in vitro proof-of-principle study of sonobactericide', *Scientific Reports*. Nature Publishing Group, 8(1). doi: 10.1038/s41598-018-21648-8.

LAURENS, N., KOOLWIJK, P. and DE MAAT, M. P. M. (2006) 'Fibrin structure and wound healing', *Journal of Thrombosis and Haemostasis*, 4(5), pp. 932–939. doi: 10.1111/j.1538-7836.2006.01861.x.

Lazarus, C., Pouliopoulos, A. N., Tinguely, M., Garbin, V. and Choi, J. J. (2017) *Clustering dynamics of microbubbles exposed to low-pressure 1-MHz ultrasound*, *The Journal of the Acoustical Society of America*. Acoustical Society of America (ASA). doi: 10.1121/1.5010170.

Lebeaux, D., Ghigo, J.-M. and Beloin, C. (2014) 'Biofilm-related infections: bridging the gap between clinical management and fundamental aspects of recalcitrance toward antibiotics.', *Microbiology and molecular biology reviews : MMBR*. American Society for Microbiology (ASM), 78(3), pp. 510–43. doi: 10.1128/MMBR.00013-14.

Lee, J. Y., Carugo, D., Crake, C., Owen, J., de Saint Victor, M., Seth, A., Coussios, C. and Stride, E. (2015) 'Nanoparticle-Loaded Protein-Polymer Nanodroplets for Improved Stability and Conversion Efficiency in Ultrasound Imaging and Drug Delivery', *Advanced Materials*. Wiley-Blackwell, 27(37), pp. 5484–5492. doi: 10.1002/adma.201502022.

Lee, M., Lee, E. Y., Lee, D. and Park, B. J. (2015) 'Stabilization and fabrication of microbubbles: applications for medical purposes and functional materials', *Soft Matter*. Royal Society of Chemistry, 11(11), pp. 2067–2079. doi: 10.1039/C5SM00113G.

Leggett, J. E. (2017) 'Aminoglycosides', *Infectious Diseases*. Elsevier, pp. 1233-1238.e1. doi: 10.1016/B978-0-7020-6285-8.00143-X.

Leighton, T. G. (1997) *The Acoustic Bubble*. 10th edn. London: Academic Press Limited. Available at: https://books.google.co.uk/books?id=0RJif-xRyGMC.

Leighton, T. G. (2007) 'What is ultrasound?', *Progress in Biophysics and Molecular Biology*, 93, pp. 3–83. doi: 10.1016/j.pbiomolbio.2006.07.026.

Lentacker, I., De Cock, I., Deckers, R., De Smedt, S. C. and Moonen, C. T. W. (2014) 'Understanding ultrasound induced sonoporation: Definitions and underlying mechanisms', *Advanced Drug Delivery Reviews*. Elsevier B.V., 72, pp. 49–64. doi: 10.1016/j.addr.2013.11.008.

Lentacker, I., Geers, B., Demeester, J., De Smedt, S. C. and Sanders, N. N. (2010) 'Design and Evaluation of Doxorubicin-containing Microbubbles for Ultrasound-triggered Doxorubicin Delivery: Cytotoxicity and Mechanisms Involved', *Molecular Therapy*. Cell Press, 18(1), pp. 101–108. doi: 10.1038/MT.2009.160.

Lentacker, I., De Smedt, S. C. and Sanders, N. N. (2009) 'Drug loaded microbubble design for ultrasound triggered delivery', *Soft Matter*. Royal Society of Chemistry, 5(11), p. 2161. doi: 10.1039/b823051j.

Leow, R. S., Wan, J. M. F. and Yu, A. C. H. (2015) 'Membrane blebbing as a recovery manoeuvre in site-specific sonoporation mediated by targeted microbubbles.', *Journal of the Royal Society, Interface*. The Royal Society, 12(105). doi: 10.1098/rsif.2015.0029.

Leung, T. S., Honeysett, J. E., Stride, E. and Deng, J. (2013) 'Light propagation in a turbid medium with insonified microbubbles', *Journal of Biomedical Optics*. SPIE-Intl Soc Optical Eng, 18(1), p. 015002. doi: 10.1117/1.jbo.18.1.015002.

Lewis, A. M. and Boose, E. R. (1995) *Estimating Volume Flow Rates Through Xylem Conduits*, *American Journal of Botany*.

Li, J., Wang, X., Zhang, T., Wang, C., Huang, Z., Luo, X. and Deng, Y. (2015) 'A review on phospholipids and their main applications in drug delivery systems', *Asian Journal of Pharmaceutical Sciences*. Elsevier, 10(2), pp. 81–98. doi: 10.1016/J.AJPS.2014.09.004.

Liang, X., Xu, Y., Gao, C., Zhou, Y., Zhang, N. and Dai, Z. (2018) 'Ultrasound contrast agent microbubbles with ultrahigh loading capacity of camptothecin and floxuridine for enhancing tumor accumulation and combined chemotherapeutic efficacy', *NPG Asia Materials*. Nature Publishing Group, p. 1. doi: 10.1038/s41427-018-0066-x.

Liljeblad, J. F. D., Bulone, V., Tyrode, E., Rutland, M. W. and Johnson, C. M. (2010) 'Phospholipid monolayers probed by vibrational sum frequency spectroscopy: Instability of unsaturated phospholipids', *Biophysical Journal*. Biophysical Society, 98(10), p. L50. doi: 10.1016/j.bpj.2010.02.009.

Limoli, D. H., Jones, C. J. and Wozniak, D. J. (2015) 'Bacterial Extracellular Polysaccharides in Biofilm Formation and Function.', *Microbiology spectrum*. NIH Public Access, 3(3). doi: 10.1128/microbiolspec.MB-0011-2014.

Lin, Y.-J., Chen, K.-T., Huang, C.-Y. and Wei, K.-C. (2016) 'Non-invasive focused ultrasound-based synergistic treatment of brain tumors', *Journal of Cancer Research and Practice*. Elsevier, 3(3), pp. 63–68. doi: 10.1016/J.JCRPR.2016.05.001.

Liu, H.-L., Hua, M.-Y., Chen, P.-Y., Chu, P.-C., Pan, C.-H., Yang, H.-W., Huang, C.-Y., Wang, J.-J., Yen, T.-C. and Wei, K.-C. (2010) 'Blood-Brain Barrier Disruption with Focused Ultrasound Enhances Delivery of Chemotherapeutic Drugs for Glioblastoma Treatment', *Radiology*, 255(2), pp. 415–425. doi: 10.1148/radiol.10090699.

Lochab, J. and Singh, V. R. (2004) *Acoustic behaviour of plastics for medical applications*, *Indian Journal of Pure & Applied Physics*. Available at: http://nopr.niscair.res.in/bitstream/123456789/9611/1/IJPAP 42%288%29 595-599.pdf (Accessed: 17 March 2019).

Lohse, M. B., Gulati, M., Johnson, A. D. and Nobile, C. J. (2017) 'Development and regulation of single- and multi-species Candida albicans biofilms', *Nature Reviews Microbiology*. Nature Publishing Group, 16(1), pp. 19–31. doi: 10.1038/nrmicro.2017.107.

Lundberg, J. O., Weitzberg, E. and Gladwin, M. T. (2008) 'The nitrate-nitrite-nitric oxide pathway in physiology and therapeutics', *Nature Reviews Drug Discovery*. Nature Publishing Group, pp. 156–167. doi: 10.1038/nrd2466.

LuTheryn, G., Glynne-Jones, P., Webb, J. S. and Carugo, D. (2019) 'Ultrasound-mediated therapies for the treatment of biofilms in chronic wounds: a review of present knowledge', *Microbial Biotechnology*. Wiley Online Library, pp. 1751-7915.13471. doi: 10.1111/1751-7915.13471.

Macia, M. D., Rojo-Molinero, E. and Oliver, A. (2014) 'Antimicrobial susceptibility testing in biofilm-growing bacteria', *Clinical Microbiology and Infection*. Elsevier, 20(10), pp. 981–990. doi: 10.1111/1469-0691.12651.

Mahringer, A. and Gert, F. (2017) ‘Nanomedicine and Neurosciences.’, in Giovanni, T. (ed.) *Fontiers in Nanomedicine*. Heidelberg, Germany: Bentham Science Publishers, pp. 115–127.

Maleki, S., Almaas, E., Zotchev, S., Valla, S. and Ertesvåg, H. (2016) ‘Alginate Biosynthesis Factories in Pseudomonas fluorescens: Localization and Correlation with Alginate Production Level.’, *Applied and environmental microbiology*. American Society for Microbiology, 82(4), pp. 1227–1236. doi: 10.1128/AEM.03114-15.

Malone, M., Bjarnsholt, T., McBain, A. J., James, G. A., Stoodley, P., Leaper, D., Tachi, M., Schultz, G., Swanson, T. and Wolcott, R. D. (2017) ‘The prevalence of biofilms in chronic wounds: a systematic review and meta-analysis of published data’, *Journal of Wound Care*. MA Healthcare London , 26(1), pp. 20–25. doi: 10.12968/jowc.2017.26.1.20.

Marsh, P. D. and Zaura, E. (2017) ‘Dental biofilm: ecological interactions in health and disease’, *Journal of Clinical Periodontology*. Wiley/Blackwell (10.1111), 44, pp. S12–S22. doi: 10.1111/jcpe.12679.

Martin, M. J., Chung, E. M. L., Goodall, A. H., Martina, A. Della, Ramnarine, K. V., Fan, L., Hainsworth, S. V., Naylor, A. R. and Evans, D. H. (2007) ‘Enhanced detection of thromboemboli with the use of targeted microbubbles’, *Stroke*. Stroke, 38(10), pp. 2726–2732. doi: 10.1161/STROKEAHA.107.489435.

Martinasso, G., Saracino, S., Maggiora, M., Oraldi, M., Canuto, R. A. and Muzio, G. (2010) ‘Conjugated linoleic acid prevents cell growth and cytokine production induced by TPA in human keratinocytes NCTC 2544’, *Cancer Letters*, 287(1), pp. 62–66. doi: 10.1016/j.canlet.2009.05.036.

Mastriani, M. (2018) ‘Quantum-Classical Algorithm for an Instantaneous Spectral Analysis of Signals: A Complement to Fourier Theory’, *Journal of Quantum Information Science*. Scientific Research Publishing, Inc., 08(02), pp. 52–77. doi: 10.4236/jqis.2018.82005.

Mathioudakis, D., Engel, J., Welters, I. D., Dehne, M. G., Matejec, R., Harbach, H., Henrich, M., Schwandner, T., Fuchs, M., Weismüller, K., Scheffer, G. J. and Mühling, J. (2011) ‘Pyruvate: Immunonutritional effects on neutrophil intracellular amino or alpha-keto acid profiles and reactive oxygen species production’, *Amino Acids*. Springer, 40(4), pp. 1077–1090. doi: 10.1007/s00726-010-0731-z.

Mautner, A., Kobkeatthawin, T. and Bismarck, A. (2017) ‘Efficient continuous removal of nitrates from water with cationic cellulose nanopaper membranes’, *Resource-Efficient Technologies*. National Research Tomsk Polytechnic University, 3(1), pp. 22–28. doi: 10.1016/j.reffit.2017.01.005.

McCarty, S. M. and Percival, S. L. (2013) ‘Proteases and Delayed Wound Healing.’, *Advances in wound care*. Mary Ann Liebert, Inc., 2(8), pp. 438–447. doi: 10.1089/wound.2012.0370.

McDannold, N., Zhang, Y. and Vykhodtseva, N. (2017) ‘The Effects of Oxygen on Ultrasound-Induced Blood-Brain Barrier Disruption in Mice.’, *Ultrasound in medicine & biology*. Elsevier, 43(2), pp. 469–475. doi: 10.1016/j.ultrasmedbio.2016.09.019.

McEwan, C., Owen, J., Stride, E., Fowley, C., Nesbitt, H., Cochrane, D., Coussios, C. C., Borden, M., Nomikou, N., McHale, A. P. and Callan, J. F. (2015) ‘Oxygen carrying microbubbles for enhanced sonodynamic therapy of hypoxic tumours’, *Journal of Controlled Release*. Elsevier, 203, pp. 51–56. doi: 10.1016/J.JCONREL.2015.02.004.

Meairs, S. and Alonso, A. (2007) ‘Ultrasound, microbubbles and the blood–brain barrier’, *Progress in Biophysics and Molecular Biology*. Pergamon, 93(1–3), pp. 354–362. doi: 10.1016/J.PBIOMOLBIO.2006.07.019.

Mehta, R. and Champney, W. S. (2002) '30S ribosomal subunit assembly is a target for inhibition by aminoglycosides in Escherichia coli.', *Antimicrobial agents and chemotherapy*. American Society for Microbiology (ASM), 46(5), pp. 1546–9. doi: 10.1128/AAC.46.5.1546-1549.2002.

Meiers, J., Zahorska, E., Röhrig, T., Hauck, D., Wagner, S. and Titz, A. (2020) 'Directing Drugs to Bugs: Antibiotic-Carbohydrate Conjugates Targeting Biofilm-Associated Lectins of Pseudomonas aeruginosa', *Journal of medicinal chemistry*. NLM (Medline), 63(20), pp. 11707–11724. doi: 10.1021/acs.jmedchem.0c00856.

Miles, A. A., Misra, S. S. and Irwin, J. O. (1938) 'The estimation of the bactericidal power of the blood.', *The Journal of hygiene*. Cambridge University Press, 38(6), pp. 732–49. Available at: http://www.ncbi.nlm.nih.gov/pubmed/20475467 (Accessed: 18 March 2019).

Miller, M. B. and Bassler, B. L. (2001) 'Quorum Sensing in Bacteria', *Annual Review of Microbiology*. Annual Reviews 4139 El Camino Way, P.O. Box 10139, Palo Alto, CA 94303-0139, USA , 55(1), pp. 165–199. doi: 10.1146/annurev.micro.55.1.165.

Miyaue, S., Suzuki, E., Komiyama, Y., Kondo, Y., Morikawa, M. and Maeda, S. (2018) 'Bacterial Memory of Persisters: Bacterial Persister Cells Can Retain Their Phenotype for Days or Weeks After Withdrawal From Colony–Biofilm Culture', *Frontiers in Microbiology*. Frontiers Media S.A., 9(JUN), p. 1396. doi: 10.3389/fmicb.2018.01396.

Mohammad, S., Mortazavi, J., Darvish, L., Abounajmi, M., Zarei, S., Zare, T., Taheri, M. and Nematollahi, S. (2015) 'Alteration of Bacterial Antibiotic Sensitivity After Short-Term Exposure to Diagnostic Ultrasound', *Iranian Red Crescent Medical Journal*, 17(11). doi: 10.5812/ircmj.26622.

Mulvana, H., Stride, E., Hajnal, J. V. and Eckersley, R. J. (2010) 'Temperature Dependent Behavior of Ultrasound Contrast Agents', *Ultrasound in Medicine & Biology*. Elsevier, 36(6), pp. 925–934. doi: 10.1016/J.ULTRASMEDBIO.2010.03.003.

Müsken, M., Pawar, V., Schwebs, T., Bähre, H., Felgner, S., Weiss, S. and Häussler, S. (2018) 'Breaking the vicious cycle of antibiotic killing and regrowth of biofilm-residing pseudomonas aeruginosa', *Antimicrobial Agents and Chemotherapy*. American Society for Microbiology, 62(12). doi: 10.1128/AAC.01635-18.

Nalawade, T. M., Bhat, K. and Sogi, S. H. P. (2015) 'Bactericidal activity of propylene glycol, glycerine, polyethylene glycol 400, and polyethylene glycol 1000 against selected microorganisms.', *Journal of International Society of Preventive & Community Dentistry*. Wolters Kluwer -- Medknow Publications, 5(2), pp. 114–9. doi: 10.4103/2231-0762.155736.

Neppiras, E. A. (1980) 'Acoustic cavitation', *Physics Reports*. North-Holland, 61(3), pp. 159–251. doi: 10.1016/0370-1573(80)90115-5.

Nesbitt, H., Sheng, Y., Kamila, S., Logan, K., Thomas, K., Callan, B., Taylor, M. A., Love, M., O'Rourke, D., Kelly, P., Beguin, E., Stride, E., McHale, A. P. and Callan, J. F. (2018) 'Gemcitabine loaded microbubbles for targeted chemo-sonodynamic therapy of pancreatic cancer', *Journal of Controlled Release*. Elsevier, 279, pp. 8–16. doi: 10.1016/J.JCONREL.2018.04.018.

Ng, K. and Liu, Y. (2002) 'Therapeutic ultrasound: Its application in drug delivery', *Medicinal Research Reviews*, 22(2), pp. 204–223. doi: 10.1002/med.10004.

O'Brien, W. D. (2007) 'Ultrasound-biophysics mechanisms', *Progress in Biophysics and Molecular Biology*. NIH

Public Access, pp. 212–255. doi: 10.1016/j.pbiomolbio.2006.07.010.

O'Toole, G. A. (2011) 'Microtiter dish biofilm formation assay.', *Journal of visualized experiments : JoVE*. MyJoVE Corporation, (47). doi: 10.3791/2437.

Ojha, T., Pathak, V., Drude, N., Weiler, M., Rommel, D., Rütten, S., Geinitz, B., Van Steenbergen, M. J., Storm, G., Kiessling, F. and Lammers, T. (2019) 'Shelf-life evaluation and lyophilization of PBCA-based polymeric microbubbles', *Pharmaceutics*. MDPI AG, 11(9). doi: 10.3390/pharmaceutics11090433.

Omar, A., Wright, J. B., Schultz, G., Burrell, R. and Nadworny, P. (2017) 'Microbial Biofilms and Chronic Wounds.', *Microorganisms*. Multidisciplinary Digital Publishing Institute (MDPI), 5(1). doi: 10.3390/microorganisms5010009.

Ommen, P., Zobek, N. and Meyer, R. L. (2017) 'Quantification of biofilm biomass by staining: Non-toxic safranin can replace the popular crystal violet', *Journal of Microbiological Methods*, 141, pp. 87–89. doi: 10.1016/j.mimet.2017.08.003.

Ortiz, D., Cabrales, P. and Briceño, J. C. (2013) 'Transport of nitric oxide by perfluorocarbon emulsion', *Biotechnology Progress*, 29(6), pp. 1565–1572. doi: 10.1002/btpr.1797.

Owen, J., Crake, C., Lee, J. Y., Carugo, D., Beguin, E., Khrapitchev, A. A., Browning, R. J., Sibson, N. and Stride, E. (2018) 'A versatile method for the preparation of particle-loaded microbubbles for multimodality imaging and targeted drug delivery', *Drug Delivery and Translational Research*. Springer Verlag, 8(2), pp. 342–356. doi: 10.1007/s13346-017-0366-7.

Owen, J., Kamila, S., Shrivastava, S., Carugo, D., Bernardino de la Serna, J., Mannaris, C., Pereno, V., Browning, R., Beguin, E., McHale, A. P., Callan, J. F. and Stride, E. (2018) 'The Role of PEG-40-stearate in the Production, Morphology, and Stability of Microbubbles', *Langmuir*. American Chemical Society, p. acs.langmuir.8b02516. doi: 10.1021/acs.langmuir.8b02516.

Owen, J., Rademeyer, P., Chung, D., Cheng, Q., Holroyd, D., Coussios, C., Friend, P., Pankhurst, Q. A. and Stride, E. (2015) 'Magnetic targeting of microbubbles against physiologically relevant flow conditions', *Interface Focus*. Royal Society of London, 5(5), pp. 1–12. doi: 10.1098/rsfs.2015.0001.

Paefgen, V., Doleschel, D. and Kiessling, F. (2015) 'Evolution of contrast agents for ultrasound imaging and ultrasound-mediated drug delivery', *Frontiers in Pharmacology*. Frontiers Media S.A. doi: 10.3389/fphar.2015.00197.

Palmioli, A., Sperandeo, P., Polissi, A. and Airoldi, C. (2019) 'Targeting Bacterial Biofilm: A New LecA Multivalent Ligand with Inhibitory Activity', *ChemBioChem*. Wiley-VCH Verlag, 20(23), pp. 2911–2915. doi: 10.1002/cbic.201900383.

Paolino, D., Accolla, M. L., Cilurzo, F., Cristiano, M. C., Cosco, D., Castelli, F., Sarpietro, M. G., Fresta, M. and Celia, C. (2017) 'Interaction between PEG lipid and DSPE/DSPC phospholipids: An insight of PEGylation degree and kinetics of de-PEGylation', *Colloids and Surfaces B: Biointerfaces*. Elsevier, 155, pp. 266–275. doi: 10.1016/J.COLSURFB.2017.04.018.

Park, K. D., Kim, Y. S., Han, D. K., Kim, Y. H., Lee, E. H. B., Suh, H. and Choi, K. S. (1998) 'Bacterial adhesion on PEG modified polyurethane surfaces', *Biomaterials*. Elsevier, 19(7–9), pp. 851–859. doi: 10.1016/S0142-9612(97)00245-7.

Parsek, M. R. and Singh, P. K. (2003) ‘Bacterial Biofilms: An Emerging Link to Disease Pathogenesis’, *Annual Review of Microbiology*. Annual Reviews 4139 El Camino Way, P.O. Box 10139, Palo Alto, CA 94303-0139, USA , 57(1), pp. 677–701. doi: 10.1146/annurev.micro.57.030502.090720.

Pen, Y., Zhang, Z. J., Morales-García, A. L., Mears, M., Tarmey, D. S., Edyvean, R. G., Banwart, S. A. and Geoghegan, M. (2015) ‘Effect of extracellular polymeric substances on the mechanical properties of Rhodococcus’, *Biochimica et Biophysica Acta (BBA) - Biomembranes*. Elsevier, 1848(2), pp. 518–526. doi: 10.1016/J.BBAMEM.2014.11.007.

Percival, S. L., Hill, K. E., Malic, S., Thomas, D. W. and Williams, D. W. (2011) ‘Antimicrobial tolerance and the significance of persister cells in recalcitrant chronic wound biofilms’, *Wound Repair and Regeneration*. John Wiley & Sons, Ltd (10.1111), 19(1), pp. 1–9. doi: 10.1111/j.1524-475X.2010.00651.x.

Pereno, V., Aron, M., Vince, O., Mannaris, C., Seth, A., De Saint Victor, M., Lajoinie, G., Versluis, M., Coussios, C., Carugo, D. and Stride, E. (2018) ‘Layered acoustofluidic resonators for the simultaneous optical and acoustic characterisation of cavitation dynamics, microstreaming, and biological effects’, *Biomicrofluidics*. American Institute of Physics Inc., 12(3), p. 034109. doi: 10.1063/1.5023729.

Pereno, V., Lei, J., Carugo, D. and Stride, E. (2020) ‘Microstreaming inside Model Cells Induced by Ultrasound and Microbubbles’, *Langmuir*. American Chemical Society, 36(23), pp. 6388–6398. doi: 10.1021/acs.langmuir.0c00536.

Persat, A., Inclan, Y. F., Engel, J. N., Stone, H. A. and Gitai, Z. (2015) ‘Type IV pili mechanochemically regulate virulence factors in Pseudomonas aeruginosa.’, *Proceedings of the National Academy of Sciences of the United States of America*. National Academy of Sciences, 112(24), pp. 7563–8. doi: 10.1073/pnas.1502025112.

Pishchany, G. and Skaar, E. P. (2012) ‘Taste for blood: Hemoglobin as a nutrient source for pathogens’, *PLoS Pathogens*. Public Library of Science, 8(3). doi: 10.1371/journal.ppat.1002535.

Pitt, W. G., McBride, M. O., Lunceford, J. K., Roper, R. J. and Sagers, R. D. (1994) ‘Ultrasonic enhancement of antibiotic action on gram-negative bacteria.’, *Antimicrobial agents and chemotherapy*, 38(11), pp. 2577–82. Available at: http://www.ncbi.nlm.nih.gov/pubmed/7872751 (Accessed: 16 March 2019).

Pitt, W. G. and Ross, S. A. (2003) ‘Ultrasound increases the rate of bacterial cell growth.’, *Biotechnology progress*. NIH Public Access, 19(3), pp. 1038–44. doi: 10.1021/bp0340685.

Povey, M. J. W. and Mason, T. J. (1998) *Ultrasound in food processing*. 1st edn. London: Blackie Academic & Professional.

Price, B. L., Lovering, A. M., Bowling, F. L. and Dobson, C. B. (2016) ‘Development of a Novel Collagen Wound Model To Simulate the Activity and Distribution of Antimicrobials in Soft Tissue during Diabetic Foot Infection’. doi: 10.1128/AAC.01064-16.

Privett, B. J., Shin, J. H. and Schoenfisch, M. H. (2010) ‘Electrochemical nitric oxide sensors for physiological measurements.’, *Chemical Society reviews*. NIH Public Access, 39(6), pp. 1925–35. doi: 10.1039/b701906h.

Pulsipher, K. W., Hammer, D. A., Lee, D. and Sehgal, C. M. (2018) ‘Engineering Theranostic Microbubbles Using Microfluidics for Ultrasound Imaging and Therapy: A Review’, *Ultrasound in Medicine & Biology*. Elsevier, 44(12), pp. 2441–2460. doi: 10.1016/J.ULTRASMEDBIO.2018.07.026.

Rahman, M. F. A., Arshad, M. R., Manaf, A. A. and Yaacob, M. I. H. (2012) *An investigation on the behaviour of*

PDMS as a membrane material for underwater acoustic sensing.

Rediske, A. M., Roeder, B. L., Brown, M. K., Nelson, J. L., Robison, R. L., Draper, D. O., Schaalje, G. B., Robison, R. A. and Pitt, W. G. (1999) ‘Ultrasonic enhancement of antibiotic action on Escherichia coli biofilms: an in vivo model.’, *Antimicrobial agents and chemotherapy*. American Society for Microbiology, 43(5), pp. 1211–4. Available at: http://www.ncbi.nlm.nih.gov/pubmed/10223938 (Accessed: 12 June 2018).

Reinders, A., Hee, C.-S., Ozaki, S., Mazur, A., Boehm, A., Schirmer, T. and Jenal, U. (2016) ‘Expression and Genetic Activation of Cyclic Di-GMP-Specific Phosphodiesterases in Escherichia coli’, *Journal of Bacteriology*. American Society for Microbiology, 198(3), pp. 448–462. doi: 10.1128/JB.00604-15.

Ren, H., Wu, J., Colletta, A., Meyerhoff, M. E. and Xi, C. (2016) ‘Efficient eradication of mature Pseudomonas aeruginosa biofilm via controlled delivery of nitric oxide combined with antimicrobial peptide and antibiotics’, *Frontiers in Microbiology*, 7(AUG), pp. 1–8. doi: 10.3389/fmicb.2016.01260.

Renner, L. D. and Weibel, D. B. (2011) ‘Physicochemical regulation of biofilm formation’, *MRS Bulletin*. NIH Public Access, pp. 347–355. doi: 10.1557/mrs.2011.65.

Reyes, E. A. P., Bale, M. J., Cannon, W. H. and Matsen, J. M. (1981) ‘Identification of Pseudomonas aeruginosa by pyocyanin production on Tech agar’, *Journal of Clinical Microbiology*. American Society for Microbiology (ASM), 13(3), pp. 456–458. doi: 10.1128/jcm.13.3.456-458.1981.

Rhoads, D. D., Wolcott, R. D. and Percival, S. L. (2008) ‘Biofilms in wounds: management strategies’, *Journal of Wound Care*. MA Healthcare London , 17(11), pp. 502–508. doi: 10.12968/jowc.2008.17.11.31479.

Ricci, S., Dinia, L., Del Sette, M., Anzola, P., Mazzoli, T., Cenciarelli, S. and Gandolfo, C. (2012) ‘Sonothrombolysis for acute ischaemic stroke’, in Ricci, S. (ed.) *Cochrane Database of Systematic Reviews*. Chichester, UK: John Wiley & Sons, Ltd. doi: 10.1002/14651858.CD008348.pub2.

Richard, A. M., Diaz, J. H. and Kaye, A. D. (2014) ‘Reexamining the risks of drinking-water nitrates on public health.’, *The Ochsner journal*. Ochsner Clinic, L.L.C. and Alton Ochsner Medical Foundation, 14(3), pp. 392–8. Available at: http://www.ncbi.nlm.nih.gov/pubmed/25249806 (Accessed: 29 October 2020).

Rmaile, A., Carugo, D., Capretto, L., Aspiras, M., De Jager, M., Ward, M. and Stoodley, P. (2014) ‘Removal of interproximal dental biofilms by high-velocity water microdrops.’, *Journal of dental research*. International Association for Dental Research, 93(1), pp. 68–73. doi: 10.1177/0022034513510945.

Robson, M. C. (2004) ‘Pathophysiology of Chronic Wounds’, in *Surgery in Wounds*. Berlin, Heidelberg: Springer Berlin Heidelberg, pp. 29–40. doi: 10.1007/978-3-642-59307-9_2.

Rodgers, S. D., Camphausen, R. T. and Hammer, D. A. (2000) ‘Sialyl Lewis(x)-mediated, PSGL-1-independent rolling adhesion on P-selectin’, *Biophysical Journal*. Biophysical Society, 79(2), pp. 694–706. doi: 10.1016/S0006-3495(00)76328-4.

Rovers, T. A. M., Sala, G., van der Linden, E. and Meinders, M. B. J. (2016) ‘Temperature is key to yield and stability of BSA stabilized microbubbles’, *Food Hydrocolloids*. Elsevier, 52, pp. 106–115. doi: 10.1016/J.FOODHYD.2015.05.038.

Runyan, C. M., Carmen, J. C., Beckstead, B. L., Nelson, J. L., Robison, R. A. and Pitt, W. G. (2006) ‘Low-frequency ultrasound increases outer membrane permeability of Pseudomonas aeruginosa’, *The Journal of General and Applied Microbiology*. Applied Microbiology, Molecular and Cellular Biosciences Research Foundation, 52(5), pp.

295–301. doi: 10.2323/jgam.52.295.

Rutherford, S. T. and Bassler, B. L. (2012) ‘Bacterial quorum sensing: its role in virulence and possibilities for its control.’, *Cold Spring Harbor perspectives in medicine*. Cold Spring Harbor Laboratory Press, 2(11). doi: 10.1101/cshperspect.a012427.

Rutkowska, M., Namieśnik, J. and Konieczka, P. (2017) ‘Ultrasound-Assisted Extraction’, in *The Application of Green Solvents in Separation Processes*. Elsevier Inc., pp. 301–324. doi: 10.1016/B978-0-12-805297-6.00010-3.

Rychak, J. J. and Klibanov, A. L. (2014) ‘Nucleic acid delivery with microbubbles and ultrasound.’, *Advanced drug delivery reviews*. NIH Public Access, 72, pp. 82–93. doi: 10.1016/j.addr.2014.01.009.

S. Ferreira, A., F. Silva-Paes-Leme, A., R.B. Raposo, N. and S. da Silva, S. (2015) ‘By Passing Microbial Resistance: Xylitol Controls Microorganisms Growth by Means of Its Anti-Adherence Property’, *Current Pharmaceutical Biotechnology*. Bentham Science Publishers, 16(1), pp. 35–42. Available at: http://www.ingentaconnect.com/content/ben/cpb/2015/00000016/00000001/art00005 (Accessed: 11 June 2018).

Saidkhani, V., Asadizaker, M., Khodayar, M. J. and Latifi, S. M. (2016) ‘The effect of nitric oxide releasing cream on healing pressure ulcers.’, *Iranian journal of nursing and midwifery research*. Wolters Kluwer -- Medknow Publications, 21(3), pp. 322–30. doi: 10.4103/1735-9066.180389.

de Saint Victor, M., Barnsley, L. C., Carugo, D., Owen, J., Coussios, C. C. and Stride, E. (2019) ‘Sonothrombolysis with Magnetically Targeted Microbubbles’, *Ultrasound in Medicine and Biology*. Elsevier USA, 45(5), pp. 1151–1163. doi: 10.1016/j.ultrasmedbio.2018.12.014.

Salazar, J., Alarcón, M., Huerta, J., Navarro, B. and Aguayo, D. (2017) ‘Phosphoethanolamine addition to the Heptose I of the Lipopolysaccharide modifies the inner core structure and has an impact on the binding of Polymyxin B to the Escherichia coli outer membrane’, *Archives of Biochemistry and Biophysics*. Academic Press, 620, pp. 28–34. doi: 10.1016/J.ABB.2017.03.008.

Salta, M., Capretto, L., Carugo, D., Wharton, J. A. and Stokes, K. R. (2013) ‘Life under flow: A novel microfluidic device for the assessment of anti-biofilm technologies.’, *Biomicrofluidics*. American Institute of Physics, 7(6), p. 64118. doi: 10.1063/1.4850796.

Sang, S. Y., Coakley, R., Lau, G. W., Lymar, S. V., Gaston, B., Karabulut, A. C., Hennigan, R. F., Hwang, S. H., Buettner, G., Schurr, M. J., Mortensen, J. E., Burns, J. L., Speert, D., Boucher, R. C. and Hassett, D. J. (2006) ‘Anaerobic killing of mucoid Pseudomonas aeruginosa by acidified nitrite derivatives under cystic fibrosis airway conditions’, *Journal of Clinical Investigation*. American Society for Clinical Investigation, 116(2), pp. 436–446. doi: 10.1172/JCI24684.

Santin, M. D., King, D. A., Foiret, J., Haak, A., O’Brien, W. D. and Bridal, S. L. (2010) ‘Encapsulated contrast microbubble radial oscillation associated with postexcitation pressure peaks’, *The Journal of the Acoustical Society of America*. Acoustical Society of America (ASA), 127(2), pp. 1156–1164. doi: 10.1121/1.3277216.

Sarkar, K., Katiyar, A. and Jain, P. (2009) ‘Growth and dissolution of an encapsulated contrast microbubble: effects of encapsulation permeability.’, *Ultrasound in medicine & biology*. NIH Public Access, 35(8), pp. 1385–96. doi: 10.1016/j.ultrasmedbio.2009.04.010.

Schulz, G. and Stechmiller, J. (2006) ‘Wound Healing and Nitric Oxide Production: Too Little or Too Much May

Impair Healing and Cause Chronic Wounds', *The International Journal of Lower Extremity Wounds*. Sage PublicationsSage CA: Thousand Oaks, CA, 5(1), pp. 6–8. doi: 10.1177/1534734606286633.

Schurr, M. J. (2013) 'Which bacterial biofilm exopolysaccharide is preferred, Psl or alginate?', *Journal of bacteriology*. American Society for Microbiology, 195(8), pp. 1623–6. doi: 10.1128/JB.00173-13.

Schutt, C. E., Ibsen, S. D., Thrift, W. and Esener, S. C. (2014) 'The influence of distance between microbubbles on the fluid flow produced during ultrasound exposure', *The Journal of the Acoustical Society of America*. Acoustical Society of America (ASA), 136(6), pp. 3422–3430. doi: 10.1121/1.4898422.

Segers, T., Lassus, A., Bussat, P., Gaud, E. and Frinking, P. (2019) 'Improved coalescence stability of monodisperse phospholipid-coated microbubbles formed by flow-focusing at elevated temperatures', *Lab on a Chip*. Royal Society of Chemistry, 19(1), pp. 158–167. doi: 10.1039/c8lc00886h.

Seliwiorstow, T., De Zutter, L., Houf, K., Botteldoorn, N., Baré, J. and Van Damme, I. (2016) 'Comparative performance of isolation methods using Preston broth, Bolton broth and their modifications for the detection of Campylobacter spp. from naturally contaminated fresh and frozen raw poultry meat', *International Journal of Food Microbiology*. Elsevier B.V., 234, pp. 60–64. doi: 10.1016/j.ijfoodmicro.2016.06.040.

Sharma, D., Misba, L. and Khan, A. U. (2019) 'Antibiotics versus biofilm: An emerging battleground in microbial communities', *Antimicrobial Resistance and Infection Control*. BioMed Central Ltd., pp. 1–10. doi: 10.1186/s13756-019-0533-3.

Sharma, P. K., Gibcus, M. J., van der Mei, H. C. and Busscher, H. J. (2005) 'Influence of fluid shear and microbubbles on bacterial detachment from a surface.', *Applied and environmental microbiology*. American Society for Microbiology, 71(7), pp. 3668–73. doi: 10.1128/AEM.71.7.3668-3673.2005.

She, P., Chen, L., Qi, Y., Xu, H., Liu, Y., Wang, Y., Luo, Z. and Wu, Y. (2016) 'Effects of human serum and apo-Transferrin on *Staphylococcus epidermidis* RP62A biofilm formation', *MicrobiologyOpen*. Blackwell Publishing Ltd, 5(6), pp. 957–966. doi: 10.1002/mbo3.379.

Shi, H., Liu, H., Luan, S., Shi, D., Yan, S., Liu, C., Li, R. K. Y. and Yin, J. (2016) 'Effect of polyethylene glycol on the antibacterial properties of polyurethane/carbon nanotube electrospun nanofibers', *Royal Society of Chemistry Advances*, 6, pp. 19238–19244. doi: 10.1039/c6ra00363j.

Singh, A., Prakash, P., Achra, A., Singh, G., Das, A. and Singh, R. (2017) 'Standardization and classification of in vitro biofilm formation by clinical isolates of Staphylococcus aureus', *Journal of Global Infectious Diseases*. Medknow Publications, 9(3), pp. 93–101. doi: 10.4103/jgid.jgid_91_16.

Singh, S., Singh, S. K., Chowdhury, I. and Singh, R. (2017) 'Understanding the Mechanism of Bacterial Biofilms Resistance to Antimicrobial Agents.', *The open microbiology journal*. Bentham Science Publishers, 11, pp. 53–62. doi: 10.2174/1874285801711010053.

Sirsi, S. and Borden, M. (2009) 'Microbubble Compositions, Properties and Biomedical Applications.', *Bubble science engineering and technology*. NIH Public Access, 1(1–2), pp. 3–17. doi: 10.1179/175889709X446507.

Sirsi, S. R. and Borden, M. A. (2014) 'State-of-the-art materials for ultrasound-triggered drug delivery', *Advanced Drug Delivery Reviews*. Elsevier B.V., 72, pp. 3–14. doi: 10.1016/j.addr.2013.12.010.

Smith, S. A., Travers, R. J. and Morrissey, J. H. (2015) 'How it all starts: Initiation of the clotting cascade.', *Critical reviews in biochemistry and molecular biology*. NIH Public Access, 50(4), pp. 326–36. doi:

10.3109/10409238.2015.1050550.

Sommer, R., Wagner, S., Rox, K., Varrot, A., Hauck, D., Wamhoff, E.-C., Schreiber, J., Ryckmans, T., Brunner, T., Rademacher, C., Hartmann, R. W., Brö, M., Imberty, A. and Titz, A. (2017) 'Glycomimetic, Orally Bioavailable LecB Inhibitors Block Biofilm Formation of Pseudomonas aeruginosa'. doi: 10.1021/jacs.7b11133.

Soren, O., Rineh, A., Silva, D. G., Cai, Y., Howlin, R. P., Allan, R. N., Feelisch, M., Davies, J. C., Connett, G. J., Faust, S. N., Kelso, M. J. and Webb, J. S. (2020) 'Cephalosporin nitric oxide-donor prodrug DEA-C3D disperses biofilms formed by clinical cystic fibrosis isolates of Pseudomonas aeruginosa', *Journal of Antimicrobial Chemotherapy*. Oxford University Press, 75(1), pp. 117–125. doi: 10.1093/jac/dkz378.

Stiefel, P., Rosenberg, U., Schneider, J., Mauerhofer, S., Maniura-Weber, K. and Ren, Q. (2016) 'Is biofilm removal properly assessed? Comparison of different quantification methods in a 96-well plate system', *Applied Microbiology and Biotechnology*. Springer Berlin Heidelberg, 100(9), pp. 4135–4145. doi: 10.1007/s00253-016-7396-9.

Stiefel, P., Schmidt-Emrich, S., Maniura-Weber, K. and Ren, Q. (2015) 'Critical aspects of using bacterial cell viability assays with the fluorophores SYTO9 and propidium iodide.', *BMC microbiology*. BioMed Central, 15, p. 36. doi: 10.1186/s12866-015-0376-x.

Van Stormbroek, B., Zampoli, M. and Morrow, B. M. (2019) 'Nebulized gentamicin in combination with systemic antibiotics for eradicating early *Pseudomonas aeruginosa* infection in children with cystic fibrosis', *Pediatric Pulmonology*. John Wiley & Sons, Ltd. doi: 10.1002/ppul.24254.

Stride, E. (2008) 'The influence of surface adsorption on microbubble dynamics.', *Philosophical transactions. Series A, Mathematical, physical, and engineering sciences*. The Royal Society, 366(1873), pp. 2103–15. doi: 10.1098/rsta.2008.0001.

Stride, E. and Edirisinghe, M. (2008) 'Novel microbubble preparation technologies', *Soft Matter*. Royal Society of Chemistry, 4(12), p. 2350. doi: 10.1039/b809517p.

Stride, E. and Edirisinghe, M. (2009) 'Novel preparation techniques for controlling microbubble uniformity: a comparison', *Medical & Biological Engineering & Computing*. Springer-Verlag, 47(8), pp. 883–892. doi: 10.1007/s11517-009-0490-8.

Stride, E. P. and Coussios, C. C. (2009) 'Cavitation and contrast: the use of bubbles in ultrasound imaging and therapy', *Proceedings of the Institution of Mechanical Engineers, Part H: Journal of Engineering in Medicine*, 224. doi: 10.1243/09544119JEIM622.

Stride, E. and Saffari, N. (2003) 'Microbubble ultrasound contrast agents: A review', *Proceedings of the Institution of Mechanical Engineers, Part H: Journal of Engineering in Medicine*, 217(6), pp. 429–447. doi: 10.1243/09544110360729072.

Sun, C., Sboros, V., Butler, M. B. and Moran, C. M. (2014) 'In vitro acoustic characterization of three phospholipid ultrasound contrast agents from 12 to 43 MHz.', *Ultrasound in medicine & biology*. Elsevier, 40(3), pp. 541–50. doi: 10.1016/j.ultrasmedbio.2013.10.010.

Sun, Y., Dowd, S. E., Smith, E., Rhoads, D. D. and Wolcott, R. D. (2008) 'In vitro multispecies Lubbock chronic wound biofilm model', *Wound Repair and Regeneration*. John Wiley & Sons, Ltd, 16(6), pp. 805–813. doi: 10.1111/j.1524-475X.2008.00434.x.

Suzuki, S., Gerner, P. and Lirk, P. (2018) 'Local anesthetics', in *Pharmacology and Physiology for Anesthesia: Foundations and Clinical Application*. Elsevier, pp. 390–411. doi: 10.1016/B978-0-323-48110-6.00020-X.

Swanson, E. J., Mohan, V., Kheir, J. and Borden, M. A. (2010) 'Phospholipid-Stabilized Microbubble Foam for Injectable Oxygen Delivery', *Langmuir*. American Chemical Society, 26(20), pp. 15726–15729. doi: 10.1021/la1029432.

Taglialegna, A., Lasa, I. and Valle, J. (2016) 'Amyloid Structures as Biofilm Matrix Scaffolds.', *Journal of bacteriology*. American Society for Microbiology, 198(19), pp. 2579–88. doi: 10.1128/JB.00122-16.

Takalkar, A. M., Klibanov, A. L., Rychak, J. J., Lindner, J. R. and Ley, K. (2004) 'Binding and detachment dynamics of microbubbles targeted to P-selectin under controlled shear flow', *Journal of Controlled Release*. Elsevier, 96(3), pp. 473–482. doi: 10.1016/j.jconrel.2004.03.002.

Talu, E., Lozano, M. M., Powell, R. L., Dayton, P. A. and Longo, M. L. (2006) 'Long-term stability by lipid coating monodisperse microbubbles formed by a flow-focusing device.', *Langmuir : the ACS journal of surfaces and colloids*. NIH Public Access, 22(23), pp. 9487–90. doi: 10.1021/la062095+.

Tassew, D. D., Mechesso, A. F., Park, N.-H., Song, J.-B., Shur, J.-W. and Park, S.-C. (2017) 'Biofilm formation and determination of minimum biofilm eradication concentration of antibiotics in Mycoplasma hyopneumoniae.', *The Journal of veterinary medical science*. Japanese Society of Veterinary Science, 79(10), pp. 1716–1720. doi: 10.1292/jvms.17-0279.

Terheyden, J. H., Wintergerst, M. W. M., Falahat, P., Berger, M., Holz, F. G. and Finger, R. P. (2020) 'Automated thresholding algorithms outperform manual thresholding in macular optical coherence tomography angiography image analysis', *PLOS ONE*. Edited by I. Grulkowski. Public Library of Science, 15(3), p. e0230260. doi: 10.1371/journal.pone.0230260.

Thomas, D. D., Liu, X., Kantrow, S. P., Lancaster, J. R. and Jr. (2001) 'The biological lifetime of nitric oxide: Implications for the perivascular dynamics of NO and O2', *Proceedings of the National Academy of Sciences*. National Academy of Sciences, 98(1), pp. 355–360. doi: 10.1073/pnas.011379598.

Thomson, C. H. (2011) 'Biofilms: do they affect wound healing?', *International Wound Journal*, 8(1), pp. 63–67. doi: 10.1111/j.1742-481X.2010.00749.x.

Tinkov, S., Bekeredjian, R., Winter, G. and Coester, C. (2009) 'Microbubbles as ultrasound triggered drug carriers', *Journal of Pharmaceutical Sciences*. Elsevier, 98(6), pp. 1935–1961. doi: 10.1002/JPS.21571.

Tong, J., Ding, J., Shen, X., Chen, L., Bian, Y., Ma, G., Yao, Y. and Yang, F. (2013) 'Mesenchymal Stem Cell Transplantation Enhancement in Myocardial Infarction Rat Model under Ultrasound Combined with Nitric Oxide Microbubbles', *PLoS ONE*. Edited by P. Rameshwar. Public Library of Science, 8(11), p. e80186. doi: 10.1371/journal.pone.0080186.

Tonnesen, M. G., Feng, X. and Clark, R. A. F. (2000) 'Angiogenesis in Wound Healing', *Journal of Investigative Dermatology Symposium Proceedings*, 5(1), pp. 40–46. doi: 10.1046/j.1087-0024.2000.00014.x.

Touzel, R. E., Sutton, J. M. and Wand, M. E. (2016) 'Establishment of a multi-species biofilm model to evaluate chlorhexidine efficacy', *Journal of Hospital Infection*. W.B. Saunders, 92(2), pp. 154–160. doi: 10.1016/J.JHIN.2015.09.013.

Truchado, P., Gil, M. I., Larrosa, M. and Allende, A. (2020) 'Detection and Quantification Methods for Viable but

Non-culturable (VBNC) Cells in Process Wash Water of Fresh-Cut Produce: Industrial Validation', *Frontiers in Microbiology*. Frontiers Media S.A., 11. doi: 10.3389/fmicb.2020.00673.

Tzu-Yin, W., Wilson, K. E., Machtaler, S. and Willmann, J. K. (2013) 'Ultrasound and microbubble guided drug delivery: mechanistic understanding and clinical implications.', *Current pharmaceutical biotechnology*. NIH Public Access, 14(8), pp. 743–52. Available at: http://www.ncbi.nlm.nih.gov/pubmed/24372231 (Accessed: 13 September 2018).

Unger, E. C., Matsunaga, T. O., McCreery, T., Schumann, P., Sweitzer, R. and Quigley, R. (2002) 'Therapeutic applications of microbubbles', *European Journal of Radiology*. Elsevier, 42(2), pp. 160–168. doi: 10.1016/S0720-048X(01)00455-7.

Unger, E. C., McCreery, T., Shen, D., Wu, G., Sweitzer, R. and Wu, Q. (1998) 'Gas-filled liposomes as ultrasound contrast agents for blood pool, thrombus-specific and therapeutic applications', *The Journal of the Acoustical Society of America*. Acoustical Society of America, 103(5), pp. 3001–3001. doi: 10.1121/1.422981.

Unger, E. C., Porter, T., Culp, W., Labell, R., Matsunaga, T. and Zutshi, R. (2004) 'Therapeutic applications of lipid-coated microbubbles', *Advanced Drug Delivery Reviews*, 56, pp. 1291–1314. doi: 10.1016/j.addr.2003.12.006.

Unger, E., Porter, T., Lindner, J. and Grayburn, P. (2014) 'Cardiovascular drug delivery with ultrasound and microbubbles', *Advanced Drug Delivery Reviews*. Elsevier, 72, pp. 110–126. doi: 10.1016/J.ADDR.2014.01.012.

Valenti, P., Catizone, A., Frioni, A. and Berlutti, F. (2015) 'Lactoferrin and Cystic Fibrosis Airway Infection', in *Diet and Exercise in Cystic Fibrosis*. Elsevier, pp. 259–270. doi: 10.1016/B978-0-12-800051-9.00030-4.

Valenti, P., Frioni, A., Rossi, A., Ranucci, S., De Fino, I., Cutone, A., Rosa, L., Bragonzi, A. and Berlutti, F. (2017) 'Aerosolized bovine lactoferrin reduces neutrophils and pro-inflammatory cytokines in mouse models of *Pseudomonas aeruginosa* lung infections', *Biochemistry and Cell Biology*. NRC Research Press, 95(1), pp. 41–47. doi: 10.1139/bcb-2016-0050.

VanCleave, T. T., Pulsifer, A. R., Connor, M. G., Warawa, J. M. and Lawrenz, M. B. (2017) 'Impact of gentamicin concentration and exposure time on intracellular Yersinia pestis', *Frontiers in Cellular and Infection Microbiology*. Frontiers Media S.A., 7(DEC), p. 505. doi: 10.3389/fcimb.2017.00505.

Vladisavljević, G. T. (2016) 'Integrated Membrane Processes for the Preparation of Emulsions, Particles and Bubbles', in *Integrated Membrane Systems and Processes*. Oxford, UK: John Wiley & Sons, Ltd, pp. 79–140. doi: 10.1002/9781118739167.ch5.

Vohra, P. and Jasuja, K. (2016) 'Recent update in ultrasound contrast agents', *International Journal of Scientific Reports*, 2(10), p. 274. doi: 10.18203/issn.2454-2156.IntJSciRep20163401.

Volk, P. D. A. and Moreland, J. G. (2014) 'ROS-containing endosomal compartments: Implications for signaling', in *Methods in Enzymology*. Academic Press Inc., pp. 201–224. doi: 10.1016/B978-0-12-397925-4.00013-4.

Wagner, C., Aytac, S. and Maria Hänsch, G. (2011) 'Biofilm growth on implants: Bacteria prefer plasma coats', *International Journal of Artificial Organs*. Int J Artif Organs, 34(9), pp. 811–817. doi: 10.5301/ijao.5000061.

Wagner, S., Hauck, D., Hoffmann, M., Sommer, R., Joachim, I., Müller, R., Imberty, A., Varrot, A. and Titz, A. (2017) 'Covalent Lectin Inhibition and Application in Bacterial Biofilm Imaging', *Angewandte Chemie International Edition*. Wiley-VCH Verlag, 56(52), pp. 16559–16564. doi: 10.1002/anie.201709368.

Walsh, J. W., Hoffstad, O. J., Sullivan, M. O. and Margolis, D. J. (2016) 'Association of diabetic foot ulcer and death in a population-based cohort from the United Kingdom', *Diabet. Med*, 33, pp. 1493–1498. doi: 10.1111/dme.13054.

Wang, C., Yang, F., Xu, Z., Shi, D., Chen, D., Dai, J., Gu, N. and Jiang, Q. (2013) 'Intravenous release of NO from lipidic microbubbles accelerates deep vein thrombosis resolution in a rat model', *Thrombosis Research*. Elsevier Ltd, 131(1), pp. e31–e38. doi: 10.1016/j.thromres.2012.11.002.

Wang, L., Fan, D., Chen, W. and Terentjev, E. M. (2015) 'Bacterial growth, detachment and cell size control on polyethylene terephthalate surfaces', *Scientific Reports*, 5(1), p. 15159. doi: 10.1038/srep15159.

Wang, R., Starkey, M., Hazan, R. and Rahme, L. G. (2012) 'Honey's Ability to Counter Bacterial Infections Arises from Both Bactericidal Compounds and QS Inhibition.', *Frontiers in microbiology*. Frontiers Media SA, 3, p. 144. doi: 10.3389/fmicb.2012.00144.

Wang, S., Samiotaki, G., Olumolade, O., Feshitan, J. A. and Konofagou, E. E. (2014) 'Microbubble Type and Distribution Dependence of Focused Ultrasound-Induced Blood–Brain Barrier Opening', *Ultrasound in Medicine & Biology*. Elsevier, 40(1), pp. 130–137. doi: 10.1016/J.ULTRASMEDBIO.2013.09.015.

Wang, X., Gkanatsas, Y., Palasubramaniam, J., Hohmann, J. D., Chen, Y. C., Lim, B., Hagemeyer, C. E. and Peter, K. (2016) 'Thrombus-Targeted Theranostic Microbubbles: A New Technology towards Concurrent Rapid Ultrasound Diagnosis and Bleeding-free Fibrinolytic Treatment of Thrombosis.', *Theranostics*. Ivyspring International Publisher, 6(5), pp. 726–38. doi: 10.7150/thno.14514.

Watters, C. M., Burton, T., Kirui, D. K. and Millenbaugh, N. J. (2016) 'Enzymatic degradation of in vitro Staphylococcus aureus biofilms supplemented with human plasma.', *Infection and drug resistance*. Dove Press, 9, pp. 71–8. doi: 10.2147/IDR.S103101.

Weitzberg, E., Hezel, M. and Lundberg, J. O. (2010) 'Nitrate-nitrite-nitric oxide pathway: Implications for anesthesiology and intensive care', *Anesthesiology*. Lippincott Williams and Wilkins, pp. 1460–1475. doi: 10.1097/ALN.0b013e3181fcf3cc.

Weller, G. E. R., Villanueva, F. S., Klibanov, A. L. and Wagner, W. R. (2002) 'Modulating targeted adhesion of an ultrasound contrast agent to dysfunctional endothelium', *Annals of Biomedical Engineering*, 30(8), pp. 1012–1019. doi: 10.1114/1.1513565.

Westerhof, N., Stergiopulos, Nikos, Noble, M. I. M., Westerhof, N., Stergiopulos, Nikolaos and Noble, M. I. M. (2010) 'Law of Poiseuille', in *Snapshots of Hemodynamics*. Springer US, pp. 9–14. doi: 10.1007/978-1-4419-6363-5_2.

Wilks, S. A., Morris, N. S., Thompson, R., Prieto, J. A., Macaulay, M., Moore, K. N., Keevil, C. W. and Fader, M. (2020) 'An effective evidence-based cleaning method for the safe reuse of intermittent urinary catheters: In vitro testing', *Neurourology and Urodynamics*. John Wiley and Sons Inc., 39(3), pp. 907–915. doi: 10.1002/nau.24296.

Williams, D., Enoch, S., Miller, D., Harris, K., Price, P. and Harding, K. G. (2005) 'Effect of sharp debridement using curette on recalcitrant nonhealing venous leg ulcers: A concurrently controlled, prospective cohort study', *Wound Repair and Regeneration*. Wiley/Blackwell (10.1111), 13(2), pp. 131–137. doi: 10.1111/j.1067-1927.2005.130203.x.

Witte, M. B. and Barbul, A. (2002) 'Role of nitric oxide in wound repair.', *American journal of surgery*, 183(4), pp. 406–12. Available at: http://www.ncbi.nlm.nih.gov/pubmed/11975928 (Accessed: 11 June 2018).

Wolcott, R. D., Kennedy, J. P. and Dowd, S. E. (2009) ‘Regular debridement is the main tool for maintaining a healthy wound bed in most chronic wounds’, *Journal of Wound Care*. MA Healthcare London , 18(2), pp. 54–56. doi: 10.12968/jowc.2009.18.2.38743.

Wolcott, R. D., Rhoads, D. D. and Dowd, S. E. (2008) ‘Biofilms and chronic wound inflammation’, *Journal of Wound Care*. MA Healthcare London , 17(8), pp. 333–341. doi: 10.12968/jowc.2008.17.8.30796.

Woldman, Y. Y., Sun, J., Zweier, J. L. and Khramtsov, V. V. (2009) ‘Direct chemiluminescence detection of nitric oxide in aqueous solutions using the natural nitric oxide target soluble guanylyl cyclase’, *Free Radical Biology and Medicine*, 47(10), pp. 1339–1345. doi: 10.1016/j.freeradbiomed.2009.09.007.

Wong, K. K., Huang, I., Kim, Y. R., Tang, H., Yang, E. S., Kwong, K. K. and Wu, E. X. (2004) ‘In vivo study of microbubbles as an MR susceptibility contrast agent’, *Magnetic Resonance in Medicine*. John Wiley and Sons Inc., 52(3), pp. 445–452. doi: 10.1002/mrm.20181.

Wood, T. K., Knabel, S. J. and Kwan, B. W. (2013) ‘Bacterial persister cell formation and dormancy’, *Applied and Environmental Microbiology*. American Society for Microbiology (ASM), pp. 7116–7121. doi: 10.1128/AEM.02636-13.

Wu, H., Moser, C., Wang, H.-Z., Høiby, N. and Song, Z.-J. (2015) ‘Strategies for combating bacterial biofilm infections’, *International Journal of Oral Science*. Nature Publishing Group, 7(1), pp. 1–7. doi: 10.1038/ijos.2014.65.

Wu, J. and Nyborg, W. L. (2008) ‘Ultrasound, cavitation bubbles and their interaction with cells’, *Advanced Drug Delivery Reviews*. Elsevier, 60(10), pp. 1103–1116. doi: 10.1016/J.ADDR.2008.03.009.

Wu, S.-Y., Aurup, C., Sanchez, C. S., Grondin, J., Zheng, W., Kamimura, H., Ferrera, V. P. and Konofagou, E. E. (2018) ‘Efficient Blood-Brain Barrier Opening in Primates with Neuronavigation-Guided Ultrasound and Real-Time Acoustic Mapping’, *Scientific Reports*. Nature Publishing Group, 8(1), p. 7978. doi: 10.1038/s41598-018-25904-9.

Wu, S.-Y., Chen, C. C., Tung, Y.-S., Olumolade, O. O. and Konofagou, E. E. (2015) ‘Effects of the microbubble shell physicochemical properties on ultrasound-mediated drug delivery to the brain.’, *Journal of controlled release : official journal of the Controlled Release Society*. NIH Public Access, 212, pp. 30–40. doi: 10.1016/j.jconrel.2015.06.007.

Xin, Z., Lin, G., Lei, H., Lue, T. F. and Guo, Y. (2016) *Clinical applications of low-intensity pulsed ultrasound and its potential role in urology*, *Translational Andrology and Urology*. AME Publishing Company. doi: 10.21037/tau.2016.02.04.

Xu, L.-C. C., Wo, Y., Meyerhoff, M. E. and Siedlecki, C. A. (2017) ‘Inhibition of bacterial adhesion and biofilm formation by dual functional textured and nitric oxide releasing surfaces’, *Acta Biomaterialia*. Acta Materialia Inc., 51, pp. 53–65. doi: 10.1016/j.actbio.2017.01.030.

Xu, Q., Nakajima, M., Ichikawa, S., Nakamura, N. and Shiina, T. (2008) ‘A comparative study of microbubble generation by mechanical agitation and sonication’, *Innovative Food Science & Emerging Technologies*. Elsevier, 9(4), pp. 489–494. doi: 10.1016/J.IFSET.2008.03.003.

Xu, X., Song, R., He, M., Peng, C., Yu, M., Hou, Y., Qiu, H., Zou, R. and Yao, S. (2017) ‘Microfluidic production of nanoscale perfluorocarbon droplets as liquid contrast agents for ultrasound imaging’, *Lab on a Chip*. The Royal

Society of Chemistry, 17(20), pp. 3504–3513. doi: 10.1039/C7LC00056A.

Yazdanpanah, L., Nasiri, M. and Adarvishi, S. (2015) 'Literature review on the management of diabetic foot ulcer WJD 5 th Anniversary Special Issues (4): Diabetes-related complications', *World J Diabetes*, 6(1), pp. 37–53. doi: 10.4239/wjd.v6.i1.37.

Ye, J., He, H., Gong, J., Dong, W., Huang, Y., Wang, J., Chen, G. and Yang, V. C. (2013) 'Ultrasound-mediated targeted microbubbles: a new vehicle for cancer therapy', *Frontiers of Chemical Science and Engineering*, 7(1), pp. 20–28. doi: 10.1007/s11705-013-1311-z.

Yeh, E., Pinsky, B. A., Banaei, N. and Baron, E. J. (2009) 'Hair Sheep Blood, Citrated or Defibrinated, Fulfills All Requirements of Blood Agar for Diagnostic Microbiology Laboratory Tests', *PLoS ONE*. Edited by A. J. Ratner. Public Library of Science, 4(7), p. e6141. doi: 10.1371/journal.pone.0006141.

Yusof, N. S. M., Babgi, B., Alghamdi, Y., Aksu, M., Madhavan, J. and Ashokkumar, M. (2016) 'Physical and chemical effects of acoustic cavitation in selected ultrasonic cleaning applications', *Ultrasonics Sonochemistry*. Elsevier, 29, pp. 568–576. doi: 10.1016/J.ULTSONCH.2015.06.013.

Zapata, A. and Ramirez-Arcos, S. (2015) 'A Comparative Study of McFarland Turbidity Standards and the Densimat Photometer to Determine Bacterial Cell Density', *Current Microbiology*. Springer US, 70(6), pp. 907–909. doi: 10.1007/s00284-015-0801-2.

Zhang, H., Dudley, E. G. and Harte, F. (2017) 'Critical Synergistic Concentration of Lecithin Phospholipids Improves the Antimicrobial Activity of Eugenol against Escherichia coli.', *Applied and environmental microbiology*. American Society for Microbiology, 83(21), pp. e01583-17. doi: 10.1128/AEM.01583-17.

Zhao, S., Borden, M., Bloch, S. H., Kruse, D. E., Ferrara, K. W. and Dayton, P. A. (2004) 'Increasing binding efficiency of ultrasound targeted agents with radiation force', in *Proceedings - IEEE Ultrasonics Symposium*, pp. 1114–1117. doi: 10.1109/ULTSYM.2004.1417975.

Zhuang, X., Dávila-Contreras, E. M., Beaven, A. H., Im, W. and Klauda, J. B. (2016) 'An extensive simulation study of lipid bilayer properties with different head groups, acyl chain lengths, and chain saturations', *Biochimica et Biophysica Acta (BBA) - Biomembranes*. Elsevier, 1858(12), pp. 3093–3104. doi: 10.1016/J.BBAMEM.2016.09.016.

van der Zwaag, S., van den Ende, D. A. and Groen, W. A. (Pim) (2013) 'Sensing and Energy Harvesting Novel Polymer Composites', in *Materials Experience: Fundamentals of Materials and Design*. Elsevier Inc., pp. 221–234. doi: 10.1016/B978-0-08-099359-1.00016-3.

UNIVERSITY OF
Southampton